

Synthesis of Novel Extractants for Back-end Fuel Technology

By

SHIKHA SHARMA

(CHEM01200904012)

Bhabha Atomic Research Centre, Mumbai

A thesis submitted to the

Board of Studies in Chemical Sciences

In partial fulfillment of requirements

for the Degree of

DOCTOR OF PHILOSOPHY

of

HOMI BHABHA NATIONAL INSTITUTE



June, 2015

HOMI BHABHA NATIONAL INSTITUTE

Recommendations of the Viva Voce Committee

As members of the Viva Voce Committee, we certify that we have read the dissertation prepared by **Shikha Sharma** entitled “**Synthesis of novel extractants for back-end fuel technology**” and recommend that it may be accepted as fulfilling the thesis requirement for the award of Degree of Doctor of Philosophy.

 _____ **Date:** 22.03.2016

Chairman: Prof. S. Chattopadhyay

 _____ **Date:** 22.03.2016

Guide/convener: Prof. Sunil Kumar Ghosh

 _____ **Date:** 22.03.2016

External Examiner: Prof. A. K. Singh

 _____ **Date:** 22.03.2016

Member 1: Prof. S. Banerjee

 _____ **Date:** 22.03.2016

Member 2: Prof. S. K. Nayak

 _____ **Date:** 22.03.2016

Technical Adviser: Dr. P. S. Dhami

Final approval and acceptance of this thesis is contingent upon the candidate's submission of the final copies of the thesis to HBNI. I hereby certify that I have read this thesis prepared under my direction and recommend that it may be accepted as fulfilling the thesis requirement.

Date: 22/03/2016

Place: Mumbai


Prof. Sunil. K. Ghosh

STATEMENT BY AUTHOR

This dissertation has been submitted in partial fulfillment of requirements for an advanced degree at Homi Bhabha National Institute (HBNI) and is deposited in the Library to be made available to borrowers under rules of the HBNI.

Brief quotations from this dissertation are allowable without special permission, provided that accurate acknowledgement of source is made. Requests for permission for extended quotation from or reproduction of this manuscript in whole or in part may be granted by the Competent Authority of HBNI when in his or her judgment the proposed use of the material is in the interests of scholarship. In all other instances, however, permission must be obtained from the author.



Shikha Sharma

DECLARATION

I, hereby declare that the investigation presented in the thesis has been carried out by me.

The work is original and has not been submitted earlier as a whole or in part for a degree / diploma at this or any other Institution / University.



Shikha Sharma

List of Publications arising from the thesis

JOURNAL

- [1] “Comparative studies on radiolytic degradation of deuterium labeled and unlabeled tributyl phosphates”, **Shikha Sharma**, Sunil K. Ghosh, Devidas B. Naik, Prem S. Dhama, Joti N. Sharma, *J. Radioanal. Nucl. Chem.*, 2014, 302, 583-591.
- [2] “ α -Dialkylamino *N,N*-diisobutylacetamides: a new class of anion exchanger with intramolecular buffering properties”, **Shikha Sharma**, Sunil K. Ghosh, Anitha M, Joti N. Sharma, *RSC Adv.*, 2014, 4, 27837-42.
- [3] “Dialkylmethyl-2-(*N,N*-diisobutyl)acetamidoammonium iodide as a ruthenium selective ligand from nitric acid medium”, **Shikha Sharma**, Sunil K. Ghosh, Joti N. Sharma, *J Hazard. Mater.*, 2015, 295, 17-21.
- [4] “Design, synthesis and extraction studies of a new class of conformationally constrained (*N,N,N',N'*-tetraalkyl) 7-oxabicyclo[2.2.1]heptane-2,3-dicarboxamides”, **Shikha Sharma**, Surajit Panja, A. Bhattachariya, Prem S. Dhama, Preetam M. Gandhi, Sunil K. Ghosh, *Dalton Trans.*, 2015, 44, 12771-12779.
- [5] “Synthesis and characterization of two different inorganic-organic hybrid isopolyoxomolybdates with α -dipropylammonium *N,N*-diisobutylacetamide by varying reaction conditions”, **Shikha Sharma**, Sunil K. Ghosh, Mukesh kumar, Joti N. Sharma, *Polyhedron*, 2015, 100, 290-295.
- [6] “Efficient transport of Am(III) from nitric acid medium using a new conformationally constrained (*N,N,N',N'*-tetr-2-ethylhexyl) 7-oxabicyclo[2.2.1]heptane-2,3-dicarboxamide across a Supported Liquid Membrane”, **Shikha Sharma**, Surajit Panja, Prem S. Dhama, Preetam M. Gandhi, Sunil K. Ghosh, *J. Hazard. Mater.*, 2016, 305, 171-177.
- [7] “Synthesis and Extraction Studies with a Rationally Designed Diamide Ligand Selective to Actinide(IV) pertinent to Plutonium Uranium Redox Extraction Process, **Shikha Sharma**, Surajit Panja, A. Bhattachariya, Prem S. Dhama, Preetam M. Gandhi, Sunil K. Ghosh, *Dalton Trans.*, 2016, 45, 0000-0000 (DOI: 10.1039/C6DT00748A).
- [8] “Sorption of ruthenium by dipropylmethyl-2-(*N,N*-diisobutyl)acetamide ammonium iodide impregnated Amberlite XAD-4 resin from nitric acid medium”, **Shikha Sharma**, Sunil K. Ghosh, Joti N. Sharma, *Sep. Sci. Technol.*, 2016, 0000-0000 (DOI:10.1080/01496395.2016.1142563)

Conferences

- 1) Synthesis of deuterium labeled tributyl phosphates as radiation stable nuclear extractants. **Shikha Sharma**, Sunil K. Ghosh, in the Proceedings of conference *ISMC-2013* held in BARC, Mumbai during Dec 9-13, 2012.
- 2) Radiolytic degradation studies on deuterium labeled and unlabeled tributyl phosphates. **Shikha Sharma**, S. K. Ghosh, D. B. Naik, P. S. Dhama, J. N. Sharma, in the Proceedings of conference *TSRP-2014* held in BARC, Mumbai during, Jan 6-9, 2014.
- 3) Radiolytic and Hydrolytic Degradation Studies Of d_n -TBPs and Use of ^{239}Pu for their Extraction Evaluation, **Shikha Sharma**, S. K. Ghosh, D. B. Naik, P. S. Dhama, J. N. Sharma, in the Proceedings of conference *ARCEBS-2014* held in SINP, Kolkata during, Jan 12-18, 2014.
- 4) Synthesis of stable and selective nuclear extractants for back end fuel technology, **Shikha Sharma**, S. K Ghosh, in the Proceedings of conference *RSM-2014* held in CKT College, Mumbai during, Feb 21-22, 2014.
- 5) Solvent extraction evaluation of novel bi-functional extractants α -dialkylamino N,N' -diisobutylacetamides: An anion exchanger with intramolecular buffering properties, **Shikha Sharma**, S. K. Ghosh, Anitha M, J. N. Sharma, in the Proceedings of conference *SESTEC-2014* held in BARC, Mumbai during, Feb 25-28, 2014.

- 6) α -Dialkylamino *N,N*-Diisobutylacetamides as a New Class of Anion Exchanger with Intramolecular Buffering Properties, , **Shikha Sharma**, S. K. Ghosh, Anitha M, J. N. Sharma, in the Proceedings of conference *ISMC-2014* held in BARC, Mumbai during, Dec 9-13, 2014.
- 7) Selective sorption of ruthenium from acidic medium by Amberlite xad-4 resin impregnated with iodide salt of *N,N*'-diisobutyl(α -trialkylammonium)-acetamide, **Shikha Sharma**, S. K. Ghosh, J. N. Sharma, in the Proceedings of conference *NUCAR-2014* held in BARC, Mumbai during, Feb 9-13, 2015.



Shikha Sharma

Dedicated to

***My Beloved Parents
&
Brother***

ACKNOWLEDGEMENTS

This thesis would not have been possible without the support of many people. I feel short of words in expressing my gratitude for their help at various stages of this work.

First and foremost, I would like to express my sincere gratitude to my research guide **Dr. Sunil K Ghosh** for his continuous support to my work, his patience, encouragement, enthusiasm and immense knowledge. His intellectual ideas and guidance helped me in my research work. I express my deep sense of gratitude for his support and for energizing me to overcome all the hurdles. I am deeply indebted to him.

I wish to express my sincere gratitude to **Shri J. N. Sharma** for his valuable guidance, helpful suggestions and encouragement to learn the subject more deeply.

I am highly grateful to **Prof. S. Chattopadhyay**, Head, BOD for giving me an excellent opportunity to carry out my research work in Bio-Organic division. I would like to thank members of my doctoral committee; **Prof. S. Chattopadhyay, Prof. S. K. Nayak, Prof. Sharmila Banerjee** and **Dr. P.S. Dhami** for their encouragement, insightful comments and fruitful ideas during the course of the thesis work.

I cannot find words to express my gratitude to **Dr. Rekha Singh** for helping me learn experimental techniques. She has been there all the time to encourage and motivate me to work skillfully and helped me to overcome all the obstacles on my path.

My sincere thanks to **Dr. Surajit Panja** for his help in conducting various experiments and devoting his valuable time for my research work. I am also thankful to **Dr. Arunasis** and **Dr. Mukesh Kumar** for their support. This acknowledgement would be incomplete without saying thanks to a lot of people who helped me in getting crucial experimental data when there was dearth of instrument in my division. It would not be possible to mention all the names but I will never forget their help in my life.

I would like to acknowledge my wonderful lab mates **Rekha mam, Pintu sir, Raghu sir, Gady sir, Sandeep, Minaksmi, Somu, Gangababu and Chandrakant**

for their support and help throughout my doctoral research and also for making a cheerful environment in the Lab. Whether it is a scientific or personal matter, they were always with me in all the situations. I will always cherish the moments I spend with all of them in **3-26- H**. I am also thankful to other BOD members **Angshuman sir, Akhil sir, Sucheta di, Diwakar sir, Ajish sir, Seema di, Bhaskar sir, Sunita di, Papiya di, Sampada di, Sneha, Bauri sir, Mrunesh sir** etc. for their help and support, specially for **Akhil sir** who made all the things available for me which were not there in my lab.

Apart from the intellectual support, an emotional support is always needed to conquer the hardships. For this, I would like to thank, from the bottom of my heart, my friends **Monika Gupta, Neelam Soni, Minakshmi Paramanik and Debashree Manna**. I can not forget the days and time I spend with these good friends. I extremely enjoyed my stay at 1 B dawalgiri with my superb roommates **Debashree, Aparajita, Sonika, Avi, Megha, Vijaya and Sejal**. I convey heartfelt thanks to my training school friends **Jerina, Vasundhara, Suman di, Sagufta, Juby.....** for their selfless help.

Last but not the least, my deepest gratitude (that would never be enough!) is to my beloved parents **Shri Bhagwan Sahay Sharma** and **Smt. Kavita Sharma**, who have been so caring and supportive to me all the time, whose countless sacrifices allowed me to reach this point. Immense love, affection and encouragement from my brother **Abhinav Sharma** have been invaluable in the journey towards my goal. I must thank to my cousins (**Monu, Pintu, Mukul, Kushu**) for their love and all beloved relatives (including my late **Bauji and Aunty**) for their love and moral support during my study. I am also grateful to my maternal uncle's family for making my stay a pleasant one in Mumbai.

Above all, I praise **Almighty God**, for giving me more than I expected and for being with me all the time.

.....*Shikha*

CONTENTS

	Page No.
SYNOPSIS.....	v
LIST OF FIGURES.....	xvii
LIST OF TABLES.....	xxiv
LIST OF SCHEMES.....	xxv
ABBREVIATIONS.....	xxvii

CHAPTER-I

Introduction to back-end fuel technology

1.1 Principle of a nuclear reactor.....	3
1.2 Nuclear fuel cycle	4
1.3 Radioactive waste.....	5
1.4 Nuclear fuel reprocessing and radioactive waste management... ..	7
1.4.1 <i>"PUREX" process.....</i>	9
1.4.2 <i>Actinide partitioning.....</i>	10
1.4.3 <i>Separation of fission products.....</i>	10
1.4.4 <i>Solvents used at various stages of back-end of fuel cycle.....</i>	11
1.5 Separation methods.....	19
1.5.1 <i>Solvent extraction.....</i>	19
1.5.2 <i>Membrane separation.....</i>	23
1.5.3 <i>Solid phase extraction</i>	23
1.6 Ligand and metal interations (mechanism of extraction).....	24
1.7 Theory of complexation (HSAB concept).....	27

1.8 Factors influencing the distribution of metal ion (factors affecting extraction efficiency)	28
--	-----------

1.9 Criteria for the selection of a suitable extractant	30
--	-----------

CHAPTER-II

Design, synthesis and extraction properties of a new class of anion exchanger for oxometalates

2.1 Introduction.....	34
2.2 Present work.....	36
<i>2.2.1 Synthesis of α-dialkylamino N,N-diisobutylacetamides 1-3.....</i>	<i>37</i>
<i>2.2.2 Comparison of extraction behavior of amines 1-6 at different acidities ...</i>	<i>38</i>
<i>2.2.3 Optimization of organic phase composition.....</i>	<i>39</i>
<i>2.2.4 Determination of Stoichiometry of the extracted metal complex.....</i>	<i>40</i>
<i>2.2.5 Mechanism of extraction.....</i>	<i>43</i>
<i>2.2.6 Confirmation of complexation by NMR and IR studies.....</i>	<i>44</i>
<i>2.2.7 Back extraction studies.....</i>	<i>46</i>
<i>2.2.8 Crystal study of the molybdate complexes of amino acetamide 1</i>	<i>46</i>
2.3 Conclusions.....	60
2.4 Experimental	61

CHAPTER-III

Comparative studies on radiolytic degradation of deuterium labeled and unlabeled tributyl phosphates

3.1 Introduction.....	70
3.2 Present work.....	74

3.2.1 <i>Synthesis of deuterated TBPs</i>	75
3.2.2 <i>Radiolytic stability studies of undeuterated and deuterated TBPs</i>	80
3.2.3 <i>Extraction properties of natural and deuterated TBPs</i>	85
3.2.4 <i>Hydrolysis of TBPs</i>	87
3.3 Conclusion	87
3.4 Experimental	88

CHAPTER-IV

Design, synthesis and extraction properties of conformationally constrained oxa-diamides

4.1 Introduction	96
4.2 Present Work	98
4.2.1 <i>Synthesis of OBDA extractants</i>	100
4.2.2 <i>Extraction evaluation of OBDA by solvent extraction</i>	100
4.2.3 <i>Extraction evaluation of OBDA by membrane separation</i>	114
4.2.4 <i>Synthesis and extraction studies of Pu selective rigidified oxa-diamides</i>	121
4.3 Conclusion	128
4.4 Experimental	129

CHAPTER V

Design, synthesis and extraction properties of a new class of ruthenium selective ligands

5.1 Introduction	144
5.2 Present Work	146

5.2.1 <i>Synthesis of ammonium based extractants</i>	147
5.2.2 <i>Extraction evaluation of extractants 29-31 for Ru by solvent extraction</i>	147
5.2.3 <i>Sorption studies for Ru using ligand 29 impregnated Amberlite XAD-4 resin</i>	155
5.3 Conclusions	164
5.4 Experimental	165
REFERENCES	172

Synopsis

Synthesis of novel extractants for back-end fuel technology

Due to rising energy demands and limitation of fossil fuels in developing countries, it is crucial to seek for new energy resources. Nuclear power is considered to be one of the most potential alternatives to the conventional source of energy with minimum impact on environment. Nuclear energy has an important role to play in the long term as a sustainable source of energy by the use of exothermic nuclear processes based on the neutron induced controlled fission of various fissile materials like ^{235}U , ^{239}Pu , ^{233}U etc. In nuclear processes, nuclear fuels cannot be consumed totally due to accumulation of fission products formed in these processes. In the back end of nuclear fuel cycle, unconsumed fissile materials like uranium and plutonium are recovered by reprocessing of irradiated fuel and efficient management of resulting HLW is carried out for minimizing the long term radiotoxic effects. For these purposes, separation of various metal ions from nuclear waste solutions is achieved by means of various separation processes using organic molecules called “extractants”.

Chapter 1: Introduction to back-end fuel technology.

In the first chapter a brief introduction to nuclear fuel cycle, classification of radioactive waste, nuclear fuel reprocessing and waste management processes have been presented. During reprocessing of spent nuclear fuel, the valuable fissile elements (Pu and U) are recovered using PUREX process [1]. After separation of U and Pu from dissolved spent fuel, highly radioactive liquid waste solution also called High Level Waste (HLW) remains. HLW generally contains un-extracted U, Pu, bulk of minor actinides such as Am, Np, Cm, host of fission products and lanthanides as well as activation products along with process chemicals and structural materials [2]. Since the

half lives of minor actinides range between a few hundred to millions of years, surveillance of the vitrified matrix for such a long period is debatable. Therefore, actinides and lanthanides are selectively removed from HLW by a process called “actinide partitioning” [3, 4]. Safe management of HLW also involves the separation of fission products like ^{106}Ru , ^{99}Tc , ^{93}Zr , ^{137}Cs , ^{90}Sr , ^{99}Mo , ^{107}Pd . Among them ^{106}Ru , ^{99}Tc , ^{93}Zr are beta/gamma active. ^{137}Cs , ^{90}Sr are beta/gamma active along with heat producing too and ^{99}Mo , ^{107}Pd are useful for various possible applications.

Separation of metal ions from nuclear waste is performed by means of various separation processes using organic molecules called ‘extractants’ or ‘ligands’ or ‘solvents’. Literature survey on different class of extractants used at various stages of spent fuel reprocessing has been summarized in the present chapter. Different separation methods and basic principle of solvent extraction technique are discussed. Ligand to metal interaction and criteria for selection of extractants has also been presented in this chapter.

Chapter 2: Design, synthesis and extraction properties of a new class of anion exchanger for oxometalates.

Oxometalates such as MoO_4^{2-} , $\text{Mo}_7\text{O}_{24}^{6-}$, $\text{H}_2\text{Mo}_7\text{O}_{24}^{4-}$, $\text{UO}_2(\text{CO}_3)_3^{4-}$, $\text{UO}_2(\text{SO}_4)_3^{4-}$, TcO_4^- are usually present in various nuclear waste streams. Trioctylamine (major component of Alamine 336), Aliquat 336 and Primene JMT, commonly used anion exchangers known to extract oxometalates, works capably at lower acidity but shows poor efficiency at higher acidity of aqueous phase because at higher acidity the anion exchanger site of these extractants get engaged with HNO_3 [5]. Therefore, these extractants are not suitable for nuclear waste streams that usually have high nitric acid concentration.

This chapter involves the design, synthesis and extraction properties of a new class of ammonium based anion exchangers embedded with a terminal amide group, viz. α -dialkylamino N,N -diisobutylacetamides **1-3** (Fig. 1) including evaluation of the role of amide group in extraction from relatively higher concentration of nitric acid medium. Molybdate anion has been chosen as a representative example of oxometalate for the present studies. α -Dialkylamino N,N -diisobutylacetamides **1-3** were synthesized in our laboratory as described in Fig. 1. For this, chloroacetyl chloride was reacted with diisobutylamine to give the chloracetamide which was subsequently reacted with different dialkyl amines to give the desired α -dialkylamino N,N -diisobutylacetamides **1-3** in very good overall yields. Extraction behaviour of α -amino-acetamides **1-3** was compared with routinely used anion exchangers like Alamine 336, Aliquat 336 and Primene JMT having no amide functionality. Higher %E value for molybdate has been observed with α - dialkylamino N,N -diisobutylacetamides compared to Alamine 336, Aliquat 336 and Primene JMT from the same HNO_3 acidity (Fig. 1). As α -amino-acetamide **1** (**L 1**) showed best results among all derivatives, hence it is used for further extraction studies.

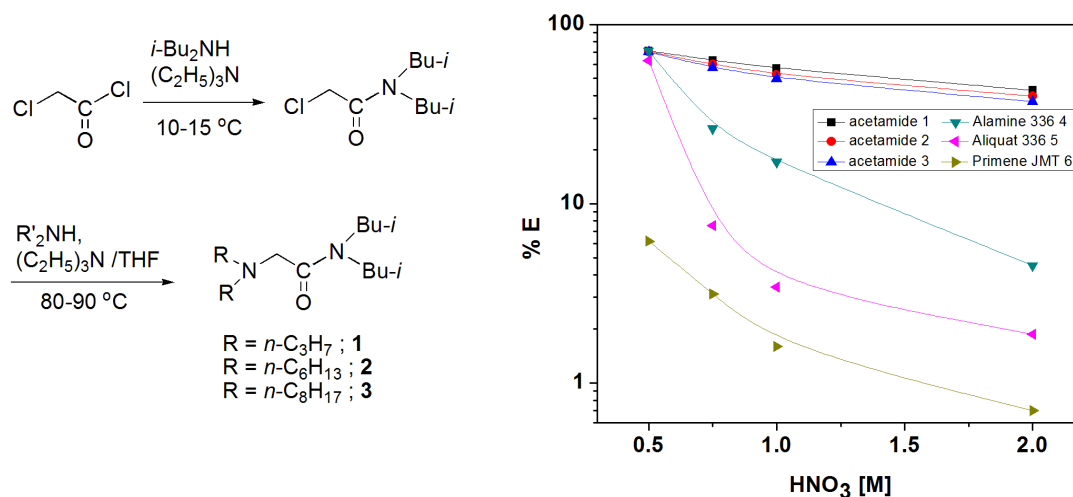


Fig. 1 Synthesis and extraction behavior of α -amino-acetamide ligands.

Various parameters which affect the solvent extraction like organic phase composition, effect of feed HNO_3 concentration, nitric acid uptake by the ligand and effect of ligand concentration have been studied to explain extraction mechanism and to evaluate the role of amide group in extraction from relatively higher concentration of nitric acid medium. The role of amide group was found to be crucial in the ligand that leads to extra acidity through the intramolecular buffering effect thus enabling the ligand to extract the molybdate anion at higher acidities.

The composition of extracted metal complex was ascertained by slope analysis method and has been found to be $(\text{LH})_2\text{MoO}_4 \cdot \text{HNO}_3$. FTIR studies have been performed to confirm the binding of HNO_3 or buffering at the amide group. NMR studies have been used to ascertain association of MoO_4^{2-} at the ammonium site of the ligand. Stripping of Mo was achieved using ammonia solution. X-Ray Crystallographic studies of α -amino-acetamide **1** with Mo were also presented in this chapter. Single crystals of two different species of Molybdate with acetamide ligand **1** [$(\text{L } \mathbf{1})_2\text{Mo}_6\text{O}_{19}$ and $(\text{L } \mathbf{1})_4\text{Mo}_8\text{O}_{24}$] were obtained under different reaction conditions (Fig. 2).

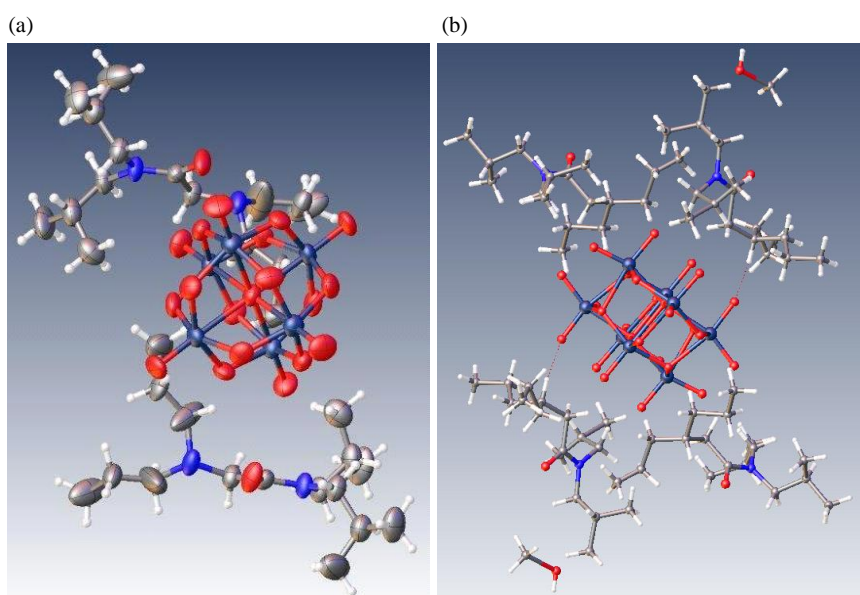


Fig. 2 Crystal structures of (a) $(\text{L } \mathbf{1})_2\text{Mo}_6\text{O}_{19}$ and (b) $(\text{L } \mathbf{1})_4\text{Mo}_8\text{O}_{24}$.

Chapter 3: Comparative studies on radiolytic degradation of deuterium labeled and unlabeled tributyl phosphates.

Valuable fissile materials, Pu and U are separated from spent nuclear fuel by PUREX process using tributyl phosphate (TBP)/*n*-dodecane as a solvent system. In the PUREX process, TBP/*n*-dodecane is continuously exposed to high radiation dose in presence of HNO₃ [1]. Thus, TBP undergoes considerable radiolytic degradation and forms varying amount of mono and dibutyl hydrogen phosphates (MBPH₂ and DBPH) [6]. These degradation products act as a complexing agents for many metals resulting in loss of selectivity, inhibit the back extraction of plutonium and cause poor phase separation. The detrimental properties of degraded TBP decrease the recycling potential of the solvent thus, needs to be disposed. This generates huge amount of organic radioactive wastes. As reviewed in literature the abstraction of hydrogen atoms from butyl chain of TBP either intramolecular or intermolecular plays key role in the degradation of TBP. Previous studies related to positive kinetic isotope effect in γ -irradiation encouraged us to hypothesize that substitution of the H atoms of butyl chain of TBP with D atoms might improve its radiolytic stability as a result of primary kinetic isotope effect *i.e.*, the higher stability of the C-D bond than compare to the C-H bond. The secondary kinetic isotope effect might also work to enhance the stability of C-O/O-P bonds.

Work present in this chapter is based on comparative radiolytic and hydrolytic degradation studies of undeuterated and deuterated TBPs. Synthesis of *d*-labelled TBPs, deuterated at four different positions *viz* (α,α)₃-*d*₆, (β,β,γ)₃-*d*₉, ($\gamma,\gamma,\delta,\delta$)₃-*d*₁₂ and per-deuterated (Fig. 3) has been achieved by four different synthetic routes with reasonably good yield and isotopic purity. A 30% solution of individual *d_n*-TBPs and undeuterated TBP in *n*-dodecane were subjected to γ -radiolytic degradation. Decay curves of different TBPs have been obtained by plotting the ratios of the residual concentrations of TBP and *d_n*-TBPs to their initial concentrations against the absorbed

dose (Fig. 3). The values for dose constant (K) and radiation chemical yield (G) were calculated. The similarities in G values for both undeuterated and d_n -TBPs in n -dodecane suggest comparable radiolytic stabilities.

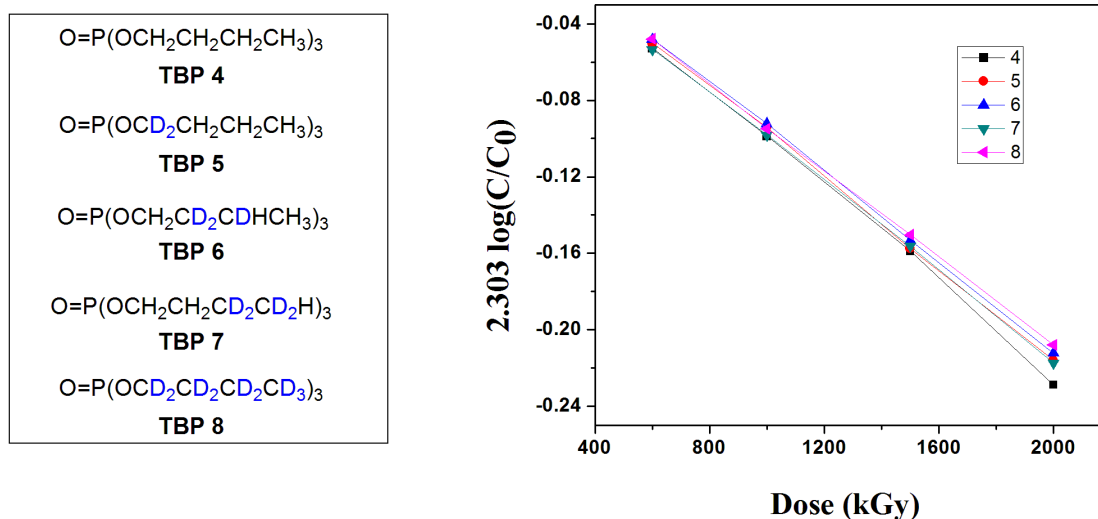


Fig. 3 Structures and γ -radiolytic degradation of d_n -TBPs.

The percentage formations of MBPH₂ and DBPH with absorbed dose for all TBPs were found to be very close. Extraction behavior for UO₂²⁺ and Pu (IV) was studied after the radiolysis and hydrolysis and the results showed similarity in extraction/ stripping behavior for all labeled or unlabeled TBP samples. The isotope effect (k_H/k_D) observed was found to be minimal in this γ -radiolytic degradation study.

Chapter 4: Design, synthesis and extraction properties of conformationally constrained oxa-diamides.

In “Actinide partitioning” process the minor actinides are extracted along with the lanthanides leaving behind most of the other elements in the raffinate. Several complexing agents have been developed over the last two decades for this purpose. Among them [4] diglycolamides (TODGA and TEHDGA), open chain ether

dicarboxylic acid diamides, were found to be the most promising. The main drawback of DGA extractants is the co-extraction of significant amount of Sr(III) and Ru(III) during actinide partitioning [7]. This leads to requirement of additional steps during stripping process.

This chapter present the design and synthesis of a novel class of conformationally constrained oxa-diamide extractants 7-oxabicyclo[2.2.1]heptane 2,3-dicarboxamides (OBDA **9-11**) and solvent extraction as well as supported liquid membrane transport studies of various actinides using these new molecules (Fig. 4). These new oxa-diamides have rigid coordination sphere created by the three donor groups (ether-oxygen and two amide groups) which are appropriately oriented for binding to a metal. Synthesis of OBDA **9-11** was achieved in three steps starting from furan and maleic anhydride in good overall yield (Fig. 4). The D-A adduct of furan and maleic anhydride was hydrogenated and subsequently reacted with different amines in the presence of DIPC to give the desired oxa-diamides **9-11**. Solvent extraction behavior of OBDA showed fast kinetics of extraction for Pu and Am. The equilibrium has been attained within two minutes only. Amongst the three OBDA ligands, *N,N*-bis-2-ethylhexyl substituted diamide (OBDA **9**) showed best results for actinide extraction and was chosen for further extraction studies. Effects of various parameters such as feed acidity, OBDA concentration and aq. nitrate ion concentration on solvent extraction behavior of Pu(IV), Eu(III) and Am(III) were studied in detail. Slope analysis method showed that Pu(IV) forms monosolvated whereas Am(III) and Eu(III) form a mixture of monosolvated and di-solvated species with OBDA. Third phase formation studies have also been performed for high concentration of Eu. The selectivity of OBDA for actinides and lanthanides with respect to other elements present in HLW has been investigated and found to be higher compared to DGA ligands especially in terms of Sr and Ru.

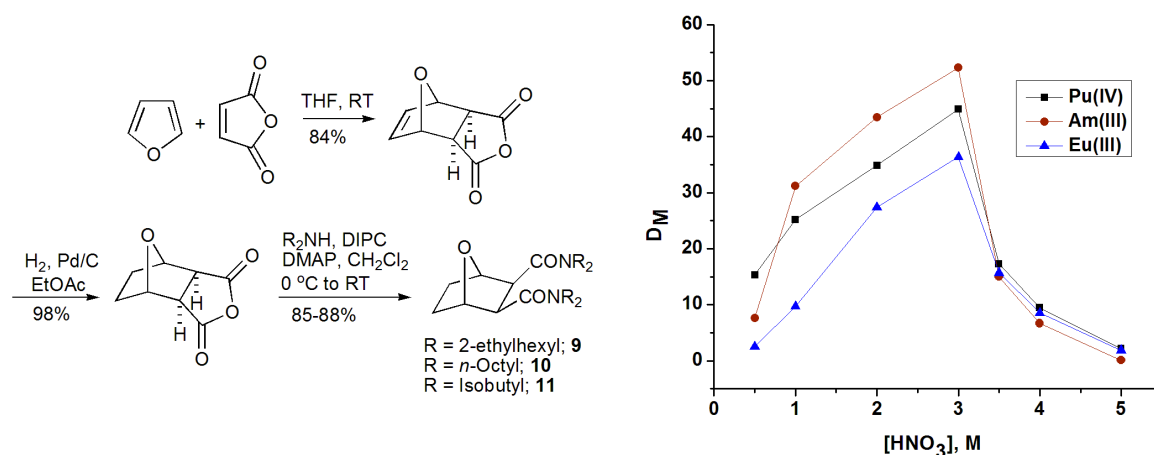


Fig. 4 Synthesis and extraction behaviour of bridged 7-oxabicyclo[2.2.1]heptane 2,3-dicarboxamides.

The present chapter also describes the transport behavior of Am(III) using OBDA **9** as the carrier across supported liquid membrane. Transport rate studies using OBDA have been carried out and found to be very fast showing ~95% transport of Am(III) within 60 min using 0.1 M OBDA in presence of 15% IDA/*n*-dodecane as carrier. The mechanism of transport was investigated by studying various parameters like feed $HNO_3/NaNO_3$ concentration, OBDA concentration in the membrane, membrane pore size, membrane thickness etc. From these studies, the mechanism of transport was found to be diffusion controlled with diffusion co-efficient value of $5.1 \times 10^{-6} \text{ cm}^2/\text{s}$ which is higher than TEHDGA. The membrane containing OBDA as a carrier showed high selectivity for tetravalent actinides and trivalent actinides and lanthanides. The OBDA based membrane was found to be stable with respect to hydrolytic stability and leaching out effect for at least six consecutive cycles of operation.

To find out the nature of metal ligand bonding, complex of $Eu(NO_3)_3 \cdot 5H_2O$ with OBDA was studied by IR and 1H NMR spectroscopy and the ligand was found to be tridentate in nature. Density functional theoretical (DFT) study was also carried out to determine the energy optimized structure of free ligand and its Am^{3+} complex which

also supported the tridentate nature of the ligand. ESI-MS spectra provided further insight of the metal ligand complex formation and showed that OBDA forms both the monosolvated and disolvated species with Eu.

This chapter also includes the synthesis of Pu selective oxa-diamides. The OBDA class of extractants showed excellent extraction behaviour but poor stability in high nitric acid medium. To overcome the problem of hydrolysis, we designed and synthesized new acid stable oxa-diamides **12** and **13** (Fig. 5) having different cavity size than OBDA created by three appropriately oriented donor groups. The synthetic route for Pu selective oxa-diamides **12** and **13** has been depicted in Fig. 5. The furan maleic anhydride D-A adduct was reacted with cyclopentadiene and resulting adduct was subjected to imide formation. Cleavage of the double bond followed by amide formation gave the desired oxa-diamides **12** and **13**. The extraction behaviour of these new oxa-diamides was evaluated by solvent extraction technique. The new oxa-diamides **12** and **13** showed good selectivity for plutonium over other metal ions present in HLW. The new oxa-diamides were found to be stable in 3 M HNO₃ medium even after 15 days.

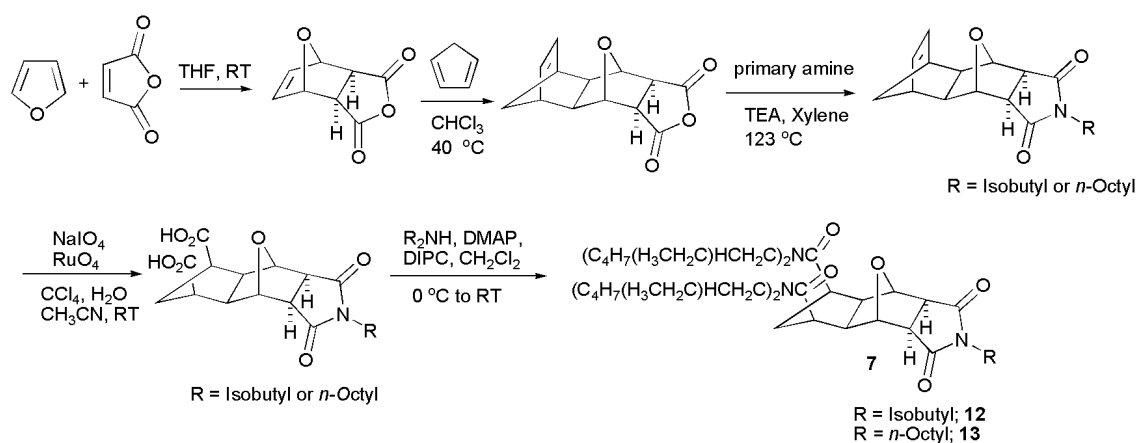


Fig. 5 Synthesis of Pu selective oxa-diamides.

Chapter 5: Design, synthesis and extraction properties of a new class of ruthenium selective ligands.

Ruthenium is one of the most hazardous fission products contained in the High-Level Waste (HLW) due to high fission yield and relatively shorter half lives of its isotopes (^{103}Ru : 39.27 d, ^{106}Ru : 1.02 y) resulting in high specific activity. It is also the most difficult fission product to separate from high level radioactive waste owing to its variable valences at different nitric acid concentrations. Ru is of particular interest because it contributes largely to beta and gamma activity of the waste and its tendency to form volatile tetroxide during vitrification [8]. Due to all these reasons, ruthenium needs to be separated from the waste to make it amenable for disposal. Suitable solvents for separation of ruthenium from nitric acid medium are rare. TBP and a few amine based extractants have been reported in literature for the same purpose although with very poor D_{Ru} values [9, 10].

This chapter deals with the synthesis and extraction behavior of a new class of quaternary ammonium iodide based ligands **14-16** having 2-(*N,N*-diisobutyl)acetamide as an alkyl appendage (Fig. 6) for separation of Ru from nitric acid medium using solvent extraction and solid phase extraction technique.

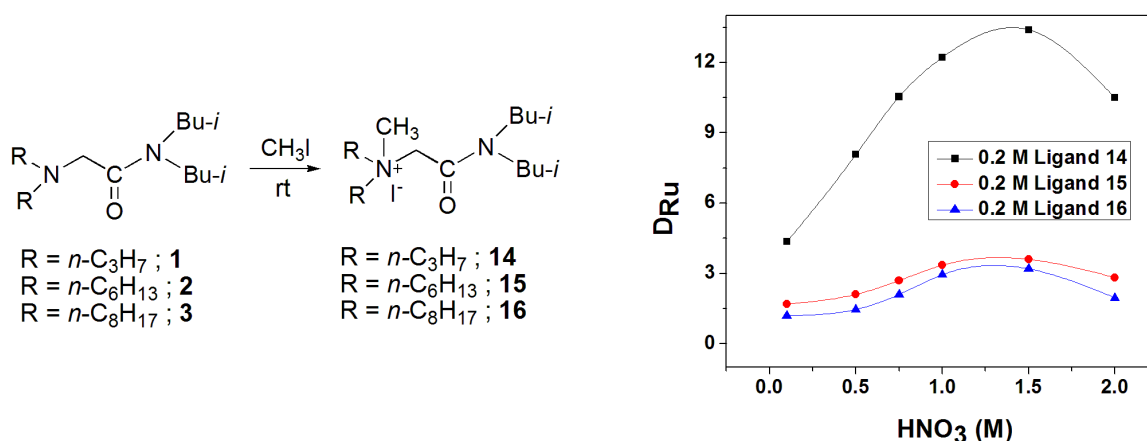


Fig. 6 Synthesis and extraction behavior of new ammonium iodide based ligands dialkylmethyl-2-(*N,N*-diisobutyl)acetamidoammonium iodide (L **14-16**).

α -Amino-acetamides **1-3** were treated with methyl iodide to obtain the desired extractants **14-16** in quantitative yield (Fig. 6). D_{Ru} was found to be significantly higher for these new ligands compare to other reported extractants (Fig. 6). The ammonium iodide **14** showed highest D_{Ru} values and was chosen for further extraction studies. The mechanism of extraction has been established by studying various parameters like feed $HNO_3/NaNO_3$ concentration, ligand concentration, aq. iodide concentration etc. Role of iodide anion in extraction process has also been investigated by performing extraction studies using same ligand with nitrate as counter ion in place of iodide. Iodide ion played an important role in the formation of the stable and extractable complex of ruthenium. No extraction was observed when iodide was replaced by nitrate anion in the ligand. The stoichiometry of the complex was ascertained by slope analysis method and was found to be 1:1 with respect to ligand L^+I^- and $Ru(NO)(NO_3)_3$. Ruthenium formed an adduct of structure $LRu(NO)(NO_3)_3I$ in the extraction medium. Stripping of ruthenium was achieved using ammonia solution. For selectivity studies, extraction behavior of ruthenium was observed in the presence of other metal ions present in nitric acid waste solution and the extractant showed good selectivity for ruthenium over Cs, Sr, Mo, Eu, Ba and Zr.

This chapter also includes the sorption studies for ruthenium (III) using ammonium iodide **14** impregnated Amberlite XAD-4 resin from nitric acid medium. Impregnated resin was prepared using wet method and characterized by IR, TGA and SEM analyses. The effect of varying concentration of Ru on sorption was studied and the maximum loading of ruthenium on impregnated resin was calculated. Ruthenium was quantitatively stripped from resin using ammonia or sodium hydroxide solution in a single contact.

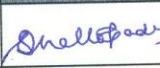
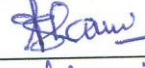
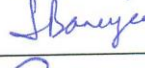
References:

- [1] Schulz W, Navratil JD, Talbot AE (1984) Science and technology of tributyl phosphate. CRC Press, Florida.
- [2] J. F. Ahearne, Special issue: Radioactive wastes, *Physics Today*, 1997, **50**, 22.
- [3] Potential Benefits and Impacts of Advanced Nuclear Fuel Cycles with Actinide Partitioning and Transmutation, in *Nuclear Science*, OECD/NEA, Paris, 2011.
- [4] J. N. Mathur, M. S. Murali and K. L. Nash, *Solvent Extr. Ion Exch.*, 2001, **19**, 357.
- [5] R. Shanker and K. S. Venkateswarlu, *Sep. Sci.*, 1976, **11**, 591.
- [6] B. J. Mincher, G. Modolo and S. P. Mezyk, *Solvent Extr. Ion Exch.* 2009, **27**, 1.
- [7] S. A. Ansari, P. N. Pathak, V. K. Manchanda, M. Hussain, A. K. Prasad and V. S. Parmar, *Solvent Extr. Ion Exch.*, 2005, **23**, 463.
- [8] A. Tokarev, A. Grandjean, Y. Guari, J. Larionova, R. Pflieger and C. Guérin, *J. Nucl. Mater.*, 2010, **400**, 25.
- [9] E. Hallaba and R. A. I. Azzam, *Z. Anorg. Allg. Chem.*, 1962, **314**, 53.
- [10] W. J. Maeck, G. L. Booman, M. E. Kussy and J. E. Rein, *Anal. Chem.*, 1961, **33**, 1775.

Name of Student: 

Date: 15.05.2015

Doctoral Committee:

S. No.	Name	Designation	Signature	Date
1.	Dr. S. Chattopadhyay	Chairman		15/5/15
2.	Dr. Sunil K. Ghosh	Guide & Convener		15/5/15
3.	Dr. P. S. Dhama	Technical Advisor		15/5/15
4.	Dr. Sharmila Banerjee	Member		15/5/15
5.	Dr. S. K. Nayak	Member		15/5/15

LIST OF FIGURES

	Page No.
CHAPTER-I	
Fig. 1.1 Worldwide production of energy by various sources.	2
Fig. 1.2 Nuclear fission of ^{235}U .	4
Fig. 1.3 Nuclear fuel cycle.	5
Fig. 1.4 Spent fuel partitioning strategies.	9
Fig. 1.5 Structures of various trialkyl phosphate ligands.	12
Fig. 1.6 Basic structure of trialkyl phosphine oxide (TRPO) ligands.	12
Fig. 1.7 Structure of carbamoyl methyl phosphine oxide (CMPO) ligands.	13
Fig. 1.8. Structure of diisodecylphosphoric acid (DIDPA) and other phosphoric acid based ligands.	14
Fig 1.9 Structure of some important Cyanex ligands.	14
Fig. 1.10. Structure of DMDBDTMA, DMDOHEMA and bicyclic malonamide.	15
Fig. 1.11. Structure of TODGA and TEHDGA.	16
Fig. 1.12 Structure of some newly developed diglycolamide ligands.	17
Fig. 1.13 Amine or ammonium salt based ligands.	18
Fig. 1.14 Crown ether and Calix-arene ligands.	18
Fig. 1.15 N- heterocyclic ligands for selective extraction of An (III).	19
Fig. 1.16 Diagrammatic presentation of Solvent extraction.	20
Fig. 1.17 Solvation of metal ion by a phosphoric group containing ligand.	25
Fig. 1.18 Ion-pair mechanism of extraction.	26
Fig. 1.19 Chelate complex of La with tetrabutyl diglycolamide [38].	27

CHAPTER-II	
Fig. 2.1 Basic framework of CMPO.	35
Fig. 2.2 Structure of α -dialkylamino <i>N,N</i> -diisobutylacetamides 1-3 (L 1-3), TOA (major component of Alamine 336) 4 , Aliquat 336 5 and Primene JMT 6	37
Fig. 2.3 %E for anion exchangers 1-6 at varying nitric acid concentrations.	39
Fig. 2.4 Variation in D_{Mo} with IDA concentration at 0.5 M nitric acid.	40
Fig. 2.5 Extraction of HNO_3 from aqueous solution by 0.2 M α -amino-acetamide 1 or Alamine 336 4 .	41
Fig. 2.6 Dependency of D_{Mo} on concentration of HNO_3 .	42
Fig. 2.7 Dependency of D_{Mo} on concentration of α -amino-acetamide 1 .	43
Fig. 2.8 Extracted metal-ligand complex in the organic phase.	43
Fig. 2.9 IR spectra of organic phase: (a) Before contact; (b) Loaded organic phase	44
Fig. 2.10 (a) 1H NMR of α -amino-acetamide 1 ; (b) 1H NMR of complex of MoO_4^{2-} with α -amino-acetamide 1 .	45
Fig. 2.11 Cluster packing of complex 8 , $(LH)_2[Mo_6O_{19}]$, in the crystal. The dark blue balls are Mo; red balls: O; Light blue balls: N; gray balls: C; white balls: H.	51
Fig. 2.12 Space filled cluster packing of complex 8 , $(LH)_2[Mo_6O_{19}]$, in the crystal. The dark blue balls are Mo; red balls: O; Light blue balls: N; gray balls: C; white balls: H.	51
Fig. 2.13 The hexamolybdate anion with a pair of anti-parallel cationic ligand in complex 8 , $(LH)_2[Mo_6O_{19}]$. The inter ligand hydrogen bonds ($N-H \cdots O=C$) are	52

shown as red dotted lines; The dark blue balls are Mo; red balls: O; Light blue balls: N; gray balls: C; white balls: H.	
Fig. 2.14 The hexamolybdate anion surrounded by four anti-parallel dimeric units of ligand in the complex $(LH)_2[Mo_6O_{19}]$ 8 . The dark blue balls are Mo; red balls: O; Light blue balls: N; gray balls: C; white balls: H.	52
Fig. 2.15 Cluster packing of complex 9 , $(LH)_4[Mo_8O_{26}] (MeCN)_2$. The dark blue balls are Mo; red balls: O; Light blue balls: N; gray balls: C; white balls: H.	56
Fig. 2.16 Space filled cluster packing of complex 9 , $(LH)_4[Mo_8O_{26}] (MeCN)_2$. The dark blue balls are Mo; red balls: O; Light blue balls: N; gray balls: C; white balls: H.	56
Fig. 2.17 The octamolybdate anion surrounded by eight ligands in complex 9 , $(LH)_4[Mo_8O_{26}] (MeCN)_2$. The dark blue balls are Mo; red balls: O; Light blue balls: N; gray balls: C; white balls: H.	57
Fig. 2.18 ORTEP diagram of complex 9 , $(LH)_4[Mo_8O_{26}] (MeCN)_2$. The ligand N–H···O–Mo bondings are shown as dotted lines; The dark blue balls are Mo; red balls: O; Light blue balls: N; gray balls: C; white balls: H.	57
Fig. 2.19 1H NMR spectrum of α -amino-acetamide 1 .	66
Fig. 2.20 1H NMR spectrum of complex of MoO_4^{2-} with α -amino-acetamide 1 .	66
CHAPTER-III	
Fig. 3.1 Structure of tributyl phosphate.	70
Fig. 3.2 Structures of different d_n -TBPs viz $(\alpha,\alpha)_3-d_6$ TBP 11 , $(\beta,\beta,\gamma)_3-d_9$ TBP	75

12 , ($\gamma,\gamma,\delta,\delta$) ₃ - <i>d</i> ₁₂ TBP 13 and per-deuterated TBP 14 .	
Fig. 3.3 ¹ H NMR spectrum of (α,α) ₃ - <i>d</i> ₆ TBP 11	76
Fig. 3.4 ¹ H NMR spectrum of (β,β,γ) ₃ - <i>d</i> ₉ TBP 12 .	78
Fig. 3.5 ¹ H NMR spectrum of ($\gamma,\gamma,\delta,\delta$) ₃ - <i>d</i> ₁₂ TBP 13 .	79
Fig. 3.6 Degradation curves of TBPs saturated with 1.5 M nitric acid as a function of absorbed dose. A, B, C, D, E are individual 30% solution of TBP 10 and its deuterated analogs 11-14 in <i>n</i> -dodecane, respectively.	81
Fig. 3.7 Degradation curves of TBPs saturated with 3.0 M nitric acid as a function of absorbed dose. A, B, C, D, E are 30% solution of TBP 10 and its deuterated analogs 11-14 in <i>n</i> -dodecane, respectively.	81
Fig. 3.8 MBPH ₂ formation as a function of absorbed dose for TBPs saturated with 3 M nitric acid. A, B, C, D, E are individual 30% solution of TBP 10 and its deuterated analogs 11-14 in <i>n</i> -dodecane, respectively.	83
Fig. 3.9 MBPH ₂ formation as a function of absorbed dose for TBPs saturated with 1.5 M nitric acid. A, B, C, D, E are individual 30% solution of TBP 10 and its deuterated analogs 11-14 in <i>n</i> -dodecane, respectively.	84
Fig. 3.10 DBPH formation as a function of absorbed dose for TBPs saturated with 3.0 M nitric acid. A, B, C, D, E are individual 30% solution of TBP 10 and its deuterated analogs 11-14 in <i>n</i> -dodecane, respectively.	84
Fig. 3.11 DBPH formation as a function of absorbed dose for TBPs saturated with 1.5 M nitric acid. A, B, C, D, E are individual 30% solution of TBP 10 and its deuterated analogs 11-14 in <i>n</i> -dodecane, respectively.	85
Fig. 3.12 Extraction of plutonium as a function of absorbed dose. Aqueous phase: 3.0 M HNO ₃ ; A, B, C, D, E are individual 30% solution of TBP 10 and its deuterated analogs 11-14 in <i>n</i> -dodecane, respectively.	86

Fig. 3.13 Extraction of plutonium as a function of absorbed dose. Aqueous phase: 0.5 M HNO ₃ (stripping conditions); A, B, C, D, E are individual 30% solution of TBP 10 and its deuterated analogs 11-14 in <i>n</i> -dodecane, respectively.	86
<i>CHAPTER IV</i>	
Fig. 4.1 Structures of important diamides and diglycolamides.	97
Fig. 4.2 Conformationally constrained oxa-diamides.	99
Fig. 4.3 Kinetics of extraction of Pu(IV) and Am(III) using 0.1 M OBDA 20a .	101
Fig. 4.4 Effect of feed HNO ₃ concentration on D _{Pu(IV)} , D _{Am(III)} and D _{Eu(III)} .	103
Fig. 4.5 Comparative extraction of Am(III) using 0.1 M OBDA 20a and 0.1 M TEHDGA III in 15% IDA/ <i>n</i> -dodecane at different feed nitric acid concentration.	103
Fig. 4.6 Plot of log D _M vs log [OBDA 20 a] for (a) Am (b) Eu and (c) Pu.	106
Fig. 4.7 Plot of log D _M vs log NO ₃ ⁻ for (a) Am (b) Eu and (c) Pu.	107
Fig. 4.8 IR spectra of (a) OBDA 20c and (b) OBDA 20c complexed with Eu(NO ₃) ₃ .5H ₂ O.	108
Fig. 4.9 ¹ H NMR of the relevant portion (a) OBDA 20c and (b) OBDA 20c complexed with Eu(NO ₃) ₃ .5H ₂ O.	109
Fig. 4.10 ESI-MS spectrum of complex of Eu(NO ₃) ₃ .5H ₂ O with OBDA 20c .	110
Fig. 4.11 Three different conformers of free OBDA obtained by geometry optimization.	113
Fig. 4.12 Energy optimized structure of Am(III) complex of OBDA.	114
Fig. 4.13 Schematic description of the SLM process.	115
Fig. 4.14 Transport of Am(III) using 0.1 M OBDA in 15% IDA/ <i>n</i> -dodecane;	116

Feed- Varying concentrations of HNO ₃ , Membrane- 0.2 μm PTFE, Strippant- pH 2 solution.	
Fig. 4.15 Transport of Am(III) using OBDA 20a as carrier at different concentrations of OBDA 20a ; Feed- 2 M HNO ₃ , Carrier- varying concentrations of OBDA 20a in 15% IDA/ <i>n</i> -dodecane, Membrane- 0.2 μm PTFE, Strippant- pH 2 solution.	117
Fig. 4.16 Plot of permeability co-efficient values against varying membrane pore size; Feed- 2 M HNO ₃ , Carrier- 0.1 M OBDA in 15% IDA/ <i>n</i> -dodecane, Membrane- PTFE membranes of varying pore size, Strippant- pH 2 solution.	118
Fig. 4.17 Transport of different elements from nitric acid medium; Feed- 2 M HNO ₃ , Carrier- 0.1 M OBDA in 15% IDA/ <i>n</i> -dodecane, Membrane- 0.2 μm PTFE, Strippant- pH 2 solution.	120
Fig. 4.18 Stability of SLM containing 0.1 M OBDA in 15% IDA in <i>n</i> -dodecane as carrier; Feed- 2 M HNO ₃ , Carrier- 0.1 M OBDA in 15% IDA/ <i>n</i> -dodecane, Membrane- 0.2 μm PTFE, Strippant- pH 2 solution.	121
Fig. 4.19 Kinetics of extraction for Pu(IV)	124
Fig.4.20 D _{Pu} at varying feed HNO ₃ concentration	125
Fig. 4.21 Plot of log D _{Pu} vs log [ligand 21b].	126
Fig.4.22 Plot of log D _{Pu} vs log [NO ₃ ⁻].	127
Fig. 4.23 IR spectrum of OBDA 20c .	140
Fig. 4.24 IR spectrum of complex of Eu(NO ₃) ₃ .5H ₂ O with OBDA 20c .	140
Fig. 4.25 ¹ H NMR spectrum of OBDA 20c .	141
Fig. 4.26 ¹ H NMR spectrum of complex of Eu(NO ₃) ₃ .5H ₂ O with OBDA 20c .	142
<i>CHAPTER V</i>	

Fig. 5.1 Structure of dialkylmethyl-2-(<i>N,N'</i> -diisobutyl)acetamidoammoniumiodides 29-31 and nitrate 32 .	146
Fig. 5.2 Variation in D_{Ru} with IDA concentration in <i>n</i> -dodecane at 1.0 M HNO_3 .	148
Fig. 5.3 Kinetics of Ru extraction with ligand 29 from 1.0 M HNO_3 .	149
Fig. 5.4 Variation in D_{Ru} with HNO_3 concentration.	150
Fig. 5.5 Variation in D_{Ru} with ligand concentration.	151
Fig. 5.6 Variation in D_{Ru} with I^- concentration.	151
Fig. 5.7 Variation in D_{Ru} with total NO_3^- concentration at 0.5 M HNO_3 .	152
Fig. 5.8 Variation in D_{Ru} with I^- concentration for ligand 32 at 1.0 M HNO_3 .	153
Fig. 5.9 TGA curves for (a) blank beads (b) pure extractant (c) impregnated beads.	156
Fig. 5.10 IR spectra of XAD-4 resin (a) before impregnation; (b) after impregnation of extractant.	157
Fig. 5.11 SEM of impregnated XAD-4 resin beads at different magnifications.	158
Fig. 5.12 Sorption of Ru on impregnated resin at different HNO_3 concentrations.	158
Fig. 5.13 Effect of metal ion concentration on sorption of Ru.	159
Fig. 5.14 Resin beads: (a) after impregnation of extractant; (b) after sorption of Ru.	160
Fig. 5.15. Langmuir isotherm plot for sorption of ruthenium on impregnated resin.	162
Fig. 5.16. Freundlich isotherm plot for sorption of ruthenium on impregnated resin.	163
Fig. 5.17 Amberlite XAD-4 resin beads; (a) before and (b) after impregnation.	169

Fig. 5.18 IR spectra of XAD-4 resin before impregnation of extractant.	171
Fig. 5.19. IR spectra of XAD-4 resin after impregnation of extractant.	171

LIST OF TABLES

CHAPTER II	Page No.
Table 2.1 Crystal data and structure refinement	48
Table 2.2. Bond Lengths for complex (LH) ₂ [Mo ₆ O ₁₉] 8	53
Table 2.3. Bond Lengths for complex 9 , (LH) ₄ [Mo ₈ O ₂₆] (MeCN) ₂ .	58
CHAPTER III	
Table 3.1 Values of <i>k</i> and <i>G</i> for different TBP	83
Table 3.2 Distribution ratios for undeuterated TBP 10 and <i>d_n</i> -TBP 11-14 before and after hydrolysis.	87
CHAPTER IV	
Table 4.1 Degradation study of OBDA 20a in HNO ₃ .	104
Table 4.2 Distribution ratio of Eu(III) in presence of different concentrations of Eu(III) in 3 M HNO ₃ for 0.1 M OBDA 20a in 15% IDA / <i>n</i> -dodecane.	111
Table 4.3 Extraction behavior of different elements present in HLLW solution using 0.1 M OBDA 20a in 15% IDA/ <i>n</i> -dodecane.	112
Table 4.4 Natural charges on the carbonyl and ethereal oxygen and carbonyl carbon atoms.	114

Table 4.5 Selectivity of 0.1 M oxa-diamide 21b in 30% IDA/ <i>n</i> -dodecane for Pu(IV) in presence of other metal ions present in HLW at 4 M HNO ₃ .	127
Table 4.6 Stripping studies for Pu (IV) extraction with oxa-diamide 21b .	128
<i>CHAPTER V</i>	
Table 5.1 Distribution ratio of ruthenium and other elements with 0.2 M ligand 29 in 30% IDA/ <i>n</i> -dodecane.	155
Table 5.2 Isotherm constants of the different models for sorption of Ru ions.	164

LIST OF SCHEMES

<i>CHAPTER-II</i>	
Scheme 2.1 Synthesis of α -dialkylamino <i>N,N</i> -diisobutylacetamides.	38
Scheme 2.2 Synthesis of metal–ligand complexes 8 and 9	48
<i>CHAPTER-III</i>	
Scheme 3.1 Major degradation products of TBP after radiolysis.	71
Scheme 3.2 Mechanism of degradation of TBP by direct radiolysis.	73
Scheme 3.3 Synthesis of (α,α) ₃ - <i>d</i> ₆ TBP 11 .	76
Scheme 3.4 Synthesis of (β,β,γ) ₃ - <i>d</i> ₉ TBP 12 .	77
Scheme 3.5 Synthesis of ($\gamma,\gamma,\delta,\delta$) ₃ - <i>d</i> ₁₂ TBP 13 .	79
Scheme 3.6 Synthesis of per-deuterated TBP 14 .	79

<i>CHAPTER-IV</i>	
Scheme 4.1 Synthesis of bridged 7-oxabicyclo[2.2.1]heptane-2,3-dicarboxamides.	100
Scheme 4.2 Synthesis of Pu selective oxa-diamides.	123
Scheme 4.3 Synthesis of imides 28a-c .	123
<i>CHAPTER-V</i>	
Scheme 5.1 Synthesis of dialkylmethyl-2-(<i>N,N'</i> -diisobutyl)acetamidoammonium iodides 29-31 and nitrate 32 .	147

ABBREVIATIONS

THF	: Tetrahydrofuran
DCM	: Dichloromethane
EtOAc	: Ethyl acetate
TEA	: Triethyl amine
EtOH	: Ethyl alcohol
MeOH	: Methyl alcohol
DIPC	: <i>N, N'</i> -Diisopropylcarbodiimide
DMAP	: Dimethylaminopyridine
DMF	: <i>N, N</i> -Dimethylformamide
NMR	: Nuclear Magnetic Resonance
IR	: Infrared spectra
ESIMS	: Electrospray Ionisation Mass Spectrometry
TLC	: Thin-Layer Chromatography
B. p.	: Boiling Point
M. p.	: Melting Point

CHAPTER 1

Introduction to back-end fuel technology

With depleting resources and rising energy demands India and other developing countries are looking for new energy sources other than fossil fuels like coal, petroleum etc. These alternative sources can be solar, hydro, wind and nuclear energy (Fig. 1.1). Amongst them, nuclear energy is considered to be most suitable alternative in terms of green process, low pollutant emission and less impact on environment. Nuclear energy can play an important role as a sustainable source of energy in the long term due to large amount of energy generation from less amount of given nuclear fuel and small amount of waste generation per unit energy production.

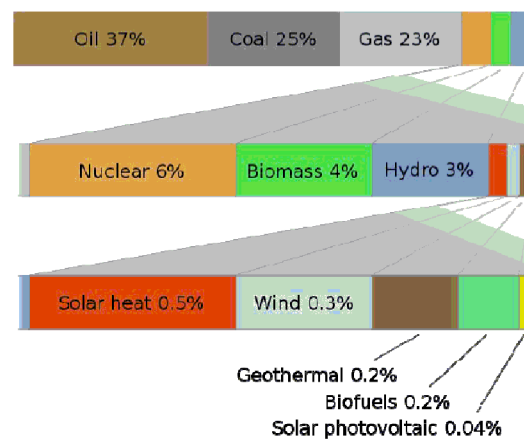


Fig. 1.1 Worldwide production of energy by various sources.

Source of the data- Renewables in global energy supply [1]

Nuclear energy is the use of nuclear processes to generate energy in the form of heat and subsequently to electricity. Presently, the nuclear fission of actinide series elements of the periodic table is being used to produce the vast majority of nuclear energy in nuclear reactors. In nuclear processes, fuel material cannot be consumed totally. For recovery of unconsumed fissile material spent fuel is reprocessed and efficient management of resulting HLW is carried out for minimizing the long term radiotoxic effects. For reprocessing and waste management purpose, metal ions are recovered

from spent nuclear fuel using various separation processes in which organic molecules play key role and are called “extractants” or “ligands” or “solvents”.

1.1 Principle of a nuclear reactor

When any fissile materials like ^{235}U , ^{239}Pu , ^{233}U etc are subjected to bombardment of neutrons, the heavy nucleus splits into two or more lighter nuclei (the fission products). The mass loss in this process appears as the huge energy according to the Einstein’s mass-energy law as kinetic energy, gamma radiation, and free neutrons. A portion of these neutrons may later be absorbed by other fissile atoms and cause further fission reactions, which release more neutrons, and so on. This is known as a nuclear chain reaction. ^{235}U is the one and only naturally occurring fissile material that undergoes fission process as shown in Equation 1.1;



Where X and Y are fission products and E denotes the released energy per fission (~ 200 MeV/ fission/ ^{235}U atom) [2]. Due to unsymmetrical fragmentation of fission nuclides a range of fission products are formed in the fission processes. In each fission process 2 to 3 neutrons are emitted which then further used to initiate the fission of another fissile atom (Fig. 1.2). But this self sustainable chain reaction can be uncontrolled chain reaction in presence of sufficient amount of fissile material and can leads to explosion. Nuclear reactors are specially designed to sustain a controlled chain reaction to produce controlled release of energy which can be subsequently used for various purposes. In reactors to control such a nuclear chain reaction, neutron poisons and neutron moderators are used to change the portion of neutrons that will go on to cause more fission.

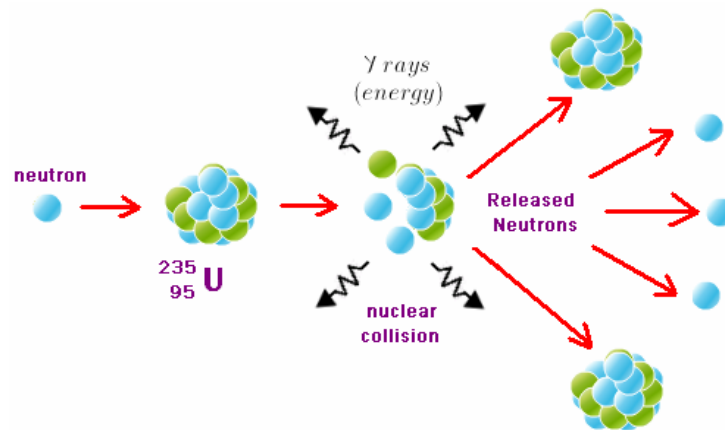


Fig. 1.2 Nuclear fission of ^{235}U .

These nuclear reactors can be classified on the basis of their applications, coolant / moderator system and energy of neutrons. Most of reactors of India which are in operation are pressurized heavy water reactors (PHWR). This is a type of thermal reactor in which natural uranium (0.7 atom % of ^{235}U and 99.3% ^{238}U) is used as the fuel and heavy water is employed as the moderator to thermalize the fast neutron [3].

1.2 Nuclear fuel cycle

Nuclear fuel cycle consist of two parts, front end and back end processes. Various steps of the front end operations are: (i) fuel mining and milling; (ii) purification; (iii) enrichment of fuel; (iv) fuel fabrication and (v) reactor operation. The back end operations include spent fuel reprocessing and radioactive waste management etc (Fig. 1.3).

In nuclear reactors, fuels cannot be consumed totally due to accumulation of fission products formed in these processes. Developed countries like USA, where the availability of uranium is sufficient, do not bother about the uranium and hence they adopted the once through fuel cycle (OTC) or open fuel cycle in which the spent fuel is directly disposed into the deep repositories in remote areas.

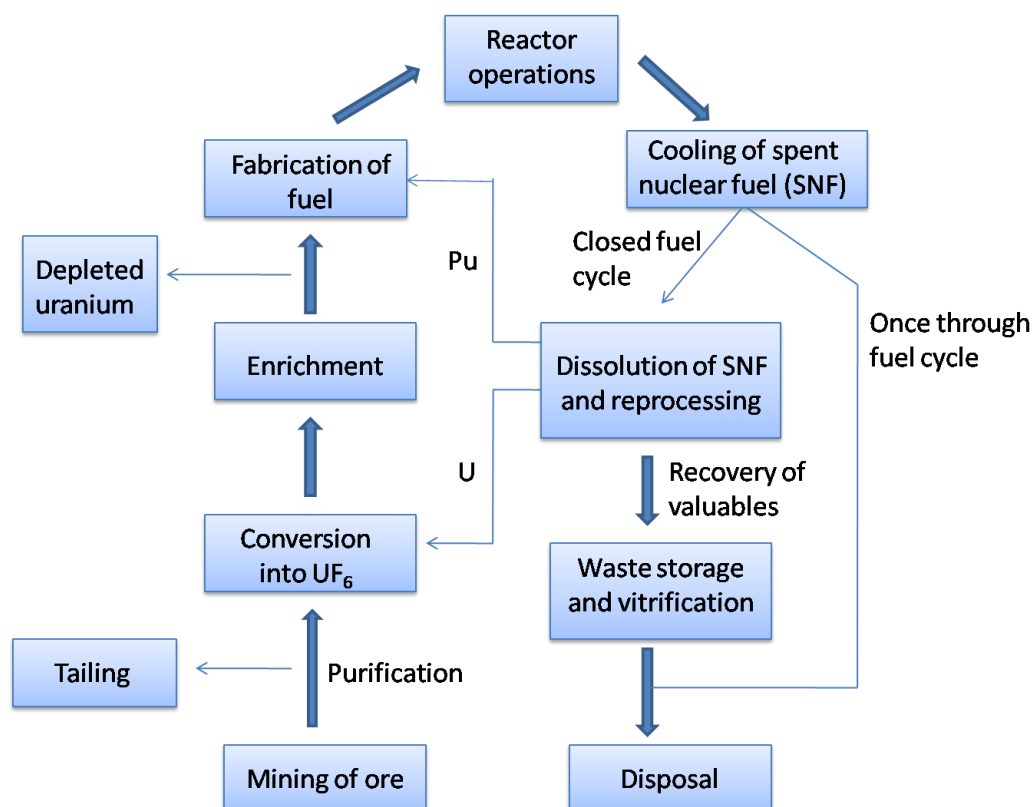


Fig. 1.3 Nuclear fuel cycle.

In developing countries like India, due to the limited natural sources of fissile material (^{235}U), the future of nuclear energy program is dependent on the availability of artificially made fissile elements like ^{233}U and ^{239}Pu which are obtained by tail end of nuclear processes. Therefore, closed nuclear fuel cycle or reprocessing fuel cycle (RFC) is the required option in which recyclable fissile elements (Plutonium and Uranium) are reprocessed for recycling and efficient management of resulting HLW is carried out before disposal using various partitioning strategies for minimizing the long term radiotoxic effects [4].

1.3 Radioactive waste

Like other industries, nuclear reactors also produce radioactive waste containing appreciable amount of radioactivity. The major concentration of waste is originated from nuclear fuel reprocessing in back end of nuclear fuel cycle. The fuel rods coming

after burning in reactors contains about 99.99% of radioactivity which is produced in fission process and only a very small portion ($<0.01\%$) is allocated in other systems of reactors. Depending on associated radioactivity, waste can be characterized as low level, intermediate level and high level waste [5].

Waste having activity less than 1 microcurie per liter of solution called as low level waste (LLW). This waste is allowed to cool for a few months and then subjected to shallow land burial. The LLW comprises about 90% of the total volume of the radioactive waste, while it contains $< 1\%$ radioactivity of all the radioactive waste. While the activity level in intermediate level waste (ILW) solution is ranges from 1 microcurie to 1 curie per liter. Main sources of ILW are components of nuclear reactor, materials originating from the treatment of high active waste, resins used for concentration of activity, chemical sludge, reprocessing equipments etc. Due to higher radioactivity level ILW is solidified in concrete or bitumen for disposal. It contains 7% volume and 4% radioactivity of total radioactive waste.

If the radioactivity level of waste is higher than 1 curie per liter, the waste is termed as High Level Waste (HLW). It comprises of the wastes originating from spent nuclear fuel reprocessing and its various liquid streams etc. It contains long lived alpha emitting actinides, lanthanides, other beta-gamma emitting fission products and smaller amount of U and Pu. HLW comprises major radioactivity of nuclear waste and occupies 3% of total volume, yet $>95\%$ of total radioactivity generated in nuclear fuel cycle. For safe management, HLW is first immobilized in glass matrices followed by containment in stainless steel canisters and then finally disposed off in deep geological repositories, the process is called "concentration and containment" [6]. But direct disposal of HLW is a challenging task due to the presence of long lived minor actinides and other radioactive fission products. In order to develop efficient and environmental

friendly process for separation of various radio-nuclides from HLW solution for its safe management, continuous efforts are being made by separation science chemists worldwide.

1.4. Nuclear fuel reprocessing and radioactive waste management

As described earlier, in nuclear reactors U and Pu cannot be consumed totally. Most of the fissile material remains unused due to accumulation of various fission products produced, many of which are neutron poison, account for loss in neutron economy and also the loss of valuable fissile materials. As a result, the spent fuel contains large amount of unreacted fissile materials such as ^{239}Pu and U along with minor actinides and fission products. Developing countries like India where availability of fissile material is limited, recovery of valuable unreacted fissile materials is essential to sustain the future nuclear energy program. Thus, the spent fuel is reprocessed to separate and recover unreacted plutonium and uranium. During reprocessing of spent nuclear fuel, the recyclable fissile elements (Plutonium and Uranium) are recovered using solvent extraction process leaving behind very highly radioactive liquid waste solution which is later concentrated to yield the High Level Waste (HLW). HLW generally contains un-extracted U, Pu and bulk of minor actinides such as Am, Np, Cm and host of fission product elements like Ru, Tc, Pd, Zr, Cs, Sr, Mo and lanthanides as well as activation products along with process chemicals and structural materials such as Fe, Cr, Ni, Zr and Al etc [7]. The most accepted approach for the management of HLW is to vitrify it in the solid and stable matrix and then disposal in deep geological repositories in remote areas. But the dumping of HLW is associated with long term hazard and contamination risk. The long term hazard of spent fuel and HLW is because of the presence of actinides, particularly the transuranic elements (TRUs), while the short and long term contamination risks are due to the mobility of fission products in

the geosphere and the possibility of their entering in biosphere. Half lives of minor actinides range between a few hundreds to millions of years, therefore, repositories containing actinides requires surveillance for such a long period which is questionable from economical as well as environmental safety considerations. Moreover, the vitrified mass of HLW can be a source of high radioactive contamination by the decay of beta/gamma emitting highly mobile fission products. If actinides are not removed from the spent fuel, it will require millions of years to reduce radio toxicity of the waste to an accepted level from environment point of view. For that reason the method of separation of long lived radionuclide followed by transmutation called “Partitioning and Transmutation” (P&T) is being adopted worldwide [8, 9]. The partitioning of the long-lived actinides and high-yield fission products could contribute to reduce the radioactive account and its associated radiotoxicity by a factor of 100 or more, reduce the time needed to approach the radioactivity to acceptable level and also reduce contamination risk associated with high-level waste. Residual waste can be vitrified and then buried in subsurface repositories with much reduced risk and cost after partitioning of actinides and fission products. Most of the partitioning strategies used for reprocessing and to make the waste amenable for safe disposal rely on the following four separations: (1) Partitioning of U and/or Pu from spent-fuel; (2) Co-extraction of the trivalent actinides and lanthanides; (3) Separation of beta/gamma emitting, heat generating fission products and (4) Separation of the trivalent actinides from trivalent lanthanides (Fig. 1.4).

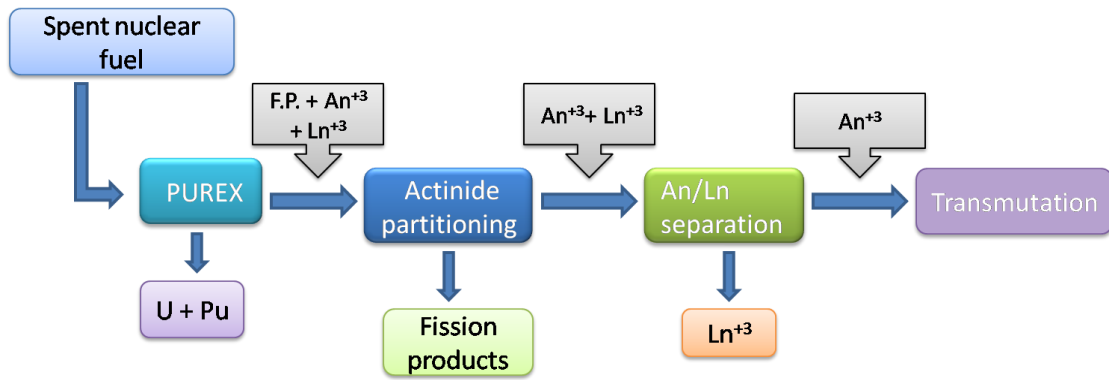


Fig. 1.4 Spent fuel partitioning strategies.

1.4.1 “PUREX” process

PUREX is “plutonium uranium redox extraction” used for separation of valuable fissile materials Pu and U from spent fuel as well as from one another. Fuel rods coming after burning in reactors are dissolved in nitric acid and the resulting solution is called “dissolver solution”. From this dissolver solution U and Pu are recovered by PUREX process using 30% tributyl phosphate (TBP) in *n*-dodecane leaving behind the minor actinides (trivalent and pentavalent), fission products and structural elements [10]. Separation of U from Pu is carried out by adjustment of their oxidation states using external chemicals. Pu (III) and other actinides and lanthanides present in +3 or lower oxidation states are not extracted by TBP *n*-dodecane system. The chemical reactions involved in the process for U and Pu extraction can be given by Equations 1.2 and 1.3.



However, the process has some drawbacks also. Some amount of Ru, Tc and Zr is co-extracted with TBP-dodecane system [11]. Nitro-nitrato complexes of ruthenium which are present in nitric acid waste medium are fairly extractable by TBP and not easy to

strip. Ruthenium also remains in the solvent after stripping of uranium and plutonium and the recovered solvents consequently have a high residual activity.

In PUREX process, TBP- *n*-dodecane solvent system is continuously exposed to a high radiation dose in presence of HNO₃ result in degradation of TBP to dibutyl hydrogen phosphate and monobutyl hydrogen phosphates (DBPH and MBPH₂) [12]. These degradation products extract many undesired metal ions, causes difficult stripping of Pu and poor phase separation during various steps of the extraction process.

1.4.2 Actinide partitioning

“Partitioning and transmutation” (P&T) [13] of actinide elements has been considered as a way of reducing the burden of geological repositories. This process will lead to generation of extra energy by transmutation process and simultaneously would reduce the need for long term surveillance of repositories.

Presence of trivalent lanthanide interfere the selective extraction of trivalent actinide from high level waste because of similar chemical properties and several times higher concentration of lanthanides than that of actinides. Concentration of Lns is found to be about one third of the total mass of the fission products. Consequently to get rid of this complexity, the separation process (P&T) is divided in two steps. In first step co-extraction of An(III) and Ln(III) is accomplished to get rid of all the alpha activities and one third part of the fission products (lanthanides) and the step is identified as “Actinide Partitioning” [14]. In the second step the separation of trivalent An from trivalent Ln is achieved for transmutation purpose.

1.4.3 Separation of fission products

The waste resulting from raffinate of PUREX process contains small quantities of An and Ln elements along with many fission products, such as, Mo, Tc, Ru, Cs, Zr, Sr, Y,

Nb, Rh, Pd, Ba etc. The presence of some fission products in HLW increase the contamination risk due to beta/gamma activity and high mobility of some of them [15]. Therefore, safe management of HLW also involves the separation of fission products like ^{106}Ru , ^{99}Tc , ^{93}Zr , ^{137}Cs , ^{90}Sr , ^{99}Mo , ^{107}Pd . Among them ^{106}Ru , ^{99}Tc , ^{93}Zr are beta/gamma active. ^{137}Cs , ^{90}Sr are beta/gamma active along with heat producing too and ^{99}Mo , ^{107}Pd are useful for their various possible applications [16-18].

Tc and Mo form a special class of fission products that exists in the form of oxometalate anions in nuclear waste as MoO_4^{2-} , $\text{Mo}_7\text{O}_{24}^{6-}$, $\text{H}_2\text{Mo}_7\text{O}_{24}^{4-}$, TcO_4^- . ^{99}Tc is a long lived β decay nuclide and TcO_4^- is mobile under environmental conditions. ^{99}Mo has large biological significance and act as a source of $^{99\text{m}}\text{Tc}$ which is used for medical modeling purposes. Ru has high specific activity and form volatile RuO_4 . It is difficult to separate Ru from waste due to its variable valences at different nitric acid concentrations. Cesium and Strontium are found to be major heat contributors of high level waste. Ligands used for separation of fission products depend on individual nature of particular metal ion.

1.4.4 Solvents used at various stages of back-end of fuel cycle

(i) Trialkyl phosphates

Trialkyl phosphates are included in the family of organophosphorus ligands. It is generally known, that for organophosphorus class of extractants, the extractability of metal ion increases in the following order: Organophosphine oxide > Organophosphonate > Organophosphate. Amongst the trialkyl phosphates, TBP is the most promising extractant and used in PUREX process for extraction of uranium and plutonium [10]. TBP is a monodentate ligand having one phosphoryl group (Fig. 1.5) and is a neutral molecule. It extract Pu and U by solvation mechanism. It is classified in the class of hard donor ligand as it has oxygen as coordination site. The extractant do

not show extraction for other actinides and lanthanides of nuclear waste. Although shows some extraction for Ru, Zr and Tc. But the D values for these metal ions are very poor. Triamyl phosphate (TAP) and triisobutyl phosphate (TIBP) (Fig. 1.5) are other ligands of the same family but rarely used.

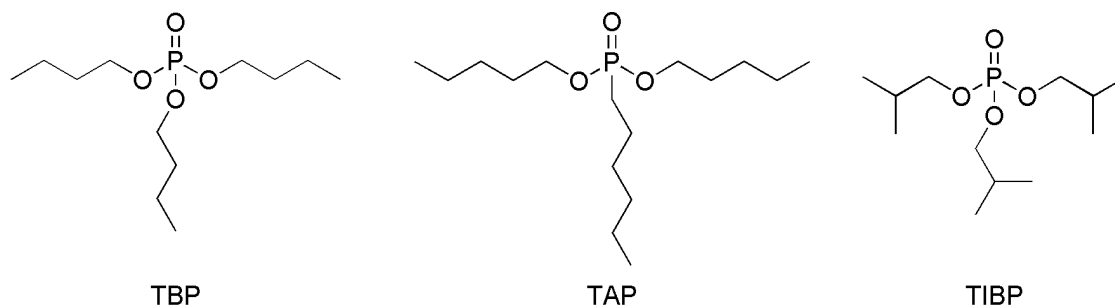


Fig. 1.5 Structures of various trialkyl phosphate ligands.

(ii) Trialkyl phosphine oxide (TRPO)

TRPO is also included in organophosphorus family of extractants. TRPO is a class of ligand where R group can be butyl, isoamyl or octyl (Fig. 1.6). It is used for actinide partitioning and extract trivalent actinides only at low acidity (≤ 1 M HNO_3) [19]. At higher acidity the coordination site of the ligand gets engaged with HNO_3 . So, this class of ligand is only useful in case of waste stored at lower acidity and not found to be promising for HLW (~ 3 M HNO_3). A relatively higher concentration of ligand (30%) is required for actinide partitioning. Poor stripping of actinides is another disadvantage of TRPO.

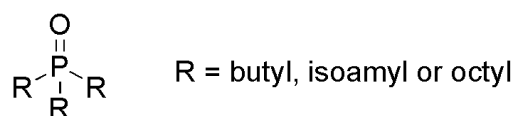


Fig. 1.6 Basic structure of trialkyl phosphine oxide (TRPO) ligands.

(iii) Carbamoyl methylphosphine oxide (CMPO)

This is bidentate neutral extractant of organophosphorous family namely octyl(phenyl)-*N,N*-diisobutylcarbamoyl methylphosphine oxide (CMPO-1) and diphenyl-*N,N*-diisobutylcarbamoyl methylphosphine oxide (CMPO-2). The bifunctionality of CMPO viz one amide group and one phosphoryl group are responsible for the separation of lanthanides and actinides (Fig. 1.7) [20]. CMPO shows high distribution ratio for actinides (III, IV, VI) from waste solutions having intermediate acid concentration. It also shows good selectivity for An over fission products. However, stripping of actinide ions from the loaded organic phase was found to be difficult and required multiple contacts with stripping agents. Coextraction of Zr is another drawback associated with the use of CMPO.

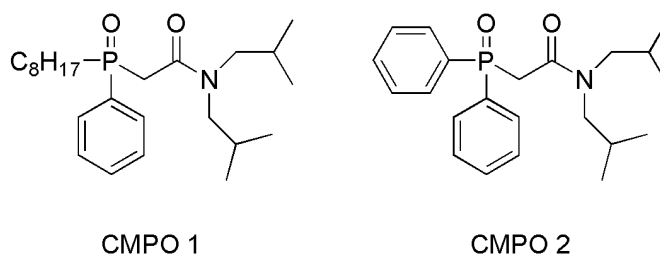


Fig. 1.7 Structure of carbamoyl methyl phosphine oxide (CMPO) ligands.

(iv) Phosphoric acid ligands

Phosphoric acid ligands (Fig. 1.8) have the same limitation as TRPO and extract actinides at lower acidity only thereby, not much useful for HLW. One of the major drawbacks associated with all organophosphorus extractants is the solid residue that results upon their incineration after use due to presence of phosphorus. More common ligand of this family is DIDPA (Fig. 1.8) [21]. Three other different derivatives of phosphoric acid ligands used in the separation process are shown in Fig 1.8. Phosphoric acid ligands are sometimes used with CMPO for synergistic extraction of U(VI)O₂.

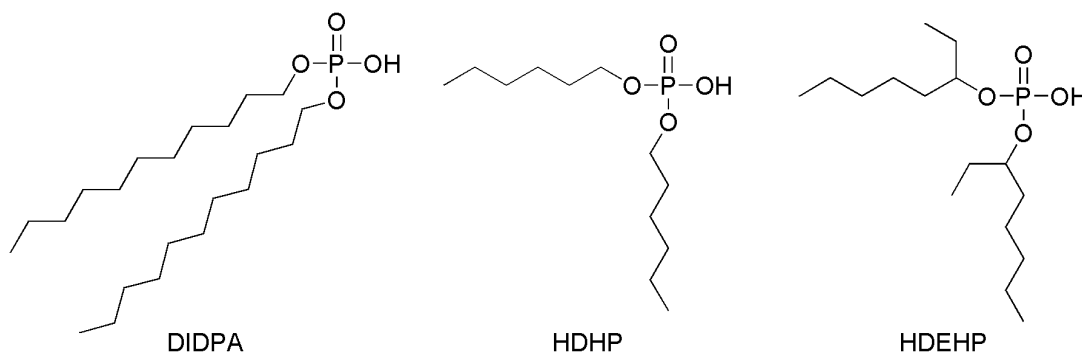


Fig. 1.8 Structure of diisodecylphosphoric acid (DIDPA) and other phosphoric acid based ligands.

(v) Cyanex ligands

Cyanex is a very broad class of ligand having cyanex 272, cyanex 923, cyanex 572, cyanex 302, cyanex 301 etc (Fig. 1.9) [22]. These ligands are used for the separation of different metals from nuclear waste solutions and employed at different stages of waste management processes. Some of sulfur donor cyanex ligand showed selective extraction of actinides over lanthanides [23]. Cyanex 301 is a soft donor ligand, containing sulphur atom. Cyanex 272 is a hard donor ligand, while cyanex 302 have both soft (S) and hard donor (O) coordinating groups. Cyanex 923 is a commercially available trialkylphosphine oxide extractant (mixture of $R_3P=O$, $R_2R'P=O$, $RR'_2P=O$ and $R'_3P=O$ with $R=C_6$ and $R'=C_8$) similar to TRPO and TOPO. While cyanex 925 is claimed as a mixture of trialkylphosphine oxides containing normal and branched octyl groups.

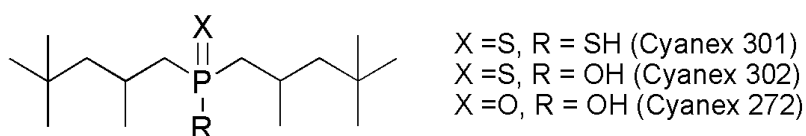


Fig. 1.9 Structure of some important Cyanex ligands.

(vi) Malonamide extractants

Considering nonincinerable nature of phosphorus based ligands, a new class of ligand “Diamides” are introduced for actinide partitioning by French researchers utilizing the CHON (carbon, hydrogen, oxygen and nitrogen) principle. These diamides are completely incinerable in nature and don't generate any solid secondary wastes at the end of the process as they can be totally convertible in to gaseous products.

These substituted bidentate malonamide extractants having two carbonyl group have been found to be promising for the partitioning of minor actinides under HLW conditions [24]. According to HSAB concept it was postulated that nitrogen atom of ligand don't participate in extraction process, only hard donor oxygen atom of amide is responsible for coordination with metal ion. Among several malonamides extractants, *N,N*-dimethyl-*N,N*-dibutyl tetradecyl malonamide (DMDBTDMA) and *N,N*-dimethyl-*N,N*-dioctyl-2-(2-hexyloxyethyl)malonamide (DMDOHEMA) have been established to be most promising (Fig. 1.10).

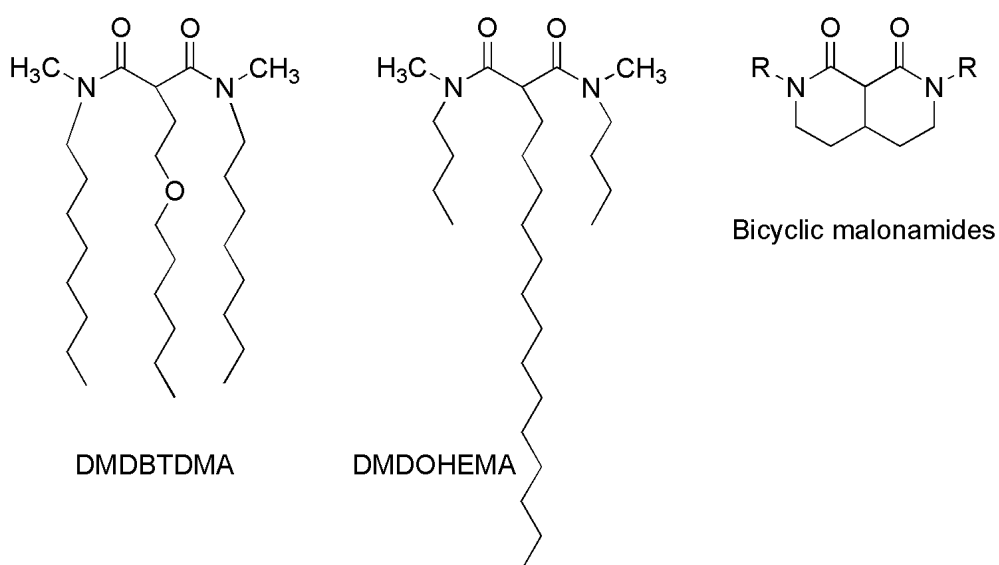


Fig. 1.10 Structure of DMDBTDMA, DMDOHEMA and bicyclic malonamide.

The salient features of malonamides ligands that make them versatile is the easy back extraction at lower HNO_3 concentration as these extractant show poor extraction at lower acidity. Although, a high concentration of malonamide ligands is require for Actinide partitioning purpose.

(vii) Diglycolamides

In recent past, a new class of ligand called diglycolamides (DGA) have been established for actinide partitioning purpose [25]. This series of ligands are the new sequence of diamide compounds obtained by introducing ether oxygen positioned between two acetamide functionalities. This one extra oxygen makes the DGA ligands tridentate result in effective complexation than diamides. Sasaki et al. synthesized a series of diglycolamides (DGA) ligands having different alkyl chains attached to amide nitrogen atom [26]. Amongst the different derivatives *N,N,N',N'*-tetraoctyldiglycolamide (TODGA) and *N,N,N',N'*-tetra-2-ethylhexyldiglycolamide (TEHDGA) (Fig. 1.11) have been found to be most promising because of their poor solubility in water, high solubility in *n*-dodecane and significantly higher extraction for trivalent actinides.

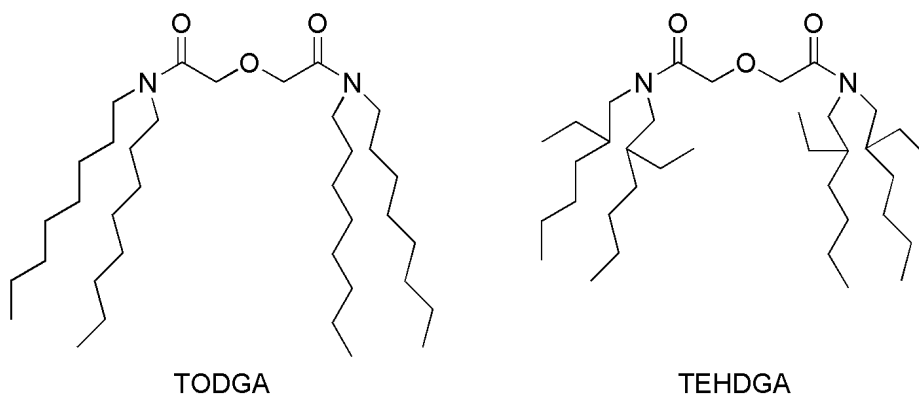


Fig. 1.11 Structure of TODGA and TEHDGA.

DGA ligands with structural modifications in their skeleton were also attempted (Fig. 1.12) but these modifications has not been resulted in making of superior extractant than TODGA and TEHDGA [27].

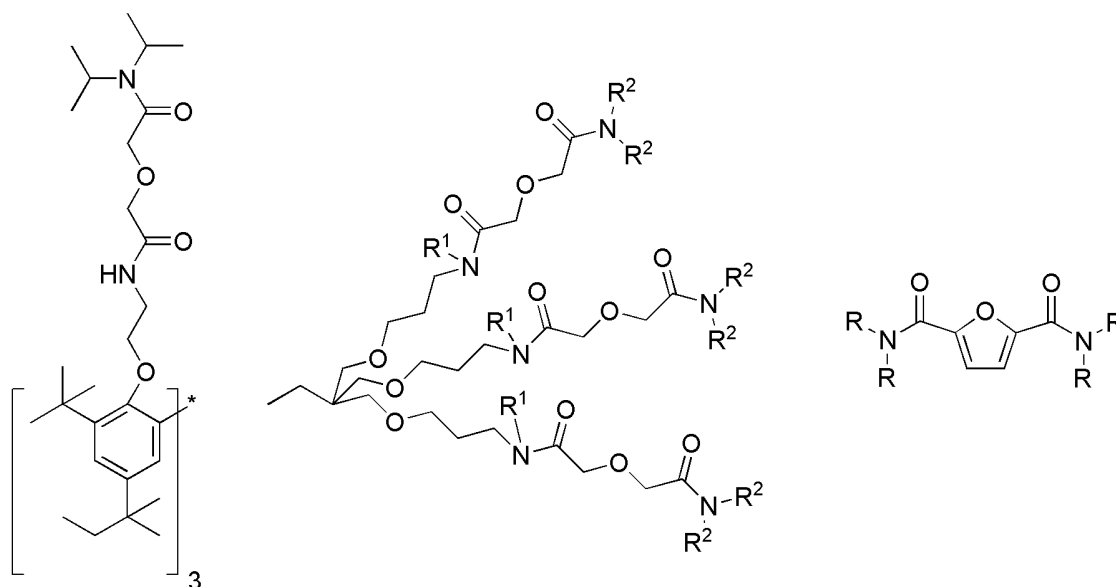


Fig. 1.12 Structure of some newly developed diglycolamide ligands.

(viii) Amines and quaternary ammonium salts

Amines and quaternary ammonium salts have been studied in detail for the extraction of oxometalate anions contained in nuclear waste solutions [28, 29]. Both the type of extractants usually works effectively at lower nitric acid concentrations (up to 0.5 M). Extraction efficiency was found to decrease with increase of acidity because at higher nitric acid concentrations the anion exchanger sites of these ligands get occupied with HNO_3 . Different amines and ammonium salts which are used for the separation of anionic metal species are presented in Fig 1.13.

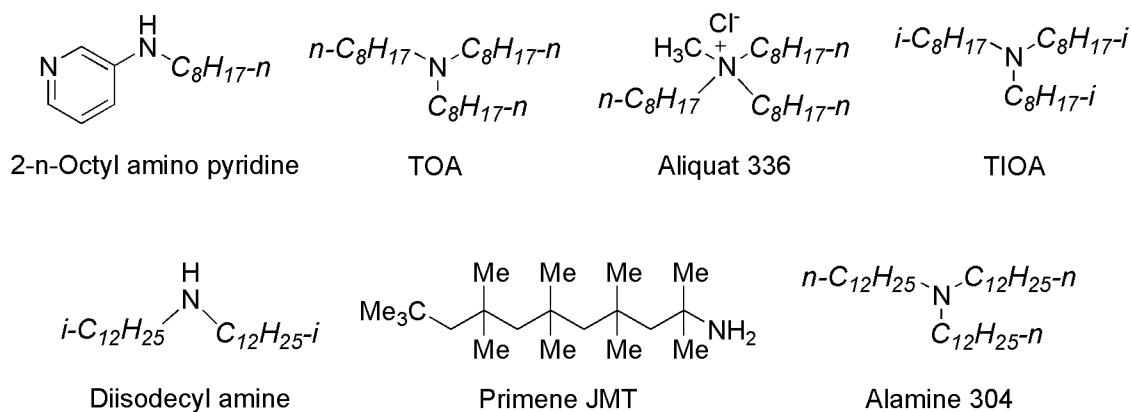


Fig. 1.13 Amine or ammonium salt based ligands.

(ix) Crown ethers and Calixarins

Macrocyclic polyethers or crown ethers are known to extract alkali metals [30]. Various crown ethers have been found to be effective for extracting either cesium or strontium from aqueous streams. Calixarenes (cyclic compounds constituted by four phenolic units linked by methylene groups, *p-tert*-butyl-calix[4]arene) were also utilized for selectively separation of cesium from other alkali cations [30]. More common crown ether and calixarene ligands are depicted in Figure 1.14.

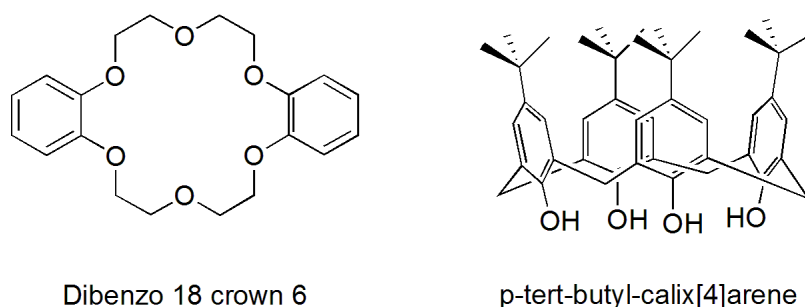


Fig. 1.14 Crown ether and Calix-arene ligands.

(x) *N*-Donor heterocyclic ligands

N-donor heterocyclic ligands based on pyridine, pyrimidine, pyrazine, 1,2,4-triazine, 1,3,5-triazine, 1,2,4-triazole, benzimidazole, benzothiazole, and benzoxazole ring systems have been studied for selective extraction of actinides over lanthanides [31]. *N*-

Donor ligands were used because they could impart better selectivity than *O*-donor ligands and extract in moderate acidities (0.1 M – 1 M) than *S*-donor ligands (pH range). BTP, BTBP, Tphen and BTphen ligands (Fig. 1.15) are extensively explored for the separation of An (III) from Ln (III).

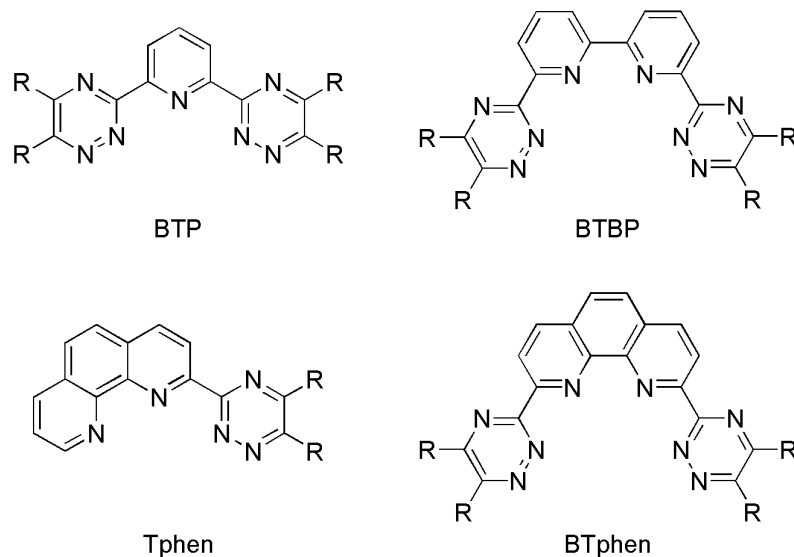


Fig. 1.15 N- heterocyclic ligands for selective extraction of An (III).

1.5 Separation methods

Separation methods generally applied for separation of metal ions from nuclear waste solutions are solvent extraction, membrane separation and solid phase extraction. All these methods utilize some common principles like equilibrium kinetics, chemical reactions, fluid mechanics, and mass transfer from one phase to another. “Solvent Extraction” or “Liquid-liquid Extraction” is considered to be the most adaptable due to the fact that separations can be carried out on a micro level as well as on a macro level [32].

1.5.1 Solvent extraction

The ability of a solute (inorganic or organic) to distribute itself between an aqueous solution and an immiscible organic solvent is applied for separation and purification of

solutes. The process is called solvent extraction and also used in metal analysis, in which a metal ion solution is brought into contact with a organic solvent, immiscible with the first, in order to bring the transfer of one or more metal ions into the organic solvent (Fig. 1.16).

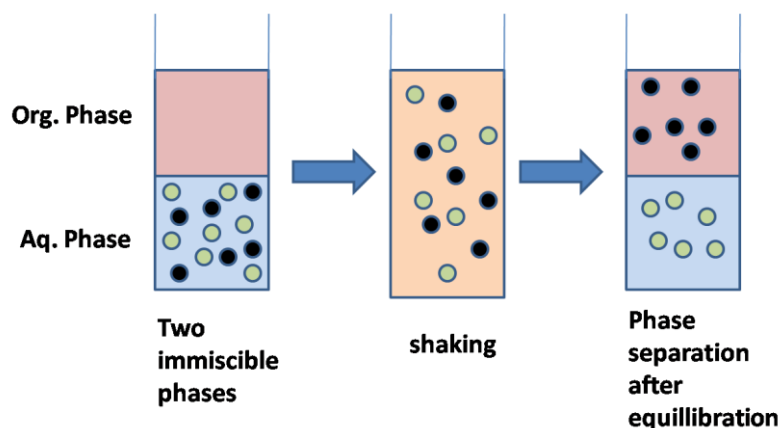


Fig. 1.16 Diagrammatic presentation of Solvent extraction.

The thermodynamics of distribution of metal ion can be explained by the Phase rule (Equation 1.4) which can be written as:

$$C - P + 2 = F \quad (1.4)$$

Where C, P and F denotes the number of components, number of phases and degrees of freedom respectively. For a binary system such as liquid-liquid extraction, number of phase is two *i.e.* $P = 2$ and no of components can be three or more including two solvents and one or more solutes. When a system contains only one solute *i.e.* $C = 3$, three degrees of freedom are associated with the system so at a particular temperature and pressure, the concentration of solute in any phase can be find out by knowing its concentration in the other phase. Therefore, the ratio of concentration of solute in the two phases is constant as long as the temperature and pressure of system remain the same. According to Nernst distribution law, the concentration of a particular species (M) in the organic phase and in the aqueous phase at equilibrium can be expressed as



In Equation 1.5, the term in subscripts “org” and “aq” denote the organic and aqueous phases respectively. If the solute species (M) remains same in both the phases, the ratio of solute concentration in the organic phase to that in the aqueous phase is termed as the “distribution coefficient” (K_d) or “partition coefficient” (Equation 1.6).

$$K_d = M_{(\text{org})} / M_{(\text{aq})} \quad (1.6)$$

However, in the metal ion separation using organic extractants, the ligand forms a complex with the metal ion and then gets transferred to the organic phase. In such cases, the chemical species of the metal ion in the two phases are not the same. Hence, a term “distribution ratio” is coined to define the ratio of total concentration of the metal ion in the organic phase to that in the aqueous phase.

Distribution ratio

The distribution ratio, D , is defined as the ratio of the total concentration of metal ions in the organic phase to that of in the aqueous phase. Here total concentration of metal represents all forms of metal ion in that particular phase. For a given metal species M it can be written as (Equation 1.7):

$$D_M = [M]_{t,\text{org}} / [M]_{t,\text{aq}} \quad (1.7)$$

In Equation 1.7, when M is present in various differently complexed forms in the aqueous phase and in the organic phase, $[M]_t$ refers to the sum of the concentrations of all M species in a given phase (the subscript t indicates total M).

Percentage extraction

The percent extraction “ E ”, is more commonly used term for expressing the extraction efficiency in separation science and can be related to “ D ” as shown in Equation 1.8.

$$\%E = 100 \times (V_{\text{org}} [M]_{\text{org}} / \{V_{\text{org}} [M]_{\text{org}} + V_{\text{aq}} [M]_{\text{aq}}\})$$

$$\text{Or} = 100 \times [D / (D + V_{\text{org}}/V_{\text{aq}})] \quad (1.8)$$

Where, V represents solvent volume of two phases. When the volume ratio of two phases are one then the % E can be expressed as Equation 1.9.

$$\%E = D / (D + 1) \quad (1.9)$$

Separation factor

It is a measure of the ability of the system to separate two metal ions. If there are more than one metal ion (metal ions A and B) and the desired metal ion is A then, the selectivity of the solvent for metal ion A as against B is defined as the ratio of the distribution ratio of A to the distribution ratio of B. The separation factor (S.F.) is related to the individual distribution ratios as shown in Equation 1.10.

$$\text{S.F.} = D_A / D_B \quad (1.10)$$

Decontamination factor

The ability of a process to remove a contaminant from a product is expressed by decontamination factor. For example, if a process has a 1:9 mixture of M_A to M_B , and the product is a 1:99 mixture of M_A and M_B , then the decontamination factor (for the removal of M_A) of the process is $0.11 / 0.01 = 11$.

The solvent extraction technique can be applied on pilot as well as plant scale. Technique has its own pros and cons. The advantages are (1) Easy handling and processing (2) better selectivity (3) % Extraction can be increased by simply increasing the organic/aqueous volume ratio (4) Relatively faster mass transfer. Some disadvantages associated with the technique are requirement of large inventories of solvents, third phase formation and large volumes of secondary waste produced.

Despite of suffering from various limitations, solvent extraction techniques are used for laboratory to industrial scale for processing of waste streams.

1.5.2 Membrane separation

Another frequently used technique for metal ion separation is use of membranes. Membrane separation technology has replaced solvent extraction technique due to a number of advantages like that of operational simplicity, high selectivity, simple technology and low energy requirements [33]. A membrane is a permeable or semi-permeable barrier like a thin polymeric film, which allows the mobility of some species and restricts the others. The membrane can be charged or neutral, porous or non-porous and acts as a permeable solid or liquid phase.

In liquid membrane separation methods, a membrane containing organic phase is kept in between the two aqueous phases; one phase containing metal ion (feed or source phase) and the other which receives the metal ion (strip or receiver phase). Several types of liquid membranes are extensively studied such as: supported liquid membranes *viz* flat-sheet supported liquid membrane (FSSLM), hollow fiber supported liquid membrane (HFSLM) and non-supported liquid membranes *viz* bulk liquid membrane, liquid emulsion membrane. One of the most important characteristics of liquid membrane extraction technique is that unlike solvent extraction, in membrane separations three steps namely the extraction and stripping of the metal ion along with regeneration of the carrier (ligand) can be carried out in a single stage.

1.5.3 Solid phase extraction

Limitations of solvent extraction techniques, lead to the development of new technologies such as membrane separation, electrodialysis and solid phase extraction for metal ion recovery and separation. Solid phase extraction (SPE) has been extensively studied for separation of metal ions from various streams because of its

advantages of high enrichment factor, high recovery, rapid phase separation, low cost, low consumption of organic solvents. Solid phase extraction has led to the development of solvent impregnated resins (SIR) [34]. SIRs are prepared by the simple immobilization of a common extracting agent onto an insoluble, non-functionalized polymer support. For maintain the advantage of solvent extraction processes in SIRs, selection of a suitable solid support is required having specific surface area, macroporosity and hydrophobicity. Solid supports mostly used for the preparation of SIRs are: (I) acrylic polymers (Amberlite XAD 7, Amberlite XAD 8 (II) divinylbenzene polymers (Amberlite XAD 2, Amberlite XAD 4). Amberlite XAD resin is widely used to develop SIRs due to its good physical and chemical properties such as porosity, high surface area, durability and purity.

1.6 Ligand and metal interactions (mechanism of extraction)

The extraction of the metal ion by the organic ligand comprises of three steps: (1) dehydration of metal ion, (2) complexation of metal ion with extractant and (3) transfer of metal-ligand complex to the organic phase. Actually the metal ion has the tendency to remain in aqueous phase only, due to its poor solubility in organic phase and high solubility in aqueous phase. The aqueous phase solubility of charged metal ion is attributable to ion-dipole interactions. It is necessary to neutralize the charge of metal ion in order to increase the solubility of charge metal ions in organic diluents so that it could be extracted in organic phase from aqueous phase. For this purpose a suitable extractant (ligand) molecule is dissolved in organic phase to complex with the metal ions that forms neutral species having solubility in organic diluent and thus subsequently extracted in the organic phase. Actually the role of the complex forming extracting agent is largely to replace the coordinated water from around the metal ion to

give a species that is more likely to be soluble in organic solvents. The mechanism of extraction of metal ion or the complexation of metal ion with ligand can be any of the following types.

(i) Solvation mechanism: Solvation is the process in which the water molecule of inner coordination sphere of metal ion is replaced by the ligand donor atoms such as 'O', 'N' or 'S' etc. When the ligand molecule is neutral, the complexation mechanism between metal and ligand is found to be solvation only and the metal ion can be transferred into the organic phase only if the ligand molecules can solvate the metal ion. Most of separations processes related to nuclear waste are based on this type of mechanism. The solvating power of the ligand depends on strength of complexation between metal and ligand.

Esters of organophosphorus acids ($=P=O$) and a number of related compounds constitute a class of organic solvents which show remarkable solvating properties, whose essential functional group is the semipolar $P=O$ bond with the oxygen atom having good steric availability. Separation of actinides by organophosphorus extractants has may be taken as a typical example of solvation mechanism [20] (Fig. 1.17).

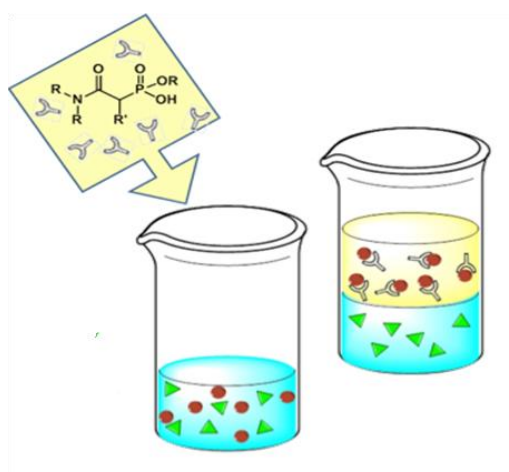


Fig. 1.17 Solvation of metal ion by a phosphoric group containing ligand.

(ii) Ion-pair mechanism: This mechanism is followed in case of anionic or cationic ligands which bind with metal ions and forms neutral ion-pair (Fig. 1.18). The best example of this type of mechanism is extraction of oxometalates by amines and quaternary ammonium salts. The ion-pair complexes are stabilized in the polar diluents like nitrobenzene, dichloromethane, etc. which increase the efficacy of metal ion extraction. Metal ion complexation by crown ethers and related compounds at higher acidity is another example of ion-pair extraction. Ion pair formation involves two types of extractants *viz.* a) Acidic Extractants: These extractants provide anions which complex with metal cations by liberating protons, e.g. sulphonic acids, carboxylic acids and organophosphoric acids [35]. (b) Basic Extractants: These extractants provide cations for aqueous anionic species of metal ions, e.g. amines and quaternary ammonium salts [36].

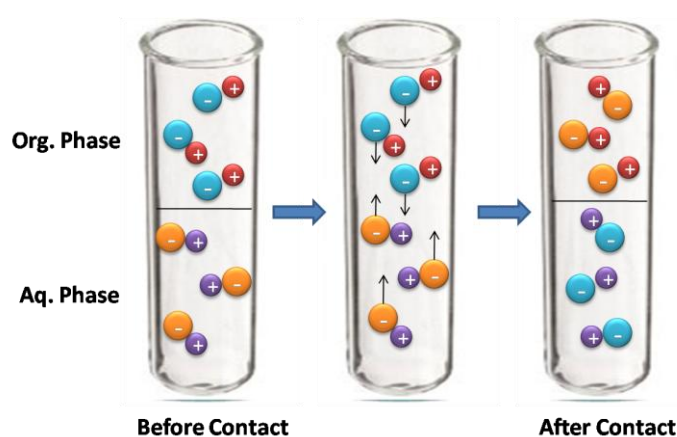


Fig. 1.18 Ion-pair mechanism of extraction.

(iii) Chelation mechanism: A chelating ligand forms a cyclic metal-chelate complex (Fig. 1.19) with the metal ion which is entropically more stable, thus making the metal ion more lipophilic. For chelation purpose the ligand molecule should have at least two donor atoms per molecule. This type of mechanism is exemplified by the extraction of actinides and lanthanides by diglycolamide ligands [37].

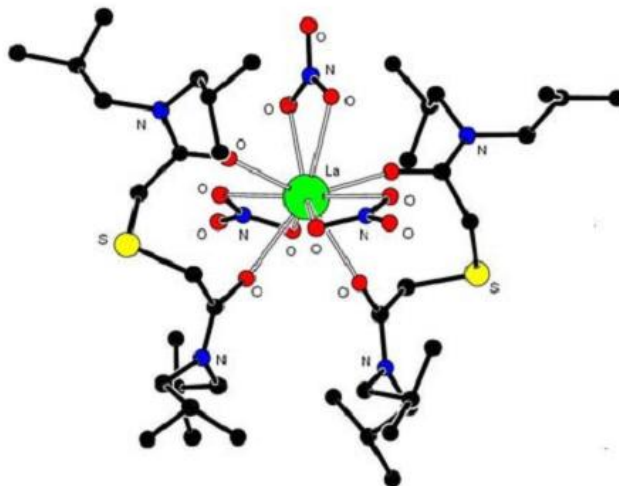


Fig. 1.19 Chelate complex of La with tetrabutylglycolamide [38].

(iv) Synergistic extraction: In synergism phenomenon, extraction of metal ions in the presence of two or more extractants is found to be more than that expected from the sum of extraction employing individual extractants. One of the examples of synergistic extraction is the extraction of U(VI) by a mixture of Alamine 336 and a neutral oxodonor ligand like DHOA, TBP or TOPO [39].

1.7 Theory of complexation (HSAB concept)

Actinides forms complexes with ligands through electrostatic interactions where covalency playing a minor role. Stability of complexes between metal ions and ligands is based on the concept of hard and soft acids and bases (HSAB) [40]. In metal ligand complexation metal ion behaves as a lewis acid and ligand behaves as a lewis base. Those metal ions are called hard which have a small radius, high charge and do not possess valence shell electrons that are easily distorted. The soft metal ions have the opposite characteristics. Ligand can also categorize on the same basis. According to HSAB concept, hard metal ions prefer binding to the hard ligands, whereas the soft metal ions prefer binding to soft ligand to give stable complexes. Actinides as ‘hard

acids' cations interact strongly with hard ligands having donor groups such as 'O' or 'F' atoms rather than soft ligands with 'N', 'S' or 'P' etc. coordinating groups. On the contrary, as compared to Ln, An show more preference to soft donor ligands because of f-orbital participation [31]. Fission products present in nuclear waste like Cs, Sr form complexes with hard donor ligands where as Mo, Tc, Ru, Pd form complexes with both hard and soft donor ligands.

Macrocyclic ligands possess excellent size selective complexing ability for alkali and alkaline earth metals due to their pre-organized conformation, size selective nature and hydrophilic interior /hydrophobic exterior [30]. Crown ethers have been employed as polydentate neutral donors in synergistic extraction of actinides from weak acidic solutions and as ion-pair extractants from strong acid solutions. Separation of Cs and Sr is based on size selective complexation with crown ethers.

1.8 Factors influencing the distribution of metal ion (factors affecting extraction efficiency)

Some of the important factors which affect the distribution of metal ions are nature and concentration of solute (metal ions), extractant, diluent, acidity of the aqueous phase, salting agent presence in the aqueous phase, and temperature etc. [41]. These factors take an important part to achieve the desired separation. Some of them are described in detail.

1.8.1 Selection of diluents

Selection of a suitable diluent for effective separation is very important. The boiling point of the diluent should not be too low to be evaporate in extraction process. The polarity of solvent also matters; the ligand as well as formed metal ligand complex should be fully dissolved in the solvent to prevent third phase formation. Polarity of the diluent can be altered by using enough amount of a polar organic material called phase

modifier to avoid third phase in extraction. Similarly, viscosity, the relative specific gravities, the degree of miscibility of the two phases, tendency to form emulsions, flammability and toxicity should also be considered. Most of the solvent usually used in extraction of metal ions are organic diluents such as dodecane and other hydrocarbons.

1.8.2 Acidity of the aqueous phase

The distribution ratio of metal is greatly influenced by the acidity of the aqueous phase, so it is necessary to optimize the concentration of H^+ ions for maximum extraction. In some cases acid competes with the metal species to bind with the coordination sites of the ligands that result in decreased extraction with increasing acid concentration.

1.8.3 Salting agents

The addition of high concentrations of inorganic salts to the aqueous phase significantly increases the distribution ratio of many metal complexes if the inorganic salt has any component of extracted species. This is due to the common ion effect or salting-out effect as well as the strong ability of these ions to bind water around them thereby depleting the aqueous phase for use as a solvent (saturation effect).

1.8.4 Masking

Masking or sequestering agents are introduced to improve the separation factor for metal pairs that are difficult to separate. Such type of masking agent is chosen that forms water-soluble complexes with the undesired metals in extraction process and prevent their extraction by the extracting agents.

1.8.5 Backwashing or scrubbing

Backwashing is a supplementary technique used to increase separations of the different metals. The organic phase containing desired and some amount of undesired metal ions,

is shaken with a fresh aqueous phase containing the optimum reagent /salting agent concentration, acidity, etc. This results in a redistribution of the undesired metal species in the aqueous phase since their distribution ratios are low, while most of the metals of interest will remain in the organic phase, since their distribution ratio is high.

1.9 Criteria for the selection of a suitable extractant

A number of factors are taken into account while choosing a suitable extractant for metal ion separation [42]. These are as follows:

1.9.1 Extractability

Extractability is measured by the distribution ratio of the particular metal for the extractant. It is desirable to be as large as possible for a good extractant so that minimum possible extraction steps will be enough to recover desired metal quantitatively. This is only possible when the extractant has better complexation ability for metal ion of interest.

1.9.2 Selectivity

Selectivity of an extractant is as important as extractability. For all useful extraction operation the selectivity must be as high as possible otherwise additional steps will be required to further separate it from co-extracted metal ions which would increase additional waste volumes.

1.9.3 Solubility of extractant

The extractant should have high solubility in nonpolar paraffinic organic diluents which are generally used in solvent extraction process like dodecane, kerosene etc. With this, the extractant should have low solubility in the aqueous feed solutions.

1.9.4 Easy and cost effective synthesis

To perform the extraction process at a reasonable cost the synthesis of extractant should be easy and cost effective. The synthetic procedure should have as less steps as possible. Synthesis should be done using easily available and cheap starting materials.

1.9.5 Recoverability

Easy regeneration of the extractant for recycling is also important to make the process cost effective. For this purpose easy stripping of the metal ions from the organic phase is necessary. After stripping most of the time the extractant is purified by distillation, so the extractant should have high relative volatility than other components of organic phase and should be thermally stable under the distillation temperature.

1.9.6 Stability of extractant

extractant should be stable in particular extraction conditions. For separation of metal ions from spent nuclear fuel the extractant should have high resistance to radiolytic and hydrolytic degradation during operation.

1.9.7 Chemical Reactivity

The extractant should be chemically stable and inert towards the other components of the extraction as well as towards the common materials used in the process.

1.9.8 Viscosity, Vapour Pressure, Freezing Point

Extractant should have low viscosity for easy flowing nature and high Inter Facial Tension (IFT) so that the faster rate of phase disengagement can achieve for clear separation of two phases. Vapour pressure should be high for nonvolatility and the extractant should not be freeze at room temperature.

1.9.9 Density

For a clear phase separation a large difference in density between extract and aqueous phases is necessary. This is especially important for extraction devices utilizing gravity for phase separation.

1.9.10 Other Criteria

1. For health and safety purpose extractant should not have toxicity and flammability.
2. Corrosivity of the solvent leads to the typical problems with materials used in the process.

CHAPTER 2

*Design, synthesis and extraction properties of a
new class of anion exchanger for oxometalates*

2.1 Introduction

Some metal ions, present in acidic nuclear waste, form a special class that exists as oxygenated anionic species called oxoanions or oxometalates. Most commonly present species are: MoO_4^{2-} , $\text{Mo}_7\text{O}_{24}^{6-}$, $\text{H}_2\text{Mo}_7\text{O}_{24}^{4-}$, $\text{UO}_2(\text{CO}_3)_3^{4-}$, $\text{UO}_2(\text{SO}_4)_3^{4-}$ and TcO_4^- etc [43, 44]. Separation of U is necessary for further recycling for future nuclear power plants. ^{99}Tc is a β decay nuclei and mobile under environment conditions. On the other hand, ^{99}Mo is used as $^{99\text{m}}\text{Tc}$ generator which has large biological applications in various fields including imaging of various organs [45-47]. Thus these anions are needed to be separated from the waste. For separation of these metal anions, ion exchangers are used as an extractant. Amines and ammonium salts are more commonly employed for this purpose (Fig 1.13) [36, 44, 48-55]. Trioctylamine (TOA), a major constituent of Alamine 336 is known to extract oxometalates from nitric acid waste solutions by an anion-exchange mechanism [56-60]. Aliquat 336 and Primene JMT are also applied for the same purpose [28, 56, 61]. A mixture of kerosene and alcohols or ketones is usually used as the diluent with these amines [62, 63].

While the extraction is based on anion or cation exchange mechanism, the extraction process is greatly affected by concentration of cationic, anionic species present in the medium as well as acidity of feed solution and the distribution ratio strongly depends on these three parameters. Alamine 336 and other amine based cationic anion exchangers works efficiently at lower acidity but shows poor results at higher acidity of aqueous phase [44]. Because at higher acidity the anion exchanger sites of these extractants get engaged with nitrate anion of nitric acid thus not available for binding the metal anion.

Recently, iminodiamides have been introduced for extraction of oxometalates from nitric acid medium. Iminodiamides are the imino analogs of TODGA and produced by replacement of ether oxygen of TODGA by secondary and tertiary imino

groups which act as an anion exchanger site [64-66]. Some of them [66] have shown good results for extraction of oxometalates even from higher acidity of aqueous phase. Still, the role of amide groups in these extractants to enable them for work efficiently at higher acidity has not been discussed. In order to find out the contribution of this amide group for extraction of oxometalate at higher acidity, there is a need to evaluate the exact role of amide group in extraction process.

It is known that the amide group in CMPO (Fig. 2.1) can suppress the effect of competing HNO_3 and retains its ability to work at higher acidity [67, 68]. This behaviour is termed as intramolecular buffering effect [69]. We applied the same principle to make a new class of anion exchangers for oxometalates that might work at higher HNO_3 concentrations. Mo has been chosen as an example of oxometalate for present extraction studies.

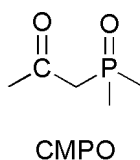


Fig. 2.1 Basic framework of CMPO.

Mo forms extensive range of oxometalate clusters consists of isopolyacids or heteropolyacids [70, 71]. Polyoxometalates (POM) are popular target for studies because they specifically have richness of their structures and possible applications in a variety of fields, including catalysis, analysis, medicine, photochemistry, chemical sensors, capacitors, memory, electrochemical cell and so on [72-75]. Several research attempts have been made to functionalize the POMs with an organic component which gives rise to the formation of organic–inorganic hybrid materials where POMs work as building blocks. As the POM anions contain many oxygen atoms which act as good

hydrogen bond acceptors, functionalization of these POMs with organic molecules having many hydrogen atoms give rise to interesting supramolecular chemistry [76,77].

Crystal structure of POM anion with Bu_4N^+ as a mixed $[\text{Mo}_6\text{O}_{19}]^{2-}$ and $[\text{Mo}_8\text{O}_{26}]^{4-}$ i.e. $[n\text{-Bu}_4\text{N}]_8[\text{Mo}_6\text{O}_{19}]_2[\alpha\text{-(Mo}_8\text{O}_{26})]$ [78] has been reported recently. Crystals of $[\text{Mo}_6\text{O}_{19}]^{2-}$ and $[\text{Mo}_8\text{O}_{26}]^{4-}$ have also been made using different ligands [77, 79, 80]. Complexes of POM with organic amino type ligands associated with other metals such as Cu, Co have been prepared and characterized by X-ray crystallography [81-83]. But, individual complexes of $[\text{Mo}_6\text{O}_{19}]^{2-}$ and $[\text{Mo}_8\text{O}_{26}]^{4-}$ with the same ligand are not known.

2.2 Present work

We have designed a new class of anion exchangers, dialkylamino-mono-amides using buffering effect principle. In addition to the imino group, the extractants have one more functionality i.e. a terminal amide group. The new extractants are derivatives of trialkylamines in which the one octyl chain is replaced with one terminal amide functionality. The extractants are expected to have good extraction behavior at higher acidity due to the presence of amide group. Its simpler structure would help us to evaluate the exact role of amide group by comparison with its analogous trioctylamine having no amide functionality. This chapter describes the synthesis and extraction behaviour of α -dialkylamino *N,N*-diisobutylacetamides **1-3** (Fig. 2.2), a new class of ammonium based extractants embedded with a terminal amide group. The extraction behavior of these amides for molybdenum was compared with commonly used anion exchangers like Alamine 336 **4**, Aliquat 336 **5** and Primene JMT **6** (Fig. 2.2) which do not possess buffering amidic functionalities.

This chapter also included the condition dependent crystal engineered syntheses of two polyoxomolybdate complexes of acetamide ligand **1** and their X-ray

crystallographic characterization considering the great importance of inorganic-organic hybrid materials of polyoxomolybdate anions and alkylammonium based cations.

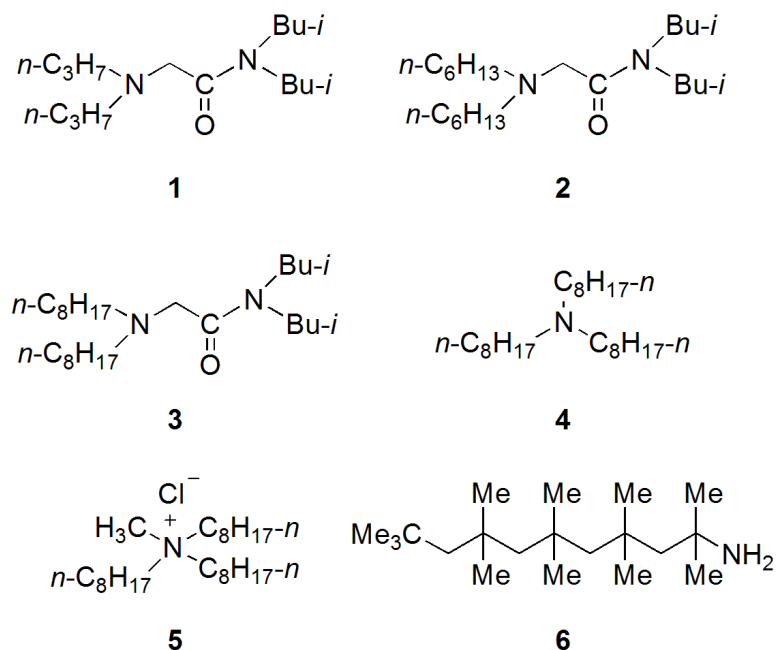
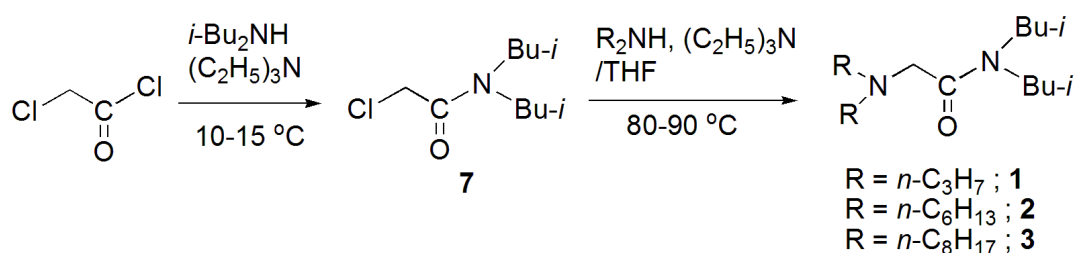


Fig. 2.2 Structure of α -dialkylamino *N,N*-diisobutylacetamides **1-3** (L **1-3**), TOA

(major component of Alamine 336) **4**, Aliquat 336 **5** and Primene JMT **6**.

2.2.1 Synthesis of α -dialkylamino *N,N*-diisobutylacetamides **1-3**

α -Dialkylamino *N,N*-diisobutylacetamides **1-3** were synthesized in only two simple steps starting from commercially available material chloroacetyl chloride and diisobutylamine as shown in Scheme 2.1. Chloroacetyl chloride was reacted with diisobutyl amine in presence of triethylamine to give amide **7** in good yield (85%). Amide **7** was subsequently heated with respective dialkylamines in different reaction conditions to give the desired α -dialkylamino *N,N*-diisobutylacetamides **1-3** in very good overall yield as shown in Scheme 2.1. In case of **1**, where R group is propyl, the substrate amine was used in excess to neutralize the HCl generated during the reaction. But in case of **2** and **3** where R group is long alkyl chain like hexyl and octyl, triethylamine was used as base.



Scheme 2.1 Synthesis of α -dialkylamino *N,N*-diisobutylacetamides.

2.2.2 Comparison of extraction behavior of amines 1-6 at different acidities

To find out the contribution of amide group a comparison of distribution ratios of conventional extractants having no amide functionality has been carried out with acetamides **1-3** at different acidities. For this a solution of 0.2 M each of extractants **1-6** dissolved in 30% IDA/*n*-dodecane was prepared and equilibrated with aqueous solution containing 450 mg/L molybdenum at varying nitric acid concentrations from 0.5 M to 2.0 M (Fig. 2.3). It can be seen by the plots that %E decreases with increase in nitric acid concentration for all the extractants. This can be explained by the fact that at higher acidities nitrate of HNO_3 competes with metal anion to bind with the anion exchanger site therefore the anion exchanger site will be comparatively less available for metal ion to bind with. By plots it also evident that the relative decrease, in case of Alamine 336, Aliquat 336 and Primene JMT is much higher compared to acetamides **1-3**. At lower concentrations of HNO_3 , %E for Mo is higher for all the extractants except Primene JMT **3**. But at higher concentrations of nitric acid, %E of Mo sharply decreases for conventional extractants. However this fact is not true for acetamides **1-3**. For them the values of % E was found to be much better compared to Alamine 336, Aliquat 336 and Primene JMT at higher HNO_3 concentrations. Good extraction behavior of acetamides **1-3** even at higher nitric acid concentrations can be explained by the presence of amidic group in acetamides **1-3**, that allowed retaining the extraction

ability at higher HNO_3 concentration by intramolecular buffering effect of amidic group.

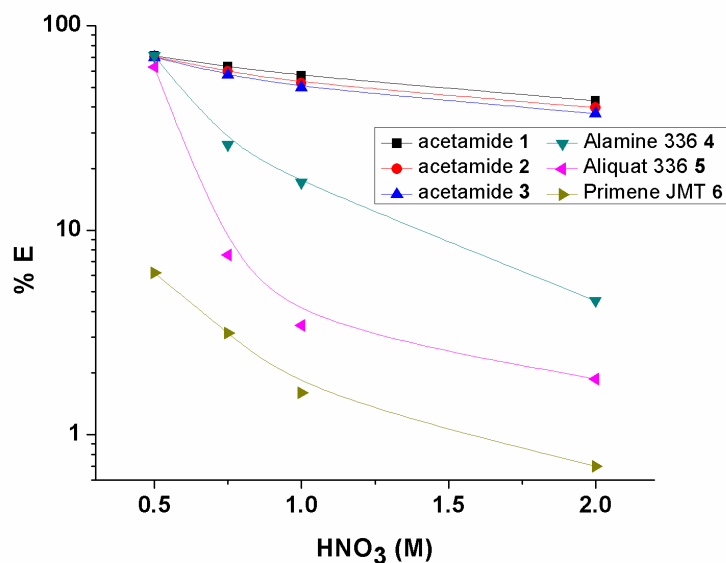


Fig. 2.3 %E for anion exchangers **1-6** at varying nitric acid concentrations.

The effect of length of alkyl chain attached to imino nitrogen is also clear from this comparison. The acetamide having shortest alkyl chain has highest extraction ability although the difference is not very high. Probably the higher extraction ability of acetamide **1** is attributed to the less steric hindrance at anion exchanger site. From this observation acetamide **1** was chosen for further studies as it has shown better extraction behavior.

2.2.3 Optimization of organic phase composition

Phase modifier is used with extractant and diluent in organic phase to prevent the third phase at various stages of extraction process. In the view of the polar nature of metal-ligand complex and their poor solubility in *n*-dodecane, IDA [84, 85] has been chosen as a phase modifier to avoid poor phase separation for the present extraction study. To establish the most suitable organic phase composition, D_{M_0} was evaluated at different

concentrations of phase modifier and acetamide **1**. Concentration of IDA was varied from 0-100% and acetamide **1** from 0.1-0.3 M (Fig. 2.4).

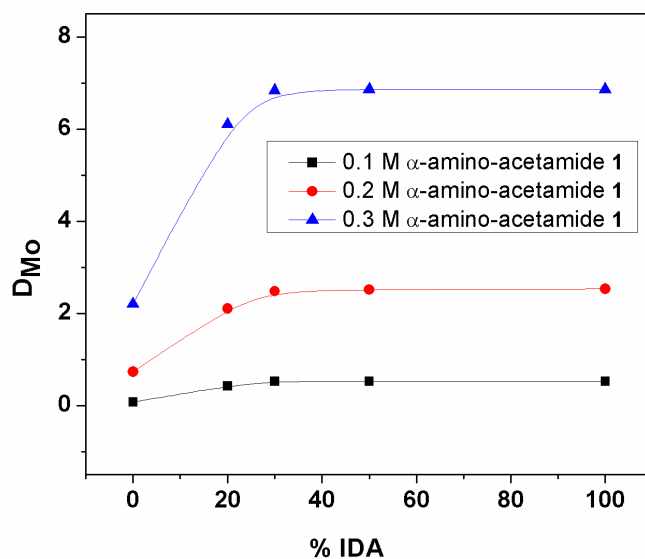


Fig. 2.4 Variation in D_{Mo} with IDA concentration at 0.5 M nitric acid.

It was observed that with increase in IDA concentration in solvent, initially there was considerable increase in the D_{Mo} values for all extractant concentrations, but, remained unchanged beyond 30% IDA. Considering these results, 0.2 M α -amino-acetamide **1** dissolved in 30% IDA/*n*-dodecane was fixed as the optimal organic phase composition for present extraction studies.

2.2.4 Determination of Stoichiometry of the extracted metal complex

In order to ascertain the stoichiometry of extracted metal complex, extraction studies *viz.* acid uptake property of the ligand, influence of acidity and ligand concentration on D_{Mo} have been performed.

2.2.4.1 Acid uptake behavior of ammonium acetamide 1 and Alamine 336

Nitric acid uptake is a common property exhibited by amidic extractants. α -amino-acetamide **1**, having both the amine and amidic functional groups, also expected to show similar properties. Therefore, the extraction of nitric acid was studied for Alamine 336 and amino-acetamide **1**. For this acid distribution studies, equal volumes of organic phase containing 0.2 M anion exchangers Alamine 336 or acetamide **1** in 30% IDA/*n*-dodecane and an aqueous phase of varying initial acidity (0.1 to 4.0 M HNO₃) were equilibrated. The acid concentration in the organic and aqueous phase was estimated by potentiometric titration with 0.1 M NaOH. The variation of [HNO₃]_{org} as a function of initial aqueous nitric acid concentration in aqueous phase for both the extractants is depicted in Fig. 2.5.

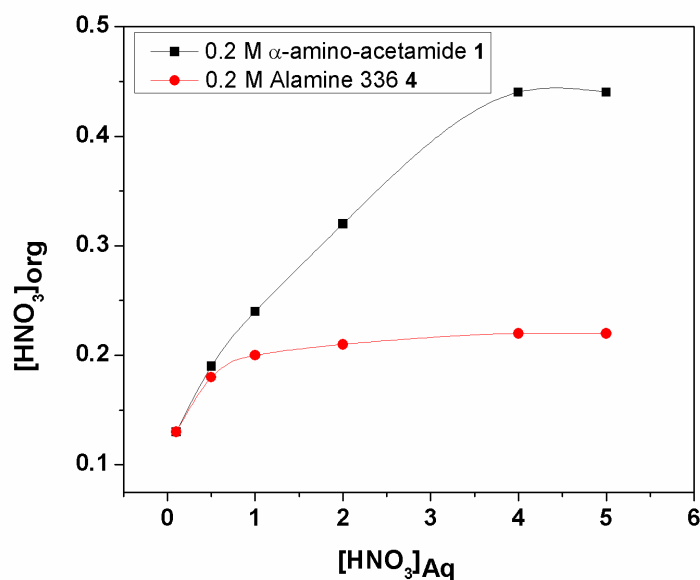


Fig. 2.5 Extraction of HNO₃ from aqueous solution by 0.2 M α -amino-acetamide **1** or Alamine 336 **4**.

For Alamine 336 the ratio of [HNO₃]_{org} to [Alamine 336] is 1:1 even for higher acidity (5 M HNO₃). In contrast for α -amino-acetamide **1**, the ratio of [HNO₃]_{org} to [acetamide **1**] increases from 1:1 to 2:1 as the aqueous nitric acid concentration increases from 0.5 M to 4.0 M. At 0.5 M HNO₃ all the ammonium site of α -amino-acetamide **1** is get

protonated by HNO_3 and shows 1:1 composition for HNO_3 and acetamide **1** in organic phase, above it the amide group of α -amino-acetamide **1** starts taking up of nitric acid, partial protonation of amide group was seen at 2 M HNO_3 and complete protonation was observed at 4 M HNO_3 . The above findings also confirmed that during pre-equilibration of acetamide **1** with 0.5 M nitric acid the species formed in the organic phase is L.HNO_3 .

It is clear from the Fig. 2.5 that the ratio of $[\text{HNO}_3]_{\text{org}}$ to [Alamine 336] is 1:1 whereas that of α -amino-acetamide **1** it was 1.5:1 in the range of 0.5 to 2 M aqueous phase HNO_3 concentration and finally 2:1 above 4 M nitric acid.

2.2.4.2 Influence of acidity on D_{M_0}

The influence of nitric acid on D_{M_0} was established by plotting $\log D_{M_0}$ vs $\log [\text{HNO}_3]$. Nitric acid concentration was varied from 0.5 M to 2 M (Fig. 2.6). It was found that D_{M_0} values linearly decreases with increasing nitric acid concentration. The plot of $\log D_{M_0}$ vs $\log [\text{HNO}_3]$ is a straight line with a slope of -0.85 ± 0.02 that suggest involvement of one molecule of nitric acid in the extraction process.

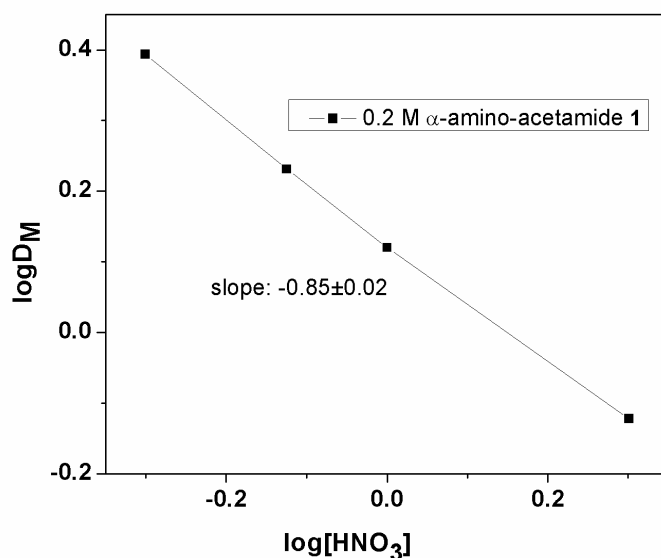


Fig. 2.6 Dependency of D_{M_0} on concentration of HNO_3 .

2.2.4.3 Effect of ligand concentration

For determination of metal to ligand ratio participate in extraction process variation of D_{Mo} was plotted as a function of concentration of amino-acetamide **1** at two different concentration of feed HNO_3 . D_{Mo} values found to be increases with an increase in the concentration of **1** for both the feed acidities. The plots are straight line with positive slopes of 2.34 ± 0.05 and 2.04 ± 0.02 for 0.5 M and 2 M HNO_3 , respectively (Fig. 2.7).

The obtained observations suggest that in the range of 0.5 to 2 M of feed HNO_3 concentrations, the metal ligand composition in the organic phase is $(LH)_2MoO_4 \cdot HNO_3$ (Fig. 2.8).

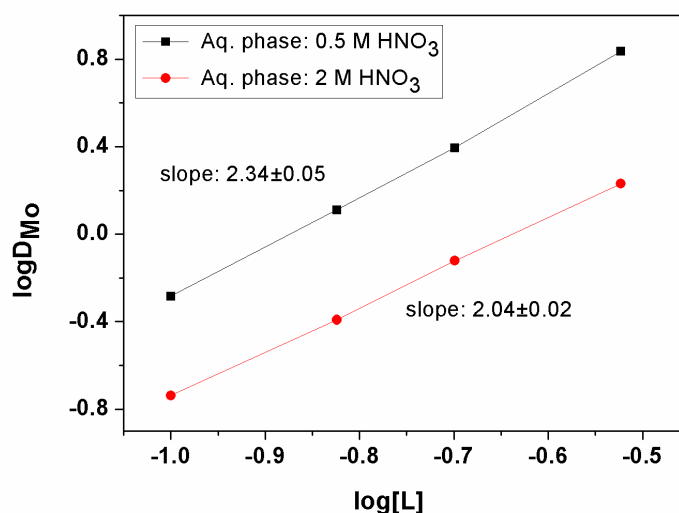


Fig. 2.7 Dependency of D_{Mo} on concentration of α -amino-acetamide **1**.

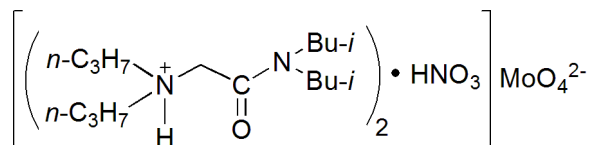


Fig. 2.8 Extracted metal-ligand complex in the organic phase.

2.2.5 Mechanism of extraction

Nitric acid concentration range of our extraction studies was 0.5-2.0 M, where molybdenum mainly exists as H_2MoO_4 [86]. Based on the above findings it can be

conclude that, extraction of Mo by amino-acetamide **1** is an anion exchange process and may be represented as Equation 2.1 in the acid range of 0.5 to 2 M HNO₃.



2.2.6 Confirmation of complexation by NMR and IR studies

The above complexation was further confirmed by FTIR and ¹H-NMR studies. FTIR spectra of loaded organic phase was recorded and compared with IR spectra of organic phase before contact as shown in Fig. 2.9. The value of $\nu_{\text{C=O}}$ of the organic phase was 1639 cm⁻¹ before contact to aqueous feed. After contact with 450 mg/L Mo in 1 M HNO₃, a shoulder for $\nu_{\text{C=O}}$ at 1554 cm⁻¹ appeared in addition to the 1639 cm⁻¹ peak (Fig. 2.9). This lowering of $\nu_{\text{C=O}}$ can be attributed to coordination of HNO₃ with the amide C=O that lowers the C=O bond strength and result in shifting of vibrational frequencies at lower value. Thus the IR results are consistent with the complexation observations postulated before in Equation 2.1.

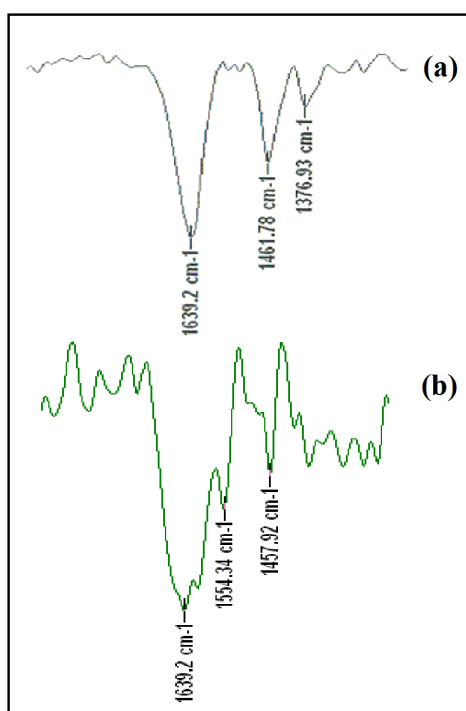


Fig. 2.9 IR spectra of organic phase: (a) Before contact; (b) Loaded organic phase.

To ascertain, the coordination site for Mo, organic phase containing 0.2 M α -amino-acetamide **1** in 30% IDA/*n*-dodecane was saturated with Mo by giving sufficient number of contacts with fresh aqueous phase containing 450 mg/L of Mo in 1 M HNO₃. The obtained yellow precipitate of metal-ligand complex in the organic phase was filtered, subsequently the residue was rinsed several times with chloroform to discard excess ligand and the obtained product was subjected to ¹H NMR. The ¹H NMR of the solution of the complex in CDCl₃ shows a downfield shift of δ values and broadening of the peaks corresponding to CH₂ α -to amine group *viz.* 2.53 (4 H, t, $J = 7.4$ Hz, $2 \times \text{CH}_2\text{CH}_2\text{N}$) vs 2.71-2.95 (4 H, brs, $2 \times \text{CH}_2\text{CH}_2\text{N}$) and 3.35 (2 H, s, CH₂CO) vs 3.6-3.78 (2 H, brs, CH₂CO) are clearly discernible. Presented NMR data is evincing that the exchange of MoO₄²⁻ occurs at ammonium site (Fig. 2.10).

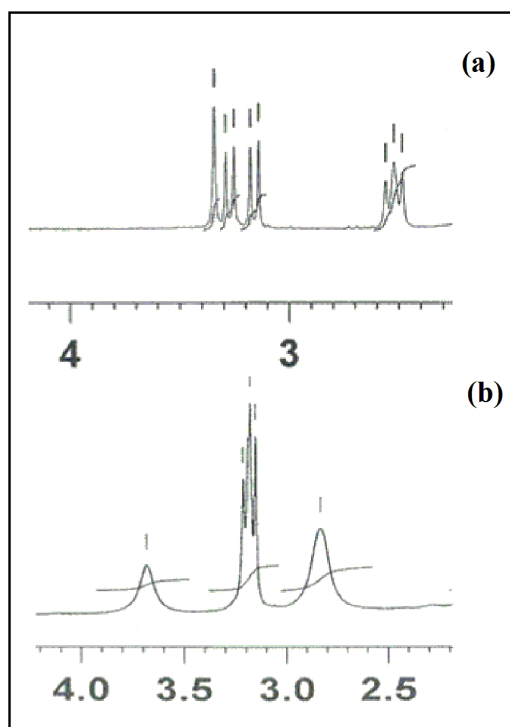


Fig. 2.10 (a) ¹H NMR of α -amino-acetamide **1**; (b) ¹H NMR of complex of MoO₄²⁻ with α -amino-acetamide **1**.

2.2.7 Back extraction studies

For back extraction studies the organic phase 0.2 M α -amino-acetamide **1** in 30% IDA/*n*-dodecane was equilibrated with aqueous phase containing 450 mg/L of Mo dissolved in 0.5 M nitric acid. Loaded organic phase was contacted with 10% NH₃ solutions. It was observed that 10% NH₃ is suitable for 90% recovery of molybdenum from loaded organic phase after three successive contacts.

2.2.8 Crystal study of the molybdate complexes of amino-acetamide **1**.

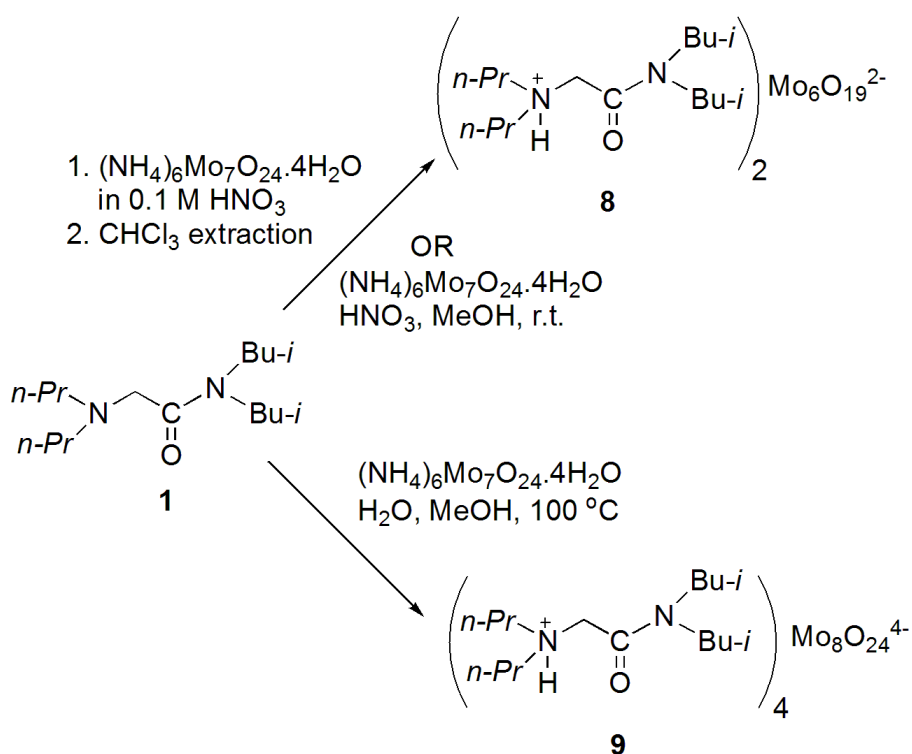
In order to find out the nature of bonding between oxomolybdate and amino-acetamide ligand **1** single crystal study of the molybdate complexes with amino-acetamide **1** was performed. Mo has the tendency to form a range of polyoxomolybdates consists of isopolyacids or heteropolyacids. The chemistry of isopolyacids of Mo is not yet fully understood because the extent of hydration and protonation of various species in solution is not known precisely. The fact that a solid can be crystallized from solution under appropriate conditions of acidity, concentration, temperature, etc. does not prove that the ion had the same structure in solution. The species of Mo present in the solution is dependent on the concentration of Mo as well as pH of the solution. At lower concentrations of Mo ($\leq \mu\text{M}$) only mononuclear species MoO₄⁻ is found in the solution and as the concentration increases the polynuclear species start to form [86]. When the pH is lowered, the first step in polyacid formation from [MoO₄]²⁻ is to increase the coordination number of Mo from 4 to 6 by addition of water molecules. Above pH = 6, [MoO₄]²⁻ is the predominant species. When the pH of the solution is between 4-5, [Mo₇O₂₄]⁶⁻ also known as paramolybdate is the species present while at pH range of 2-3, the octamolybdate [Mo₈O₂₆]⁴⁻ is preferentially formed [87]. It is known that in the molybdate system the equilibrium between various species in solution is attained quickly [87]. The Lindqvist anionic hexamolybdate [Mo₆O₁₉]²⁻ has

been structurally characterized only as isolated salt in solid state [87]. The interesting aspects of structure chemistry of the octamolybdate anion, $[\text{Mo}_8\text{O}_{26}]^{4-}$ is seen in varied structural patterns in the solid state [88]. Seven isomeric forms viz. α – η of octamolybdates, $[\text{Mo}_8\text{O}_{26}]^{4-}$ are known [88-90]. Functionalization of polyoxometalates with an organic component leads to the formation of organic–inorganic hybrid materials which shows interesting supramolecular chemistry [76, 77].

We obtained two new polyoxomolybdate based inorganic-organic hybrid compounds from ligand **1** and ammonium molybdate just by altering reaction conditions. The different structural features of these two complexes suggest that different polyoxometalate clusters play a key role in the process of assembling of ligands.

2.2.8.1 Synthesis of molybdate complexes of amino-acetamide **1**

Two different metal ligand complexes were obtained using ligand (L) **1** and $(\text{NH}_4)_6\text{Mo}_7\text{O}_{24}\cdot 4\text{H}_2\text{O}$ in three different conditions (Scheme 2). When the chloroform solution of ligand **1** was repeatedly contacted with fresh solution of $(\text{NH}_4)_6\text{Mo}_7\text{O}_{24}\cdot 4\text{H}_2\text{O}$ in 0.1 M aqueous HNO_3 and the resultant organic phase was concentrated, a yellow precipitate was obtained which on crystallization from acetonitrile provided a yellow complex $(\text{LH})_2[\text{Mo}_6\text{O}_{19}]$ **8** (Scheme 2.2). The same complex **8** was achieved when a 0.5 M nitric acid solution of $(\text{NH}_4)_6\text{Mo}_7\text{O}_{24}\cdot 4\text{H}_2\text{O}$ and a methanolic solution of ligand **1** were mixed and stirred at room temperature. Interestingly, when $(\text{NH}_4)_6\text{Mo}_7\text{O}_{24}\cdot 4\text{H}_2\text{O}$ was dissolved in water, mixed with a methanolic solution of ligand **1** and heated at 100 °C, a colorless complex $(\text{LH})_4[\text{Mo}_8\text{O}_{26}]$ **9** was formed.



Scheme 2.2 Synthesis of metal–ligand complexes **8** and **9**

2.2.8.2 Single crystal structures of molybdate complexes of amino-acetamide **1**

The complex **8** crystallizes in the monoclinic space group $I2/a$ while complex **9** crystallizes in the triclinic space group $P\bar{1}$. The crystal data and the refinement statistics is shown in Table 2.1.

Table 2.1 Crystal data and structure refinement

Compound	8	9
Empirical formula	$\text{Mo}_6\text{O}_{19}, 2(\text{C}_{16}\text{H}_{35}\text{N}_2\text{O})$	$\text{Mo}_8\text{O}_{26}, 4(\text{C}_{16}\text{H}_{35}\text{N}_2\text{O}), 2(\text{C}_2\text{H}_3\text{N})$
Formula weight	1420.54	2351.46
Temperature/K	293(2)	293(2)
Crystal system	monoclinic	triclinic
Space group	$I2/a$	P-1
$a/\text{\AA}$	24.8703(11)	11.8091(11)

b/Å	11.1774(3)	12.1612(11)
c/Å	20.4442(9)	18.2009(13)
α /°	90	77.755(7)
β /°	119.195(6)	81.247(7)
γ /°	90	87.642(7)
Volume/Å ³	4961.2(4)	2524.6(4)
Z	4	1
ρ_{calc} /mg/mm ³	1.902	1.547
m/mm ⁻¹	12.706	8.471
F(000)	2832.0	1200.0
Crystal size/mm ³	0.4585 × 0.288 × 0.1217	0.5939 × 0.3818 × 0.1877
2 Θ range for data collection	8.144 to 139.73°	7.574 to 140.192°
Index ranges	-27 ≤ h ≤ 29, -13 ≤ k ≤ 13, -24 ≤ l ≤ 23	-12 ≤ h ≤ 14, -14 ≤ k ≤ 14, -22 ≤ l ≤ 21
Reflections collected	8318	16607
Independent reflections	4616[R(int) = 0.0621]	9390[R(int) = 0.0809]
Data/restraints/parameters	4616/48/332	9390/24/535
Goodness-of-fit on F ²	1.007	1.133
Final R indexes [I ≥ 2 σ (I)]	R ₁ = 0.0946, wR ₂ = 0.2501	R ₁ = 0.1100, wR ₂ = 0.2873
Final R indexes [all data]	R ₁ = 0.1164, wR ₂ = 0.2812	R ₁ = 0.1319, wR ₂ = 0.3204
Largest diff. peak/hole / e Å ⁻³	1.92/-3.29	3.48/-2.54

The crystal structure of complex **8** [91] shows that the protonated ligand (LH⁺) **1** forms a cage-like structure in which the Mo₆O₁₉ fits in the cavity (Figs. 2.11 and 2.12). The counterions (LH⁺)-**1** regularly distribute in the interspaces formed by the polyanions. A pair of (LH⁺)-**1** ligand molecules orient in anti-parallel fashion with formation of two inter-ligand hydrogen bonds between amide oxygen atom of one ligand molecule and

the quaternary nitrogen atom of other ligand molecule (Fig. 2.13). The inter ligand N–H···O=C H- bond distance is 2.92 Å. Each $[\text{Mo}_6\text{O}_{19}]^{2-}$ anion is surrounded by six $(\text{LH}^+)-\mathbf{1}$ cations but its surrounding is not uniform. Each cluster anion is surrounded by two H-bonded dimeric $(\text{LH}^+)-\mathbf{1}$ cations and two $(\text{LH}^+)-\mathbf{1}$ cations not H-bonded to each other but to other protonated ligand molecules. The cage-like structure is then formed by hydrophobic interactions among intermolecular hydrogen bonded ligand dimers surrounding the central metal cluster (Fig. 2.14). The distances of quaternary N in $(\text{LH}^+)-\mathbf{1}$ cations and the nearest Mo in adjacent polyanions range from 4.77 to 5.31 Å. Three kinds interactions *viz.* the Van der Waals forces, electrostatic attractions between $(\text{LH}^+)-\mathbf{1}$ cations and polyanions $[\text{Mo}_6\text{O}_{19}]^{2-}$ and several hydrogen bonds between oxygen atoms of the polyanions and the hydrogens attached to carbon atoms of $(\text{LH}^+)-\mathbf{1}$ have been observed between $(\text{LH}^+)-\mathbf{1}$ cations and polyanion layers. The shortest C–H/O distance observed was 3.41 Å [between C(16)–O(10)]. The structure of $[\text{Mo}_6\text{O}_{19}]^{2-}$ anion in complex **8** shows slightly distorted cage of six molybdenum atoms located octahedrally around a central oxygen atom, with 12 oxygen atoms disposed in Mo–O–Mo units and one terminal oxygen attached to each molybdenum. Three distinct types of Mo–O bond lengths are observed. The terminal Mo–O bond lengths are shorter with a typical length of 1.66 Å and the bridging Mo–O bonds have a typical length of 1.91 Å. The central Mo–O bond lengths are the longest with a typical value of 2.32 Å. The exact values are presented in Table 2.2.

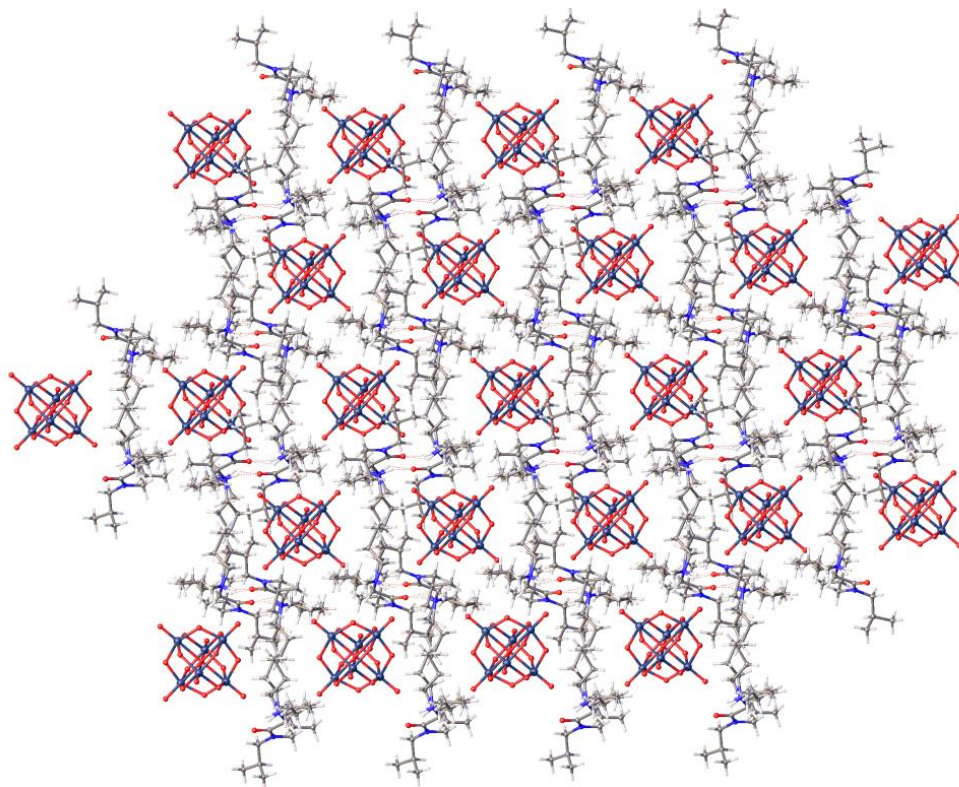


Fig. 2.11 Cluster packing of complex **8**, (LH)₂[Mo₆O₁₉], in the crystal. The dark blue balls are Mo; red balls: O; Light blue balls: N; gray balls: C; white balls: H.

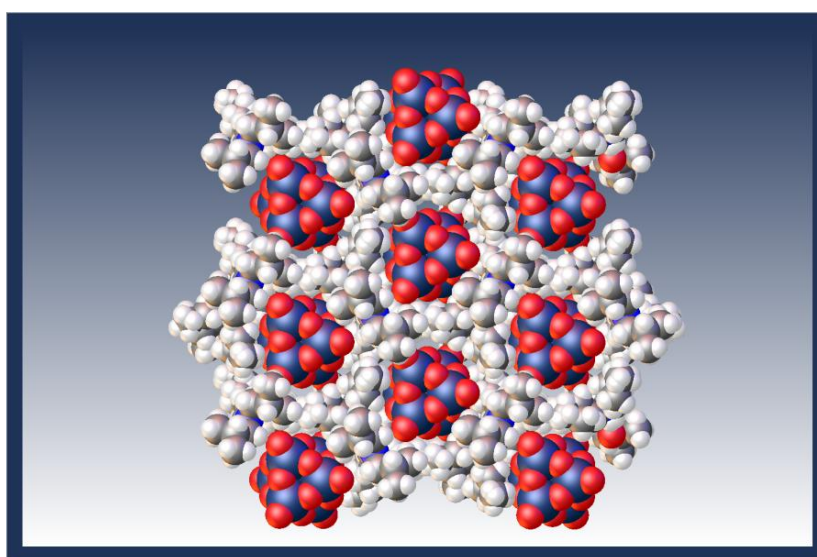


Fig. 2.12 Space filled cluster packing of complex **8**, (LH)₂[Mo₆O₁₉], in the crystal. The dark blue balls are Mo; red balls: O; Light blue balls: N; gray balls: C; white balls: H.

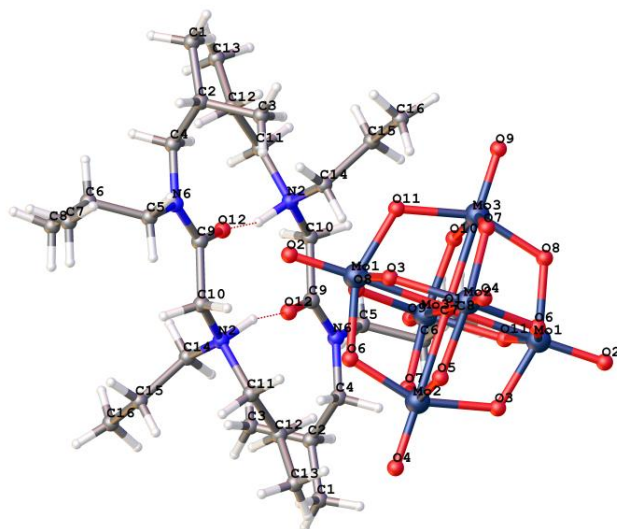


Fig. 2.13 The hexamolybdate anion with a pair of anti-parallel cationic ligand in complex **8**, $(\text{LH})_2[\text{Mo}_6\text{O}_{19}]$. The inter ligand hydrogen bonds ($\text{N-H}\cdots\text{O}=\text{C}$) are shown as red dotted lines; The dark blue balls are Mo; red balls: O; Light blue balls: N; gray balls: C; white balls: H.

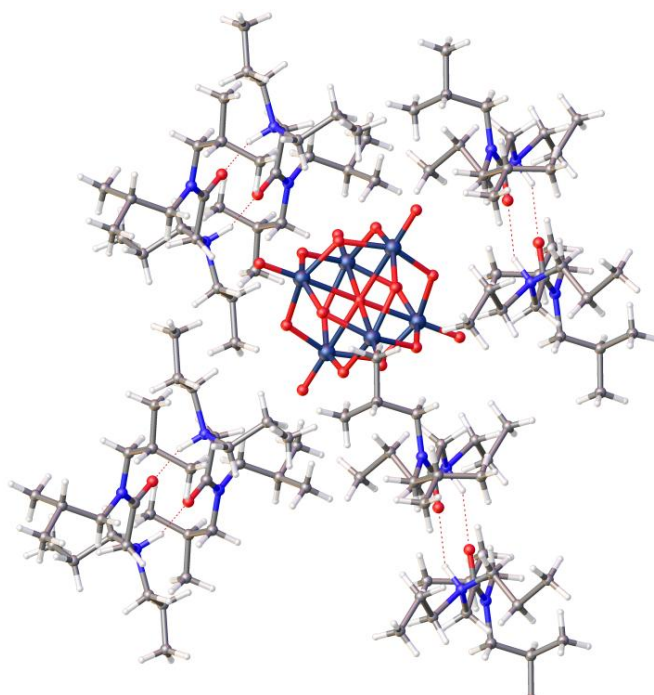


Fig. 2.14 The hexamolybdate anion surrounded by four anti-parallel dimeric units of ligand in the complex $(\text{LH})_2[\text{Mo}_6\text{O}_{19}]$ **8**. The dark blue balls are Mo; red balls: O; Light blue balls: N; gray balls: C; white balls: H.

Table 2.2 Bond Lengths for complex (LH)₂[Mo₆O₁₉] **8**.

Atom	Atom	Length/Å	Atom	Atom	Length/Å
Mo3	O10	1.919(5)	O12	C9	1.224(12)
Mo3	O8	1.898(8)	C10	N2	1.476(12)
Mo3	O7	1.910(7)	C10	C9	1.555(14)
Mo3	O9	1.654(7)	N2	C11	1.64(3)
Mo3	O11	1.945(9)	N2	C14	1.38(3)
Mo3	O1	2.329(7)	N2	C11A	1.29(4)
Mo2	O4	1.664(7)	N2	C14A	1.66(4)
Mo2	O7	1.920(7)	C9	N6	1.317(12)
Mo2	O5	1.914(5)	C2	C1	1.517(17)
Mo2	O6	1.898(8)	C2	C3	1.490(18)
Mo2	O1	2.308(7)	C2	C4	1.501(15)
Mo2	O3	1.934(8)	C11	C12	1.52(3)
O10	Mo3 ¹	1.919(5)	C6	C5	1.487(17)
O8	Mo1 ¹	1.937(7)	C6	C7	1.502(17)
O2	Mo1	1.665(7)	C6	C8	1.52(2)
Mo1	O8 ¹	1.937(7)	C5	N6	1.484(13)

Mo1	O11	1.882(9)	C4	N6	1.462(13)
Mo1	O6 ¹	1.951(8)	C15	C16	1.67(2)
Mo1	O1	2.3183(8)	C15	C14	1.58(4)
Mo1	O3	1.893(8)	C12	C13	1.54(2)
O5	Mo2 ¹	1.914(5)	C13	C12A	1.81(4)
O6	Mo1 ¹	1.951(8)	C16	C15A	1.53(3)
O1	Mo3 ¹	2.329(7)	C15A	C14A	1.52(4)
O1	Mo2 ¹	2.308(7)	C12A	C11A	1.50(6)

¹ Atoms generated by symmetry operation (-1/2-X,+Y,-Z).

The crystal structure for complex **9** [92] shows that octamolybdate anion is present in β -form and the protonated ligand (LH⁺) **1** forms a different cage structure (Figs. 2.15 and 2.16) to accommodate the polyanion in the cavity. Each β -[Mo₈O₂₆]⁴⁻ anion is surrounded by eight (LH⁺)-**1** cationic ligands (Fig. 2.17). Two MeCN molecules per cluster anion are incorporated into the interstitial positions held by hydrophobic interaction with the ligands and a weak C-H \cdots O hydrogen bonding interaction (C \cdots O distance 3.1 Å) with β -[Mo₈O₂₆]⁴⁻ anion (Fig. 2.18). The size of the cavity in this cage-structure is bigger than that in complex **8**. The clustering of ligand here is different and there is no inter-ligand hydrogen bond present as in complex **8**. The quaternary ammonium N of each ligand molecule, however, makes hydrogen bond with one of the oxygen atoms of metal cluster as shown in Figs. 2.17 and 2.18. Each anionic cluster β -[Mo₈O₂₆]⁴⁻ is strongly H-bonded to two (LH⁺)-**1** and weakly H-bonded to another two (LH⁺)-**1** (N-H \cdots O-Mo) with a typical bond length of 2.82 and 2.9 Å, respectively. Remaining four (LH⁺)-**1** ligands are not H-bonded to the cluster but H-bonded to

adjacent cluster anions. Besides H-bonding interactions, there exist three weak kinds of interactions between (LH⁺)-1 cations and inorganic cluster anions: the Van der Waals force, electrostatic attractions between cations (LH⁺)-1 and polyanions β -[Mo₈O₂₆]⁴⁻ and several H-bond between oxygen atoms of the polyanions and the C-H of (LH⁺)-1 ligands. The shortest C-H/O distance observed was 3.08 Å [between C(7)-O(6)]. The distances of quarternary N in (LH⁺)-1 cations and the nearest Mo in adjacent polyanions range from 4.48 to 4.54 Å. The β -isomeric octamolybdate cluster anion β -[Mo₈O₂₆]⁴⁻ is made up of Mo₆O₂₄ ring capped on opposite faces by two MoO₆ octahedra with overall eight edge-sharing MoO₆ octahedra. There are two classes of Mo-O bonds, the terminal Mo-O with a typical bond length between 1.70 and 1.72 Å and three types of bridging Mo-O bonds. The doubly bridged Mo-O(μ_2), triply bridged Mo-O(μ_3) and quintly bridged Mo-O(μ_5) having bond length in the range of 1.884(6)-1.917(7)Å, 1.932(6)-2.357(7)and 2.134(6)-2.482(7)Å, respectively. In each type of bonds, the *trans* Mo-O bonds to terminal oxygen atoms are considerably long compared to the ones of *trans* to the bridging oxygen atoms, which can be related to *trans* effect of terminal oxygen atom on the Mo-O bonds. The detailed of Mo-O bonds are presented in Table 2.3.

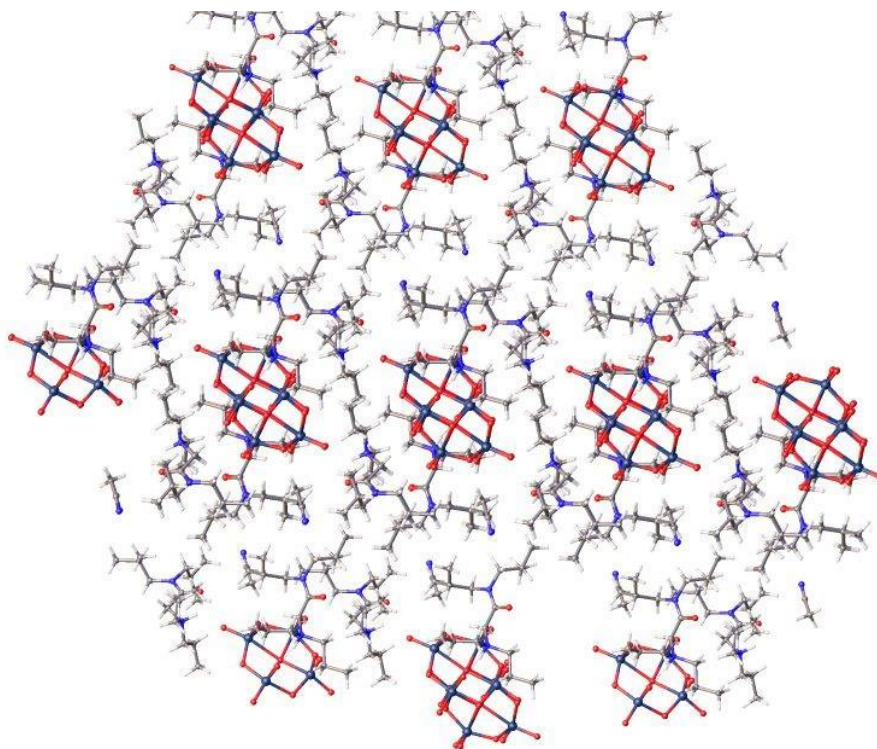


Fig. 2.15 Cluster packing of complex **9**, $(\text{LH})_4[\text{Mo}_8\text{O}_{26}] (\text{MeCN})_2$. The dark blue balls are Mo; red balls: O; Light blue balls: N; gray balls: C; white balls: H.

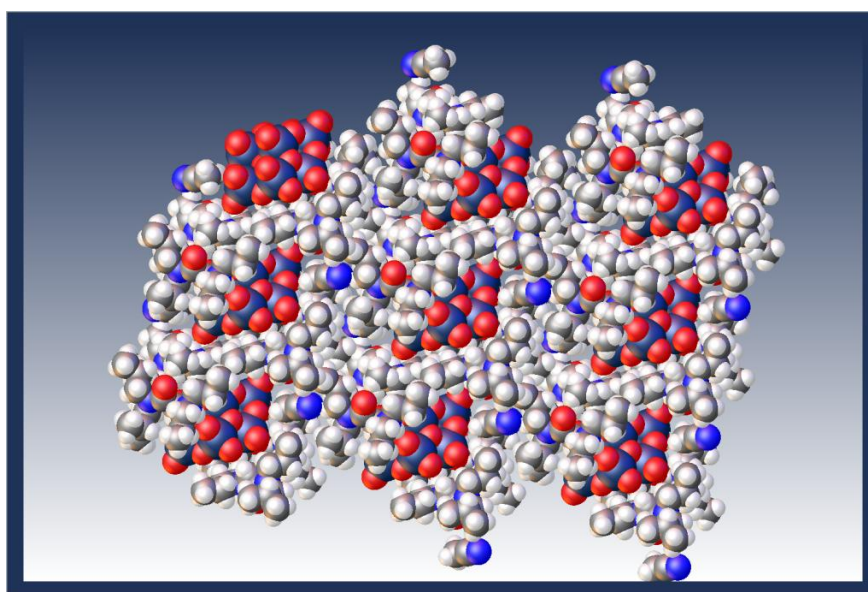


Fig. 2.16 Space filled cluster packing of complex **9**, $(\text{LH})_4[\text{Mo}_8\text{O}_{26}] (\text{MeCN})_2$. The dark blue balls are Mo; red balls: O; Light blue balls: N; gray balls: C; white balls: H.

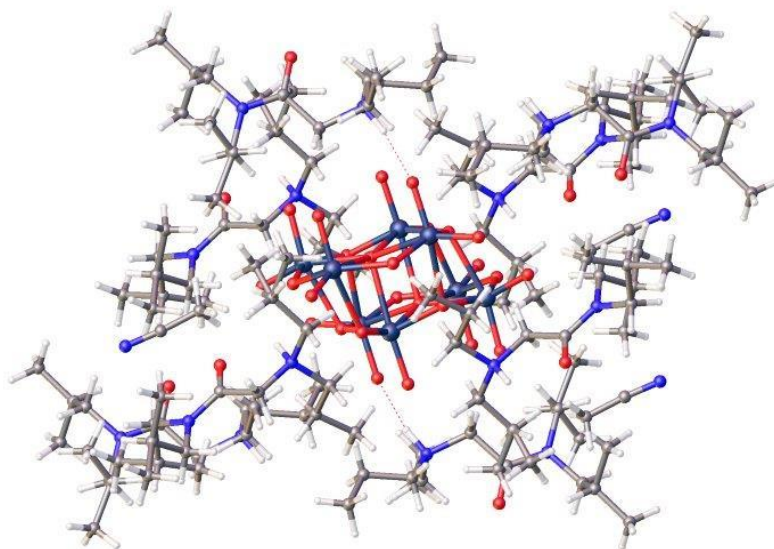


Fig. 2.17 The octamolybdate anion surrounded by eight ligands in complex **9**, $(\text{LH})_4[\text{Mo}_8\text{O}_{26}] (\text{MeCN})_2$. The dark blue balls are Mo; red balls: O; Light blue balls: N; gray balls: C; white balls: H.

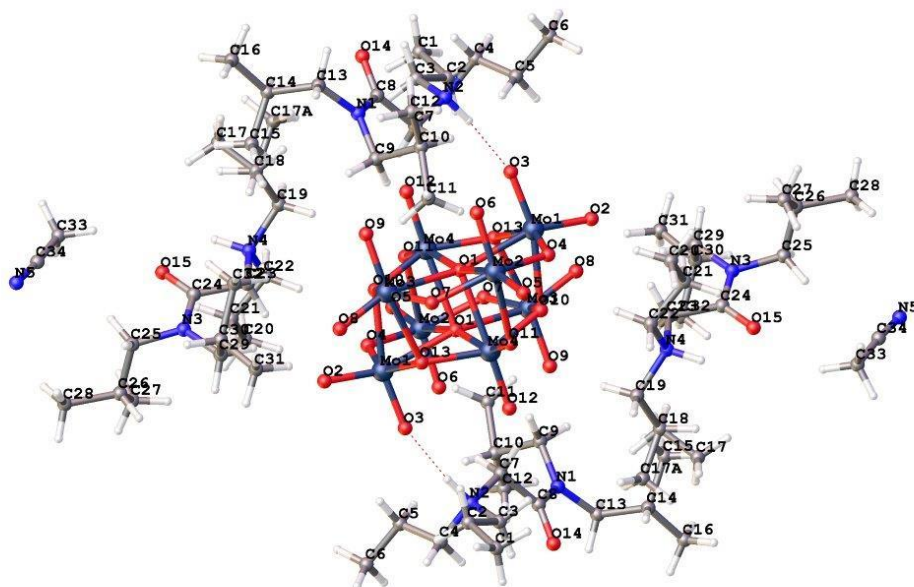


Fig. 2.18 ORTEP diagram of complex **9**, $(\text{LH})_4[\text{Mo}_8\text{O}_{26}] (\text{MeCN})_2$. The ligand N-H...O-Mo bondings are shown as dotted lines.

Table 2.3 Bond Lengths for complex **9**, (LH)₄[Mo₈O₂₆] (MeCN)₂.

Atom	Atom	Length/Å	Atom	Atom	Length/Å
C1	C2	1.529(16)	C30	C31	1.500(17)
C2	C3	1.510(16)	C30	C32	1.58(2)
C3	N2	1.495(14)	Mo1	O1	2.351(7)
C4	C5	1.460(17)	Mo1	O2	1.729(6)
C4	N2	1.481(14)	Mo1	O3	1.721(7)
C5	C6	1.54(2)	Mo1	O4	1.884(6)
C7	C8	1.518(16)	Mo1	O10 ¹	2.316(7)
C7	N2	1.512(13)	Mo1	O13	1.989(7)
C8	N1	1.346(14)	Mo2	O1	2.482(7)
C8	O14	1.244(13)	Mo2	O4	1.917(7)
C9	C10	1.59(3)	Mo2	O5	1.711(6)
C9	N1	1.484(14)	Mo2	O6	1.719(7)
C10	C11	1.57(3)	Mo2	O7	1.917(8)
C10	C12	1.32(3)	Mo2	O11 ¹	2.271(7)
C13	C14	1.540(19)	Mo3	O1	2.308(7)
C13	N1	1.462(15)	Mo3	O7	1.884(7)
C14	C15	1.47(2)	Mo3	O8	1.695(7)

C14	C16	1.50(2)	Mo3	O9	1.706(7)
C17	C18	1.29(4)	Mo3	O10	1.998(6)
C19	N4	1.510(15)	Mo3	O13 ¹	2.357(7)
C19	C18	1.493(19)	Mo4	O1	2.134(6)
C20	C21	1.519(19)	Mo4	O1 ¹	2.388(7)
C21	C22	1.514(17)	Mo4	O10	1.962(7)
C22	N4	1.510(13)	Mo4	O11	1.753(6)
C23	C24	1.520(14)	Mo4	O12	1.715(7)
C23	N4	1.487(11)	Mo4	O13	1.932(6)
C24	N3	1.351(13)	O1	Mo4 ¹	2.387(7)
C24	O15	1.212(12)	O10	Mo1 ¹	2.316(7)
C25	C26	1.52(2)	O11	Mo2 ¹	2.271(7)
C25	N3	1.464(14)	O13	Mo3 ¹	2.357(7)
C26	C27	1.45(3)	C34	N5	1.19(3)
C26	C28	1.56(2)	C34	C33	1.36(3)
C29	C30	1.486(17)	C17A	C18	1.43(3)
C29	N3	1.476(12)			

¹ Atoms generated by symmetry operation (-X,1-Y,2-Z)

2.3 Conclusions

In conclusion, α -amino-acetamides have been designed and synthesized as a new class of anion exchangers to extract molybdate anions from higher nitric acid medium. These acetamides showed better extraction behavior compared to the conventional anion exchangers, Alamine 336, Aliquat 336 and Primene JMT. The presence of amide group was critical to this success because of its intramolecular buffering effect. This study has highlighted the exact role of the amide group in retaining the extraction ability at higher acidities. Stoichiometry of metal ligand complex was ascertained by slope analysis method and was found to be $(\text{LH})_2\text{MoO}_4\cdot\text{HNO}_3$. FTIR and NMR of loaded organic indicated MoO_4^{2-} exchanged at ammonium site while buffering effect takes place at amide group.

Individual complexes of $[\text{Mo}_6\text{O}_{19}]^{2-}$ and $[\text{Mo}_8\text{O}_{26}]^{4-}$ with the same ligand are not known and we have provided two new homopolyoxomolybdate complexes of the same ligand from ammonium molybdate and acetamide **1** just by changing the reaction conditions. Based on the single-crystal analysis of these inorganic-organic hybrid compounds, the functionalized ammonium cation of ligand **1** has been incorporated for charge balance. In complex **8**, only weak (C–H \cdots O–Mo) H-bonding interaction between ligand **1** and hexamolybdate anion has been observed. The hexamolybdate anion is embedded in the cage formed by inter ligand H-bondings with antiparallel arrangement of two ligand molecules. Interestingly, complex **9** exhibits strong hydrogen-bonding between ligand **1** and β -octamolybdate anion (N–H \cdots O–Mo). Different reaction conditions may be developed using the ligand for the synthesis of other inorganic-organic hybrid polyoxomolybdates with interesting structural features and molecular properties.

2.4 Experimental

General Details:

All reactions were performed in oven-dried (120 °C) or flame-dried glass apparatus under dry N₂ or argon atmosphere.

NMR Study:

¹H NMR and ¹³C NMR spectra were recorded on a Bruker 200 MHz spectrometer. Spectra were referenced to residual chloroform (δ 7.26 ppm, ¹H; 77.00 ppm, ¹³C). Chemical shifts are reported in ppm (δ); multiplicities are indicated by s (singlet), d (doublet), t (triplet), q (quartet), quint (pentet), m (multiplet) and br (broad). Coupling constants, J, are reported in Hertz. ¹³C spectra were recorded with broadband proton decoupling.

IR Study:

IR spectra were recorded on a Nicolet Impact 410 FT IR spectrophotometer in NaCl cells or in KBr discs. Peaks are reported in cm⁻¹.

Melting Points: Melting points (mp) were determined on a Fischer John's melting point apparatus and are uncorrected.

TLC: Analytical thin-layer chromatography was performed using homemade Acme silica gel plates (about 0.5 mm).

Column Chromatography: Column Chromatography was performed using Silica Gel 230-400 mesh (for flash chromatography) obtained from Sisco Research Laboratories Pvt. Ltd.

Chemicals

Nitric acid, *n*-dodecane and isodecyl alcohol (IDA) were obtained from local sources. Alamine 336, Aliquat 336, Primene JMT, diisobutylamine, dioctylamine, dihexylamine, dipropylamine, ammonium molybdate tetrahydrate [(NH₄)₆Mo₇O₂₄·4H₂O] and other chemicals used were of analytical grade. The solvents

were dried and distilled from the indicated drying agents: THF from sodium/benzophenone; triethyl amine from CaH_2 and then stored over calcium metal.

Synthetic procedures for 1-3

N,N-Diisobutylchloroacetamide **7**

A solution of diisobutylamine (525 μL , 1 equiv, 3 mmol) in dry CH_2Cl_2 (3 mL) was drop-wise added to a stirred solution of chloroacetyl chloride (290 μL , 1.2 equiv, 3.6 mmol) in dry CH_2Cl_2 (6 mL) followed by drop-wise addition of dry triethylamine (420 μL , 1 equiv, 3 mmol) at 10-15 $^\circ\text{C}$. The reaction mixture was allowed to attain to room temperature and stirred for 24 h. The reaction mixture was diluted with water and extracted with ethyl acetate-petroleum ether mixture. The organic extract was dried over anhydrous sodium sulfate and concentrated under reduced pressure. The residue was purified by distillation to give chloracetamide **7** (523 mg, 85%).

$^1\text{H NMR}$ (200 MHz, CDCl_3): δ 0.82-1.0 (12 H, m, $2 \times \text{CHMe}_2$), 1.80-2.16 (2 H, m, $2 \times \text{CHMe}_2$), 3.14 (2 H, d, $J = 7.6$ Hz, NCH_2CH), 3.20 (2 H, d, $J = 7.6$ Hz, NCH_2CH), 4.08 (2 H, s, COCH_2Cl).

α -Dipropylamino *N,N*-diisobutylacetamide **1**

Dipropylamine (20 mL, 3 equiv, 146 mmol) was added to a stirred solution of chloracetamide **7** (10 g, 1 equiv, 48.7 mmol) in dry THF (20 mL) and the solution was heated at 80 $^\circ\text{C}$ for 3 d. The reaction mixture was diluted with water and extracted with 10% ethyl acetate-petroleum ether. The combined organic extract was dried over anhydrous sodium sulfate and concentrated under reduced pressure. The residue was distilled to give α -dipropylamino *N,N*-diisobutylacetamide **1** (10.52 g, 80%).

$^1\text{H NMR}$ (200 MHz, CDCl_3): δ 0.80-0.95 (18 H, m, $6 \times \text{CH}_3$), 1.40-1.59 (4 H, m, $2 \times \text{CH}_2\text{CH}_2\text{N}$), 1.82-2.07 (2 H, m, $2 \times \text{CHMe}_2$), 2.53 (4 H, t, $J = 7.4$ Hz, $2 \times \text{CH}_2\text{CH}_2\text{N}$),

3.16 (2 H, d, $J = 7.4$ Hz, $\text{NCH}_2\text{CHMe}_2$), 3.27 (2 H, d, $J = 7.8$ Hz, $\text{NCH}_2\text{CHMe}_2$), 3.35 (2 H, s, CH_2CO).

^{13}C NMR (150 MHz, CDCl_3): δ 11.8, 19.9, 20.1 (4 C), 26.1 (2 C), 27.3 (2 C), 52.5, 54.3, 56.1 (2 C), 57.8, 171.1.

Elemental analysis calcd. for $\text{C}_{16}\text{H}_{34}\text{N}_2\text{O}$; C, 71.06; H, 12.67; N, 10.36%; Found C, 71.16; H, 12.67; N, 10.46%.

α -Dihexylamino N,N -diisobutylacetamide **2**

A mixture of chloracetamide **7** (1 g, 1equiv, 4.87 mmol) and dihexylamine (1.42 mL, 1.25 equiv, 6.09 mmol) in triethylamine (3 mL) was heated at 90 °C for 20 h. The reaction mixture was diluted with water and extracted with 10% ethyl acetate-petroleum ether. The combined organic extract was dried over anhydrous sodium sulfate and concentrated under reduced pressure. The residue was purified by column chromatography to give amide α -dihexylamino N,N -diisobutylacetamide **2** (1.31 g, 76 %).

^1H NMR (500 MHz, CDCl_3): δ 0.83-0.93 (18 H, m, $6 \times \text{CH}_3$), 1.22-1.33 (12 H, m, $6 \times \text{CH}_2$), 1.39-1.47 (4 H, m, $2 \times \text{CH}_2\text{CH}_2\text{N}$) 1.86-1.95 (1 H, m, CHMe_2), 1.96-2.05 (1 H, m, CHMe_2), 2.48 (4 H, t, $J = 7.5$ Hz, $2 \times \text{CH}_2\text{NCH}_2\text{CO}$), 3.16 (2 H, d, $J = 7.5$ Hz, $\text{NCH}_2\text{CHMe}_2$), 3.28 (2 H, s, CH_2CO), 3.29 (2 H, d, $J = 9$ Hz, $\text{NCH}_2\text{CHMe}_2$).

^{13}C NMR (125 MHz, CDCl_3): δ 13.9 (2 C), 20.0 (2 C), 20.2 (2 C), 22.6, 26.2 (2 C), 27.0 (2 C), 27.2 (2 C), 27.4, 31.8 (2 C), 52.6, 54.4 (2 C), 54.5, 57.7, 171.2.

Elemental analysis calcd. for $\text{C}_{22}\text{H}_{46}\text{N}_2\text{O}$; C, 74.51; H, 13.07; N, 7.9%; Found: C, 74.46; H, 13.0; N, 7.92%.

α -Dioctylamino *N,N*-diisobutylacetamide **3**

A mixture of chloracetamide **7** (1 g, 1equiv, 4.87 mmol) and di-*n*-octylamine (1.84 mL, 1.25 equiv, 6.09 mmol) in triethylamine (3 mL) was heated at 90 °C for 20 h. The reaction mixture was diluted with water and extracted with 8% ethyl acetate-petroleum ether. The combined organic extract was dried over anhydrous sodium sulfate and concentrated under reduced pressure. The residue was purified by column chromatography to give amide α -dioctylamino *N,N*-diisobutylacetamide **3** (1.46 g, 73 %). **¹H NMR (500 MHz, CDCl₃):** δ 0.83-0.96 (18 H, m, 6 \times CH₃), 1.20-1.34 (20 H, m, 10 \times CH₂), 1.39-1.48 (4 H, m, 2 \times CH₂CH₂N), 1.86-1.96 (1 H, m, CHMe₂), 1.96-2.07 (1 H, m, CHMe₂), 2.48 (4 H, t, J = 8 Hz, 2 \times CH₂NCH₂CO), 3.17 (2 H, d, J = 7.5 Hz, NCH₂CHMe₂), 3.29 (2 H, s, CH₂CO), 3.30 (2 H, d, J = 7.5 Hz, NCH₂CHMe₂).

¹³C NMR (125 MHz, CDCl₃): δ 14.1 (2 C), 20.1 (2 C), 20.2 (2 C), 22.6 (2 C), 26.3, 27.1 (2 C), 27.5, 27.6 (2 C), 29.3 (2 C), 29.6 (2 C), 31.8 (2 C), 52.7, 54.4 (2 C), 54.5, 57.8, 171.3.

Elemental analysis calcd. for C₂₆H₅₄N₂O; C, 76.03; H, 13.25; N, 6.82%; Found: C, 76.07; H, 13.01; N, 6.72%.

Molybdenum feed solutions

Ammonium molybdate solutions were prepared by dissolving appropriate amount in nitric acid. Quantitative determination of molybdenum was carried out using ICP-AES (Inductively coupled plasma atomic emission Spectrophotometry technique). Detection limit for molybdenum was 1 ppm. Error in molybdenum analysis was within $\pm 5.0\%$.

Extraction studies

Prior to extraction experiments, organic phase containing the anion exchangers was pre equilibrated with equal volume of 0.5 M HNO₃ to minimize variation in nitric acid

concentration during extraction. For determination of distribution ratio (D_{Mo}), organic phase was equilibrated with equal volume of aqueous phase containing molybdate anion for 1 h in a glass vial. All the extraction experiments were carried out in a thermostated water bath maintained at temperature 25 ± 1 °C. After phase separation by centrifugation, the organic and the aqueous phase was separated and the aqueous phase was analyzed for molybdenum concentration by ICP-AES after suitable dilutions. The concentration of molybdenum in the organic phase was calculated by mass balance. The distribution ratio D_{Mo} was determined as the ratio of metal concentration in organic phase to that in aqueous phase. Percentage extraction of metal ion was determined by Equation 2.2:

$$\%E = (D_{Mo} / D_{Mo} + 1) \times 100 \quad (2.2)$$

Errors in D_M values were within $\pm 5\%$. The nitric acid concentrations of aqueous and organic phases were determined by potentiometric titration with 0.1 M NaOH using a Metrohm 905 Titrando device.

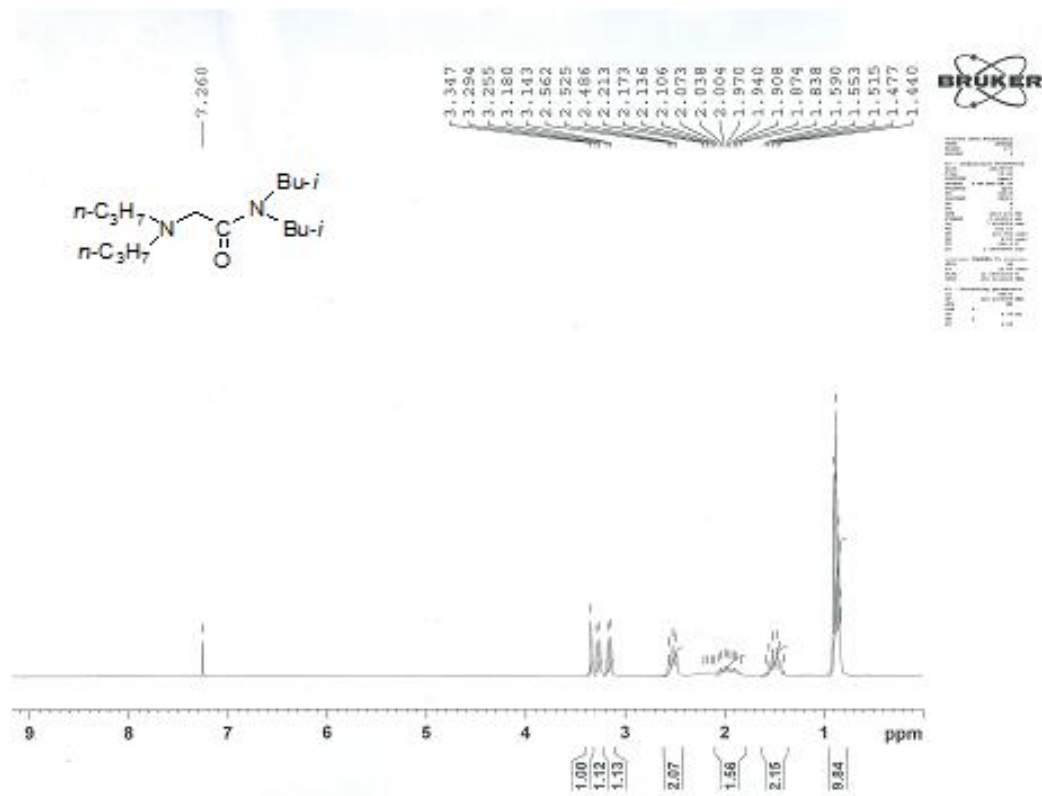


Fig. 2.19 ^1H NMR spectrum of α -amino-acetamide 1.

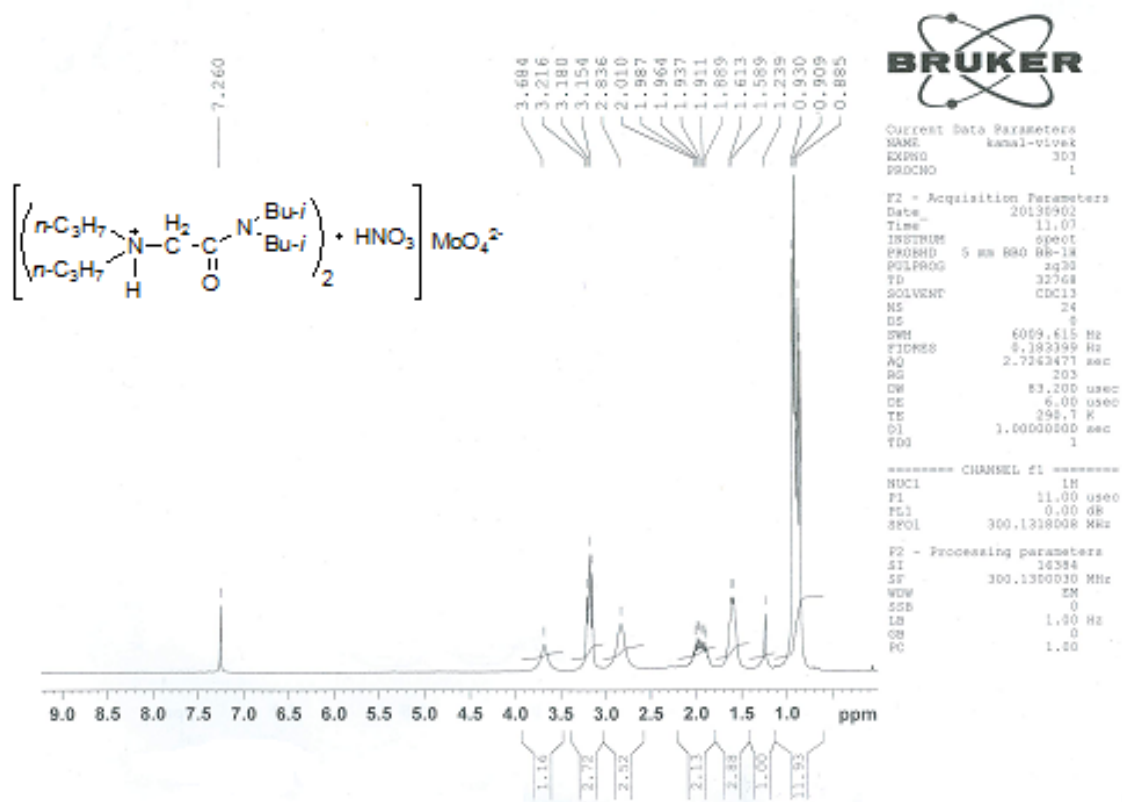


Fig. 2.20 ^1H NMR spectrum of complex of MoO_4^{2-} with α -amino-acetamide 1.

Synthesis of complex (LH)₂[Mo₆O₁₉] 8 (route A):

A solution of acetamide **1** (271 mg, 1 mmol) in chloroform (5 mL) was repeatedly contacted with fresh solution of (NH₄)₆Mo₇O₂₄·4H₂O (46 mg, 0.037 mmol) in 0.1 M aqueous HNO₃ (5 mL). The chloroform extract was concentrated under reduced pressure to give a yellow precipitate of metal ligand complex. The precipitate was triturated with 10% ethyl acetate-hexane solution to remove excess ligand **1**. The light yellow solid residue was then crystallized from acetonitrile to obtain the yellow crystalline complex **8** (603 mg, 85%). **IR (KBr):** $\bar{\nu}$ 3450, 3109, 2960, 2877, 1643 (C=O), 1464, 1387, 1257, 1157, 953 (Mo=O), 800, 592 (Mo-O-Mo), 436 cm⁻¹.

Synthesis of Mo crystal (LH)₂[Mo₆O₁₉] 8 (route B):

A solution of (NH₄)₆Mo₇O₂₄·4H₂O (84 mg, 0.068 mmol) in 0.5 M HNO₃ (3 mL) was added to a solution of acetamide **1** (55 mg, 0.204 mmol) in MeOH (2 mL) and the reaction mixture was stirred at room temperature for 5 h. The reaction mixture was filtered and the yellow precipitate was washed with 10% ethyl acetate-hexane solution to remove the excess ligand **1**. The yellow powder was crystallized from acetonitrile to give light yellow crystals of complex **8** (79 mg, 81%).

Synthesis of Mo crystal (LH)₄[Mo₈O₂₆] 9:

A solution of (NH₄)₆Mo₇O₂₄·4H₂O (42 mg, 0.034 mmol) in water (2 mL) was added to a solution of acetamide **1** (64.3 mg, 0.238 mmol) in MeOH (1 mL). The reaction mixture was stirred at 100 °C for 3 h, brought to room temperature and concentrated under reduced pressure to give a white precipitate. The precipitate was filtered and washed with 10% ethyl acetate-hexane solution to remove the excess ligand **1**. The

white powder was crystallized from acetonitrile to give colourless crystals of complex **9** (59 mg, 74%). **IR (KBr):** $\bar{\nu}$ 3467, 2964, 2939, 2875, 1647 (C=O), 1471, 1431, 1369, 944, 913 (Mo=O), 848, 714, 664 (Mo-O-Mo), 557, 525 cm^{-1} .

X-ray crystallographic studies

Single crystal X-ray diffraction data were collected on Agilent Supernova system equipped with a microfocus Cu-source ($\lambda = 1.54184 \text{ \AA}$) and a Titan CCD detector. The crystals were separated, coated with paraffin oil and mounted on a loop for X-ray diffraction data collection at room temperature (293K). The data reduction and analysis were carried out with CrysAlisPro software suit. Analytical absorption correction using a multifaceted crystal model based on expressions derived by Clark & Reid [93] and as implemented in the CrysAlisPro software suit was carried out for both the crystals. The structures were solved by direct method using Shelxs and refined using Shelxl softwares [94] using Olex2 interface [95]. All the nonhydrogen atoms were refined anisotropically and hydrogens were generated at their idealized positions and refined isotropically according to riding model.

CHAPTER 3

*Comparative studies on radiolytic degradation of
deuterium labeled and unlabeled tributyl phosphates*

3.1 Introduction

PUREX process is used for recovery of unused fissile materials remained in spent fuel after nuclear processes [96]. The process is followed worldwide due to its high efficiency. Tributyl phosphate **10** (TBP) (Fig. 3.1) [97] is used as a solvent in this process for extraction of U and Pu from the spent fuel. TBP is also used in front-end of nuclear fuel cycle for extraction of uranium from various resources as well as for isolation and purification of rare-earth elements, used in nuclear reactors.

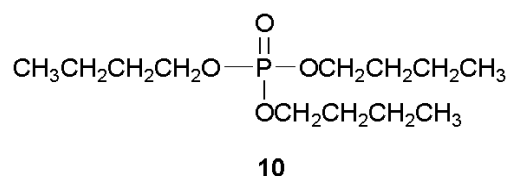
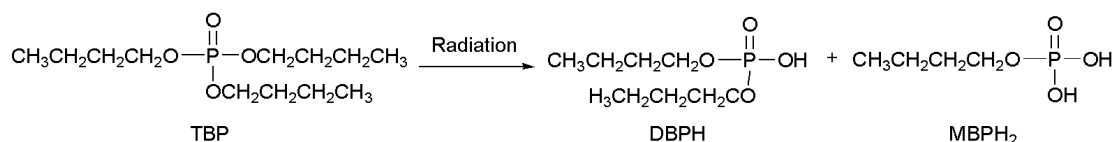


Fig. 3.1 Structure of tributyl phosphate.

In the separation process of metal ions from spent nuclear fuel, the extractants have to face highly radioactive environment and acidic conditions due to the presence of large quantities of α, β, γ emitting nuclei present in spent fuel and HNO_3 dissolver, respectively. Most of the extractants and diluents used for separation purposes are made up of organic molecules which are prone to degrade by the highly acidic oxidizing media provided by nitric acid. Highly radioactive solutions also rapidly decompose the molecules by the radiolytic production of organic radicals [98]. Sometimes the degraded products of the extractant don't affect the separation processes considerably if they don't coordinate with any metal ion present in feed solution. In those cases, degradation of the extractant can be ignored. But if the degradation products coordinate with undesired metal ions then they adversely affects the various steps of extraction by several means and it becomes imperative to improve the radiolytic and hydrolytic stability of the extractant.

In PUREX process, 30% TBP is used in *n*-dodecane to recover Pu and U from highly active spent fuel from 3-4 M HNO₃. Thus, TBP/*n*-dodecane is continuously exposed to a high radiation dose in contact with HNO₃. In case of TBP, the hydrolytic degradation is minimal but radiolytic degradation is known to be considerable [99]. Under radiolytic conditions, TBP tends to undergo degradation to different extent forming varying amount of harmful mono and dibutyl hemiesters of phosphoric acid (DBPH and MBPH₂) [12, 100-102] (Scheme 3.1). Besides, some other products like TBP dimers, oxygenated derivatives of TBP/TBP dimers also produced during radiolysis in smaller extent compare to MBPH₂ and DBPH [103-107]. In neat HNO₃ medium, TBP is quite stable but in presence of radiation HNO₃ also affects the degradation of TBP. The radiolysis of TBP in the presence of HNO₃ produce nitrated phosphates [101, 108, 109].



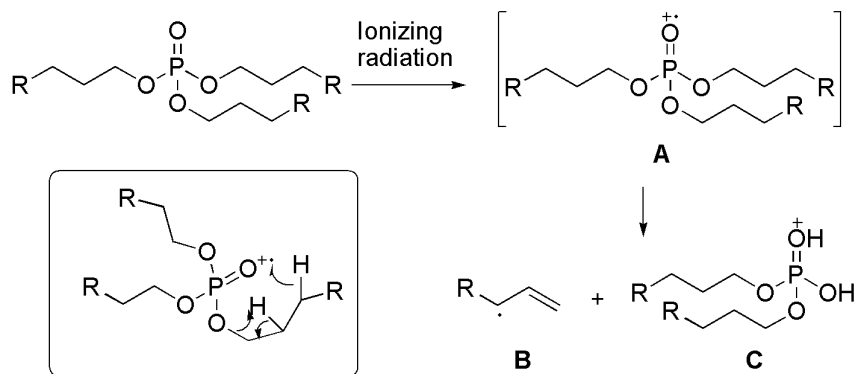
Scheme 3.1 Major degradation products of TBP after radiolysis.

Sometimes it is found that the diluents also sensitize the degradation of extractant in radiolytic conditions. Besides the own degradation products of TBP, diluent such as *n*-dodecane or kerosene also play important role in radiolytic degradation of TBP. Diluents form various products by diluent nitration and also produce higher molecular weight acidic phosphates from TBP radiolysis. Stable diluents with higher ionization potential than TBP also increase the production of DBPH [110, 111]. MBPH₂ and DBPH along with other degradation products act as an extract for many metal ions present in PUREX feed. This result in loss of metal ion selectivity during the process. These acidic products bind with Pu and inhibit it's back

extraction. Therefore recovered solvent which has contaminated with significant amount of Pu bonded with hemiacids, has a huge of residual activity [112-115]. The degradation products also cause poor phase separation during various stages of the extraction processes [12], thus impair the performance of the solvent. The deleterious properties of the degraded solvent make it unsuitable for further recycling and thus, the solvent needs to be disposed. This leads to generation of good amount of organic radioactive wastes which are highly radiotoxic and hazardous to the environment as it contains Pu along with other active metals. Therefore, in order to reduce the amount of organic radioactive waste, it becomes crucial to improve the radiolytic stability of TBP.

Degradation of TBP involves two possible degradation pathways such as direct and indirect radiolysis. In direct radiolysis, the ionizing radiation interacts with TBP and causes its degradation. In indirect process, the reactive species initially created by direct radiolysis of the medium *i.e.* dodecane, water and HNO₃ diffuse into bulk solution and reacts with TBP.

From the radiolysis study of neat TBP and other trialkyl phosphates, Wilkinson and Williams [116] have proposed a conceivable degradation pathway for direct radiolysis as depicted in Scheme 3.2. Ionizing radiation initiates the degradation of TBP by the formation of the oxygenated radical cation **A**. This initially formed radical cation subsequently undergoes intramolecular rearrangement by abstraction of hydrogen from butyl chain and hence produces a hydrocarbon fragment **B** and protonated hemiester of phosphoric acid **C**. As an allyl radical is stabilized, *n*-alkyl substituents having 3 carbon atoms and beyond favored this degradation pathway.



Scheme 3.2 Mechanism of degradation of TBP by direct radiolysis.

In indirect process, the reactive species primarily formed by the direct radiolysis of the medium. These species are hydroxyl radical ($\dot{\text{O}}\text{H}$), nitrogen trioxide radical ($\dot{\text{N}}\text{O}_3$), nitrogen dioxide radical ($\dot{\text{N}}\text{O}_2$) and alkane radicals ($\dot{\text{C}}_n\text{H}_{2n+1}$) etc. The initially formed $\dot{\text{O}}\text{H}$ radical abstract a hydrogen atom from the butyl chain of TBP and mainly produce a γ C-centered radical $(\text{C}_4\text{H}_9\text{O})_2\text{P}(=\text{O})(\dot{\text{C}}_4\text{H}_8\text{O})$ [117]. This C-centered radical can react with oxygen, and subsequently superoxide elimination and hydrolysis gives DBPH. Other than these reactions, C-centered radical also produces all possible TBP dimers and higher molecular weight phosphates. TBP dimers are formed by combination of two C-centered TBP radicals while a combination of a C-centered TBP radical and an alkane radical produce higher molecular weight phosphates. Formations of some nitrated derivatives also take place by addition of $\dot{\text{N}}\text{O}_3$ or $\dot{\text{N}}\text{O}_2$ radicals [99]. The above processes clearly indicate that abstraction of hydrogen atom (H) either intramolecular or intermolecular plays key role in the degradation of TBP.

According to kinetic isotope effect the rate of reaction is dependent on the isotopic identity of an atom in a reactant. When the isotopic substitution is performed in a chemical bond which is forming or deforming in rate determining step, it greatly modify the reaction rate and is called primary kinetic isotope effect. For example, the primary kinetic isotope effect on the deprotonation of C-H acids *i.e.* $k_{\text{H}}/k_{\text{D}} = 2-7$ [118].

In some exceptional cases, $k_H/k_D = 24-70$ or more. This is attributed to the participation of quantum mechanical tunnel effects [119]. In such type of cases replacement of H atoms with D atoms results in higher stability of respective molecules.

Literature shows some evidences of positive kinetic isotope effect for substitution of hydrogen by deuterium with γ -irradiation. Gillbro and Lund has shown an unusual formation of alkyl radicals in γ -irradiated single crystals of *n*-decane- d_{22} doped with 0.1-0.25 mol% of *n*-decane wherein $\text{CH}_3\dot{\text{C}}\text{HCH}_2$ - type radical are present in about 100 times more amount than that expected to be formed by the direct action of γ -irradiation [120]. Miwa and co-workers have shown a large kinetic isotope effect ($k_H/k_D = 8.6-10.1$) in the intramolecular H abstraction while a moderate to low kinetic isotope effect ($k_H/k_D = 1.7-3.1$) in intramolecular deprotonation [121].

3.2 Present work

Previous studies related to positive kinetic isotope effect in γ -irradiation encouraged us to hypothesize that substitution of the H atoms of the butyl chain of TBP with D atoms might improve its radiolytic stability as a result of primary kinetic isotope effect [118, 119, 122-128] *i.e.*, the higher stability of the C-D bond than compare to the C-H bond. The secondary kinetic isotope effect [129] might also work to enhance the stability of C-O/O-P bonds. Hence, deuterium might act as an effective protecting group for hydrogen and might improve the hydrolytic and radiolytic stability of TBP. Beside this, deuterium has some unique properties. D has smaller effective radius and this property is very useful in kinetics of complexation/decomplexation, as many extractants do not tolerate substitutions in complexation process during extraction because of increase in the steric crowding. The other interesting property of deuterium is that it is NMR active. The spin value of deuterium is $I = 1$ result in easy characterization of deuterated compounds by NMR.

To this end we synthesized different *d*-labelled TBPs deuterated at four different positions of butyl chain viz (α,α)₃-*d*₆ labeled **11**, (β,β,γ)₃-*d*₉ labeled **12**, ($\gamma,\gamma,\delta,\delta$)₃-*d*₁₂ labeled **13** and per-deuterated TBPs **14** (Fig. 3.2) with good to excellent isotopic purities (60-99%). A comparative study of degradation behavior of deuterated TBPs (*d_n*-TBPs) in comparison with undeuterated TBP was performed. Extraction behavior of all *d_n*-TBPs was also compared after absorption of particular doses.

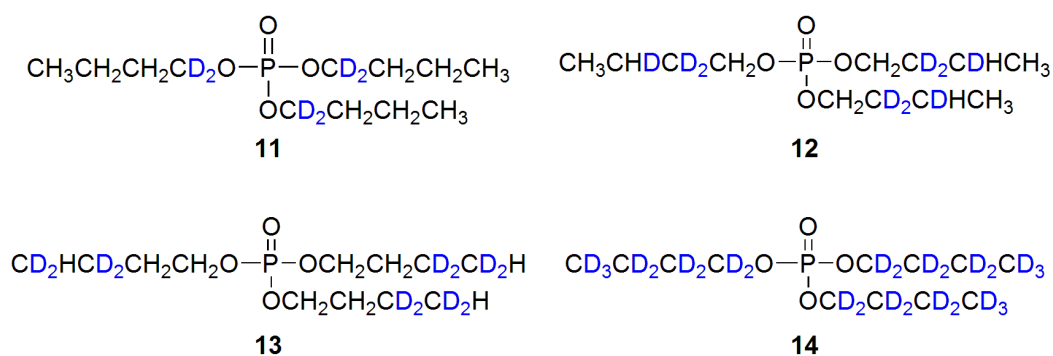
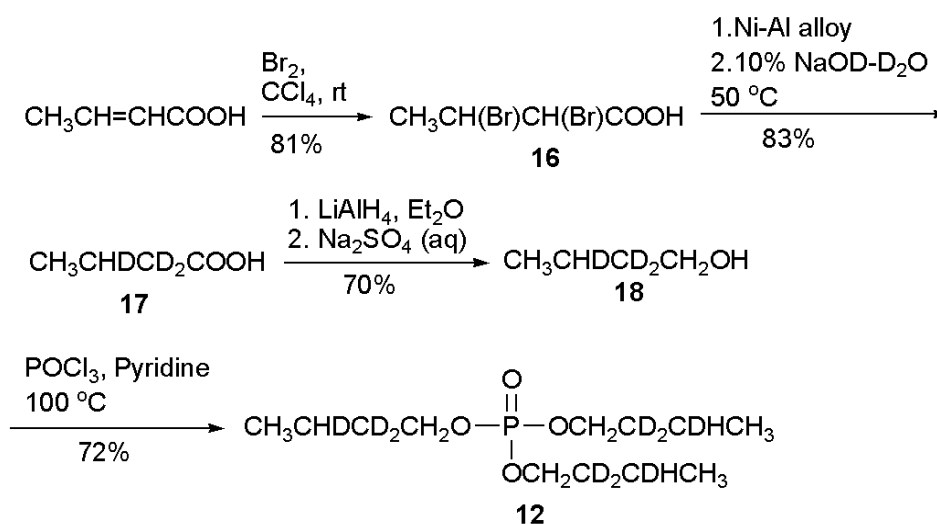


Fig. 3.2 Structures of different *d_n*-TBPs viz (α,α)₃-*d*₆ TBP **11**, (β,β,γ)₃-*d*₉ TBP **12**, ($\gamma,\gamma,\delta,\delta$)₃-*d*₁₂ TBP **13** and per-deuterated TBP **14**.

3.2.1 Synthesis of deuterated TBPs

Undeuterated TBP was obtained from commercial source and used after distillation while deuterated TBPs were synthesized using various steps in our laboratory as presented in Schemes 3.3-3.6. (α,α)₃-*d*₆ TBP **11** has already been reported and the synthesis has been briefly described by Lamouroux et. al. [105] with 31% yield starting from (α,α)-dideuterated butanol **15** and POCl₃. We also achieved the same starting from butanoic acid and with an overall improved yield of 77%. Reduction of butanoic acid with lithium aluminium deuteride (99 atom % D) gave the (α,α)-dideuterated butanol **15** in 88% yield (Scheme 3.3). (α,α)-dideuterated butanol **15** further reacted with freshly distilled POCl₃ in benzene solution in the presence of pyridine as a base to give the desired (α,α)₃-*d*₆ TBP **11** with very high isotopic purity (99%) as ascertained by ¹H

Synthesis of $(\beta,\beta,\gamma)_3-d_9$ TBP **12** was achieved from commercially available crotonic acid. As presented in Scheme 3.4, bromination of crotonic acid has been carried out to give 2,3-dibromobutyric acid **16** as a white solid in very good yield (81%). Acid **16** was further subjected to a reductive debromination and incorporation of deuterium was also carried out in the same step. Debromination has been achieved using Ni–Al alloy with 10% NaOH in D_2O in closed conditions as reported for 2,3-dibromovaleric acid [130]. The reaction was mediated by NaOD formed in situ. This provided the $\beta,\beta,\gamma-d_3$ butyric acid **17** in 83% yield and with 60% isotopic purity as adjudged from 1H NMR (Fig. 3.4). The deuterated acid **17** was reduced with lithium aluminium hydride to give $\beta,\beta,\gamma-d_3$ butanol **18** in 70% yield. To obtain $(\beta,\beta,\gamma)_3-d_9$ TBP **12**, $\beta,\beta,\gamma-d_3$ butanol **18** was reacted with $POCl_3$ and pyridine following the same procedure used for the synthesis of **11**.



Scheme 3.4 Synthesis of $(\beta,\beta,\gamma)_3-d_9$ TBP **12**.

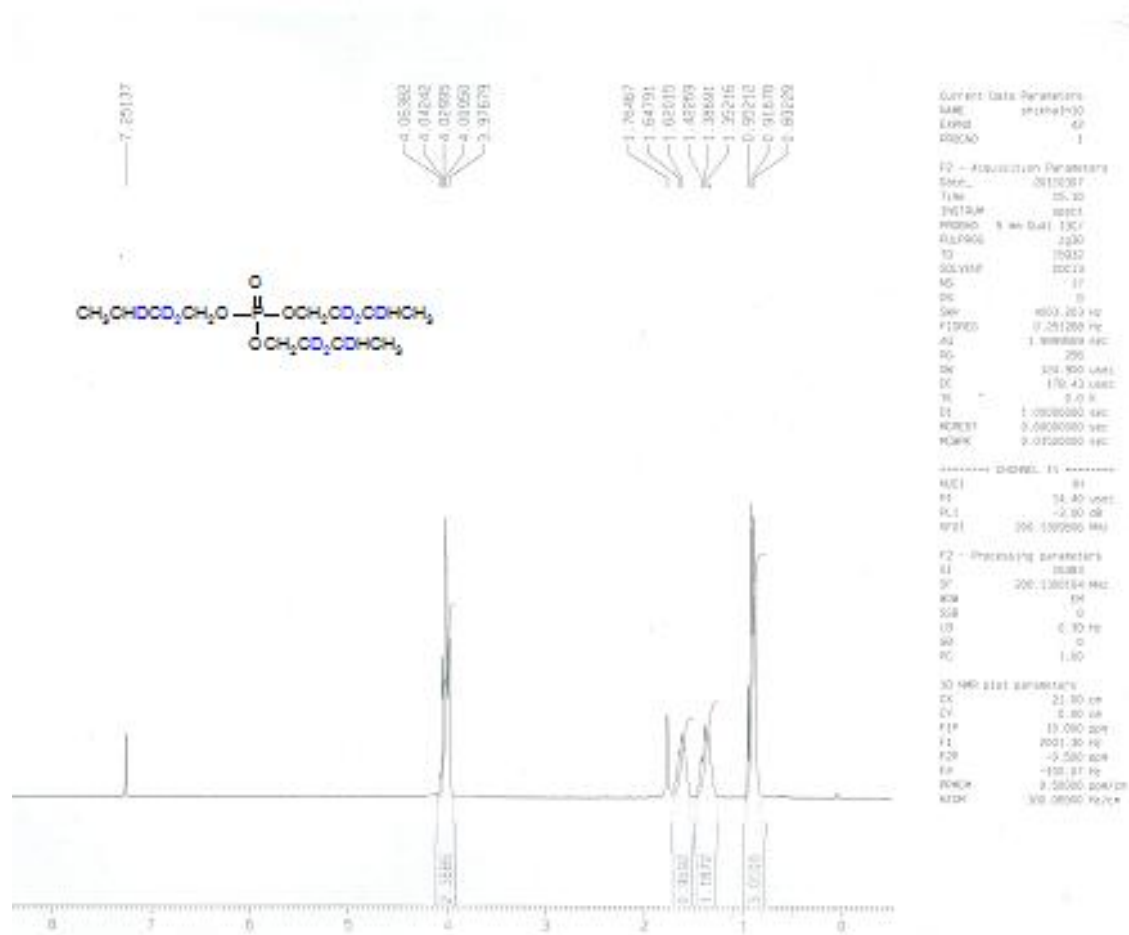


Fig. 3.4 ^1H NMR spectrum of $(\beta,\beta,\gamma)_3\text{-}d_9$ TBP **12**.

The synthesis of $(\gamma,\gamma,\delta,\delta)_3\text{-}d_{12}$ TBP **13** is presented in Scheme 3.5. The synthesis was started with but-3-yne-1-ol. First we tried to reduce but-3-yne-1-ol using D_2 gas in the presence of Pd catalyst, but the yield of the desired material was poor. We modified the route and first but-3-yne-1-ol was reacted with POCl_3 in presence of pyridine (Scheme 3.5) to obtain tri-3-butynylphosphate **19** in 78% yield. The phosphate **19** was reduced using deuterium gas (deuterium content 60%) in the presence of catalytic amount of Pd/C to give $(\gamma,\gamma,\delta,\delta)_3\text{-}d_{12}$ TBP **13** in very good yield (91%). Isotopic purity (60 %) of **13** was ascertained by ^1H NMR (Fig 3.5).

3.2.2 Radiolytic stability studies of undeuterated and deuterated TBPs

In the PUREX process, TBP solvent system is used in the form of a 30% TBP **10** solution in *n*-dodecane [96]. Considering this fact, to obtain a simulated condition, a set of solutions containing of 30% each of TBP **10** or its individual deuterated analogs **11**–**14** in *n*-dodecane were prepared. These solutions are saturated separately with 3.0 or 1.5 M HNO₃. Thus saturated organic phases of total 10 separate samples were taken in different vials and irradiated with γ -rays using ⁶⁰Co source. Decay curves were obtained by quantitative analysis of the irradiated samples using gas chromatography. For decay curves the ratios of the residual concentrations of TBP or *d_n*-TBPs to their initial concentrations were plotted against the absorbed dose as shown in Figs. 3.6 and 3.7 (for 1.5 M HNO₃ and 3.0 M HNO₃, respectively). The slope of the lines in the plots signifies the extent of degradation by irradiation. From these plots it is evident that the decrease in the concentrations of TBP and *d_n*-TBPs on irradiation was almost same. The slope of the lines was estimated using Eq. (3.1) as defined by Mincher and Curry [131].

$$C = C_0 \exp(-kd) \quad (3.1)$$

Here, C is the concentration in mol L⁻¹ of TBPs after irradiation, C₀ is the initial concentration of TBPs before irradiation, d is the dose absorbed by the sample in kGy and the coefficient k (kGy⁻¹) is dose constant. The dose constant is useful to evaluate the degree of the radiolytic degradation by irradiation and can be obtained from the slope of the decay curves. From Figs. 3.6 and 3.7, the slopes for *d_n*-TBPs and undeuterated TBP were found to be almost same, and are shown in Table 3.1. It therefore, signifies that the labeling of deuterium on TBP, apparently, has not resulted in any enhancement on the stability during irradiation.

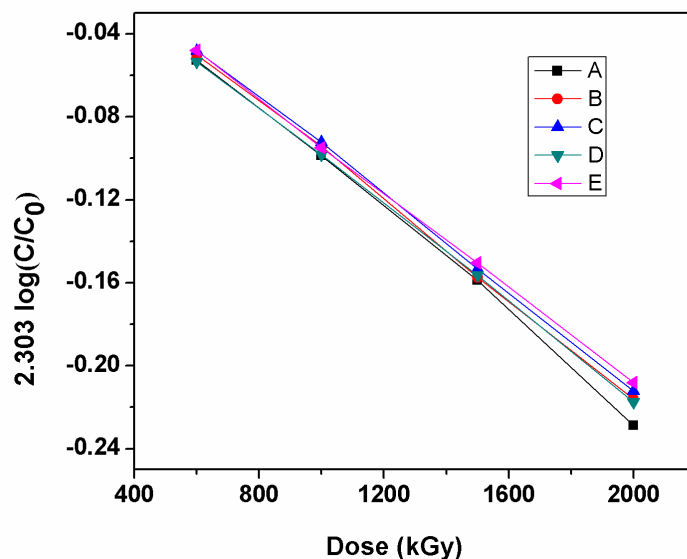


Fig. 3.6 Degradation curves of TBPs saturated with 1.5 M nitric acid as a function of absorbed dose. A, B, C, D, E are individual 30% solution of TBP **10** and its deuterated analogs **11-14** in *n*-dodecane, respectively.

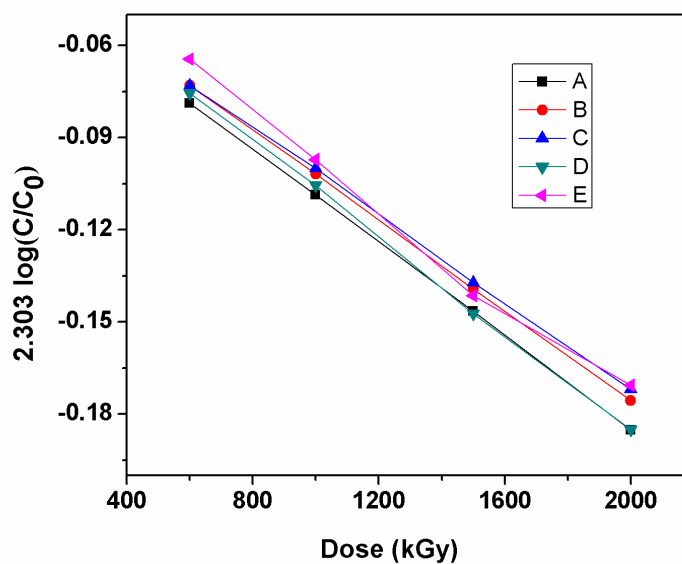


Fig. 3.7 Degradation curves of TBPs saturated with 3.0 M nitric acid as a function of absorbed dose. A, B, C, D, E are 30% solution of TBP **10** and its deuterated analogs **11-14** in *n*-dodecane, respectively.

The plots also indicated that at an absorbed dose of 2000 kGy, the percentage reduction in TBPs were from 30 to ~25% for samples saturated with 3.0 M nitric acid. It corresponds to about 17% degradation on the basis of 100% TBP. While, for samples saturated with 1.5 M nitric acid this reduction was from 30 to ~24%, which corresponds to about 20% degradation of 100% TBP. This difference is not significant, thus, implies similar degradation pattern in both the conditions.

For evaluation of the extent of degradation, the radiation chemical yield ‘G’ is also considered to be an important factor. ‘G’ can be defined as μmole of TBP decreased by absorption of 1 Joule of energy, is calculated by using Eq. (3.2) [132].

$$G = 10^3 \cdot C_0 \cdot k / \rho \quad (3.2)$$

Where ρ is the density of 30% solutions of undeuterated/ d_n -TBPs in n -dodecane in g/mL. G values were calculated for each sample of d_n -TBPs from the Equation 3.2. Obtained G values (Table 3.1) were found to be almost similar for each sample and also found to be close to the reported value of unlabeled TBP [133]. Almost similar G values for all TBP samples supports comparable radiolytic stabilities of both undeuterated and d_n -TBPs in n -dodecane.

We were also interested to see the percentage formation of MBPH₂ and DBPH in each sample as these two major degradation products of TBP have detrimental effect on PUREX process. The % MBPH₂ and DBPH formed after irradiation were plotted against the absorbed dose. At 2000 kGy, the % formation of MBPH₂ was about 5.5 and 7% (with respect to 100% TBP) for solvent saturated with 3.0 and 1.5 M nitric acid, respectively as shown in Figs 3.8 and 3.9. Likewise, DBPH formation was about 3.7 and 4.5% for solvent saturated with 3.0 and 1.5 M nitric acid, respectively as shown in

Figs. 3.10 and 3.11. Here also, the results were found to be very close for undeuterated and deuterated TBPs.

Table 3.1 Values of k and G for different TBPs.

	k (kGy ⁻¹)		G (μ mol. J ⁻¹)	
	1.5 M	3.0 M	1.5 M	3.0 M
TBP 10	-1.253E-4	-0.7608E-4	0.168 ± 0.02	0.102 ± 0.05
(α,α) ₃ - d_6 TBP 11	- 1.194E-4	-0.7344E-4	0.159 ± 0.04	0.098 ± 0.05
(β,β,γ) ₃ - d_9 TBP 12	-1.178E-4	-0.7106E-4	0.156 ± 0.01	0.094 ± 0.09
($\gamma,\gamma,\delta,\delta$) ₃ - d_{12} TBP 13	-1.171E-4	-0.7884E-4	0.154 ± 0.07	0.104 ± 0.02
Per-deuterated TBP 14	-1.171E-4	-0.7701E-4	0.147 ± 0.04	0.099 ± 0.06

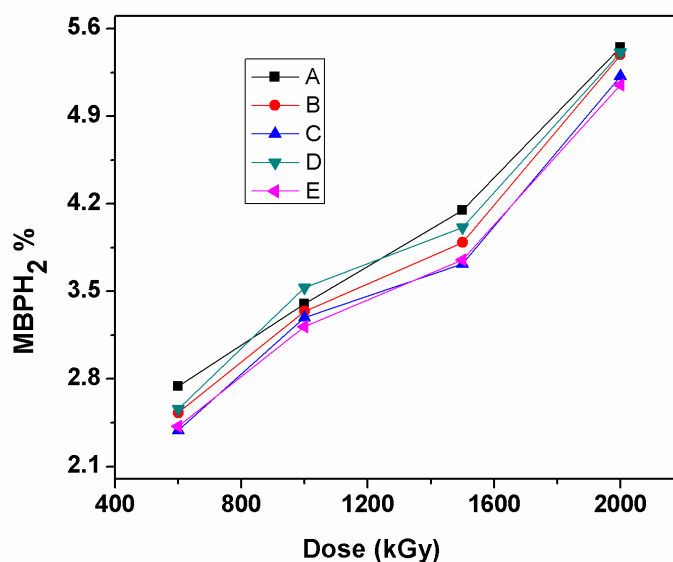


Fig. 3.8 MBPH₂ formation as a function of absorbed dose for TBPs saturated with 3.0 M nitric acid. A, B, C, D, E are individual 30% solution of TBP **10** and its deuterated analogs **11-14** in *n*-dodecane, respectively.

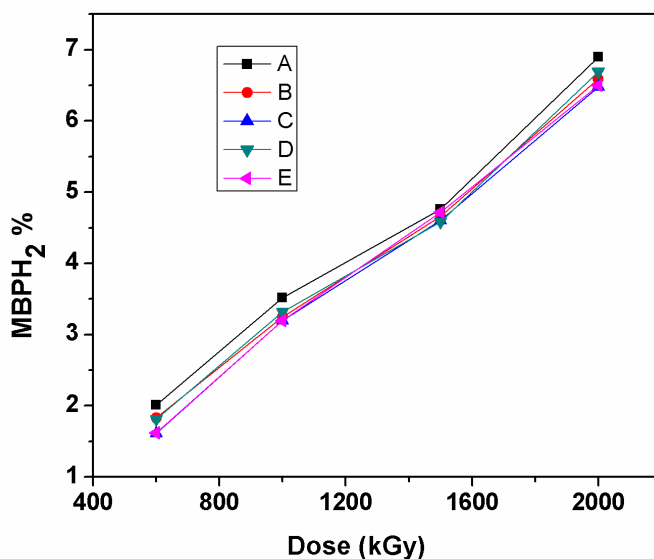


Fig. 3.9 MBPH₂ formation as a function of absorbed dose for TBPs saturated with 1.5 M nitric acid. A, B, C, D, E are individual 30% solution of TBP **10** and its deuterated analogs **11-14** in *n*-dodecane, respectively.

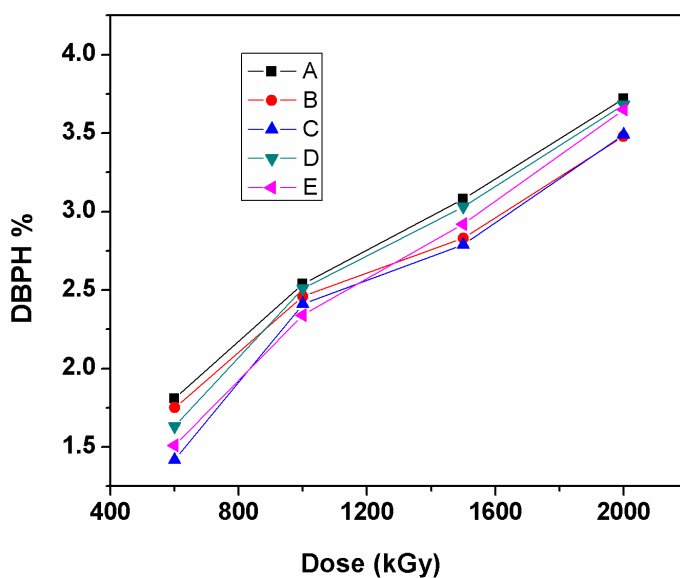


Fig. 3.10 DBPH formation as a function of absorbed dose for TBPs saturated with 3.0 M nitric acid. A, B, C, D, E are individual 30% solution of TBP **10** and its deuterated analogs **11-14** in *n*-dodecane, respectively.

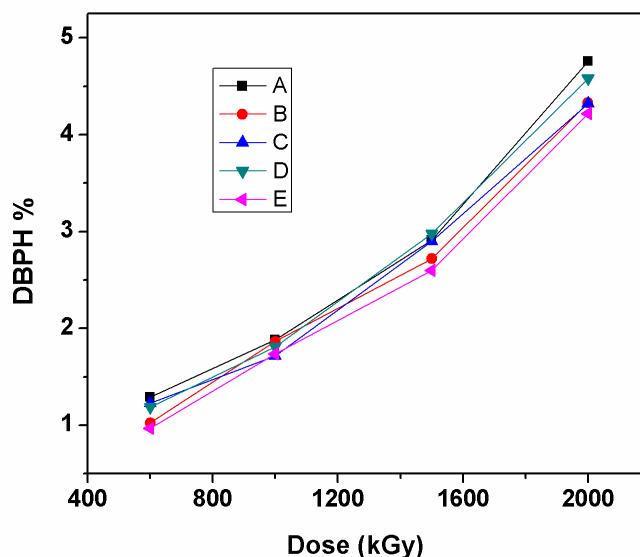


Fig. 3.11 DBPH formation as a function of absorbed dose for TBPs saturated with 1.5 M nitric acid. A, B, C, D, E are individual 30% solution of TBP **10** and its deuterated analogs **11-14** in *n*-dodecane, respectively.

3.2.3 Extraction properties of natural and deuterated TBPs

In order to evaluate extraction properties of undeuterated and d_n - TBPs after absorption of particular doses, the distribution ratios of Pu(IV) for the irradiated solvents (saturated with 1.5 M nitric acid) were plotted as a function of absorbed dose. Results are shown in Fig. 3.12 for feed acidity 3.0 M HNO₃ (extraction condition) and Fig. 3.13 for feed acidity 0.5 M HNO₃ (stripping condition). Distribution ratios were found to increase with increase in absorbed dose for all samples. The higher D_{Pu} values at higher absorbed doses, for both the feed acidities, are due to the presence of acidic degradation products like DBPH and MBPH₂. As the formation of these acidic compounds increase with increase in absorbed dose, the D_{Pu} also increases with dose at both the acidities [112]. The extraction behaviors of deuterated TBPs were found to be comparable with undeuterated one.

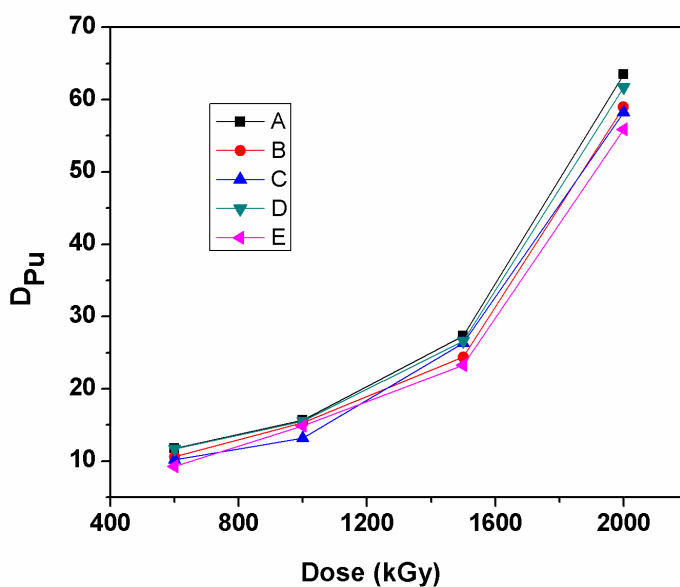


Fig. 3.12 Extraction of plutonium as a function of absorbed dose. Aqueous phase: 3.0 M HNO₃; A, B, C, D, E are individual 30% solution of TBP **10** and its deuterated analogs **11-14** in *n*-dodecane, respectively.

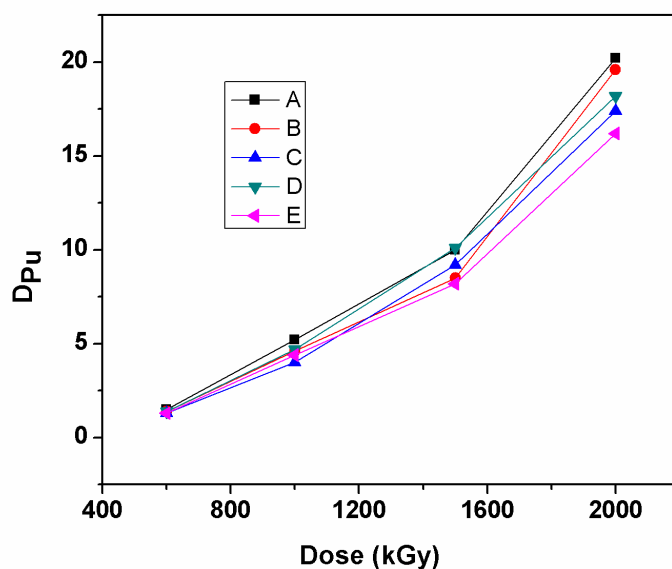


Fig. 3.13 Extraction of plutonium as a function of absorbed dose. Aqueous phase: 0.5 M HNO₃ (stripping conditions); A, B, C, D, E are individual 30% solution of TBP **10** and its deuterated analogs **11-14** in *n*-dodecane, respectively.

3.2.4 Hydrolysis of TBPs

As the TBP has to face highly acidic conditions along with radiolytic environment in extraction process, it is also important to evaluate and compare the hydrolytic stability of undeuterated and d_n -TBPs. The hydrolysis experiments were carried out in 4.0 M nitric acid at room temp for 1 month. No degradation product was found by gas chromatographic analysis for all TBPs. Distribution ratios for UO_2^{2+} (VI) and Pu(IV) were also determined and values are given in Table 3.2 shows no change in distribution ratios after hydrolysis. The trend was same for all TBPs.

Table 3.2 Distribution ratios for undeuterated TBP **10** and d_n -TBPs **11-14** before and after hydrolysis.

Metal ion	[HNO ₃] Feed (M)	Distribution ratio				
		TBP 10	(α,α) ₃ - d_6 TBP 11	(β,β,γ) ₃ - d_9 TBP 12	($\gamma,\gamma,\delta,\delta$) ₃ - d_{12} TBP 13	Per-deuterated TBP 14
UO_2^{2+}	3.0	11.08	11.17	11.28	11.12	11.30
(before hydrolysis)	0.01	0.15	0.18	0.16	0.18	0.15
UO_2^{2+}	3.0	12.11	11.50	11.14	11.80	12.10
(after hydrolysis)	0.01	0.16	0.19	0.18	0.19	0.16
Pu(IV)	3.0	5.09	4.66	4.98	4.70	4.99
(before hydrolysis)	0.5	0.11	0.12	0.09	0.11	0.13
Pu(IV)	3.0	5.02	4.78	4.98	4.77	4.88
(after hydrolysis)	0.5	0.12	0.11	0.13	0.09	0.10

3.3 Conclusion

The radiolytic and hydrolytic stability of deuterium labeled tributyl phosphates (d_n -TBPs) in comparison with undeuterated TBP in n -dodecane has been studied. The

results showed very similar extent of degradation for undeuterated and deuterated TBPs. Extraction behavior was also showed similar trend for all irradiated TBPs. Therefore, it is apparent that deuteration at different positions on butyl chains of TBP has not resulted in any enhancement of stability under present radiolytic and hydrolytic conditions. Earlier the deuterium labeled TBPs have been subjected to radiolytic study to find out the mechanism of dimerization of TBP by mass spectroscopy but the comparison of their relative stabilities of labeled and unlabeled TBPs have not been attempted. The present study is the only effort made in this direction to quantify such an effect although with neutral results. This may be due to more complex mechanisms involved in the radiolysis of multicomponent system involving TBP, the hydrocarbon diluent and aqueous nitric acid. The solvent constitute large amount of diluent (*n*-dodecane) and it is already known [12, 134] that the degradation of TBP is sensitized by the diluents, therefore, stability of dodecane is also to be considered. Even though the results are neutral, the study can be useful for the researchers working in this direction.

3.4 Experimental

General Details

As described in chapter 2.

Synthesis of d_n -TBPs

Synthesis of $(\alpha,\alpha)_3-d_6$ TBP 11

Synthesis of $\alpha,\alpha-d_2$ -butanol **15**: A 250 mL three-necked flask equipped with a reflux condenser, a dropping funnel and a magnetic stirrer was charged with lithium aluminum deuteride (2 g, 47.6 mmol) under nitrogen atmosphere. The flask was cooled on an ice-water bath and dry diethyl ether (100 mL) was carefully introduced into it via the dropping funnel. A solution of butyric acid (5.5 mL, 60 mmol) in diethyl ether (50

mL) was then added slowly into the flask at 0 °C. After completion of addition the reaction mixture was slowly allowed to come to room temperature. The reaction mixture was then heated under reflux for 10 h. For quenching of excessive LiAlH₄ the reaction mixture was cooled on an ice-water bath and quenched carefully with a saturated solution of sodium sulphate. After quenching reaction mixture becomes thick. Diethyl ether (50 mL) was added to the thick reaction mixture and filtered through a Celite pad. The residue was washed with diethyl ether and the combined filtrate was evaporated. The residue was distilled to give α,α -d₂-butanol **15** (4.02 g, 52.81 mmol, 88%) as a colourless liquid. Obtained α,α -d₂-butanol **15** was stored over molecular sieves for next reaction. Isotopic purity: 99%. **B. P.** 117-120 °C.

IR (film): 3337, 2960, 2930, 2873, 2196, 2097, 1464, 1379, 1159, 967 cm⁻¹.

¹H NMR (200 MHz, CDCl₃): δ 0.93 (3 H, t, $J = 7.2$ Hz, CH₃CH₂), 1.32- 1.46 (2 H, m, CH₃CH₂), 1.46-1.61 (2 H, m, CH₂CD₂), 1.71-1.91 (1 H, br, OH).

Synthesis of (α,α)₃-d₆ TBP **11**: A 50 mL two-necked round-bottomed flask, fitted with a reflux condenser, a stirring bar and a dropping funnel was charged with α,α -d₂-butanol **15** (5 g, 65.7 mmol), pyridine (5.8 mL, 71.5 mmol) and dry benzene (6 mL). The content of the flask was cooled in an ice-salt mixture (-5 °C) and a freshly distilled phosphorus oxychloride (2.0 mL, 21.7 mmol) was dropwise added with vigorous stirring. After the addition was complete, the reaction mixture was brought to room temperature and heated under reflux for 3 h. The reaction mixture was cooled to room temperature, diluted with water and extracted with hexanes. The organic extract was washed with water, dried over anhydrous sodium sulfate and concentrated under reduced pressure. The residue was distilled to give (α,α)₃-d₆ TBP **11** (4.54 g, 16.7 mmol, 77%). Isotopic purity: 99%. **B.P.** 179-185 °C (20 mm Hg).

IR (film): 2959, 2934, 2874, 2222, 2143, 1456, 1275, 1013, 922, 874, 856, 802, 754 cm⁻¹.

¹H NMR (200 MHz, CDCl₃): δ 0.93 (3 H, t, $J = 7.2$ Hz, CH₃CH₂), 1.31-1.46 (2 H, m, CH₃CH₂), 1.56-1.71 (2 H, m, CH₃CH₂CH₂);

GC-MS: t_R 14.2 min; m/z 273 (M+1, 0.7%), 215 (21), 157 (20), 127 (14), 99 (100).

Synthesis of (β,β,γ)-*d*₉ TBP **12**

Synthesis of 2,3-dibromobutyric acid **16**: A solution of bromine (1.0 mL, 20 mmol) in carbon tetrachloride (20 mL) was added to a stirred solution of crotonic acid (1.70 mL, 20 mmol) at room temperature. Few drops of water were added to initiate the reaction. The solution was concentrated and the residue was crystallized from ethyl acetate-hexane to give 2,3-dibromobutyric acid **16** as a white solid (3.99 g, 16.23 mmol, 81%).

M.P. 87-90 °C.

¹H NMR (200 MHz, CDCl₃): δ 1.91 (3 H, d, $J = 5.8$ Hz, CH₃CHBr), 4.35-4.50 (2 H, m, CHBrCHBr), 7.67 (1 H, br, COOH).

Synthesis of β,β,γ -*d*₃ butyric acid **17**: Following the procedure described in the literature, [130] Ni/Al alloy (1.2 g) was gradually added to a vigorously stirred solution of the acid **16** (1.9 g, 7.7 mmol) in 10% NaOH in D₂O (12 mL) under nitrogen atmosphere. During the addition, the temperature of the reaction mixture was maintained below 50 °C. Minimal exposure to the environment is maintained during the reaction. The reaction mixture was stirred at 50 °C for 2 h, cooled to room temperature and filtered through a Celite pad. The residue was washed with a small amount of water and the combined filtrate was acidified with concentrated hydrochloric acid till pH ~ 1. The mixture was extracted with dichloromethane (10 × 30 mL) and the combined extract was dried over anhydrous sodium sulfate, concentrated and the residue distilled to give β,β,γ -*d*₃ butyric acid **17** (582 mg, 6.39 mmol, 83%) as a colourless liquid. Isotopic purity was found to be 60% as adjudged by ¹H NMR and no further effort was made to improve the isotopic purity. **B.P.** 164-165 °C.

¹H NMR (200 MHz, CDCl₃): δ 0.85-1.05 (3 H, m, CH₃CHD/CH₃CH₂), 1.55-1.75 (1 H, m, CH₃CHD/CH₃CH₂), 2.21- 2.41 (2 H, m, CH₂COOH/CD₂COOH).

Synthesis of β,β,γ -*d*₃ butanol **18**: Following a similar procedure described for the preparation of α,α -*d*₂-butanol **15**, the acid was reduced with LiAlH₄ to obtain **18** (7.66 g, 99.3 mmol, 70%). Isotopic purity was found to be 60% as adjudged by ¹H NMR and no further effort was made to improve the isotopic purity. **B.P.** 117-120 °C.

¹H NMR (200 MHz, CDCl₃): δ 0.81- 1.00 (3 H, m, CH₃CHD/CH₃CH₂), 1.23-1.43 (1 H, m, CH₃CHD/CH₃CH₂), 1.43-1.65 (2 H, m, CH₂CH₂OH/CD₂CH₂OH), 3.53-3.73 (2 H, m, CH₂CH₂OH/CD₂CH₂OH).

Synthesis of (β,β,γ) ₃-*d*₉ TBP **12**: Following a similar procedure described for the preparation of (α,α) ₃-*d*₆ TBP **11**, the alcohol **18** was reacted with POCl₃ to give the desired (β,β,γ) ₃-*d*₉ TBP **12** (5.9 g, 21.45 mmol, 72%). **B.P.** 180-185 °C (20 mm Hg). Isotopic purity was found to be 60% as evidenced by ¹H NMR and no further effort was made to improve the isotopic purity.

IR (film): 2957, 2932, 2903, 2110, 1456, 1263, 995, 928, 912, 862 cm⁻¹.

¹H NMR (200 MHz, CDCl₃): δ 0.80-1.00 (3 H, m, CH₃CHD/CH₃CH₂), 1.27-1.48 (1 H, m, CH₃CHD/CH₃CH₂), 1.52-1.71 (2 H, m, CH₂CH₂O/CD₂CH₂O), 3.92-4.11 (2 H, m, CH₂CH₂O/CD₂CH₂O);

GC-MS: t_R 14.09 min; m/z 275 (M⁺, 0.7%), 216 (10), 158 (21), 127 (14), 100 (100), 60 (10).

Synthesis of $(\gamma,\gamma,\delta,\delta)$ ₃-*d*₁₂ TBP **13**

Synthesis of tri-3-butynyl phosphate **19**: The titled product **19** was prepared using but-3-yne-1-ol and POCl₃ following the procedure as described for the preparation of (α,α) ₃-*d*₆ TBP **11** (12.4 g, 48.81 mmol, 78%).

GC-MS: t_R 17.03 min; m/z 255 (M+1, 0.7%), 201 (7), 149 (100), 121 (33), 99 (61).

Synthesis of $(\gamma,\gamma,\delta,\delta)_3-d_{12}$ TBP **13**: A solution of **19** (4.7 g, 18.5 mmol) in ethyl acetate (57 mL) was stirred overnight under deuterium atmosphere in the presence of Pd/C (10%, 0.235 g, 5 wt% of the substrate). The reaction mixture was filtered through a Celite pad, and the filtrate was concentrated. The residue was distilled to give to **13** (4.71 g, 16.94 mmol, 92%). Isotopic purity was found to be 60% as evidenced by ^1H NMR and no further effort was made to improve the isotopic purity.

B.P. 182-187 °C (20 mm Hg).

IR (film): 2953, 2927, 2214, 1265, 1011, 978, 907, 845, 752 cm^{-1} .

^1H NMR (800 MHz, CDCl_3): δ 0.86-0.94 (1 H, m, $\text{CD}_2\text{H}/\text{CDH}_2/\text{CH}_3$), 1.34-1.42 (2 H, m, $\text{CD}_2\text{CH}_2/\text{CH}_2\text{CH}_2$), 1.61-1.67 (2 H, m, $\text{CD}_2\text{CH}_2/\text{CH}_2\text{CH}_2$), 4.02 (2 H, q, $J = 6.4$ Hz, $\text{CH}_2\text{CH}_2\text{O}$);

GC-MS: t_R 14.02 min; m/z 278 (M^+ , 0.4%), 217 (7), 158 (19), 125 (13), 100 (100), 60 (14).

Synthesis of per-deuterated TBP **14**

Synthesis of per-deuterated TBP **14**: The titled compound **14** was made from d_9 -butanol (5.3 mL, 57.9 mmol) and POCl_3 (1.78 mL, 19.1 mmol) following the procedure as described for the preparation of $(\alpha,\alpha)_3-d_6$ TBP **11** (3.75 g, 12.8 mmol, 67%). Isotopic purity: 99%.

B.P. 180-186 °C (20 mm Hg).

IR (film): 2218, 2108, 1275, 1015, 995, 937, 916, 851, 841, 750 cm^{-1} ;

^{13}C NMR (50 MHz, CDCl_3): 12.30 (3 C, septet, $J = 18.7$), 17.32 (3 C, quintet, $J = 18.4$), 30.97 (3 C, quin, $J = 17.5$), 66.51 (3 C, quin, $J = 23.5$);

GC-MS: t_R 13.92 min; m/z 295 ($\text{M}+2$, 0.4%), 231 (12), 167 (22), 131 (9), 103 (100), 66 (14).

Irradiation with gamma ray

A set of solutions containing of 30% each of TBP **10** or its individual deuterated analogs **11-14** in *n*-dodecane were saturated with equal volume of 1.5 M or 3.0 M nitric acid. The organic phases were then separated and the nitric acid concentration in the organic phase was estimated by titration. The concentration of HNO₃ extracted by 30% *d_n*-TBPs in *n*-dodecane for aqueous phases of 1.5 M and 3 M HNO₃ were found to be 0.26-0.27 M and 0.56-0.58 M, respectively. The separated organic phases were taken in stoppered glass bottles and then irradiated with γ -rays using a ⁶⁰Co source at room temperature. The dose rate was determined by Fricke dosimeter and was found to be 22 Gy/min. For dose rate in 30% *d_n*-TBPs in *n*-dodecane system, (Z/A) corrections were made where Z and A are effective atomic number and mass number, respectively. It is expected that at this dose rate of γ -radiation would not alter the solution temperature. After absorption of particular doses, the samples were withdrawn from the chamber and analyzed for distribution ratio and degradation products.

Hydrolytic studies

Equal volumes of 30% solutions of undeuterated/*d_n*-TBPs in *n*-dodecane are separately taken in glass vials with 4 M nitric acid. The content was vigorously stirred at room temperature for 30 days. The organic phase was separated and used for degradation and solvent extraction studies.

Solvent extraction studies

The solvent extraction behavior of degraded TBPs were studied for Pu(IV) extraction. For the determination of the distribution ratio as a function of hydrolysis and radiolysis time, a small aliquot of organic solvent (0.5 mL) was contacted with equal volume of aqueous nitric acid spiked with Pu(IV) metal ion for 15 min. After centrifugation, the

organic and aqueous phases were separated and analyzed for the plutonium counts using an alpha scintillation counter. The distribution ratios were determined at the aqueous phase acidities of 3.0 and 0.5 M HNO₃ and calculated as the ratio of concentrations of the metal ion in the organic phase to that in the aqueous phase. All experiments were carried out in duplicate and the mean values are reported. The material balance for calculation of distribution ratio has a maximum error of $\pm 5.0\%$. The HNO₃ concentrations used here approximately represent the aqueous feed and strip acidities in the PUREX process. All the extraction studies were carried out at $25 \pm 1^\circ\text{C}$.

Gas chromatography–mass spectrometry analysis

The quantitative analyses of the solvent and their degradation products after hydrolysis and radiolysis were performed by gas chromatography using a Shimadzu GC 2010 instrument equipped with a flame ionization detector. The separation was achieved using a 30 m long, 0.2 mm id, and 0.25 μm thickness CP-SIL 5CB WCOT fused silica column. Helium was used as the carrier gas and the temperature program was 100°C for 1 min, increased to 300°C at the rate of 10°C per minute and held at 300°C for 20 min. Each sample was dissolve in toluene containing TOPO as an internal standard. An approximately $0.5\ \mu\text{L}$ of solution was injected manually into the column in the split mode of 50:1. For identification of the degradation products GC-MS studies were carried out using a Shimadzu GCMS QP 2010 plus instrument. The interface temperature and the ion source temperature were kept at 300°C and 250°C , respectively. The ionization energy was 70 eV. Other conditions were same as in the case of GC.

CHAPTER 4

*Design, synthesis and extraction properties of
conformationally constrained oxa-diamides*

4.1 Introduction

The combined recovery of minor actinides along with the lanthanides is carried out from HLW by the process called ‘Actinide Partitioning’. Several complexing agents or extractants have been proposed for actinide partitioning over the last 20 years [14]. The journey started with phosphorus based ligands. Several phosphorus based compounds *viz.* trialkylphosphine oxides (TRPO process) [19], diisodecylphosphoric acid (DIDPA) [21], carbamoyl organophosphorous compounds (TRUEX process) [20], etc have been developed for the same purpose. After phosphorus based ligands, amide group containing ligands came into picture as the phosphorus containing ligands are non-incinerable and do not comply with the requirements of CHON principle of extractant design. The most promising member of malonamide family was the DIAMEX reference compound *N,N'*-dimethyl-*N,N'*-dibutyl malonamide (DMDBTDMA) **I** (Fig. 4.1) [24, 135]. The significant feature of amide extractants is their complete incinerability thereby leading to reduced secondary wastes in accordance with the CHON principle and the innocuous nature of their degradation products, mainly carboxylic acids and amines, which can be washed off easily.

The multidentate diglycolamide (DGA) family of extractants were introduced recently for the same purpose [25]. The diglycolamides are open-chain ether dicarboxylic acid diamides that can form a coordination structure similar to the corresponding macrocyclic ligand, and showed the highest extractabilities among all the amides ever investigated. The change from malonamide (bidentate ligand) to DGA (tridentate ligand) significantly increased the affinity for both trivalent actinides and lanthanides. *N,N,N',N'*-tetraoctyldiglycolamide (TODGA) **II** [136, 137], and *N,N,N',N'*-tetra-2-ethylhexyldiglycolamide (TEHDGA) **III** (Fig. 4.1) [138] are the most promising extractants of DGA family for the separation of trivalent actinides and lanthanides from HLLW. The main disadvantage associated with DGA based

extractants is the co-extraction of Sr(II), Zr ions from the HLLW solution along with Ln(III) and Ac(III) [136, 139-141, 142]. Therefore, the extraction process using DGAs requires the use of masking agents to suppress the coextraction of fission product and some additional scrubbing steps during stripping.

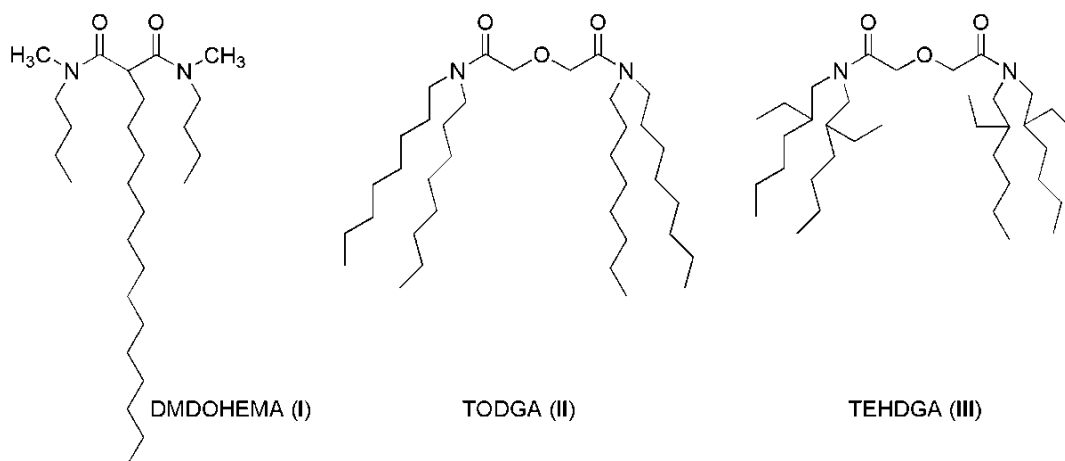


Fig. 4.1 Structures of important diamides and diglycolamides.

DGA ligands with structural modifications in their skeleton were also attempted and it was found that a small alteration in their skeleton leads to considerable change in extraction properties [143]. These modifications include (1) the increase in chain length from one carbon to two carbons between the central ether oxygen (oxydipropionamide or ODPAA)/ sulfur atom (thiadipropionamide or TDPA) and the amide moieties, [144] (2) the addition of substituents on the carbons between the central oxygen atom and the amide moieties on either one or both sides of the central oxygen, [145] (3) the replacement of the central oxygen by a (substituted) nitrogen atom or sulfur atom, [144] (4) synthesis of pillar[5]arene and calix[4]arene based DGA molecules [146, 147] (5) pre-organisation of DGA molecules on various tripodal platforms [148] and (6) synthesis of bis(DGA) [149] (7) synthesis of rigidified diglycolamides on a tetrahydrofuran platform [145]. Extraction evaluation of all above described extractants showed that these modifications changed some properties of extraction or back

extraction but did not change extraction behaviour in a meaningful way to be superior than TODGA **II** or TEHDGA **III**.

The attempt have been made so far, to design and develop a successful tridentate ligands are mostly consist of linear diglycolamides. As mentioned above, the only reported diglycolamides on a rigidified tetrahydrofuran platform (as a mixture of *cis* and *trans*-isomers) has been reported by Iqbal *et al* [145]. Similarly the only one attempt has been made to see the effect of increasing chain length from one carbon to two carbons between the central ether oxygen atom and the amide moieties in ODPa [144]. Both the modifications have shown poor extraction abilities.

In spent nuclear fuel reprocessing, solvent extraction technique is mostly used for metal ion separations from nuclear waste because it can be applied successfully at research scale as well as industrial or plant scale. The other alternate greener techniques like liquid membrane is also being investigated as an alternative to solvent extraction for nuclear industry especially where the target metal ions are present in micro concentrations in the solution. The liquid membrane technique has been extensively studied worldwide for the separation of radio nuclides [150-155]. Supported Liquid membrane (SLM) techniques are found to be particularly attractive for their possible application in actinide, lanthanide and valuable fission product separation from various waste streams generated during spent fuel reprocessing. They have the advantage of large surface to volume ratio, faster mass transfer and continuous flow [156-160].

4.2 Present Work

We have designed tridentate diamide based ligands **20** based on conformationally constrained 7-oxabicyclo[2.2.1]heptane-2,3-dicarboxylic acid where the ether-oxygen is positioned at the bridgehead and a chain of two carbon atoms between the ether oxygen and the amide moieties (Fig. 4.2). It was assumed that the rigid coordination

sphere created by the three donor groups (ether-oxygen and two amide groups) might enhance binding kinetics as the coordination atoms are appropriately oriented for binding to a metal. The arrangement of three donor groups is perfect to make a cavity in which a selective metal ion can fit. We were therefore curious to investigate the concept of rigidity effect of donor groups on an oxabicyclo[2.2.1]heptane skeleton for the selective extraction of lanthanides and actinides. The other important feature of the basic moiety of new extractant is that the cavity size can also be slightly tuned, by slight modification in the basic structure, for specific binding to enhance ionic selectivity. We have also tuned the cavity size by modification in basic moiety to see the effect of tuned cavity size on selectivity and designed the ligand **21** (Fig. 4.2). The synthesis of such conformationally constrained simple oxa-diamides have not been attempted before to study the effect of such structural modifications in rigid direction on the extraction behaviour. This chapter includes the synthesis of three conformationally constrained bridged 7-oxabicyclo[2.2.1]heptane-2,3-dicarboxamides **20 a-c** (OBDA **20 a-c**) and evaluation of their extraction behaviour for Am(III), Eu(III), Pu(IV), U(VI) from the nitric acid medium using 15% isodecyl alcohol (IDA)/*n*-dodecane as diluents. A detailed study of extraction behaviour of OBDA ligands has been performed using solvent extraction and membrane separation technique. Present study also includes synthesis and solvent extraction studies of Pu selective rigidified oxa-diamides **21a,b**. Pu selective rigidified oxa-diamides were synthesized by adjusting the distance of three donor groups of OBDA by means of structural alterations.

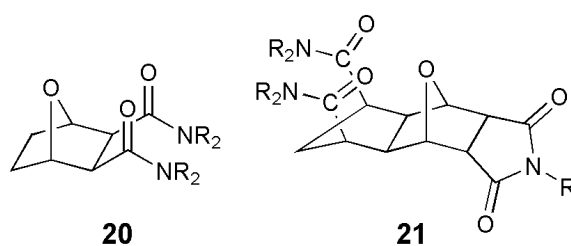
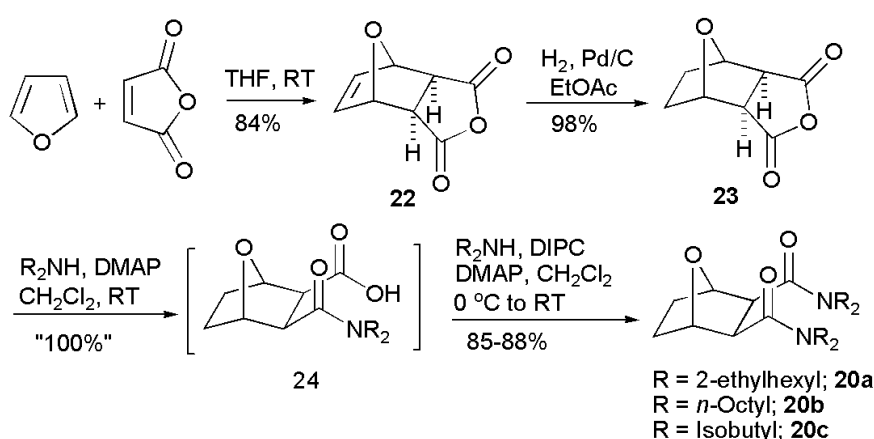


Fig. 4.2 Conformationally constrained oxa-diamides.

4.2.1 Synthesis of OBDA extractants

Three different derivatives of OBDA **20a-c** having different amine components have been synthesized from the commercially available cheap starting materials as shown in Scheme 4.1. Diels-Alder reaction of furan and maleic anhydride gave the known *exo* adduct **22** in excellent yield. The main advantage of the reaction is that the reaction gives 100% *exo* product that itself crystallizes in reaction mixture so, the step of difficult separation of *exo* and *endo* can be escaped. The *exo* adduct was then hydrogenated in dry ethyl acetate using Pd/C to give the bridged tricyclic anhydride **23** in quantitative yield. Anhydride **23** was opened up with bis 2-ethylhexylamine in presence of catalytic amount of DMAP to give the hemiamide **24** as an intermediate which was reacted *in situ* with another equiv of bis 2-ethylhexylamine in the presence of diisopropylcarbodiimide (DIPC) to give the bridged OBDA **20a** in excellent yield as an white waxy solid. The other two dicarboxamides, OBDA **20b** and OBDA **20c** were similarly made in high yields from the anhydride **23** using dioctylamine and diisobutylamine, respectively (Scheme 4.1).



Scheme 4.1 Synthesis of bridged 7-oxabicyclo[2.2.1]heptane-2,3-dicarboxamides.

4.2.2 Extraction evaluation of OBDA by solvent extraction

Evaluation of OBDA for separation of actinides and lanthanides by liquid-liquid extraction has been performed with varying extraction parameters *viz* feed acidity,

extractant concentration and nitrate ion concentration etc. Nature of bonding between metal and ligand was explained with the help of IR, NMR, ESI-MS and Density functional theoretical (DFT) study. Third phase formation, selectivity of ligand and back extraction studies were also carried out using OBDA ligands.

4.2.2.1 Optimization of organic phase composition

IDA was used as a phase modifier in organic phase along with OBDA **20a** and dodecane diluents to suppress the formation of third phase at higher acidity. 15% IDA in organic phase was found to be enough to prevent the third phase in contact with 4 M HNO₃ solution.

4.2.2.2 Kinetics of extraction

The time of equilibration required for Am(III) and Pu(IV) by OBDA_s was studied using 0.1 M OBDA **20a** in 15% IDA/*n*-dodecane in presence of 1 M HNO₃ (Fig. 4.3). OBDA **20a** showed very fast kinetics of equilibration for both Am(III) and Pu(IV). Equilibration was achieved within 2 min. Therefore, in subsequent studies, 5 min equilibration time was maintained.

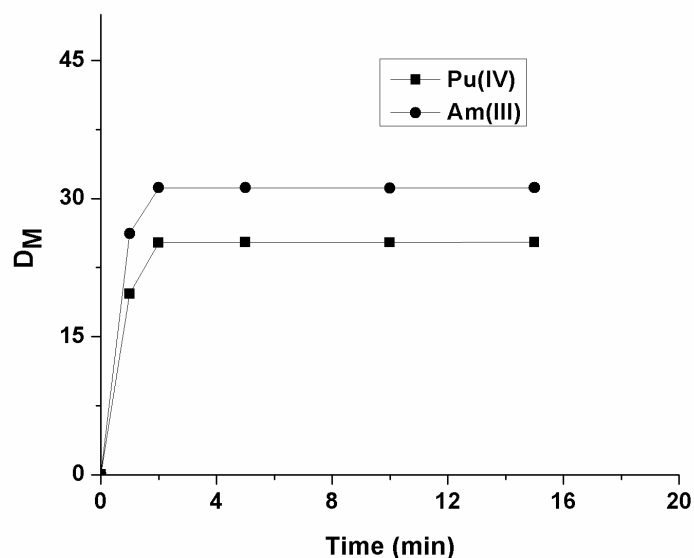


Fig. 4.3 Kinetics of extraction of Pu(IV) and Am(III) using 0.1 M OBDA **20a**.

4.2.2.3 Comparative study of D_{Am} for derivatives of OBDA

The extraction of Am(III) was also studied with two other derivatives of OBDA series OBDA **20b** and OBDA **20c** and the obtained D_{Am} values was compared with OBDA **20a**. The D_{Am} value was found to be slightly less for OBDA **20b** (42) compared to OBDA **20a** (52.3). The solubility of OBDA **20c** was poor in 15% IDA/*n*-dodecane. Hence, a solution of OBDA **20c** in 30% IDA/*n*-dodecane was studied which also showed slightly lower D_{Am} value (40) than OBDA **20a**. Therefore, further extraction studies were performed with OBDA **20a** only.

4.2.2.4 Effect of feed acidity on extraction

The effect of feed nitric acid concentration on the distribution ratio of Pu(IV), Am(III) and Eu(III) for 0.1 M OBDA **20a** in 15% IDA/*n*-dodecane was investigated to explore the feasibility of using this ligand for the separation of actinides and lanthanides (Fig. 4.4). OBDA **20a** showed interesting trend in the distribution ratio of Pu(IV), Am(III) and Eu(III). In case of OBDA **20a**, an initial increasing trend of the distribution ratios for Pu(IV), Am(III) and Eu(III) was observed with increasing feed HNO_3 concentration. Beyond 3 M HNO_3 , the distribution ratios rapidly decreased. The results obtained for Am(III) were compared with the results obtained from TEHDGA **III** to understand the effect of conformational restriction of the ligand structure on the extraction performance (Fig. 4.5). In case of TEHDGA **III**, the distribution ratio continuously increased with increasing HNO_3 concentration up to 6 M concentration. Between 3-4 M HNO_3 (the commonly used acidity of nuclear waste) D_M values for OBDA **20a** are comparable with TEHDGA **III**. Like TEHDGA **III**, OBDA **20a** is a neutral extractant. Hence, the extraction mechanism takes place via nitrate ion assisted complex formation (Eq. 4.1). The subscript 'org' refers to species in organic phase and without subscript refer to those present in aqueous phase.

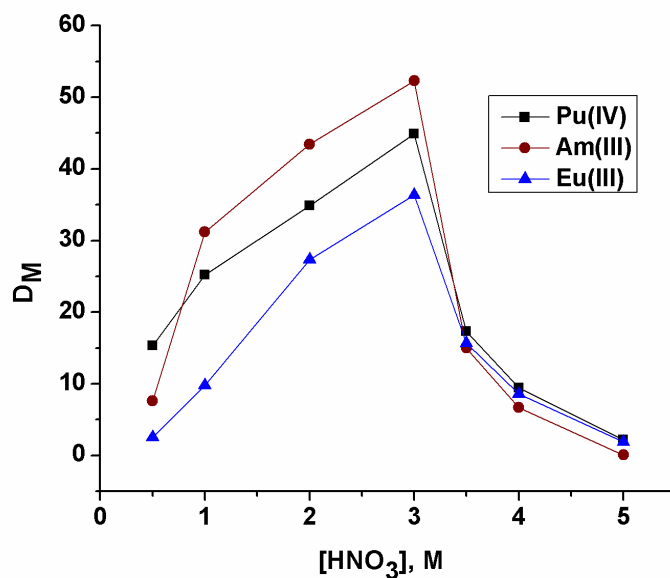
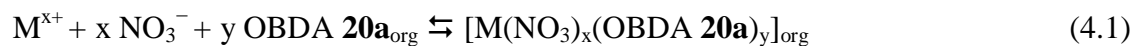


Fig. 4.4 Effect of feed HNO₃ concentration on D_{Pu(IV)}, D_{Am(III)} and D_{Eu(III)}.

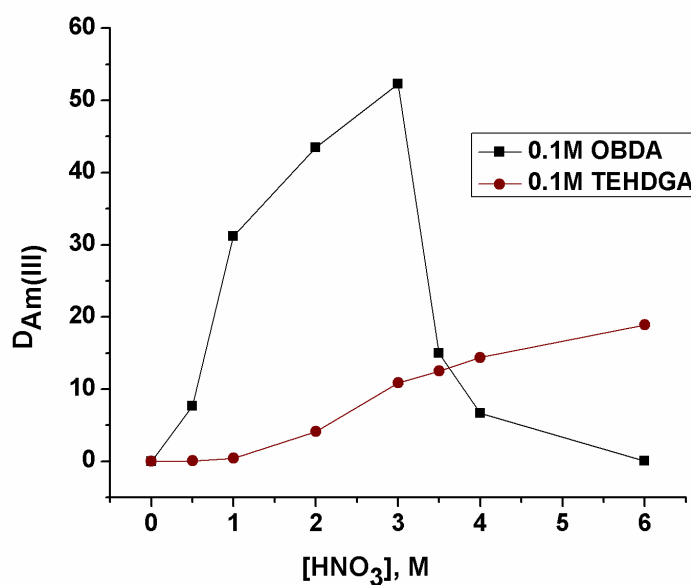


Fig. 4.5 Comparative extraction of Am(III) using 0.1 M OBDA **20a** and 0.1 M TEHDGA **III** in 15% IDA/*n*-dodecane at different feed nitric acid concentration.

So increasing nitric acid concentration leads to increased formation of neutral metal-nitrate complex leading to higher D_M value, explains the increasing trend of D_M for

OBDA **20a** with increasing nitric acid concentration. But the decreasing trend in D_M beyond 3 M HNO_3 for OBDA **20a** needed more investigation. One possible reason for this abnormal behavior could be its stability at higher HNO_3 concentration. This prompted us to study stability behavior of OBDA **20a** at different HNO_3 concentrations. OBDA was found to be sensitive for hydrolytic degradation (Table 4.1).

Table 4.1 Degradation study of OBDA **20a** in HNO_3

Time (min)	% of OBDA 20a remaining after degradation		
	0.5 M aq. HNO_3	1 M aq. HNO_3	3 M aq. HNO_3
0	100	100	100
5	99	99	98
15	99	98	10
30	98	94	0
90	91	46	-
150	88	0	-
330	61	-	-

In lower acid concentration the degradation rate was found to be slow. In 1 M HNO_3 , the OBDA **20a** was observed to be stable up to about 15 min after which the degradation started and complete hydrolysis was observed in 2.5 h. In 3 M HNO_3 , the OBDA **20a** solution in *n*-dodecane-IDA mixture is stable for a very short period of time. The hydrolysis pattern of OBDA **20a** showed that after 5 min of contact with 3 M HNO_3 , its degradation was initiated followed by rapid degradation thereafter. The complete degradation of OBDA **20a** took about 30 min resulting in the formation of bis-2-ethylhexylamine and the corresponding dicarboxylic acid, a product further independently confirmed by hydrolyzing the anhydride **23**. It was therefore needed to find out the species responsible for extraction of Pu(IV) and Am(III). Independent studies using either bis-2-ethylhexylamine or di-carboxylic acid of anhydride **23** or a

mixture of both did not show any extraction of Pu(IV) and Am(III). This clearly proved that OBDA **20a** is responsible for extraction of Pu(IV) and Am(III). The OBDA molecules that are complexed to Pu(IV) or Am(III) did not undergo hydrolysis. This has been augmented by stripping studies of the OBDA **20a** complexed to Pu(IV) or Am(III) with higher concentration of nitric acid (6 M HNO₃) where extracted metal ions are not stripped into the aqueous phase. So the combination of fast kinetics for complexation and good D_M values for Pu(IV) and Am(III) at 3-4 M acidity (normally used in HLLW) prompted us to carry out further extraction studies using OBDA **20a**.

4.2.2.5 Determination of stoichiometry of metal ligand complex

D_M was calculated at varying concentration of OBDA **20a** at a fixed aqueous acidity (1 M HNO₃). As shown by the Fig 4.6, the D_M values increases with increasing OBDA **20a** concentration in organic phase and plot of log D_M vs log [OBDA **20a**] for Pu(IV), Am(III) and Eu(III) gave straight lines with varying slopes. Slope value for Pu is close to 1 indicates that Pu(IV) forms a mono-solvated species with OBDA **20a**. While Am(III) and Eu(III) formed a mixture of mono-solvated and di-solvated species as the slope values are in between 1 and 2 *i.e.* 1.68 and 1.72 for Am and Eu, respectively.

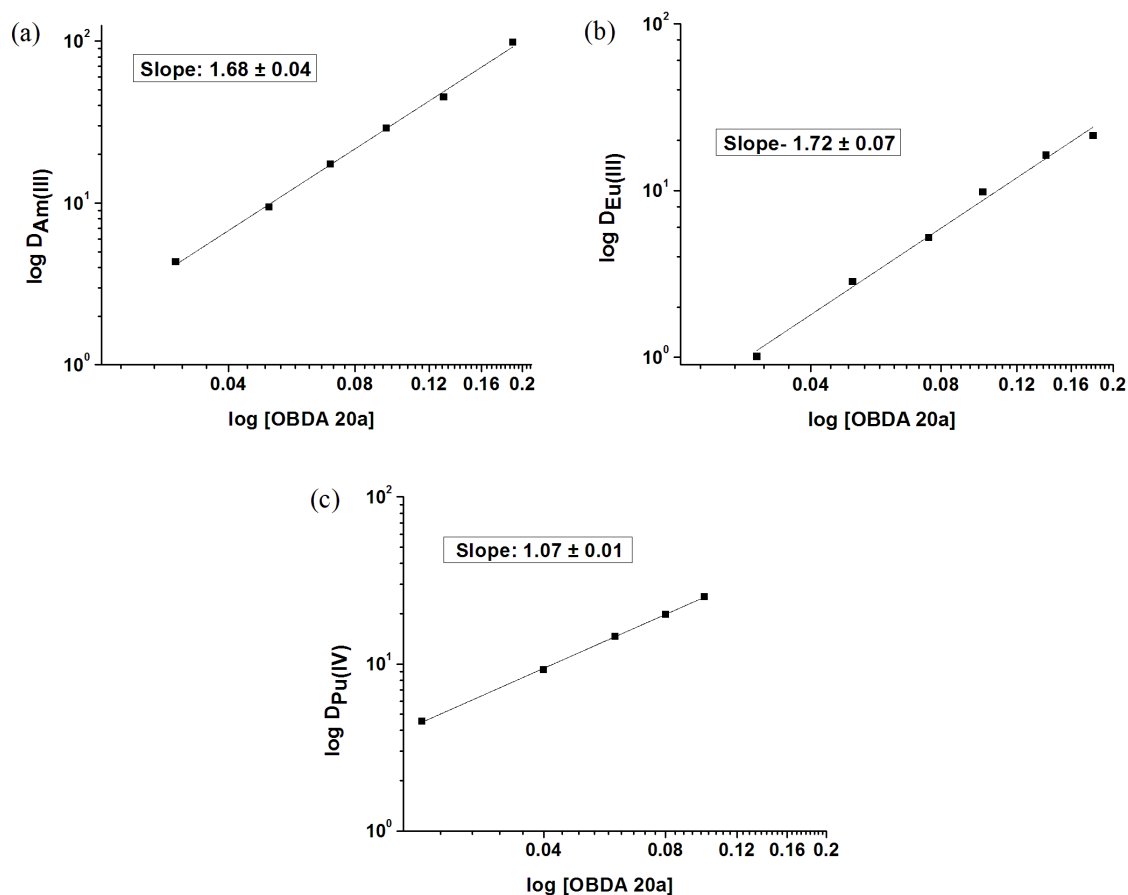


Fig. 4.6 Plot of $\log D_M$ vs $\log [\text{OBDA } 20\text{a}]$ for (a) Am (b) Eu and (c) Pu.

In order to determine the participation of nitrate ion in formation of metal extracted species the D_M values for Pu, Am and Eu were studied at different nitrate ion concentrations at a fixed aqueous acidity (1 M HNO_3). The plot of $\log D_M$ vs $\log [\text{NO}_3^-]$ showed a straight line with a slope of ~ 4 for Pu(IV) and ~ 3 for Am(III) or Eu(III) (Fig. 4.7) indicating four nitrate ions are involved in the extraction of Pu(IV) while three nitrate ions for Am(III) and Eu(III).

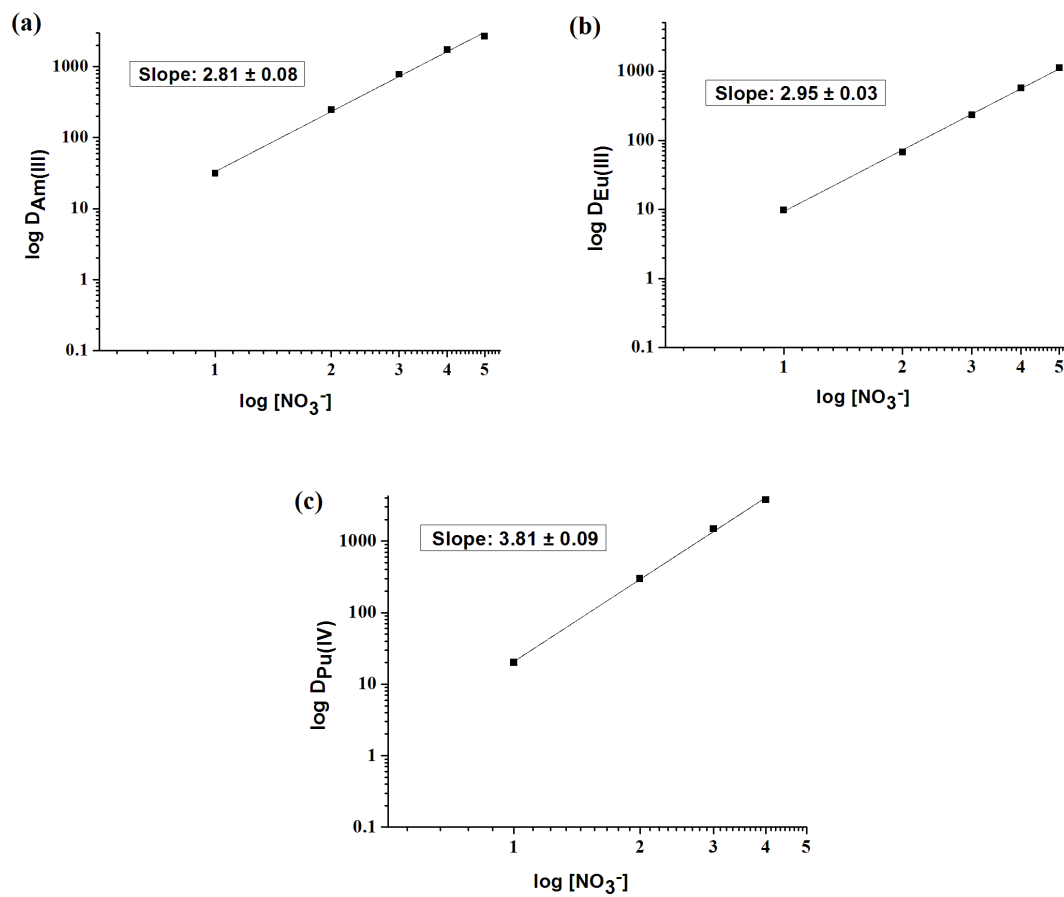


Fig. 4.7 Plot of $\log D_M$ vs $\log \text{NO}_3^-$ for (a) Am (b) Eu and (c) Pu.

4.2.2.6 FTIR, NMR and ESIMS studies of metal ligand complex

To find out the nature of bonding between metal and ligand, complex of $\text{Eu}(\text{NO}_3)_3 \cdot 5\text{H}_2\text{O}$ with OBDA **20c** was studied by IR and ^1H NMR spectroscopy. IR spectra of the obtained complex, is shown in Fig. 4.8, which indicates a strong binding of metal at the amide carbonyl group of the ligand. The $\nu_{\text{C=O}}$ for OBDA **20c** appeared at 1655 and 1632 cm^{-1} whereas for the metal-ligand complex it appeared at a lower wave number (1593 cm^{-1}). This lowering in $\nu_{\text{C=O}}$ was attributed to the coordination of the metal at the carbonyl group of the ligand which weakens the C=O character.

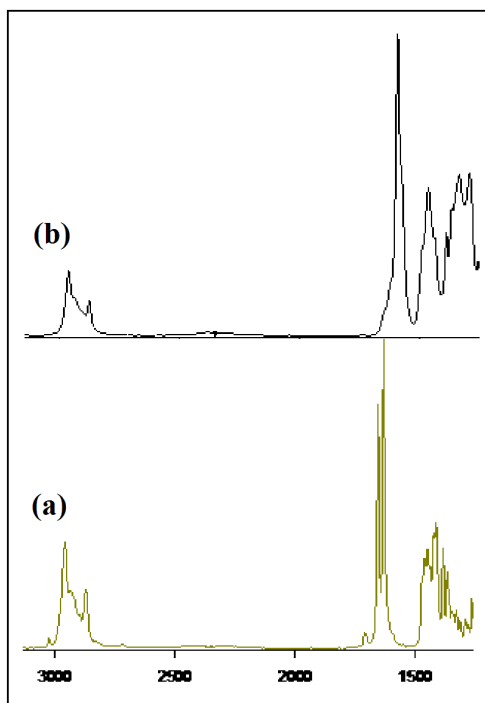


Fig. 4.8 IR spectra of (a) OBDA **20c** and (b) OBDA **20c** complexed with $\text{Eu}(\text{NO}_3)_3 \cdot 5\text{H}_2\text{O}$.

The participation of the bridgehead ether-oxygen of OBDA in binding with the metal in the metal ligand complex has been corroborated from ^1H NMR spectra (Fig. 4.9). A significant downfield shift of CH-O-CH resonance was observed after complexation with Eu [δ 4.86 (2 H, s, CHOCH) for free OBDA **20c** vs 5.96 (2 H, s, broad, CHOCH) for the complexed Eu]. NMR and IR studies confirmed the participation of amide carbonyls and bridgehead ether-oxygen of OBDA ligand in metal ligand complex formation. The OBDA ligands thus function as a tridentate ligand like DGA ligands. These deviations supports our designed principle discussed earlier that in OBDA molecule the three coordination sites (two carbonyl and one ether) are appropriately oriented for binding to a metal ion and It will, therefore, be of more interest to understand the structure and coordination modes in its complex using density functional theoretical (DFT) study.

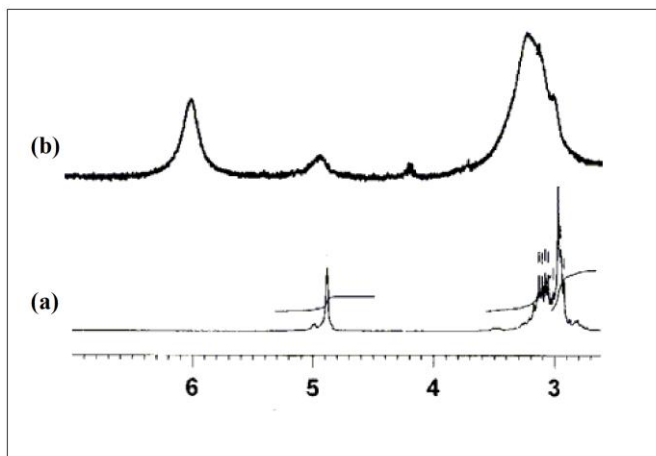
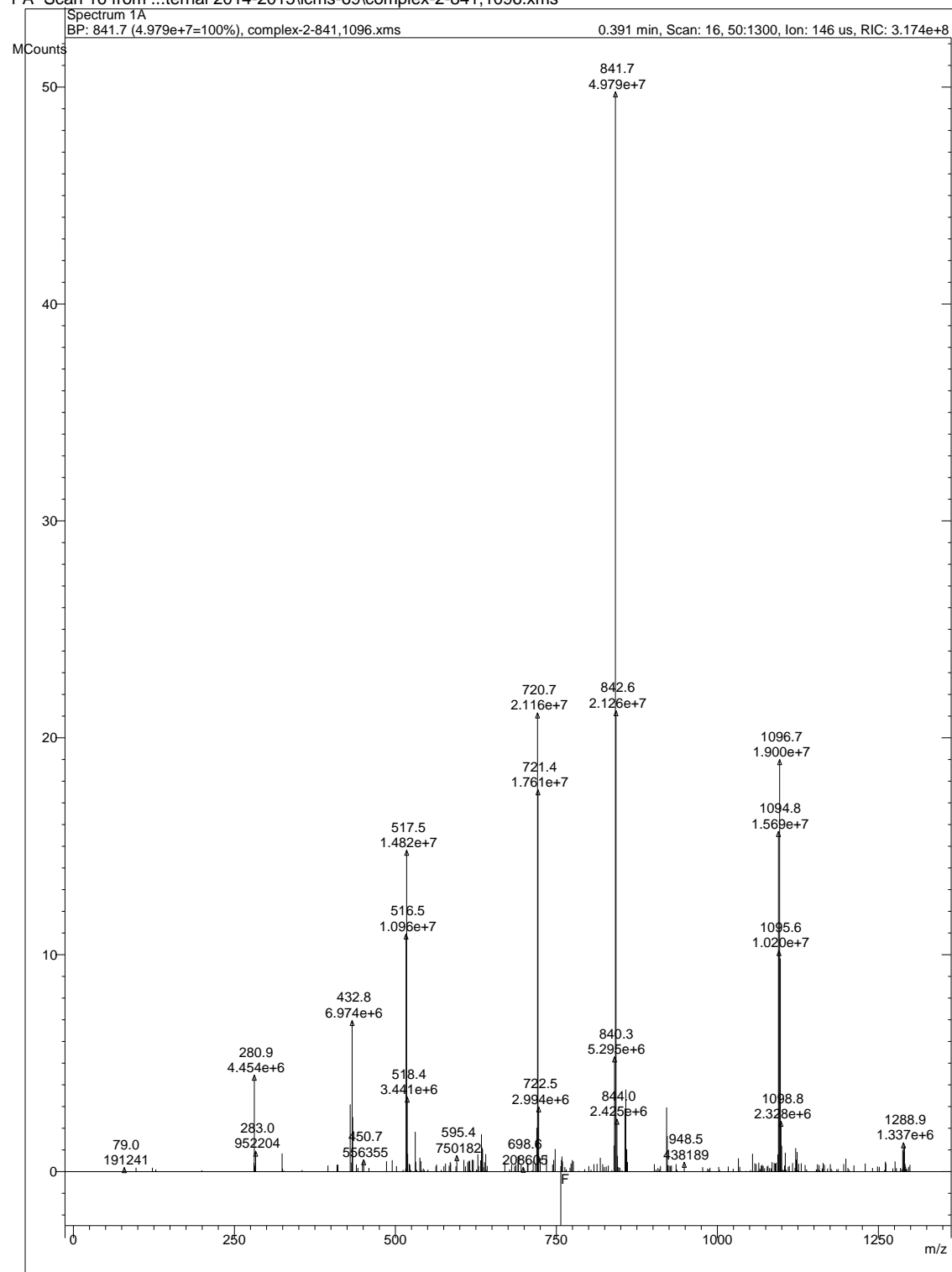


Fig. 4.9 ^1H NMR of the relevant portion of (a) OBDA **20c** and (b) OBDA **20c** complexed with $\text{Eu}(\text{NO}_3)_3 \cdot 5\text{H}_2\text{O}$.

ESI-MS spectra of the complex provided further insight of the metal ligand complex formation. From the ESIMS spectra it becomes clear that the complex obtained was a mixture of two species mono- and di-solvated. The peaks at m/z 720.7 and 841.7 correspond to $[(\text{OBDA } \mathbf{20c})\text{Eu}(\text{NO}_3)_2(\text{H}_2\text{O})_2]^+$ and $[(\text{OBDA } \mathbf{20c})\text{Eu}(\text{NO}_3)_3(\text{H}_2\text{O})_4\text{Na}]^+$, respectively while peaks at m/z 517.5 and 1096.7 correspond to $[(\text{OBDA } \mathbf{20c})_2\text{Eu}(\text{NO}_3)]^{2+}$ and $[(\text{OBDA } \mathbf{20c})_2\text{Eu}(\text{NO}_3)_2]^+$, respectively (Fig. 4.10).

Spectrum Plot - 11/19/2014 3:28 PM

1 A Scan 16 from ...ternal 2014-2015\lcms-69\complex-2-841,1096.xms

**Fig. 4.10** ESI-MS spectrum of complex of $\text{Eu}(\text{NO}_3)_3 \cdot 5\text{H}_2\text{O}$ with OBDA **20c**.

4.2.2.7 Third phase formation studies for high loading of Eu

The large concentration of the trivalent lanthanides present in the HLW often leads to the formation of third phase during ‘actinide partitioning’. In this view it is required to understand the extraction behavior of Eu(III) (surrogate for all the trivalent lanthanides) under acidic feed conditions similar to the HLW. To simulate the situation, the D_M value of Eu(III) was studied with OBDA **20a** at 3 M HNO₃ with varying concentrations of Eu. No third phase formation was observed even up to 5 g/L of Eu. Also, significant D_{Eu} was found even at higher concentrations of Eu (Table 4.2).

Table 4.2 Distribution ratio of Eu(III) in presence of different concentrations of Eu(III) in 3 M HNO₃ for 0.1 M OBDA **20a** in 15% IDA /*n*-dodecane.

[Eu] (ppm)	$D_{Eu(III)}$
100	34.21
200	31.91
500	27.85
1000	21.01
2000	18.07
5000	4.97

4.2.2.8 Back extraction studies

Easy stripping of metal ions from the loaded organic phase is an essential factor for an extractant to be considered for separation of actinides and lanthanides. For back extraction studies 0.1 M OBDA **20a** was contacted with Pu (IV) and Am (III) at 1 M HNO₃. Am(III) was found to be stripped by pH 2 solution (~90% stripping in a single contact) whereas Pu(IV) was possible to be stripped by 0.1 M Oxalic acid (~85% stripping in a single contact) from loaded OBDA **20a**.

4.2.2.9 Selectivity of OBDA for lanthanides and actinides

For actinide partitioning purpose the extractant should be enough selective for Ans and Lns over the fission products present in HLW. The selectivity of OBDA **20a** for Ans and Lns in reference to other elements present in HLLW was investigated in 3 M HNO₃. OBDA didn't show extraction for any fission product *viz* Cs, Sr, Ru, Nb and Sb. The selectivity of OBDA was found to be higher compared to TEHDGA **III** (Table 4.3). It was interesting to observe that D_{Sr} and D_U values were less compared to that observed for TEHDGA **III** (D_{Sr} ~0.65 and D_U ~ 2.1 for 0.1 M TEHDGA **III**/ 15% IDA) [138, 161] and thus offering better purification of the trivalent actinides and lanthanides over the other constituents present in HLLW.

Table 4.3 Extraction behavior of different elements present in HLLW solution using 0.1 M OBDA **20a** in 15% IDA/*n*-dodecane.

Elements	Cs	Sr	Ru	Nb	Ce	U	Pu	Eu	Sb	Am
$D_{M(OBDA)}$	<0.01	0.05	0.04	<0.01	14.86	0.5	44.29	35.46	<0.01	52.21
$D_{M(TEHDGA)}$	<0.01	0.65	0.05	<0.01	13.17	2.1	34.16	9.15	<0.01	11.15

4.2.2.10 Computational Study

DFT calculations were performed on the free OBDA with the di-methyl substituent on the amidic 'N' atoms in order to reduce the computational cost. The result shows that the ligand is most stable in the conformation, where two carbonyl oxygens of amide groups are in trans position (Fig. 4.11a). However, prior to the complexation with the metal ions both the amidic oxygens should be in cis position. Two possible conformers with the amidic oxygens in the cis position were considered (Figs. 4.11b and 4.11c) and their relative energies were compared with respect to the most stable trans conformer. The results showed that the conformer 'c' (relative energy: 5.39 kcal.mol⁻¹) is more stable than the conformer 'b' (relative energy: 11.18 kcal.mol⁻¹). FTIR studies also

showed the participation of ethereal oxygen atom in the bonding with the metal ion, which is possible if the ligand form complexes in the conformer 'c'. DFT study, therefore, substantiate the results of the FTIR studies. The slope analysis study indicated the presence of two OBDA molecules and three nitrate ions in the extracted species of Am^{3+} . The guess structure of the Am^{3+} complex was, therefore, prepared with two OBDA and three nitrate ions coordinating to the central Am^{3+} ion. The optimized geometry of the Am^{3+} complex is shown in Figure 4.12. In this complex the amidic oxygens are closer to the central Am^{3+} ion with 'Am-O' bond length of $2.51 \pm 0.02 \text{ \AA}$ as compared to the ethereal oxygen atoms ($2.70 \pm 0.04 \text{ \AA}$). The nitrate ions are, however, closer to the Am^{3+} ion as compared to the OBDA with 'Am-O' distance of $2.403 \pm 0.002 \text{ \AA}$. In order to further understand the metal-ligand bonding the natural charges on the Am^{3+} ion and coordinating sites of the ligand molecules were calculated and the results are shown in Table 4.4. The electron density on the amidic oxygen atom increased from -0.60 e to -0.641 after complexation in spite of transfer of electron density to the Am^{3+} ion. This indicates more charge polarization in the ligand molecule after complexation due to pulling of electron density by the amidic oxygen atoms from the adjacent carbon atom resulting in change in electronic charge on the amidic carbon atom from -0.412 e to 0.714 e .

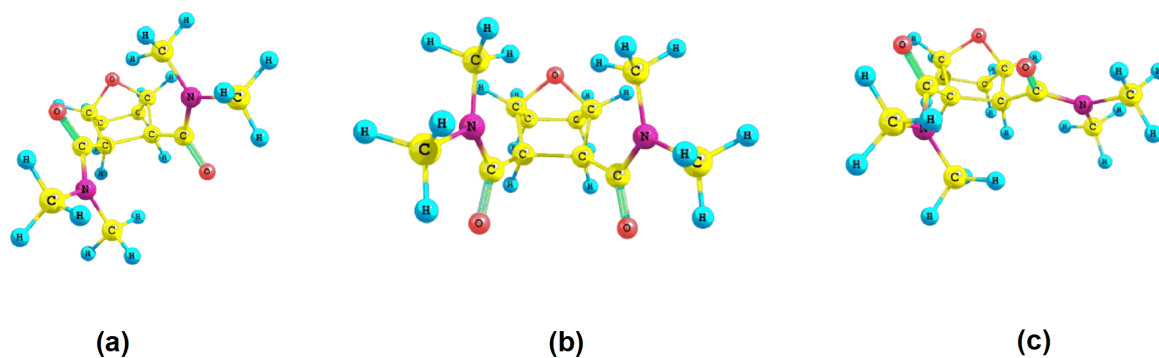


Fig. 4.11 Three different conformers of free OBDA obtained by geometry optimization

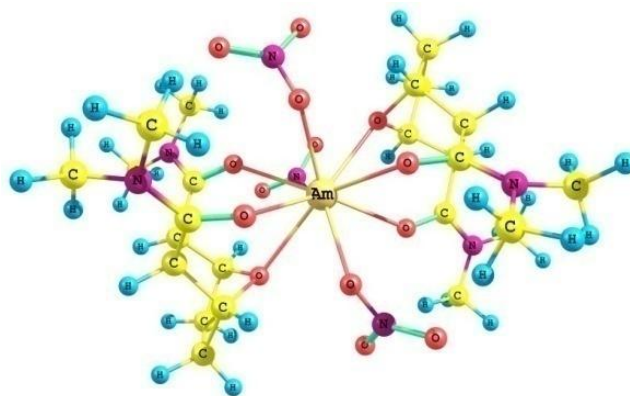


Fig. 4.12 Energy optimized structure of Am(III) complex of OBDA

Table 4.4 Natural charges on the carbonyl and ethereal oxygen and carbonyl carbon atoms.

Q(Am)	Q(O) _{amide}		Q(C) _{amide}		Q(O) _{ether}	
	In free ligand	In complex	In free ligand	In complex	In free ligand	In complex
1.582	-0.60±0.01	-0.641±0.007	-0.412	0.714	-0.572	-0.570±0.001

4.2.3 Extraction evaluation of OBDA by membrane separation technique

In the previous section it has been shown that OBDA **20a** is a good candidate for extraction of lanthanides and actinides. The molecule showed good extraction behaviour, fast kinetics, high loading capacity for lanthanides without third phase formation, very low extraction of fission products and easy stripping of the extracted metal ions. Unfortunately, the molecule was found to be less stable in nitric acid medium and the rate of hydrolysis increased with increasing feed nitric acid concentration. In carrier mediated transport mechanism across a SLM, the carrier molecule remains in contact with nitric acid for a limited period thereby acid induced hydrolysis is expected to be minimized. The above assumption and encouraging result of OBDA **20a** obtained from Solvent extraction studies therefore prompted us to explore the possibility of the use of OBDA as a carrier across a SLM to study the

transport behavior of Am(III). Hence, the effect of feed nitric acid/ nitrate concentration, carrier concentration, membrane pore size and membrane stability on the transport of Am(III) using OBDA **20a** as carrier molecule across a SLM has been studied in detail. Schematic description of the SLM processes is shown in Fig. 4.13.

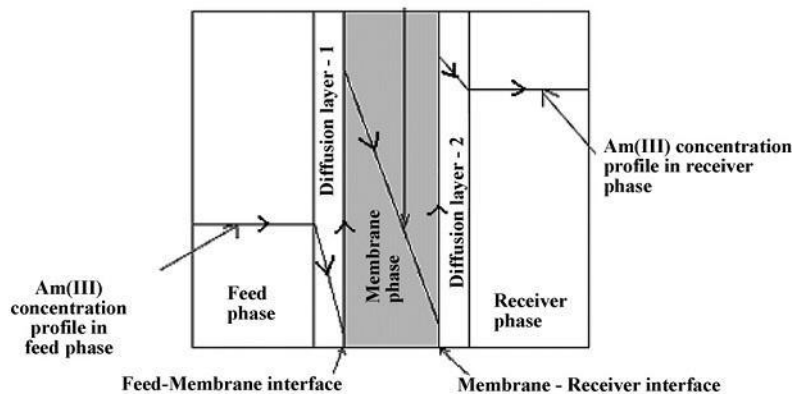


Fig. 4.13 Schematic description of the SLM process.

4.2.3.1 Effect of feed nitric acid concentration on Am transport

Dependency of Am(III) transport on feed nitric acid using 0.1 M OBDA **20a** in presence of 15% IDA/*n*-dodecane was studied. The OBDA **20a** carrier showed good transport properties over a wide range of feed nitric concentration. The transport rate was found to be very fast with 80-90% transportation of Am(III) within 1 h for feed nitric acid concentration of 1 M-4 M (Fig. 4.14). Remarkably, ~95% transport of Am(III) from 2 M HNO₃ feed was achieved within 1 h. For TEHDGA, similar transport percentage required a higher concentration of the carrier (0.2 M) and much longer time (~3 h) [155]. Such faster rate of transport is rarely observed [162, 163]. For OBDA **20a**, the order of transport of Am(III) by 0.1 M OBDA in 15% IDA/*n*-dodecane was 2 M HNO₃ > 1 M HNO₃ ≥ 3 M HNO₃ > 4 M HNO₃ >> 6 M HNO₃. But the difference in transport between the 2-4 M HNO₃ was very small.

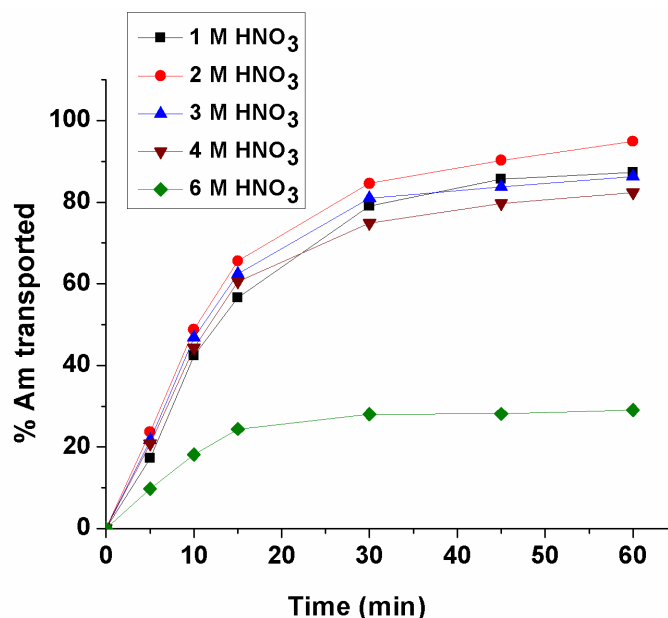


Fig. 4.14 Transport of Am(III) using 0.1 M OBDA in 15% IDA/*n*-dodecane; Feed-Varying concentrations of HNO₃, Membrane- 0.2 μm PTFE, Strippant- pH 2 solution

A closer look into the results showed that % transport is almost similar from 1 M to 4 M nitric acid concentrations and less for 6 M HNO₃. Continuous increase in Am(III) transport with increasing time up to 1 h even for a feed acidity of 4 M HNO₃ proves that acid induced hydrolysis of OBDA is not happening in SLM.

As the transport in supported liquid membrane follows diffusion controlled transport mechanism, the carrier molecule is in dynamic state within the membrane from feed-membrane interface to membrane-strip interface (Fig 4.13). Due to this dynamic state, the contact time of OBDA with feed nitric acid is decreased, thereby allowing better hydrolytic stability and OBDA based membrane is showing good transport of Am (III) over a wide range of feed HNO₃.

4.2.3.2 Effect of OBDA concentration in the membrane phase

In solvent extraction studies, extraction values always found to be increase with increasing extractant concentration but in the facilitated transport of metal ions across a SLM carrier concentration in the membrane phase plays an important role. Therefore,

the effect of carrier concentration on transport behavior was studied in detail for four different concentrations of OBDA **20a** and shown in Fig. 4.15. As evident from the Fig. 4.15, there is an initial increase in transport rate with increasing OBDA **20a** concentration from 0.05 M to 0.1 M which on further increase resulted in decreasing trend in Am(III) transport rate. Identical behavior was observed for Am(III)-TEHDGA system where it has been shown a maximum transport at 0.2 M TEHDGA concentration beyond which a decrease was observed [155].

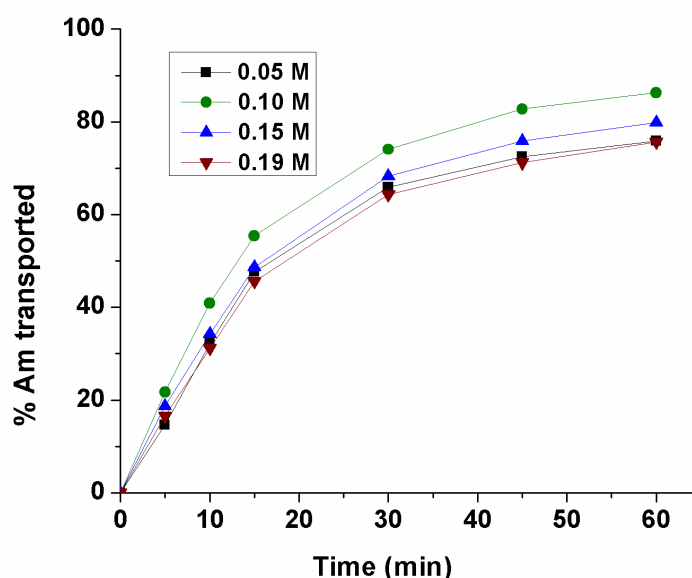


Fig. 4.15 Transport of Am(III) using OBDA **20a** as carrier at different concentrations of OBDA **20a**; Feed- 2 M HNO₃ , Carrier- varying concentrations of OBDA **20a** in 15% IDA/*n*-dodecane, Membrane- 0.2 μm PTFE, Strippant- pH 2 solution

The initial increase in transport rate with OBDA **20a** concentration is due to increase in concentration gradient of the metal-carrier complex due to complexation of Am(III) with OBDA in the feed-membrane interface. But with increasing OBDA concentration the viscosity of the membrane phase increases which decreases the transport rate according to Stoke-Einstein Equation:

$$D = kT/6\pi\eta r \dots\dots\dots (4.2)$$

Where k is the Boltzmann constant, T is the absolute temperature (K), η is the viscosity of the organic phase, r is the ionic radius of the metal ion (A^0) and D is the diffusion coefficient of the metal ion. These two factors make 0.1 M as the optimum OBDA concentration with 15% IDA/*n*-dodecane. Hence further studies on the optimization of other parameters were carried out using 0.1 M OBDA **20a** in 15% IDA/*n*-dodecane.

4.2.3.3 Effect of membrane pore size

Membrane characteristics such as membrane pore size, porosity, tortuosity, pore-structure play an important role in metal ion transport across SLM. We have studied the effect of membrane pore size on the transport of Am(III) for 0.1 M OBDA in 15% IDA as carrier. The trend of permeability co-efficient values for different pore size membranes is shown in Fig. 4.16.

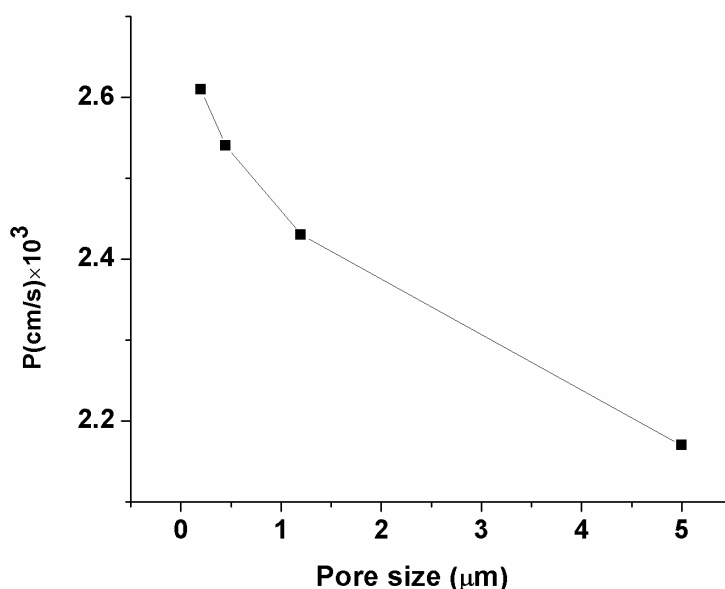


Fig. 4.16 Plot of permeability co-efficient values against varying membrane pore size; Feed- 2 M HNO_3 , Carrier- 0.1 M OBDA in 15% IDA/*n*-dodecane, Membrane- PTFE membranes of varying pore size, Strippant- pH 2 solution

As can be seen from the figure, there is a continuous decrease in transport rate of Am(III) with increasing membrane pore size for OBDA as carrier. This can be explained by Laplace's Equation:

$$P = (2\gamma/r_p)\cos\theta \dots\dots\dots (4.3)$$

where p is the trans-membrane pressure required to displace the carrier molecule from the pores of the membrane having pore size r_p . The inverse relation between p and r_p indicates that with increasing membrane pore size it is easier to replace carrier molecule from the membrane pores thus enhancing the leaching process. This signifies lower stability for membranes having higher pore size. This causes a decrease in transport rate of Am(III) at higher membrane pore sizes using OBDA as carrier.

4.2.3.4 Effect of membrane thickness

The transport of metal ions across SLM in a carrier mediated transport mechanism is diffusion controlled. The rate of diffusion is inversely proportional to the diffusional path length, *i.e.*, membrane thickness in SLM. With increasing membrane thickness the transport rate decreases which can be understood from the Equation:

$$P = (D_{Am(III)} \cdot D_0) / d_0 \tau \dots\dots\dots (4.4)$$

Where P is the permeability co-efficient, D_0 is the diffusion co-efficient, d_0 is the membrane thickness, τ is the tortuosity factor.

In order to investigate the mechanism of Am(III) transport using OBDA as carrier we carried out membrane transport studies using varying membrane thickness. The feed solution was maintained at 2 M HNO₃ with 0.1 M OBDA in 15% IDA/*n*-dodecane as the carrier. The stirring rate in this experiment was kept at 8.33 Hz (500 rpm) to reduce the aqueous diffusion film thickness to minimum value. The transport rate decreased from ~95% for 65 μm to ~76% for 325 μm in 1 h. The plot of P vs $1/d_0$ yielded a straight line from which the diffusion co-efficient value was found to be $5.1 \times$

10^{-6} cm²/s. This value is higher than Am(III)-TEHDGA system which was reported to be $\sim 1.2 \times 10^{-6}$ cm²/s [155].

4.2.3.5 Transport of metal ions

In order to see the selectivity of OBDA for Am(III) in SLM mode the transport behavior of different radionuclides was observed from 2 M HNO₃ medium. The trend is given in Fig. 4.17. As evident from the figure, none of the elements except Am(III), Ce(III), Eu(III) and Pu(IV/III) got transported to any significant amount. This proves that OBDA as a carrier in SLM provides excellent decontamination factor over fission products.

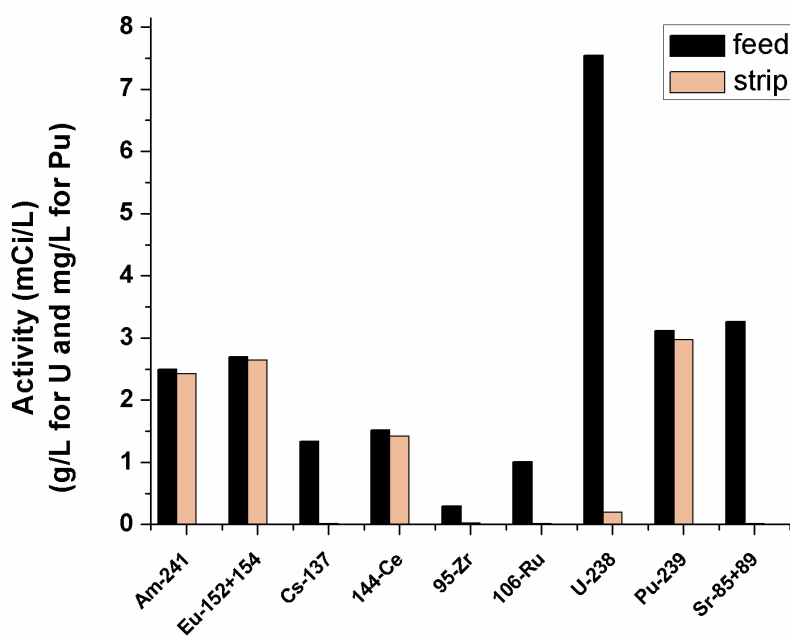


Fig. 4.17 Transport of different elements from nitric acid medium; Feed- 2 M HNO₃ , Carrier- 0.1 M OBDA in 15% IDA/*n*-dodecane, Membrane- 0.2 μm PTFE, Strippant- pH 2 solution.

4.2.3 6 Stability of membrane

Stability of membrane containing a specific carrier molecule is an important characteristic to be checked out for SLM transport studies. Stability of SLM was shown

to be dependent on the volatility of the diluent used. As mentioned by Kemperman *et al.* [164], the stability of the SLM is affected by various parameters such as leaching out of the carrier molecule from the membrane phase due to pressure gradient, chemical degradation, loss of the solvent from membrane phase due to its aqueous solubility etc. We investigated the stability pattern of the SLM containing OBDA as carrier. The transport behavior of Am was determined for a number of successive operations. The trend in Fig. 4.18 shows excellent stability of the membrane phase even after 6 cycles of continuous operation. Hence, here also we do not observed acid hydrolysis of OBDA as it is successfully recycled even for 6 continuous operations. This trend further proves our assumption of the very small time of contact of OBDA with HNO₃ in the membrane phase.

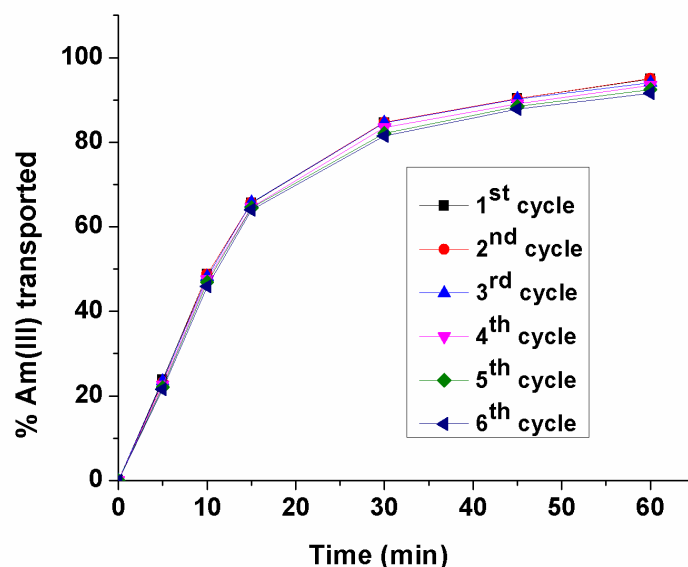


Fig. 4.18 Stability of SLM containing 0.1 M OBDA in 15% IDA in *n*-dodecane as carrier; Feed- 2 M HNO₃, Carrier- 0.1 M OBDA in 15% IDA/*n*-dodecane, Membrane- 0.2 μ m PTFE, Strippant- pH 2 solution

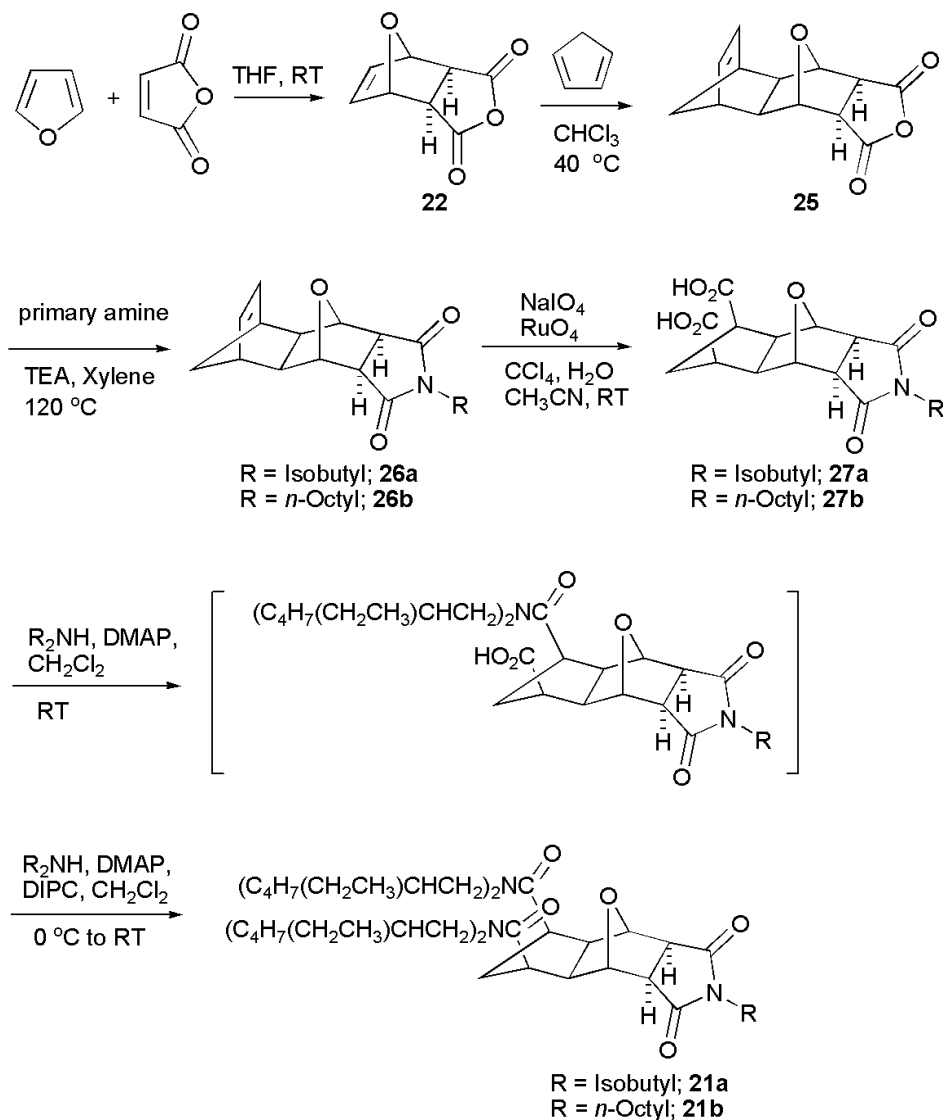
4.2.4 Synthesis and extraction studies of Pu selective rigidified oxa-diamides

In order to increase the hydrolytic stability of OBDA some structural modification was done in the OBDA ligand. We observed that the close proximity of two amide

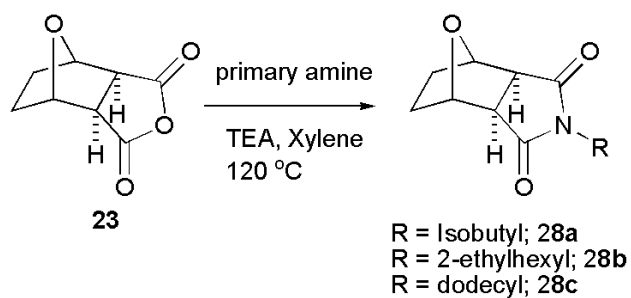
carbonyls in OBDA facilitates acid induced hydrolysis by neighbouring group participation mechanism. Therefore we synthesized new class of oxa-diamides having comparatively large distance between carbon and oxygen of two amide groups by increasing the number of carbons between amide moieties. By this way we also succeed to alter the cavity size created by three donor groups (two amides and one ether oxygen). We were curious to see the effect of slightly tuned cavity size of new oxa-diamides **21** on ionic selectivity in extraction of actinides and lanthanides.

4.2.4.1 Synthesis of Pu selective rigidified oxa-diamides

For the synthesis of new oxa-diamides (Scheme 4.2), anhydride **22** was reacted with cyclopentadiene to give Diels-Alder *endo* adduct **25**. This anhydride was opened up with one molecule of isobutyl or octyl amine in presence of triethylamine to obtain the imide **26a,b**. Imide group was introduced with an aim to stop the hydrolytic degradation as we found that the imides **28a-c** (Scheme 4.3) showed no hydrolytic degradation in HNO₃. These imides also do not participate in the extraction of any metal present in HLW (An, Ln and other fission products). In the next step, the double bond in imides **26a,b** was converted to diacids **27a,b** by RuO₄ mediated oxidative cleavage in the presence of NaIO₄. The diacids **27a,b** was allowed to react with bis(2-ethylhexyl)amine in the presence of DIPC and DMAP, by the same procedure used for synthesis of OBDA **20**, to obtain final extractants **21a,b** (Scheme 4.2).



Scheme 4.2 Synthesis of Pu selective oxa-diamides.



Scheme 4.3 Synthesis of imides **28a-c**.

4.2.4.2 Extraction studies of Pu selective rigidified oxa-diamides

Extraction behavior of oxa-diamide **21a** and **21b** was evaluated for Pu(IV) by changing various extraction parameters *viz.* feed acidity, ligand concentration, nitrate concentration etc. Stoichiometry of extracted metal ligand complex was determined by slope analysis method. Selectivity, stripping and hydrolytic stability studies were also carried out.

4.2.4.2.1 Kinetics of extraction

The time required to attain the equilibration condition for extraction of Pu(IV) was determined for 0.1 M oxa-diamide **21b** in 30% IDA/*n*-dodecane at 4 M feed HNO₃ concentration. Kinetics of extraction was found to be fast and the equilibrium was attained within 5 min (Fig. 4.19). Therefore, in subsequent studies, 10 min equilibration time was maintained.

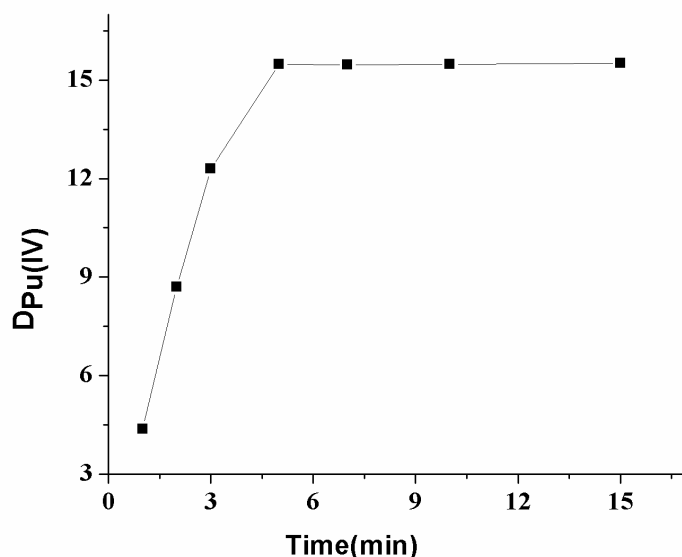


Fig. 4.19 Kinetics of extraction for Pu(IV)

4.2.4.2.2 Comparison of extraction behavior of oxa-diamide **21a** and **21b**.

For a comparison purpose, the extraction of Pu (IV) was studied with oxa-diamide ligands **21a** and **21b** using 0.1 M **21a/b** in 30% IDA/*n*-dodecane at 4 M HNO₃. D_{Pu} was

found to be 17.5 and 15.49 for oxa-diamide **21a** and **21b**, respectively. As the oxa-diamide **21b** showed better solubility in IDA/*n*-dodecane solvent system than **21a**, further extraction studies were carried out with oxa-diamide **21b**.

4.2.4.2.3 Effect of feed HNO₃ concentration on extraction of Pu(IV)

Distribution ratio values for Pu were determined at different nitric acid concentrations for 0.1 M **21b** in 30% IDA/*n*-dodecane. The values are shown in Fig. 4.20.

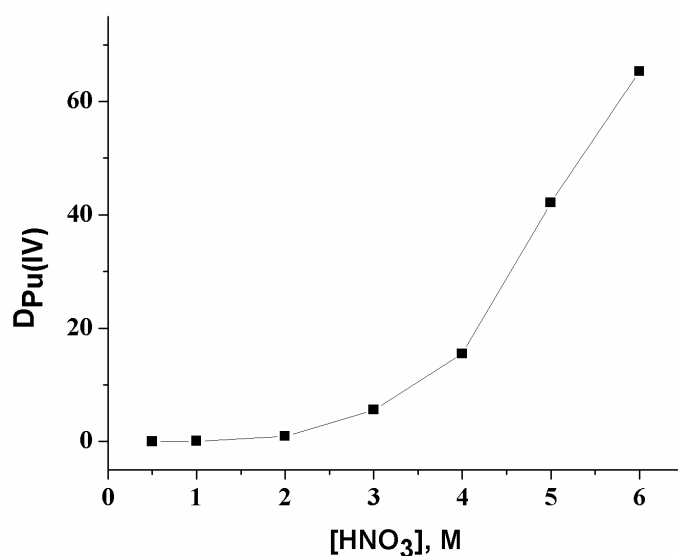
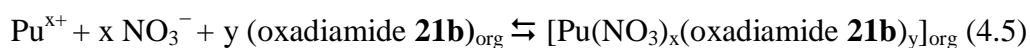


Fig. 4.20 D_{Pu} at varying feed HNO₃ concentration

D_{Pu} values were found to increase with increasing feed HNO₃ concentration. As oxa-diamide **21b** is a neutral extractant hence, the extraction mechanism takes place via nitrate ion assisted complex formation (Eq. 4.5). The subscript 'org' refers to species in organic phase and without subscript refer to those present in aqueous phase.



So increasing nitric acid concentration leads to increased formation of neutral metal-nitrate complex leading to higher D_{Pu} value, explains the increasing trend of D_{Pu} for oxa-diamide **21b** with increasing nitric acid concentration.

4.2.4.2.4 Effect of ligand concentration on extraction of Pu(IV).

For determination of stoichiometry of metal ligand complex D_{Pu} was determined at varying concentration of oxa-diamide **21b** in 30% IDA/*n*-dodecane at a fixed aqueous acidity (4 M HNO_3). As shown by the Fig 4.21, the D_{Pu} values increases with increasing ligand concentration in organic phase and plot of $\log D_{Pu}$ vs \log [ligand **21b**] gave a straight lines with slope value 1.08 indicating that Pu(IV) forms a mono-solvated species with ligand **21b**.

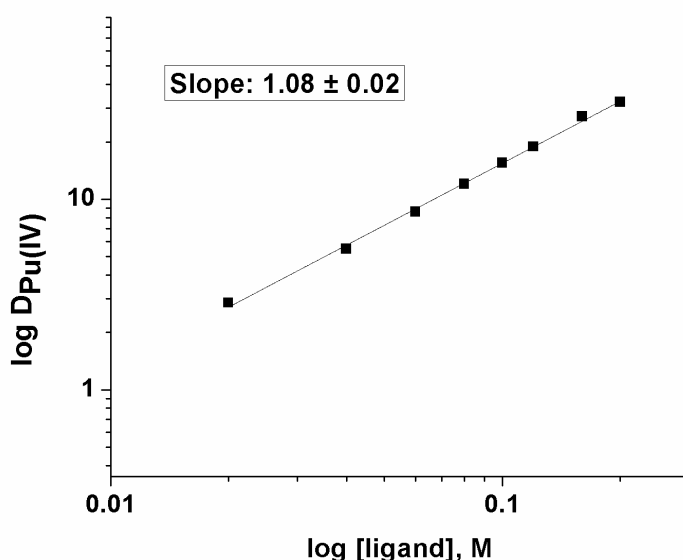


Fig. 4.21 Plot of $\log D_{Pu}$ vs \log [ligand **21b**].

4.2.4.2.5 Effect of nitrate ion concentration on extraction of Pu(IV).

In order to determine the participation of nitrate ion in formation of metal extracted species the D_{Pu} values were determined at different nitrate ion concentrations at a fixed aqueous acidity (0.5 M HNO_3) for 0.1 M **21b** in 30% IDA/*n*-dodecane. The plot of $\log D_{Pu}$ vs $\log [NO_3^-]$ showed a straight line with a slope of 4.21 (Fig. 4.22) indicating four nitrate ions are involved in the extraction of Pu(IV).

4.2.4.2.7 Stripping studies

Stripping studies were carried out for Pu(IV) at 0.5 M HNO₃ or using 0.3 M HAN + 0.2 M HNO₃. Results are shown in Table 4.6. Stripping agent 0.3 M HAN + 0.2 M HNO₃ provided better results with 80% stripping of Pu in a single contact.

Table 4.6 Stripping studies for Pu (IV) extraction with oxa-diamide **21b**.

Strippant	% Stripping (single contact)
0.5M HNO ₃	40.15
0.3M HAN +0.2M HNO ₃	80.21

4.2.4.2.8 Hydrolytic stability studies of new oxa-diamides

Hydrolytic stability of new oxa-diamides in acidic medium was checked in 4 M HNO₃.

Both the oxa-diamides **21a** and **21b** were found to be stable in 4 M HNO₃ for 15 days.

4.3 Conclusions

A conformationally constrained class of oxadiazides (OBDA) has been found to be excellent extractant for tri- and tetra-valent actinides as well as trivalent lanthanides in nitric acid medium. The synthesis of extractants are achieved from cheap commercially available materials in three steps in high yields and purity. OBDA **20a** showed excellent extraction behavior with fast kinetics, high loading capacity for lanthanides without third phase formation, very low extraction of fission products and easy stripping of the extracted metal ions. Very poor extraction of Sr(II) and Ru (III) by the ligand is advantageous because no scrubbing was needed before stripping. This class of molecules forms a mixture of mono-solvated and di-solvated species with Am and Eu as obtained by slope analysis method and ESI-MS. OBDA **20a** was found to be sensitive to hydrolytic degradation. This detrimental effect has been surpassed by fast

kinetics of complexation and hydrolytic stability of the complexed OBDA as supported by good D_M values at 3-4 M HNO_3 and stripping studies with 6 M HNO_3 . DFT study indicates the participation of both carbonyl and ethereal oxygens in the bonding with metal ion, which is also supported by FTIR and NMR studies.

Supported Liquid Membrane containing *N,N,N',N'*-Tetrakis(2-ethylhexyl)-7-oxabicyclo[2.2.1]heptane-2,3-dicarboxamides (OBDA) as carrier was found to be effective for the transport of Am(III) from HNO_3 medium. OBDA showed good hydrolytic stability in membrane phase due to decreased contact time with nitric acid in SLM and performed efficient transport of Am(III). Very high diffusion-coefficient value ($5.1 \times 10^{-6} \text{ cm}^2/\text{s}$) was observed for OBDA-Am(III) complex which is higher to that of the value reported for TEHDGA. Excellent selectivity for the trivalent and tetravalent actinides and lanthanides was observed using OBDA as carrier. Interestingly the OBDA based membrane was found to be stable at least up to 6 cycles of operation.

To overcome the setback of hydrolysis, a new class of acid stable oxa-diamides **21a,b** were synthesized having tuned cavity size created by donor groups. The new oxadiazides were found to be selective for Pu over other An, Ln and fission products found in HLW. The new extractants also showed good extraction behavior with fast kinetics, high selectivity and easy stripping of the extracted Pu.

4.4 Experimental

General Details

As described in Chapter 2.

Chemicals

Nitric acid, *n*-dodecane and isodecyl alcohol (IDA) were obtained from local sources.

Maleic anhydride, dicyclopentadiene, furan, Pd/C catalyst, diisobutyl amine, isobutyl

amine, octyl amine, dodecyl amine, dioctyl amine, bis-2ethylhexyl amine, diisopropylcarbodiimide, DMAP and other chemicals were purchased from local sources. The solvents were dried and distilled from the indicated drying agents: THF from sodium/benzophenone; chloroform from P₂O₅; ethyl acetate from CaCl₂ and then stored over molecular sieves; CH₂Cl₂ from CaH₂; xylene from sodium and all amine from CaH₂ and then stored over calcium metal.

Synthesis of diamides OBDA 20a-c

Exo-3,6-Epoxy-1,2,3,6-tetrahydrophthalic anhydride **22**

A freshly distilled furan (11 mL, 151.5 mmol) was added to a stirred solution of maleic anhydride (14.7 g, 150 mmol) in dry THF (45 mL) at room temperature. The reaction mixture was left standing for 5 days. The resulting crystals were filtered to obtain anhydride **22** (21 g, 84 %). **M.P.** 116-118 °C. **¹H NMR (200 MHz, CDCl₃):** 3.17 (2 H, s, COCHCHCO) 5.46 (2 H, s, CHOCH), 6.58 (2 H, s, CH=CH).

Exo-3,6-Epoxy-hexahydrophthalic anhydride **23**

Palladium on charcoal (400 mg, 10% Pd) was added to a solution of unsaturated anhydride **22** (4 g, 24.09 mmol) in dry ethyl acetate (72 mL). The mixture was degassed and flushed with hydrogen gas for several times followed by stirring under hydrogen atmosphere for 24 h. The mixture was filtered through celite and the filtrate was evaporated to give the saturated anhydride **23** (3.97 g, 98%). **M.P.** 112 °C. **¹H NMR (300 MHz, CDCl₃):** 1.57-1.62 (2 H, m, CH_AHCH_AH), 1.85-1.95 (2 H, m, CHH_BCHH_B), 3.18 (2 H, s, COCHCHCO), 5.03-5.05 (2 H, m, CHOCH).

General procedure-1

Preparation of OBDA 20a-c from anhydride **23** and *N,N*-dialkylamines

A solution of a *N,N*-dialkylamine (20.1 mmol) in dry CH₂Cl₂ (5 mL) was added slowly to a solution of anhydride **23** (1.68 g, 10 mmol,) in dry CH₂Cl₂ (15 mL) at room temperature followed by addition of DMAP (122 mg, 1 mmol). The reaction mixture

was stirred for 0.5 h and cooled on an ice-water bath. Diisopropylcarbodiimide (1.57 mL, 10.1 mmol) was added drop-wise to the stirred reaction mixture. The reaction mixture was allowed to attain room temperature and stirred overnight. The reaction mixture was diluted with 1/1 ethyl acetate-petroleum ether and washed with 5% citric acid solution, with water and concentrated under reduced pressure. The residue was purified by column chromatography to give OBDA **20a-c**.

***N,N,N',N'*-Tetrakis(2-ethylhexyl)-7-oxabicyclo[2.2.1]heptane-2,3-dicarboxamides
20a**

Yield: 5.56 g (88%); **M.P.** 100-103 °C. **IR (neat):** 2955, 2916, 2874, 2857, 1643, 1632, 1416 cm^{-1} ; **^1H NMR (200 MHz, CDCl_3):** δ 0.75-1.00 (24 H, m, $8 \times \text{CH}_3$), 1.05-1.41 (32 H, bs, $4 \times \text{CH}_2\text{CH}_3$, $4 \times \text{CH}(\text{CH}_2)_3\text{CH}_3$), 1.41-1.68 (4 H, m, $\text{CHCH}_2\text{CH}_2\text{CH}$), 1.72-1.95 (4 H, m, $4 \times \text{CHCH}_2\text{CH}_3$) 2.93 (2 H, s, COCHCHCO), 3.0 (4 H, d, $J = 6.4$ Hz, $2 \times \text{NCH}_2\text{CH}$), 3.15 (4 H, d, $J = 7.2$ Hz, $2 \times \text{NCH}_2\text{CH}$), 4.86 (2 H, s, $2 \times \text{CHOCH}$); **Anal. Calcd. for $\text{C}_{40}\text{H}_{76}\text{N}_2$:** C, 75.89; H, 12.1; N, 4.43%; Found C, 75.91; H, 12.18; N, 4.26%.

***N,N,N',N'*-Tetraoctyl-7-oxabicyclo[2.2.1]heptane-2,3-dicarboxamides 20b**

Yield: 5.37 g (85%); **IR (neat):** 2953, 2916, 2851, 2818, 1643, 1632, 1416, 746, 719 cm^{-1} ; **^1H NMR (300 MHz, CDCl_3):** δ 0.8-0.98 (12 H, m, $4 \times \text{CH}_3$), 1.16-1.4 (48 H, m, $24 \times \text{CH}_2$), 1.4-1.68 (4 H, m, $\text{CHCH}_2\text{CH}_2\text{CH}$), 2.85-2.95 (2 H, m, COCHCHCO), 2.95-3.2 (4 H, m, $2 \times \text{NCH}_2\text{CH}$), 3.23-3.42 (4 H, m, $2 \times \text{NCH}_2\text{CH}$), 4.86 (2 H, t, $J = 2.4$ Hz, $2 \times \text{CHOCH}$); **^{13}C NMR (75 MHz, CDCl_3):** δ 14 (2 C), 22.6 (2 C), 27 (2 C), 27.2 (2 C), 27.3 (2 C), 29 (2 C), 29.2 (3 C), 29.3 (3 C), 29.33 (3 C), 29.4 (3 C), 29.5 (2 C), 31.7 (2 C), 31.8 (2 C), 46.2 (2 C), 47.7 (2 C), 51.1 (2 C), 79.2 (2 C), 169.2 (2 C); **Anal. Calcd. for $\text{C}_{40}\text{H}_{76}\text{N}_2$:** C, 75.89; H, 12.10; N, 4.43%; Found C, 76.13; H, 12.24; N, 4.34%.

***N,N,N',N'*-Tetrabutyl-7-oxabicyclo[2.2.1]heptane-2,3-dicarboxamides 20c**

Yield: 3.51 g (86%); **M.P.** 156 °C; **IR (neat):** 2956, 2869, 1655, 1632, 1414 cm^{-1} ; **^1H NMR (300 MHz, CDCl_3):** δ 0.75-1.00 (24 H, m, $8 \times \text{CH}_3$), 1.45-1.58 (2 H, m, $\text{CH}_A\text{HCH}_A\text{H}$), 1.76-1.88 (2 H, m, CHH_BCHH_B), 1.88-2.0 (2 H, m, $2 \times \text{CH}_2\text{CH}(\text{CH}_3)_2$), 2.0-2.19 (2 H, m, $2 \times \text{CH}_2\text{CH}(\text{CH}_3)_2$), 2.8-3.2 (10 H, m, $4 \times \text{NCH}_2\text{CH}$, COCHCHCO), 4.86 (2 H, s, $2 \times \text{CHOCH}$); **^{13}C NMR (75 MHz, CDCl_3):** δ 19.9 (2 C), 20.2 (2 C), 20.5 (2 C), 20.6 (2 C), 26.2 (2 C), 27.6 (2 C), 29.5 (2 C), 51.3 (2 C), 53.8 (2 C), 55.5 (2 C), 79.4 (2 C) 170 (2 C); **Anal. Calcd. for $\text{C}_{24}\text{H}_{44}\text{N}_2$:** C, 70.54; H, 10.85; N, 6.86%; Found C, 70.74; H, 11.08; N, 6.73%.

Synthesis of new oxa-diamides**Synthesis of Deals-elder adduct 25**

Freshly distilled cyclopentadiene (37.8 mL, 15 eq, 450 mmol) was added to a suspension of exo-3,6-Epoxy-1,2,3,6-tetrahydrophthalic anhydride **22** (4.98 g, 1 eq, 30 mmol) in dry CHCl_3 and the mixture was heated to 40 °C for 4 days overnight. The resulting reaction mixture was allowed to stand overnight and the obtained white crystals were filtered and washed with 2% ethyl acetate petrol mixture to give **25**. (yield 2.78 g, 41%)

M.P. 183 °C. **^1H NMR (300 MHz, CDCl_3):** 1.2 (1 H, d, $J = 8.1$, CHH), 1.4 (1 H, d, $J = 8.1$, CHH), 2.4 (2 H, s, $\text{CH}(\text{CH}=\text{CH})\text{CH}$), 2.97 (2 H, s, $2 \times \text{CH}(\text{CHCH}=\text{CHCH})$), 3.08 (2 H, s, $2 \times \text{CHCO}$), 4.64 (2 H, s, CHOCH), 5.97 (2 H, s, $\text{CH}=\text{CH}$). **^{13}C NMR (50 MHz, CDCl_3):** 44.9 (2 C), 48.3 (2 C), 51.3, 51.9 (2 C), 80.7 (2 C), 133.4 (2 C), 171 (2 C). **IR (KBr):** 3074, 2978, 2871, 1859, 1835, 1770, 1252, 1234; **Anal. Calcd. for $\text{C}_{13}\text{H}_{12}\text{O}_4$:** C, 67.23; H, 5.21; Found C, 67.17; H, 5.123.

Synthesis of imide **26a**

Triethyl amine (1.3 mL, 1.2 eq, 9.31 mmol) and isobutyl amine (925 mL, 1.02 eq, 9.31 mmol) was added to a stirred suspension of anhydride **25** (1.8 g, 1 eq, 7.76 mmol) in xylene (7 mL). The reaction mixture was stirred for 0.5 h at room temperature, diluted with xylene (25 mL) and reflux at 120 °C for 4 h. The solvent and excess amine was evaporated under reduced pressure and the residue was purified by column chromatography using 15% ethyl acetate petrol mixture to obtain product **26a** (1.92 g, yield 86%).

M.P. 140 °C. **¹H NMR (300 MHz, CDCl₃):** 0.82 (6 H, d, $J = 6.6$, $2 \times \text{CH}_3$), 1.2 (1 H, d, $J = 7.8$, CHH), 1.37 (1 H, d, $J = 8.1$, CHH), 1.85-2.05 (1 H, s, NCH₂CH), 2.38 (2 H, s, CH(CH=CH)CH), 2.77 (2 H, s, $2 \times \text{CH}(\text{CHCH}=\text{CHCH})$), 2.92 (2 H, s, $2 \times \text{CHCO}$), 3.22 (2 H, d, $J = 7.5$, NCH₂), 4.47 (1 H, s, CHOCH), 5.96 (2 H, s, CH=CH) **¹³C NMR (75 MHz, CDCl₃):** 20 (2 C), 26.9, 44.9 (2 C), 46.2, 48.8 (2 C), 51.2 (2 C), 51.6, 79.5 (2 C), 133.4 (2 C), 177.2 (2 C). **IR (KBr):** 2966, 2930, 2864, 1696, 1405 cm⁻¹; **Anal. Calcd. for C₁₇H₂₁NO₃:** C, 71.06; H, 7.37; N, 4.87%; Found C, 71.11; H, 7.047; N, 4.67%.

Synthesis of imide **26b**

Following the procedure described for the synthesis of **26a**, octylamine (1.24 mL, 1.01 eq, 7.49 m mol) and anhydride **25** (1.72 g, 1 eq, 7.42 m mol) gave imide **26b** (2.13 g, yield 80%).

M.P. 70 °C. **¹H NMR (300 MHz, CDCl₃):** 0.85 (3 H, t, $J = 7.2$, CH₃), 1.12-1.3 (12 H, bs, $5 \times \text{CH}_2$, CHH), 1.3-1.4 (1 H, d, $J = 8.4$, CHH), 1.4-1.51 (2 H, m, NCH₂CH), 2.37 (2 H, s, CH(CH=CH)CH), 2.75 (2 H, s, $2 \times \text{CH}(\text{CHCH}=\text{CHCH})$), 2.91 (2 H, s, $2 \times$

CHCO), 3.35 (2 H, d, $J = 7.5$, NCH_2), 4.46 (1 H, s, *CHOCH*), 5.95 (2 H, s, $CH=CH$). ^{13}C NMR (75 MHz, $CDCl_3$): 14.0, 22.6, 26.7, 27.6, 29.0 (2 C), 31.7, 39.0, 44.9 (2 C), 48.7 (2 C), 51.2 (2 C), 51.5, 79.5 (2 C), 133.4 (2 C), 176.9 (2 C). IR (KBr): 2962, 2930, 2857, 1690, 1407 cm^{-1} ; Anal. Calcd. for $C_{21}H_{29}NO_3$; C, 73.44; H, 8.51; N, 4.08%; Found C, 73.58; H, 8.236; N, 4.31%.

Synthesis of diamide 21a,b from imide 26 a,b

General procedure; Sodium periodate (335 mg, 4.5 eq, 1.57 mmol) was added to a stirred solution of Imide **26a/b** (1 eq, 0.35 mmol) in a mixture of CCl_4 , CH_3CN , H_2O (1.5 mL, 1.5 mL, 2.25 mL). After 5 min of stirring, $RuO_4 \cdot xH_2O$ (1.5 wt%) was added to the reaction mixture and stirred vigorously for 3 h. The reaction mixture was concentrated, titrated with ethyl acetate and filtered through celite. The product **27a/b** was used for next reaction without any purification. For amide synthesis a solution of bis(2-ethylhexyl)amine (210 μL , 2 eq, 0.7 mmol) in dry CH_2Cl_2 was added to a solution of acid **27a/b** (1 eq, 0.35 mmol) in dry CH_2Cl_2 at room temperature followed by addition of DMAP (17 mg, 0.2 eq, 0.14 mmol). The reaction mixture was stirred for 15 min and cooled on an ice-water bath. Diisopropylcarbodiimide (110 μL , 2 eq, 0.7 mmol) was added drop-wise to the stirred reaction mixture. The reaction mixture was allowed to attain room temperature and stirred overnight. The reaction mixture was diluted with 1/1 ethyl acetate-petroleum ether mixture and washed with 5% citric acid solution, with water and concentrated under reduced pressure. The residue was purified with column chromatography to give final product **21a/b**.

Oxa-diamide 21a

Yield: 303 mg (38%); **M.P.** 184-197 °C (waxy solid); 1H NMR (300 MHz, $CDCl_3$): 0.82 (6 H, d, $J = 6.6$, $2 \times CHCH_3$), 0.83-1.05 (24 H, m, $8 \times CH_3$), 1.05-1.51 (34 H, bs, CH_2), 1.52-1.68 (4 H, bs, $4 \times CH_2CHCH_2N$), 1.85-2.0 (1H, m, $CH(CH_3)_2$), 2.49 (2 H, s,

$2 \times \text{CHCON}(\text{CH}_2)_2$), 2.73 (2 H, s, $2 \times \text{CHCO}$), 2.8-3.3 (10 H, m, $5 \times \text{NCH}_2$), 3.51-3.65 (1 H, m, CHCOC), 3.65-3.8 (1 H, m, CHCOC), 4.84 (2 H, s, CHOCH). **IR (KBr):** 2960, 2929, 2874, 2859, 1705, 1630, 1451. **Anal. Calcd. for $\text{C}_{49}\text{H}_{87}\text{N}_3\text{O}_5$:** C, 73.73; H, 10.99; N, 5.26%; Found: C, 73.49; H, 10.74; N, 5.13%.

Oxa-diamide 21b

Yield: 350 mg (41%); **M.P.** 183-196 °C (waxy solid); **^1H NMR (300 MHz, CDCl_3):** 0.80-1.05 (27 H, m, $9 \times \text{CH}_3$), 1.05-1.51 (44 H, m, CH_2), 1.52-1.68 (4 H, bs, $4 \times \text{CH}_2\text{CHCH}_2\text{N}$), 1.68-1.88 (2 H, bs, NCH_2CH_2), 2.49 (2 H, bs, $2 \times \text{CHCON}(\text{CH}_2)_2$), 2.73 (2 H, s, $2 \times \text{CHCO}$), 2.8-3.4 (10 H, m, $5 \times \text{NCH}_2$), 3.55-3.68 (1 H, m, CHCOC), 3.69-3.82 (1 H, m, CHCOC) 4.83 (2 H, s, CHOCH). **IR (KBr):** 2960, 2930, 2874, 2860, 1704, 1630, 1461, 1377. **Anal. Calcd. for $\text{C}_{53}\text{H}_{95}\text{N}_3\text{O}_5$:** C, 74.51; H, 11.21; N, 4.92%; Found C, 74.46; H, 11.02; N, 4.87%.

Synthesis of imides 28a-c

Imide **28a** and **28b-c** were synthesized by the same procedure described earlier for the synthesis of **26a** and **26b** respectively.

Imide 28a

Yield: 1.56 g (90%); **^1H NMR (200 MHz, CDCl_3):** 0.83 (6 H, d, $J = 6.8$, $2 \times \text{CH}_3$), 1.51-1.63 (2 H, m, CH_2COC), 1.75-1.88 (2 H, m, CH_2COC) 1.88-2.1 (1 H, m, $(\text{CH}_3)_3\text{CHCH}_2\text{N}$), 2.84 (2 H, s, $2 \times \text{CHCON}$), 3.25 (2 H, d, $J = 7.4$, $(\text{CH}_3)_3\text{CHCH}_2\text{N}$), 4.85-4.82 (2 H, m, CHOCH). **^{13}C NMR (50 MHz, CDCl_3):** 19.8 (2 C), 26.8, 28.5 (2 C), 46.1, 49.7 (2 C), 79 (2 C), 177.4 (2 C). **Anal. Calcd. for $\text{C}_{12}\text{H}_{17}\text{NO}_3$:** C, 68.79; H, 9.02; N, 5.01%; Found C, 68.74; H, 9.45; N, 5.30%.

Imide 28b

Yield: 1.78 g (82%) ; $^1\text{H NMR}$ (200 MHz, CDCl_3): 0.77-0.95 (6 H, m, $2 \times \text{CH}_3$), 1.1-1.35 (8 H, m, $4 \times \text{CH}_2$), 1.53-1.78 (4 H, m, $\text{CH}_2\text{CH}_2\text{COC}$), 1.78-1.93 (1 H, m, $\text{CH}_2\text{CHCH}_2\text{N}$), 2.85 (2 H, s, $2 \times \text{CHCON}$), 3.35 (2 H, d, $J = 7.4$, $\text{CH}_2\text{CHCH}_2\text{N}$), 4.84-4.87 (2 H, m, CHOCH). $^{13}\text{C NMR}$ (50 MHz, CDCl_3): 10.2, 13.9, 22.8, 23.4, 28.1, 28.5 (2 C), 30, 37.0, 42.7, 49.7 (2 C), 79 (2 C), 177.4 (2 C). **Anal. Calcd. for $\text{C}_{16}\text{H}_{25}\text{NO}_3$;** C, 74.48; H, 10.08; N, 5.32%; Found C, 74.56; H, 10.18; N, 5.13%.

Imide 28c

Yield: 2.26 g (87%); $^1\text{H NMR}$ (500 MHz, CDCl_3): 0.86 (3 H, t, $J = 7$, CH_3), 0.83-1.05 (18 H, s, $9 \times \text{CH}_2$), 1.57-1.65 (2 H, m, CH_2CO), 1.65-1.72 (2 H, m, CH_2CO) 1.8-1.85 (2 H, m, $\text{CH}_2\text{CH}_2\text{CH}_2\text{N}$), 2.83 (2 H, s, $2 \times \text{CHCON}$), 3.43 (2 H, t, $J = 7$, $\text{CH}_2\text{CH}_2\text{CH}_2\text{N}$), 4.85 (2 H, s, CHOCH). $^{13}\text{C NMR}$ (50 MHz, CDCl_3): 14.0, 22.6, 26.6, 27.5, 28.5 (2 C), 29, 29.2, 29.4, 29.4, 29.5 (2 C), 31.8, 39, 49.8(2 C), 78.9(2 C), 177.1 (2 C). **Anal. Calcd. for $\text{C}_{20}\text{H}_{33}\text{NO}_3$;** C, 71.6; H, 9.91; N, 4.18%; Found C, 71.5; H, 10.09; N, 4.18%.

Solvent extraction studies

Solutions of desired concentration of OBDA **20a-c** were prepared in *n*-dodecane (with 15% iso-decanol as the phase modifier) and agitated with an equal volume of the aqueous phase (containing the requisite quantity of $^{239}\text{Pu}/^{2420\text{a}}\text{m}$ tracer) in a rotary thermostated water bath for 5 minutes at 25.0 ± 0.1 °C. The two phases were then centrifuged and assayed by taking suitable aliquots from both the phases. The distribution ratio (D_M) is defined as the ratio of concentration of metal ion in the organic phase to that in the aqueous phase. The valency of Pu during extraction was maintained as Pu(IV). For preparation of Pu(IV) stock, NaNO_2 was used as oxidant in 1 M HNO_3 solution. The oxidized Pu(IV) solution was subsequently extracted by 0.5 M 2-thenoyltrifluoroacetone (TTA) in xylene where Pu(IV) is quantitatively extracted.

The loaded Pu was stripped by 7 M HNO₃ and equilibrated three times with xylene to remove dissolved TTA from the aqueous phase. The stripped Pu solution was used as stock for Pu(IV). For extraction studies of various fission products, HLW solution generated from PUREX process was diluted in 3 M HNO₃ and was used as feed. HLW originated from research reactor fuel reprocessing plant from a particular batch having the composition of uranium (predominantly ²³⁸U)-7.51 g/L, plutonium (predominantly ²³⁹Pu)-3.19 mg/L, ¹³⁷Cs-8.89 Ci/L, ¹⁰⁶Ru-7.99 Ci/L, ¹⁴⁴Ce-27.75 Ci/L, ⁹⁰Sr-4.0 Ci/L, ¹²⁵Sb -0.2 Ci/L, ⁹⁵Nb- 14.32 mCi/L was used. In view of high activity of HLW, it was diluted by 100 times to bring down the activity to a measurable level. Consequently, the activity of the radionuclide ¹⁵²⁺¹⁵⁴Eu became too low to determine and hence, had to be spiked. Owing to pure β activity of ⁹⁰Sr present in the diluted solution, ⁸⁵⁺⁸⁹Sr was spiked where a gamma emitter, namely, ⁸⁵Sr was used as a tracer. The acidity was finally adjusted to 3 M HNO₃. All distribution studies were carried out in duplicate and the data were reproducible within an error limit of ±5%.

Membrane separation studies

PTFE membranes (average pore size: 0.2 μm; porosity: 51%) used in the present study were procured from Sartorius, Germany. All the reagents used were of AR grade and were used as procured. ²⁴¹Am was purified according to the reported procedure [165]. ^{85,89}Sr was procured from BRIT, India and used after checking its radiochemical purity. For transport studies of various fission products, HLW originated from research reactor fuel reprocessing plant having the composition of uranium (predominantly ²³⁸U)-9.56 g/L, plutonium (predominantly ²³⁹Pu)-3.19 mg/L, ¹³⁷Cs-10.29 Ci/L, ¹⁰⁶Ru-5.59 Ci/L, ¹⁴⁴Ce-31.75 Ci/L, ⁹⁰Sr-4.0 Ci/L, ⁹⁵Zr -0.2 Ci/L was used as feed in membrane experiment. In view of high activity of HLW, it was diluted by 1000 times to bring down the activity to a measurable level. Consequently, the activity of the radionuclide

$^{152+154}\text{Eu}$ became too low to determine and hence, had to be spiked. Owing to pure β activity of ^{90}Sr present in the diluted solution, $^{85+89}\text{Sr}$ was spiked where a gamma emitter, namely, ^{85}Sr was used as a tracer. The final acidity of the feed was adjusted to 2.0 M HNO_3 .

Membrane characterization

The following membrane characteristics were measured: a) membrane thickness by a Mitutoyo digital micrometer; b) porosity of the membranes by an Electroscan 2020 environmental scanning electron microscope (ESEM) as reported earlier [158]. The effective area of the membrane flat sheet was determined to be 2.50 cm^2 .

Analysis of radionuclides

The radio assaying of ^{241}Am was done by gamma counting using a NaI(Tl) scintillation counter inter-phased to a multi channel analyzer. The activity of the radionuclides during HLW experiment was assayed with a high purity germanium detector coupled to a 4096 channel analyzer. Energies used for the various radionuclides were as follows: ^{106}Ru -621 keV, ^{137}Cs -662 keV, ^{144}Ce -133 keV, ^{241}Am -59 keV, ^{152}Eu -121.8 keV and $^{85+89}\text{Sr}$ -514 keV. Uranium analysis was carried out spectrophotometrically using Br-PADAP as chromogenic reagent. Usually, the counting statistics error was less than $\pm 2\%$.

Transport studies

Pyrex glass cell consisting of two compartments (having volume 16 mL each) was used for SLM transport experiments. The feed and strip solutions were stirred at 5 Hz (300 rpm) to prevent concentration polarization in the membrane interfaces and in the bulk of the solutions [166]. The PTFE membranes were soaked in the carrier solution

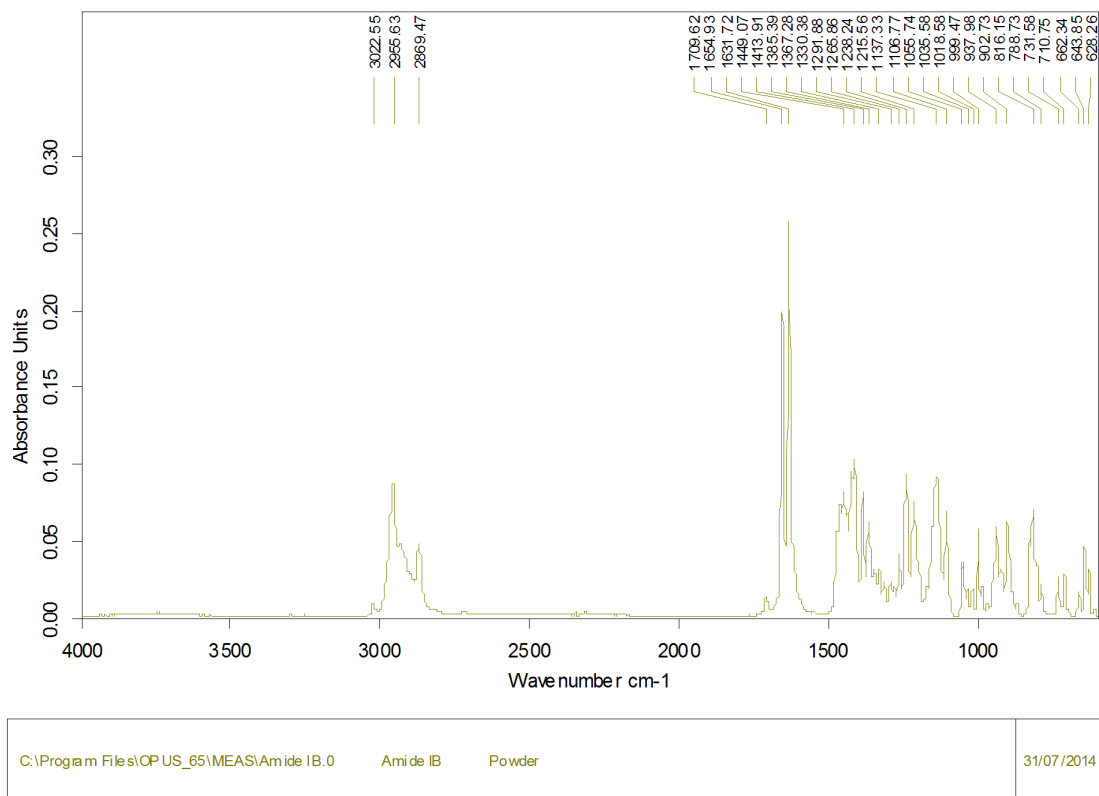
(generally 0.1 M OBDA in 15% IDA/*n*-dodecane) at least 30 min prior to experiment. The use of 15% IDA/*n*-dodecane as diluent was for prevention of third phase formation as observed in Solvent extraction studies. Subsequently, the submerged membrane was removed from the solution and wiped carefully with a tissue paper to remove the excess carrier solution on both the sides. During experiments, aliquots were removed from the feed as well as the receiver compartments in regular intervals and assay of radionuclides were done as mentioned above. Transport of hydrogen ion was monitored by volumetric titrations. The transport studies were carried out at ambient temperatures (24-26°C). During stability studies the feed and strip solutions were removed after each experiment and fresh solution of feed and strippant was put into the feed and strip compartment respectively for further transport experiment. The cumulative percent transport (%T) at a given time is determined by the following Equation,

$$\%T = 100. \frac{C_{r,t}}{C_{f,0}} \dots\dots\dots (4.6)$$

where, $C_{f,0}$ is concentrations of the metal ion in the feed phase at starting time and $C_{r,t}$ is the concentration of the metal ion in the receiver phase at a given time 't'.

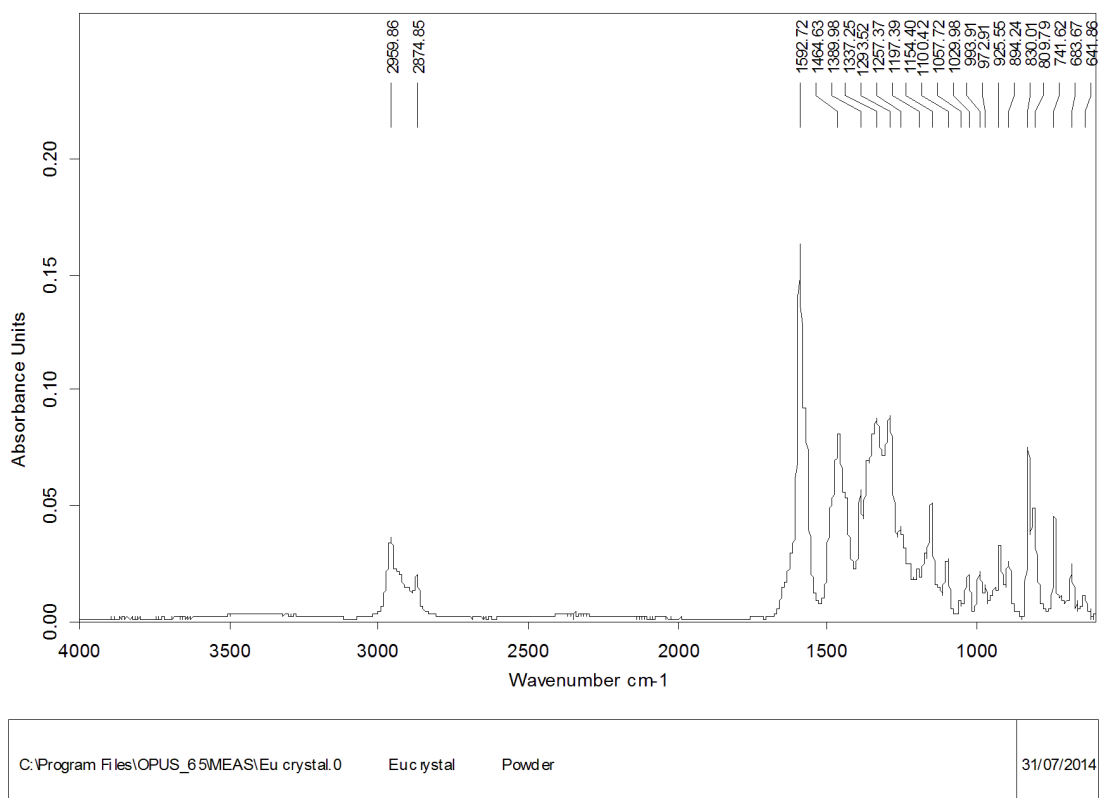
Computational methods

Gas phase geometries of the free ligand (OBDA) and its Am^{3+} complex were optimized at the GGA level of density functional theory (DFT) by using Becke's exchange functional [167] in conjunction with Perdew's correlation functional [168] (BP86) with generalized gradient approximation (GGA) where 60 electron core pseudopotentials (ECPs) along with the corresponding def-SV(P) basis set were selected for the Am^{3+} ion. All other lighter atoms were treated at the all electron (AE) level. All the calculations were performed using the TURBOMOLE program package [169, 170].



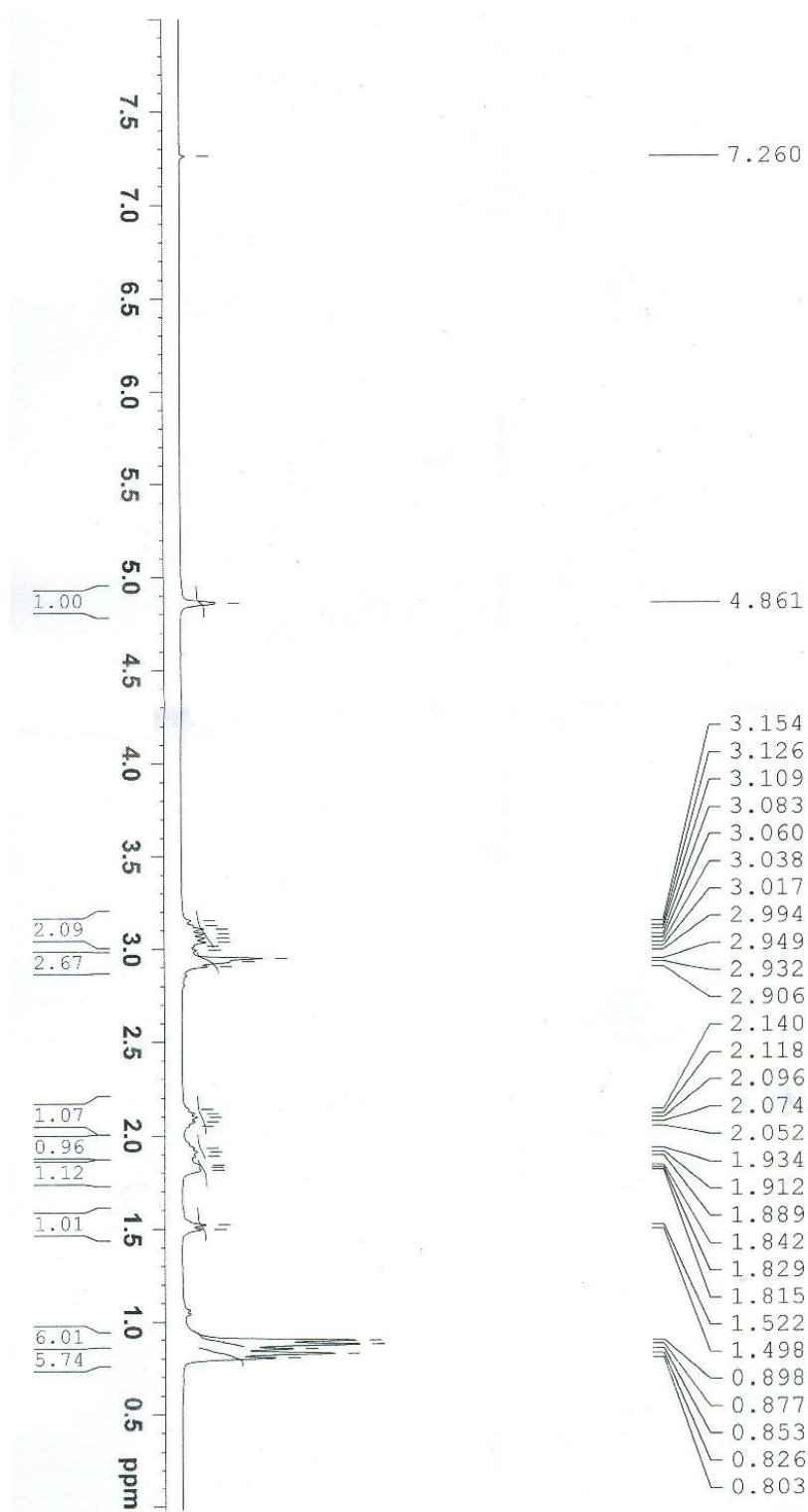
Page 1/1

Fig. 4.23 IR spectrum of OBDA **20c**.



Page 1/1

Fig. 4.24 IR spectrum of complex of $\text{Eu}(\text{NO}_3)_3 \cdot 5\text{H}_2\text{O}$ with OBDA **20c**.



exp 173



Fig . 4.25 ^1H NMR spectrum of OBDA 20c.

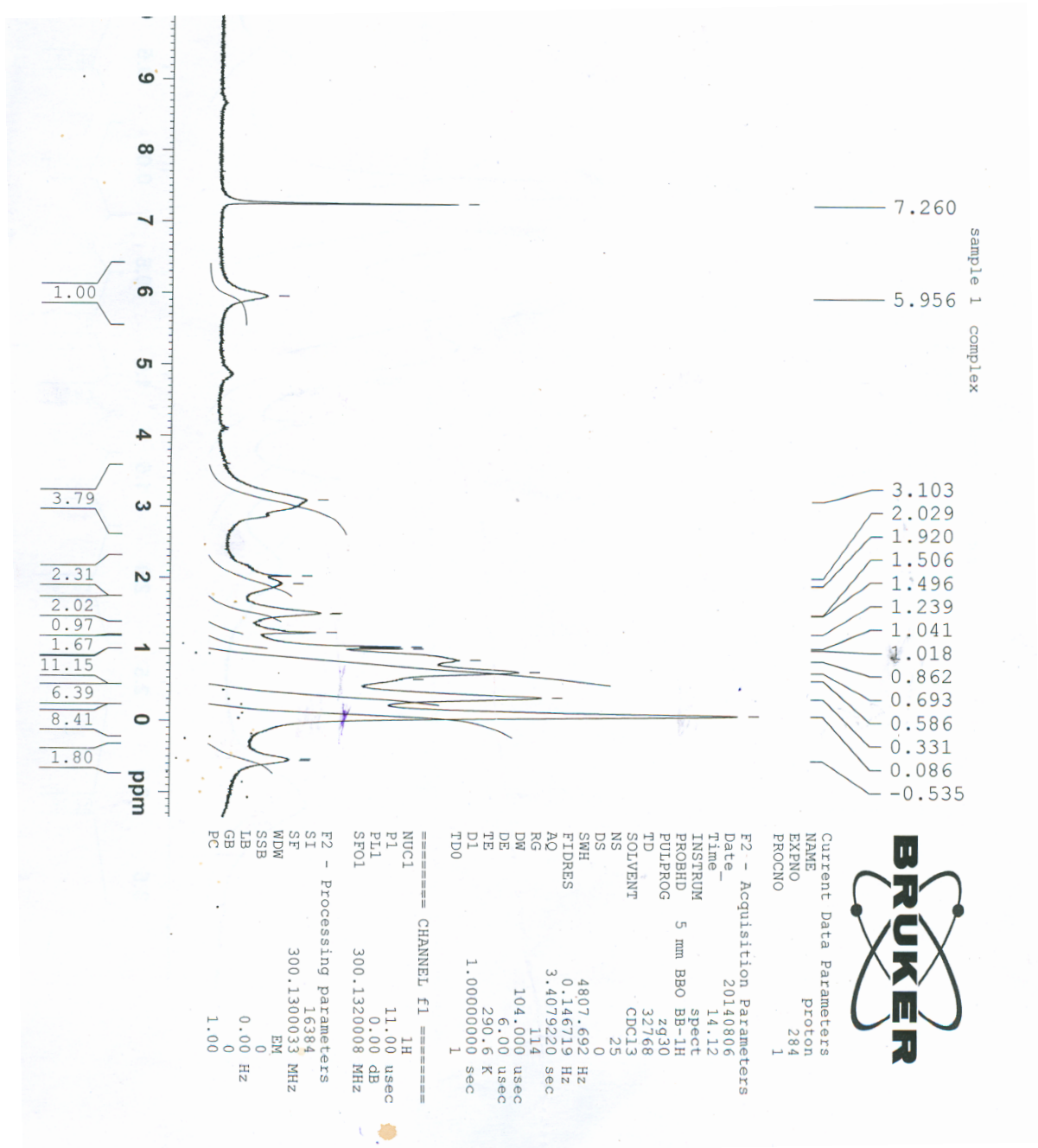


Fig . 4.26 ^1H NMR spectrum of complex of $\text{Eu}(\text{NO}_3)_3 \cdot 5\text{H}_2\text{O}$ with OBDA 20c.
(broad peaks due to paramagnetic nature)

CHAPTER 5

*Design, synthesis and extraction properties of a
new class of ruthenium selective ligands*

5.1 Introduction

Ruthenium is one of the most trouble-maker and hazardous fission products contained in nuclear waste. Radioactive hazardousness is due to its high fission yield, large beta, gamma activity and relatively shorter half lives of its isotopes (^{103}Ru : 39.27 d, ^{106}Ru : 1.02 y) resulting in high specific activity [171]. Ruthenium cause troubles at different stages of spent fuel reprocessing upto final disposal of HLW waste. Ru is of particular interest because of its tendency to form volatile tetroxide during vitrification [17]. Due to these reasons, ruthenium needs to be separated from the waste to make it amenable for disposal.

Ruthenium is the most difficult fission product to separate from nuclear waste dissolved in nitric acid because it forms a large number of complexes and exists in variable valences at different nitric acid concentrations [172].

During the treatment of nuclear waste solutions various problems are usually encountered due to the presence of ruthenium. It forms a series of nitro-nitrato complexes at different concentrations of nitric acid. These species of ruthenium are partially extractable by TBP, cause loss of selectivity during PUREX process and the product streams of U and Pu get contaminated by radioruthenium. In addition, this also results in residual radioactivity in the spent solvent as these ruthenium species are difficult to strip from the loaded TBP [173, 11]. During vitrification of the HLW, ruthenium gets oxidized to volatile tetroxide RuO_4 which gets deposited as RuO_2 on contact with steel surface leading to hot spots on the wall of the inner surface. This also causes corrosion at the inner steel surface [174].

One of the isotopes of ruthenium, ^{106}Ru , present in radioactive waste has large biological applications. It is used in brachytherapy and radiotherapy of tumors of different organs [175-177]. Beside this, Ru compounds have shown promising catalytic, analytical and theoretical applications [178-180].

Solvent extraction is a well known practice for separation of metal ions. It is used at research scale as well as industrial scale for separation of radionuclides from nuclear waste solutions. The success of the process mainly depends on the efficiency of the extractant used. Recently, solid phase extraction (SPE) technique which uses solid polymers as sorption matrix is also identified as the fast and reliable approach for quantitative metal ion separation and preconcentration [181, 182]. The main advantage of solid phase extraction in the field of nuclear industry is that the generated radioactive solid waste can be directly immobilized with polymer or cement matrix for further disposal [183]. Solid phase extraction material can be prepared by two different ways *viz* physical impregnation of a suitable extractant on the solid support *viz* solvent impregnated resins (SIR) or by chemical binding of a chelating ligand to the support material [184]. SIR, first proposed by Warshawsky [185] are prepared by immobilization or impregnation of an extracting agent on an insoluble non-functionalized solid polymer support. Amberlite XAD resins as polymer support have been extensively used for the immobilization of chelating ligands over other supporting materials including activated carbon [186], silica gel [187], polyurethane foam [188] and alumina [189]. The popularity of Amberlite XAD resins is due to their good physical and chemical properties such as porosity, uniform pore size distribution, high surface area and chemical stability toward acids, bases and oxidizing agents [190]. Amberlite XAD-4 has been used earlier as a solid sorbent for impregnation of quaternary ammonium salt based ligands [191-193].

Suitable solvents for Ru are scantily reported specially from nitric acid medium. Two solvents, namely, TBP and tetrahexylammonium iodide (THexI) have been reported for this purpose [194, 195]. These solvents have different extraction behaviour and have been reported with lower distribution ratio (D) values as ~1.3 (1.5 M HNO₃) and 0.5 (1.5 M HNO₃) for 60% TBP/kerosene and 0.2 M THexI/methylisobutylketone

respectively. Tertiary amines and quaternary ammonium salts are widely used for extraction of ruthenium [195-198, 63]. Maeck *et.al.* [195] have reported the extraction of ruthenium from nitric acid medium using THexI, where iodide ion enhanced the extraction process among halides.

5.2 Present Work

We have designed a quaternary ammonium based extractant having iodide as an anionic part for the separation of ruthenium from nitric acid medium. A specially designed alkyl appendage, 2-(*N,N*-dialkyl)acetamide was incorporated in to the quaternary ammonium centre to increase the solubility of the metal-ligand complex in the organic phase as well as to enhance extractability at higher acidity utilizing the buffering property of the dialkylamido group [67-69]. This chapter describes the synthesis of a new class of quaternary ammonium iodide based ligands **29-31** with 2-(*N,N*-diisobutyl)acetamide as an alkyl appendage (Fig. 5.1). Extraction behaviour of these extractants for ruthenium has been evaluated by solvent extraction as well as solid phase extraction technique. For solid phase extraction extractant **29** has been impregnated on Amberlite XAD-4 resin.

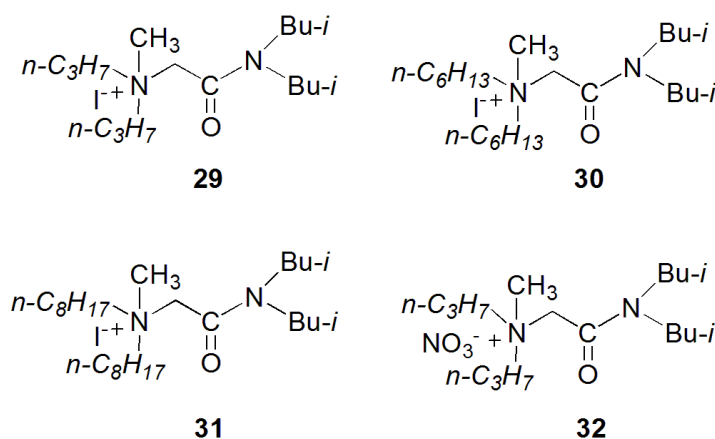
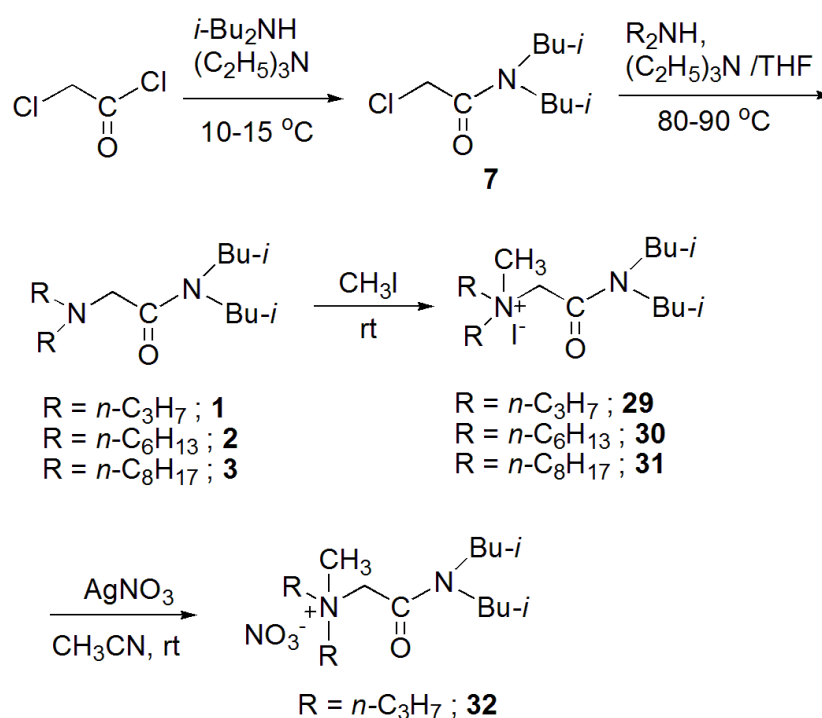


Fig. 5.1 Structure of dialkylmethyl-2-(*N,N'*-diisobutyl)acetamidoammonium iodides **29-31** and nitrate **32**.

5.2.1 Synthesis of ammonium based extractants

Synthesis of ammonium salts **29-31** have been achieved from aminoacetamides **1-3**. Synthesis of aminoacetamides **1-3** has been already described in Chapter 2. α -Dialkylamino-*N,N'*-diisobutylacetamides **1-3** was treated with 10 equivalent of methyl iodide to obtain final desired compounds dialkylmethyl-2-(*N,N'*-diisobutyl)acetamidoammonium iodides **29-31**. Dialkylmethyl-2-(*N,N'*-diisobutyl)acetamidoammonium nitrate **32** was obtained by stirring the corresponding iodide salt **29** with silver nitrate in acetonitrile (Scheme 5.1).



Scheme 5.1 Synthesis of dialkylmethyl-2-(*N,N'*-diisobutyl)acetamidoammonium iodides **29-31** and nitrate **32**.

5.2.2 Extraction evaluation of extractants **29-31** for Ru using solvent extraction technique

The solvent extraction capabilities of the synthesized ammonium based extractants were evaluated for the separation of ruthenium. Various parameters affecting D values

like concentration of phase modifier, feed HNO_3 concentration, iodide and nitrate ion concentration etc were studied in detail. Stoichiometry of extracted complex was ascertained by slope analysis method.

5.2.2.1 Determination of organic phase composition

Considering the polar nature of ligand, metal-ligand complex and their poor solubility in *n*-dodecane, IDA has been chosen as a phase modifier to mitigate the third phase formation [84, 85]. To find out the most suitable solvent composition, extraction studies were carried out at different concentrations of IDA in *n*-dodecane at 1 M HNO_3 . The ligand **29** was initially chosen to optimize the extraction conditions. The solubility of ligand was very poor in *n*-dodecane and also low when the IDA concentration was below 20%. The ligand was fully soluble in 30% IDA/*n*-dodecane to obtain a 0.1-0.2 M solution. The variation of D_{Ru} with IDA/*n*-dodecane composition is shown in Fig. 5.2 for ligand concentration of 0.1 and 0.2 M ligand **29**. The plots show that no significant change in D_{Ru} was observed with increasing IDA concentration beyond 30% in organic phase. From these observations, ligand **29** in 30% IDA/*n*-dodecane was chosen as the optimum organic phase composition for extraction studies.

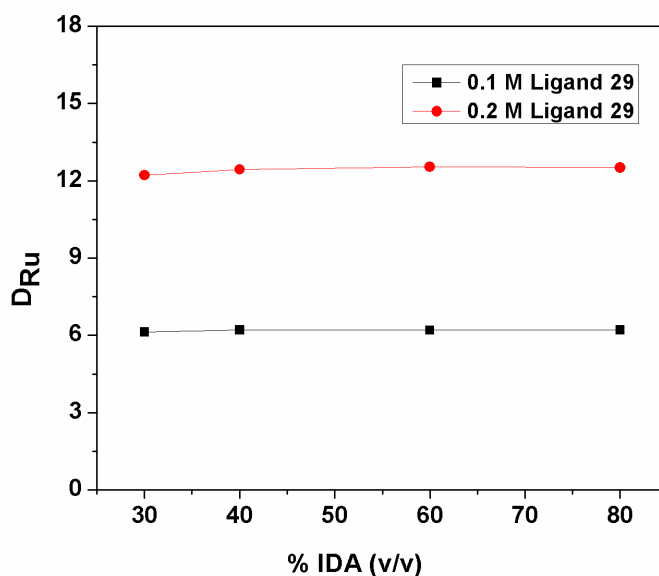


Fig. 5.2 Variation in D_{Ru} with IDA concentration in *n*-dodecane at 1.0 M HNO_3 .

5.2.2.2. Kinetics of extraction

The kinetics of extraction was evaluated by plotting the variation of D_{Ru} as a function of contact time for 0.2 M ligand **29** in 30% IDA/*n*-dodecane at 1.0 M HNO_3 concentration. Results are shown in Fig. 5.3. It was observed that equilibrium has been attained within 15 min of the equilibration implying the fast reaction between ligand **29** and ruthenium. No further increase in D_{Ru} was observed after 15 min of contact. Hence, 30 min contact time was used in all experiments for ruthenium extraction.

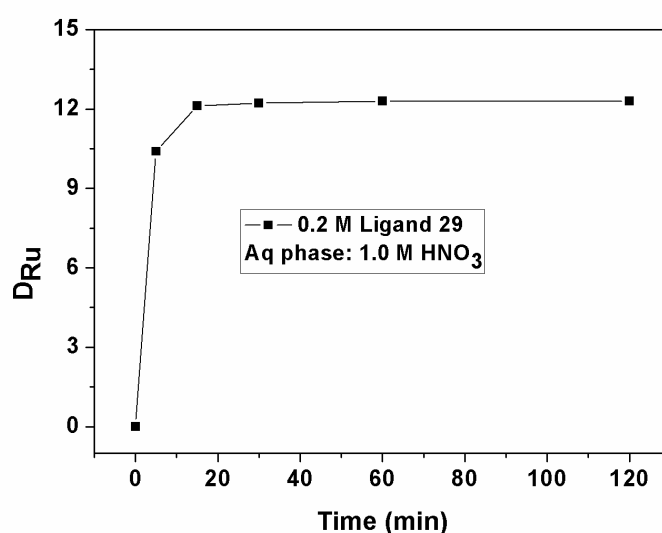


Fig. 5.3 Kinetics of Ru extraction with ligand **29** from 1.0 M HNO_3 .

5.2.2.3 Dependency of D_{Ru} on HNO_3 concentration

To see the effect of feed acidity on extraction of ruthenium, a solution of ligand **29-31** in 30% IDA/*n*-dodecane was equilibrated with aqueous solution of Ru at varying initial nitric acid concentrations in the range of 0.1-2.0 M (Fig. 5.4). As shown by the plot for ligand **29**, D_{Ru} increased with increasing nitric acid concentration upto 1.5 M HNO_3 and then falls with further increase in HNO_3 concentration. This trend was found to be similar for ligands **30** and **31** also. Increase in D_{Ru} upto 1.5 M HNO_3 can be explained by increased concentration of NO_3^- from HNO_3 which favors the formation of extractable $Ru(NO)(NO_3)_3$ complex and also by neutralization of HNO_3 due to amide

group *vis a vis* intramolecular buffering effect [67-69]. Beyond 1.5 M nitric acid concentration, the reduction in D_{Ru} was observed, probably due to the formation of non-extractable Ru species.

Ligand **29** was chosen for further studies as it has shown better extraction behavior among ligand **29-31**. Since the complex formation site of the ligand is the ammonium center, increase in steric hindrance at this site by hexyl or octyl groups therefore resulted in decrease in D_{Ru} .

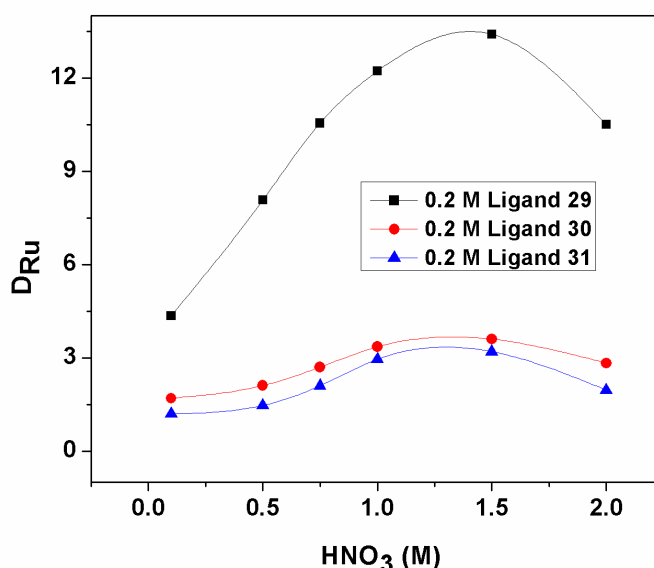


Fig. 5.4 Variation in D_{Ru} with HNO_3 concentration.

5.2.2.4 Dependency of D_{Ru} on ligand concentration

The stoichiometry of extracted complex with respect to ligand **29** (L^+T) was determined by plotting variation of D_{Ru} as a function of concentration of ligand **29** at 1.0 M HNO_3 concentration (Fig. 5.5). Ligand concentration was varied from 0.5 to 2 M. It was observed that D_{Ru} values increases with an increase in the concentration of **29**. The plot is a straight line with slope of 0.952 ± 0.019 . This indicates that metal to ligand ratio is 1:1 in the extracted complex.

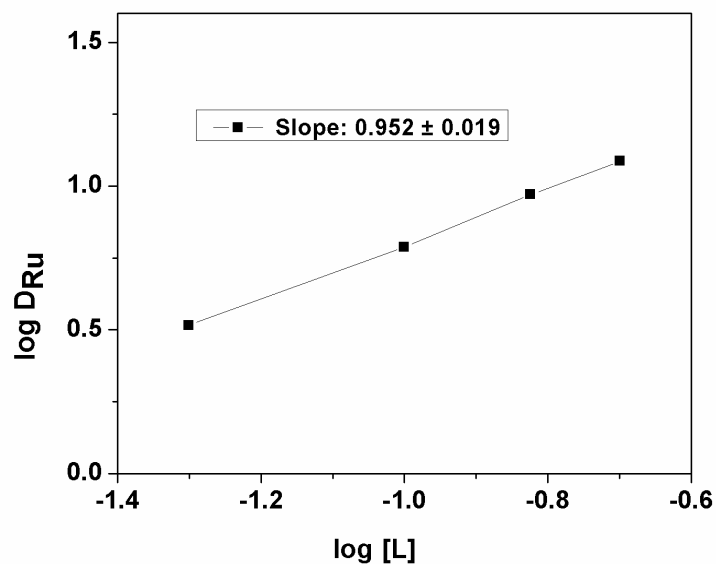


Fig. 5.5 Variation in D_{Ru} with ligand concentration.

5.2.2.5 Effect of iodide ion on extraction

The effect of iodide ion concentration on the D_{Ru} was studied for ligand **29** at 1.0 M HNO_3 with addition of NaI salt in aqueous phase (Fig. 5.6). NaI concentration was varied from 0.1 to 2 M.

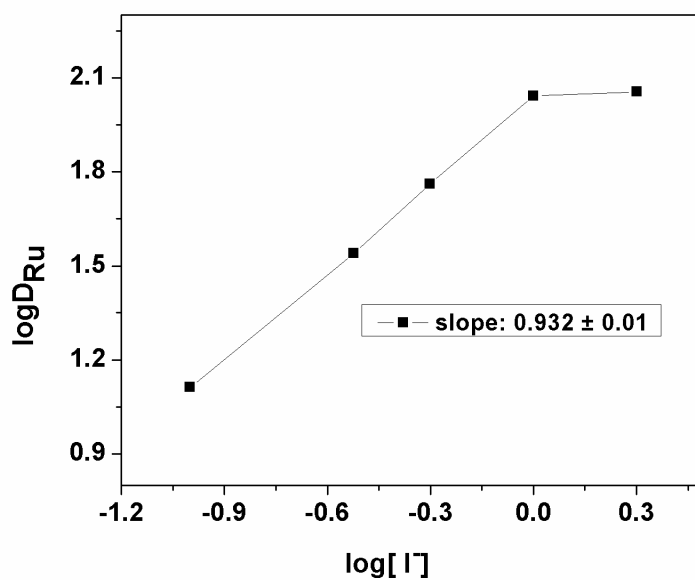


Fig. 5.6 Variation in D_{Ru} with I^- concentration.

D_{Ru} increases with added iodide ion concentration upto 1 M and then remained constant. The slope in the straight line region is 0.932 ± 0.01 indicating participation of one molecule of iodide ion in the extraction process.

5.2.2.6 Effect of nitrate ion concentration on extraction

To see the effect of nitrate ion concentration on extraction, D_{Ru} was determined for different concentrations of nitrate ions in aqueous phase. As observed by the plot, D_{Ru} showed negligible dependence on nitrate ion concentration with increasing nitrate ion in aqueous medium (Fig. 5.7). However, a small increase in the D_{Ru} was observed while addition of NaNO_3 due to law of mass action. Since, increase in D_{Ru} is not significant with nitrate concentration, it can be mentioned that there is no exchange of iodide by nitrate ion during extraction and the extracted complex form remained unchanged.

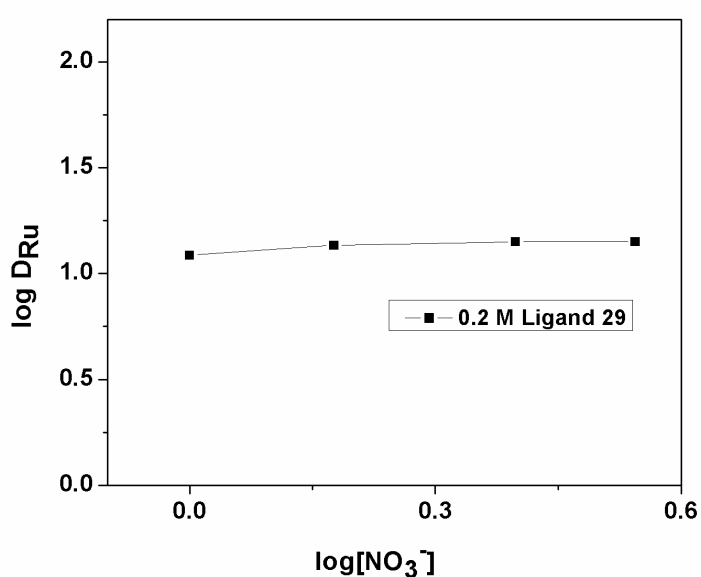


Fig. 5.7 Variation in D_{Ru} with total NO_3^- concentration at 0.5 M HNO_3 .

5.2.2.7 Role of anionic part of ligand in extraction

In order to evaluate the role of anionic part of ligand on extraction of Ru, extraction studies was preformed with ligand **32** where anion is nitrate in place of iodide. No extraction of ruthenium was observed with ligand **32** under the similar extraction conditions. However, extraction occurred when sodium iodide was added to the aqueous solution. D_{Ru} was found to be increase with increase in sodium iodide concentration and remained constant after 0.5 M NaI concentration (Fig. 5.8). This indicates the possible formation of $HRu(NO)(NO_3)_3I$ in the aqueous nitric acid medium and extracted by anion exchange mechanism where $Ru(NO)(NO_3)_3I^-$ is exchanged by nitrate ion of the solvent.

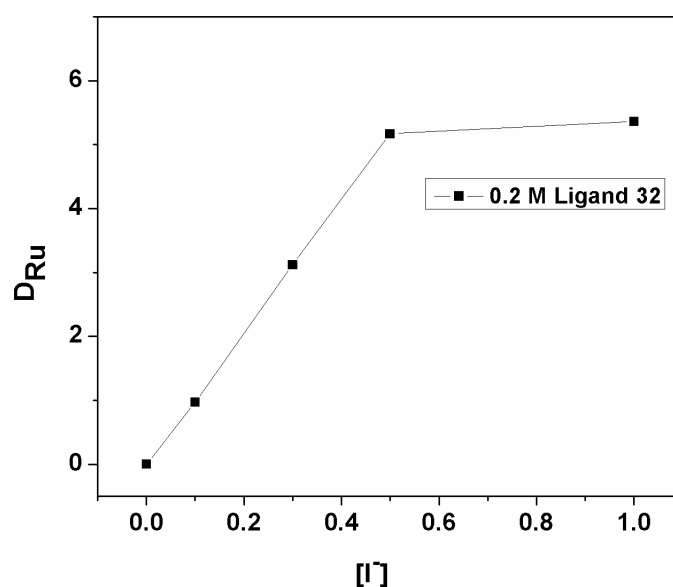


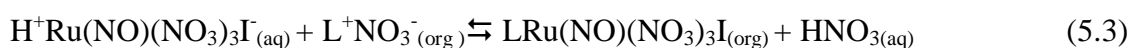
Fig. 5.8 Variation in D_{Ru} with I^- concentration for ligand **32** at 1.0 M HNO_3 .

5.2.2.8. Mechanism of extraction

From the all above observations mechanism of extraction can be explain. $Ru(NO)(NO_3)_3$ in 1 M HNO_3 exist predominantly as a neutral species [172, 194], therefore, extraction with the ligand **29**, L^+I^- , follows adduct formation mechanism as indicated in Equation 5.1.



In case of ligand **32**, which is in the form of L^+NO_3^- , no extraction of Ru was observed in absence of NaI in the aqueous medium indicating nitrate anion of ligand **32** has no role in adduct formation. However, in the presence of sodium iodide, extraction was observed and the possible extraction mechanism is indicated by Equations 5.2 and 5.3.



Thus, it is the iodide in the ligand, or iodide ion in the aqueous medium, which plays a vital role in formation of extractable adduct of the kind $\text{LRu}(\text{NO})(\text{NO}_3)_3\text{I}$. No extraction of $\text{Ru}(\text{NO})(\text{NO}_3)_3$ by ligand **32**, in the absence of NaI, also confirms that the amido group did not participate in the extraction process.

5.2.2.9 Selectivity of ligand

The extraction of ruthenium using ligand **29** was studied in the presence of other metal ions like Cs, Sr, Mo, Eu, Ba and Zr at 1.0 M nitric acid. These metal ions are chosen because they are present in acidic nuclear waste solutions [199]. The distribution ratio for Ru along with other metal ions found in nitric acid nuclear waste streams are presented in Table 5.1. Europium was chosen as representative example of trivalent lanthanide/actinides. Ligand **29** has shown high separation factor (SF) for Ru over Cs, Sr, Eu, Ba. Though, the ligand showed very small D_M values for Mo and Zr, they can be removed from the organic phase by scrubbing with suitable scrub agents.

Table 5.1 Distribution ratio of ruthenium and other elements with 0.2 M ligand **29** in 30% IDA/*n*-dodecane.

	Ru	Cs	Sr	Mo	Eu	Ba	Zr
D	5.99	0.008	0.003	0.49	0.012	0.001	0.11
S.F.		749	1997	12.22	499	5990	54.45

5.2.2.10 Stripping studies

For the stripping of ruthenium from loaded organic, the loaded organic phase was contacted separately with 5% NH₃ or 10% NaOH solution as stripping agent. It was observed that in case of NH₃ and NaOH the metal recovery was 83% and 62%, respectively, from loaded organic phase after three successive contacts.

5.2.3 Sorption studies for Ru using ligand **29** impregnated Amberlite XAD-4 resin

Dipropylmethyl-2-(*N,N*-diisobutyl)acetamidoammonium iodide **29** has been impregnated on Amberlite XAD-4 resin and investigated for sorption of Ru from nitric acid medium. Impregnated resin was characterized by IR, TGA, SEM analyses. Maximum loading of extractant on XAD resin was determined by TGA analysis and weight difference method. The effect of varying concentration of Ru on its sorption was studied for the determination of maximum loading of ruthenium on impregnated resin. Sorption data were fitted to different known isotherm models to understand the sorption process. Desorption studies were also carried out.

5.2.3.1 Determination of maximum loading of extractant **29** on Amberlite XAD-4

The maximum loading of extractant **29** on Amberlite XAD-4 resin was calculated from the weight difference between the resins after and before impregnation with the extractant which was found to be 1.54 g extractant /g of resin that corresponds to 60.6% loading. The % loading was further analyzed by thermo gravimetric analysis. The

thermograms of pure extractant and beads before and after impregnation with the extractant are shown in Fig. 5.9. The TGA curve of the extractant shows an initial slow weight loss up to 155 °C and then rapid weight loss due to decomposition. The TGA curve of the pure resin shows single-step weight loss after 380 °C due to its degradation while the TGA of impregnated resin shows two step weight losses. Weight loss of about 60% happened between 155°C and 330 °C is due to the loss of extractant. The weight loss after 380 °C is due to the degradation of the resin material. The % loading calculated from weight difference after impregnation and weight loss by TGA analysis are very close.

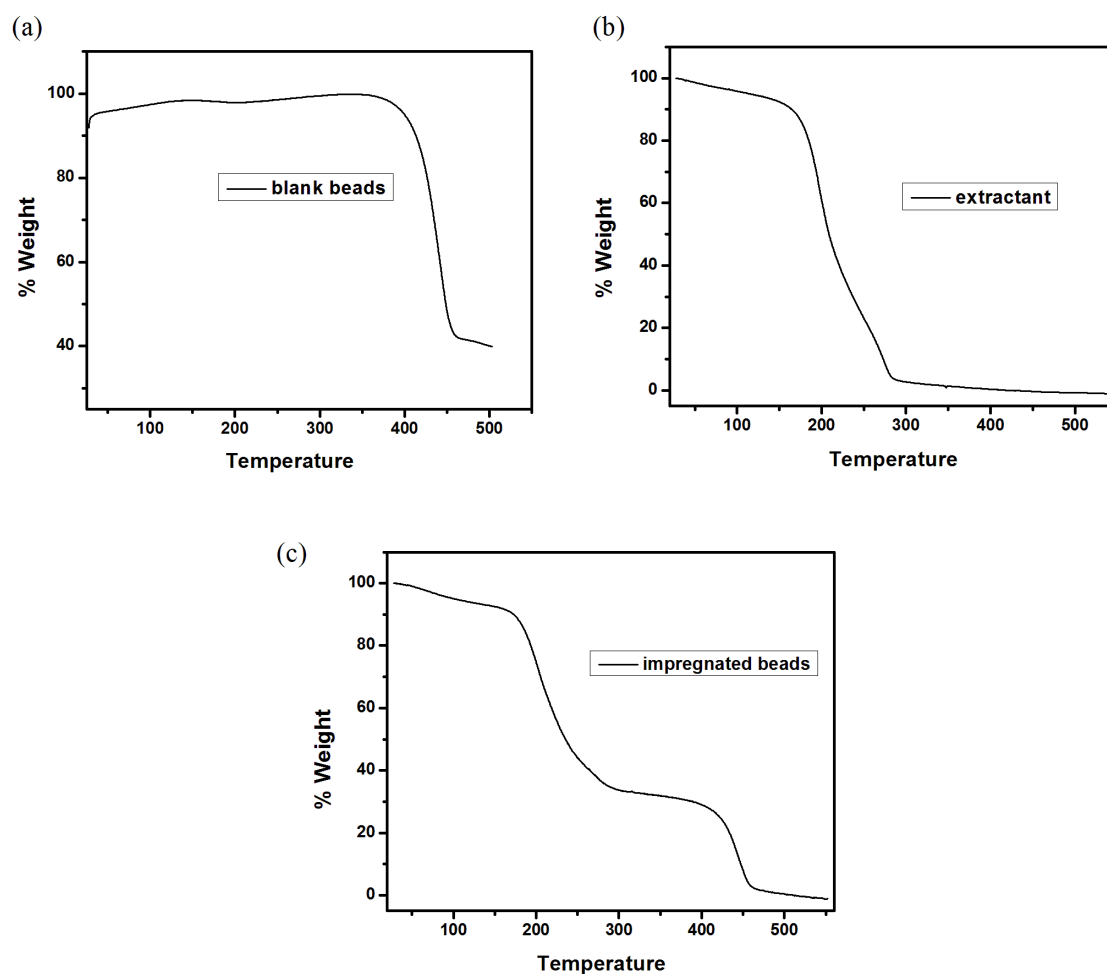


Fig. 5.9 TGA curves for (a) blank beads (b) pure extractant (c) impregnated beads.

5.2.3.2 Characterization of impregnated resin by IR

IR spectra of XAD-4 resin after impregnation of extractant clearly indicate the extractant $\nu_{C=O}$ peak at 1648 cm^{-1} which is absent in non-impregnated XAD resin, thus, confirms the impregnation of extractant (Fig. 5.10).

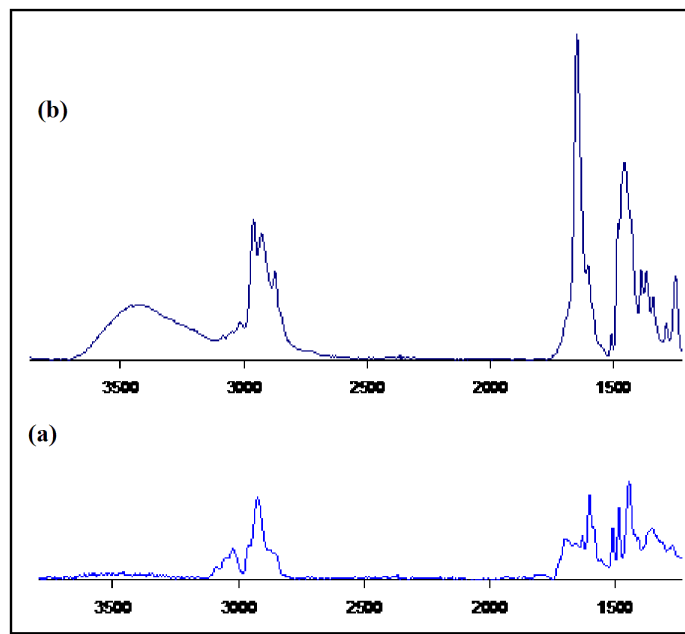


Fig. 5.10 IR spectra of XAD-4 resin (a) before impregnation; (b) after impregnation of extractant.

5.2.3.3 SEM characterization of impregnated resin

SEM is used to study the morphological changes appeared on the surface of sorbent after impregnation of extractant. Sometimes some surface defects like scales, deep cavity, shallow cavity and microcracks are seen on the surface of impregnated resin due to excess loading of extractant. The appearance of these defects can be attributed to the swelling stress of the matrix. These surface defects affect the sorption process because of possible leaching of extractant from the polymer resulting in inconsistency of sorption results [182]. Therefore, it is pertinent to check the morphology of the impregnated beads for any surface defects before performing sorption experiments. The SEM images of impregnated resin at different magnifications have been shown in Figure 5.11. The micrograph shows a spherical shape of impregnated resin beads

without surface defect hence are suitable for sorption studies. The SEM analysis also confirmed that there was no deformation effect of vacuum (used in impregnation procedure) on impregnated resin as the micrograph shows clearly a spherical shape.

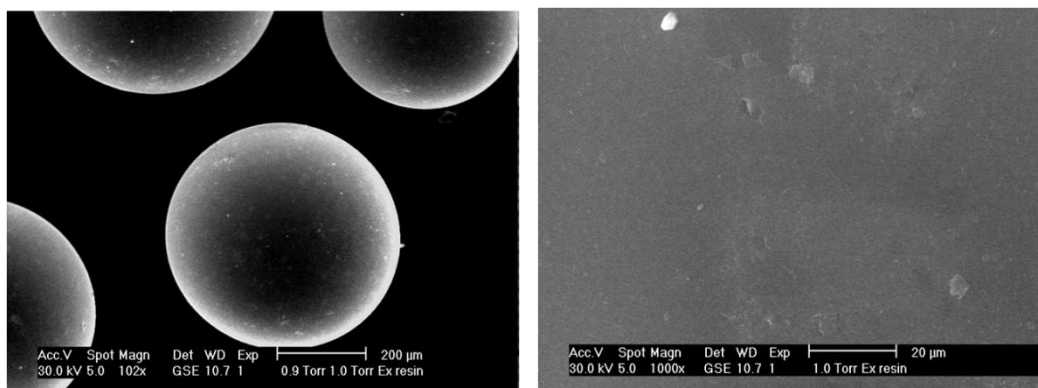


Fig.5.11 SEM of impregnated XAD-4 resin beads at different magnifications.

5.2.3.4 Effect of HNO_3 concentration on sorption of ruthenium

The effect of HNO_3 concentration on sorption of Ru was studied with the impregnated resin contained 60% (w/w) of extractant **29** and the results are shown in Figure 5.12.

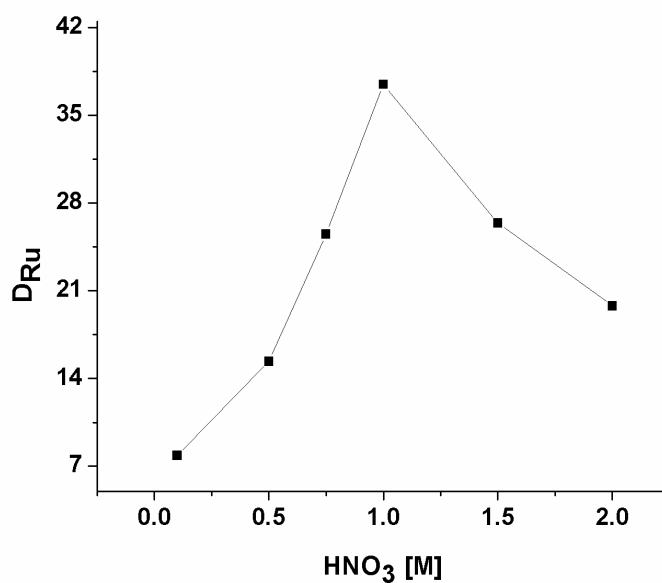


Fig. 5.12 Sorption of Ru on impregnated resin at different HNO_3 concentrations.

The sorption increases with increase in nitric acid concentration, reached to a maximum at 1 M HNO₃ and then decreases. The ruthenium gets sorbed into the resin more likely as Ru(NO)(NO₃)₃ species as described in solvent extraction studies. This species is predominant in 1 M HNO₃ concentration whereas at other nitric acid concentrations the species are different which are not extractable [194]. As the beads work best at 1 M HNO₃, further testes were carried out at this acidity only.

5.2.3.5 Maximum loading capacity of impregnated resin for Ru:

The effect of varying concentration of ruthenium on the sorption was studied to quantify the maximum sorption capacity of impregnated resin (Fig 5.13). Equilibrium sorption increases with increase in initial ruthenium concentration and remained constant after 700 mg/L. The uptake by the sorbent is initially linear because of availability of enough number of active sites, but with further metal loading free active sites decreases and finally saturation in uptake is attained. Maximum loading of ruthenium thus obtained was 5.63 mg/g of resin. The picture of ruthenium loaded impregnated resin is shown in Fig. 5.14.

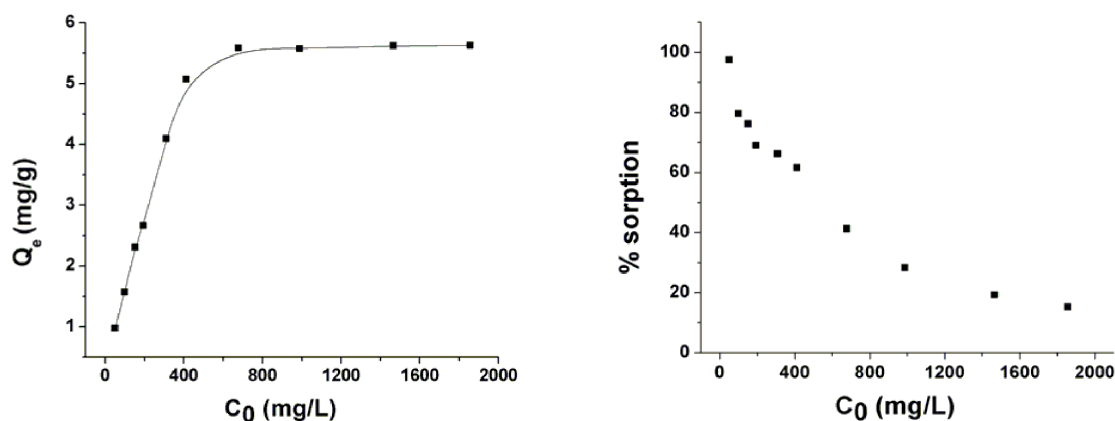


Fig. 5.13 Effect of metal ion concentration on sorption of Ru.

The % sorption decreases with increase in metal ion concentration and highest K_d value obtained was 749 for 50 mg/L of initial ruthenium concentration. No iodide loss from the impregnated resin was observed in the aqueous phase during the sorption of ruthenium. This indicates that Ru sorption is not taking place by ion exchange mechanism. The more likely mechanism would be the same as proposed in solvent extraction studies (part 5.2.2.8 of this chapter) with formation of adduct as shown in Equation 5.1.

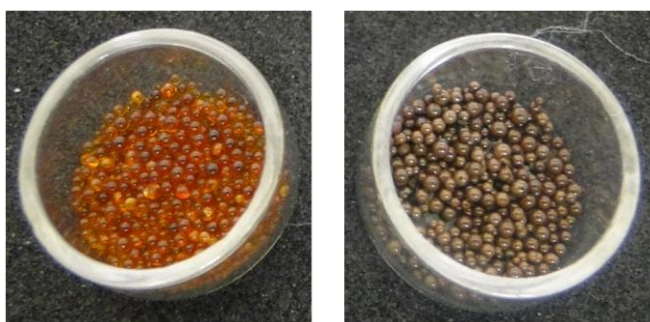


Fig. 5.14 Resin beads: (a) after impregnation of extractant; (b) after sorption of Ru.

5.2.3.6 Sorption isotherm models

To understand the equilibrium sorption behavior, sorption data were fitted to Langmuir and Freundlich isotherm models [200].

Langmuir isotherm: Langmuir isotherm is valid for a structurally homogeneous sorbent where all sorption sites are identical and finite. The model also assumes uniform sorption on the active sites present at the outer surface of sorbent and when a molecule is sorbed at that active sites, the other molecules could not be interacted with these active sites, thereby, indicating a monolayer sorption. The linear form of Langmuir Equation may be written as

$$Q_e = \frac{Q_0 K_L C_e}{1 + K_L C_e} \quad (5.4)$$

Where

C_e = Equilibrium concentration of metal ion in the bulk solution (mg/L)

Q_e = Amount of metal ion sorbed per unit weight of resin (mg/g) at equilibrium

Q_0 = monolayer sorption capacity (mg/g)

K_L = Langmuir isotherm constant (L/mg).

After linearization of Equation 5.4, we got Equation 5.5

$$\frac{1}{Q_e} = \frac{1}{Q_0} + \frac{1}{Q_0 K_L C_e} \quad (5.5)$$

A linear plot of $1/Q_e$ versus $1/C_e$ shows that the sorption obeys the Langmuir isotherm.

The values of Q_0 and K_L can be calculated from the slope and the intercept respectively.

The equilibrium parameter or separation factor, R_L is a dimensionless constant and expresses the essential features of the Langmuir isotherm (Equation 5.6).

$$R_L = \frac{1}{1 + (1 + K_L C_0)} \quad (5.6)$$

R_L value indicates the sorption nature to be either unfavorable if $R_L > 1$, linear if $R_L = 1$, favorable if $0 < R_L < 1$ and irreversible if $R_L = 0$ [200].

Sorption experiments were carried out at different initial concentrations of ruthenium at 1.0 M HNO_3 and the graph plotted between $1/Q_e$ and $1/C_e$ for the initial ruthenium concentrations (C_0) from 100 to 1000 mg/L in aqueous phase is shown in Fig. 5.15.

The higher value of correlation coefficient ($R^2 = 0.98$) indicates a good correlation between the experimental data and Langmuir sorption model. The maximum monolayer sorption capacity (Q_0) was determined to be 6.25 mg/g. The Langmuir isotherm constant (K_L) is 0.0162 L/mg and separation factor (R_L) is between 0.055-0.276 for the initial feed concentration (C_0) 100 to 1000 mg/L. Above findings indicate

a favorable Langmuir model and confirm the monolayer, homogeneous sorption of Ru under the given experimental conditions.

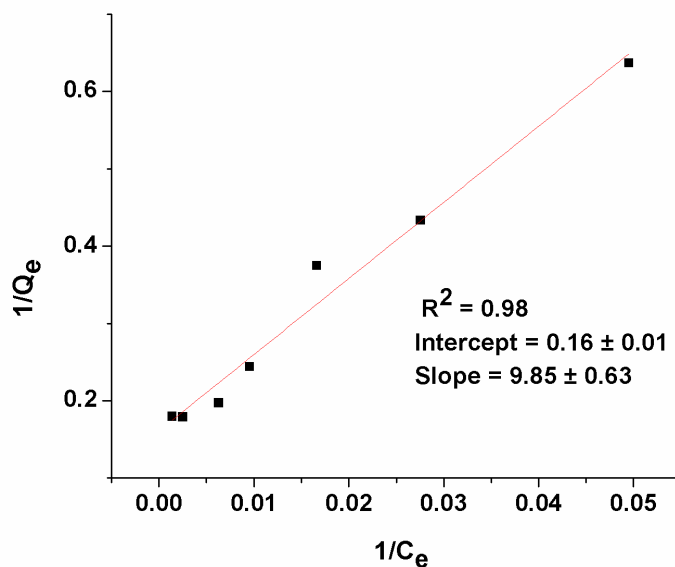


Fig. 5.15 Langmuir isotherm plot for sorption of ruthenium on impregnated resin.

Freundlich isotherm: Freundlich isotherm expresses the heterogeneity of the surface and multilayer sorption to the active sites located on the surface of the sorbent. The imperial form of Freundlich model is expressed as follows

$$Q_e = K_f \cdot C_e^{1/n} \quad (5.7)$$

Where K_f is Freundlich constant gives the information about the sorption capacity ($\text{mg} \cdot \text{g}^{-1} \text{ L}^{1/n} \text{ mg}^{-1/n}$) and n shows the sorption intensity indicating heterogeneity in sorption. After linearization of Equation (5.7) we got Equation (5.8)

$$\log Q_e = \log K_f + \frac{1}{n} \log C_e \quad (5.8)$$

Freundlich isotherm is valid only when the plot of $\log Q_e$ v/s $\log C_e$ is linear. The value of Freundlich constants (K_F and $1/n$) can be calculated from the intercept and slope of the plot respectively. K_f is an approximate indicator of sorption capacity. For favorable sorption of metal ions on surface of resin the value of sorption intensity $1/n$ should be between zero and one. For maximum heterogeneity $1/n$ should be one.

$\log Q_e$ was plotted with respect to $\log C_e$ with the data obtained from ruthenium sorption studies for the C_0 values 100-1000 mg/L. Results showed that Freundlich isotherm model is not as good as Langmuir for the present sorption data as correlation coefficient value obtained for Freundlich is 0.86 (Fig. 5.16). These studies indicated that the sorption of ruthenium is predominantly monolayer in the given experimental conditions. Although, the value of $1/n$ obtained as 0.37 indicates slight heterogeneity in sorption process.

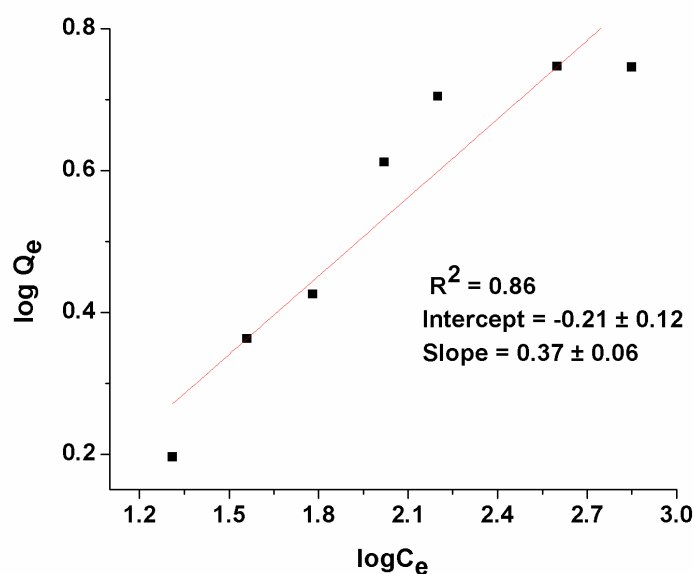


Fig. 5.16 Freundlich isotherm plot for sorption of ruthenium on impregnated resin.

Table 5.2 Isotherm constants of the different models for sorption of Ru ions.

Isotherm model	Parameters	Values
Langmuir	R^2	0.98
	Q_0	6.25 mg/g
	K_L	0.0162 L/mg
Freundlich	R^2	0.86
	K_f	$0.617 \text{ mg}\cdot\text{g}^{-1} \text{ L}^{1/n} \text{ mg}^{-1/n}$
	$1/n$	0.37

5.2.3.7 Desorption studies

Ruthenium was quantitatively desorbed from resin using ammonia or sodium hydroxide solution. Resin loaded with Ru was kept in contact with 5 % ammonia or 10% sodium hydroxide solution for 4 hrs. Desorption of ruthenium with ammonia or sodium hydroxide was found to be 85 and 97 % respectively in a single contact.

5.3 Conclusions

In conclusion, trialkyl-[2-(*N,N*-diisobutyl)acetamido]ammonium iodides, have been designed and synthesized as a new class of quaternary ammonium based ligands to extract ruthenium selectively from nitric acid medium. Ruthenium was extracted in the form of an iodide complex only. Stoichiometry of extracted complex as determined by slope analysis method showed 1:1 ratio for metal to ligand. The role of anionic part of the ligand was found to be very new and interesting in this study. The ligands having iodide as anion, L **29-31**, have shown extraction of $\text{Ru}(\text{NO})(\text{NO}_3)_3$ whereas the L **32** having nitrate as anion has not shown any extraction. The extraction with L **32** was only observed, when NaI was added in the aqueous medium. The probable mechanism for the extraction of ruthenium by L **29** is the adduct formation of the type

LRu(NO)(NO₃)₃I. Extraction of ruthenium was also studied in presence of Cs, Sr, Mo, Eu, Ba, Zr metal ions and found to be selective for Ru. The proposed ruthenium extraction method, in the present form, has been applied for extraction of Ru from a synthetic solution under simulated conditions. Its application in real radioactive waste solution needs to be examined. Moreover, this development will provide a direction for making a suitable extractant for separation of Ru from real nuclear waste streams.

Dipropylmethyl-2-(*N,N*-diisobutyl)acetamidoammonium iodide was impregnated on XAD-4 resin using wet method. Resulting impregnated resin was characterised by IR, SEM and TGA analyses. The TGA showed 60% (w/w) impregnation of extractant on resin and SEM confirms spherical shape of beads without any surface defect. Sorption of Ru was found to predominantly follow Langmuir isotherm with a slight heterogeneous multilayer coverage. Maximum sorption capacity was found to be 6.25 mg of Ru/g of resin from Langmuir sorption isotherm which is close to the experimentally obtained value of 5.63 mg/g. Highest K_d value obtained was 749 indicating reasonably good sorption of ruthenium by impregnated resin. Ruthenium was successfully desorbed from resin using ammonia or sodium hydroxide solution in a single contact. The impregnated resins can be possibly used for the recovery of Ru from various waste solutions including nuclear waste.

5.4 Experimental

General details

As described in Chapter 2.

Chemicals

Nitric acid, *n*-dodecane and isodecyl alcohol (IDA) were obtained from local sources. Diisobutylamine, dioctylamine, dihexylamine, dipropylamine, ruthenium nitrosyl nitrate, methyl iodide and other chemicals used were of analytical grade. Amines were

used after distillation. The solvents were dried and distilled from the indicated drying agents: THF from sodium/benzophenone; triethyl amine from CaH_2 and then stored over calcium metal. Amberlite XAD-4 (manufacturer Rohm and Hass Co., USA) supplied by Sigma Aldrich.

General procedure for the synthesis of trialkyl-2-(*N,N*-diisobutyl)acetamidoammonium iodide 29-31: A mixture of α -dialkylamino *N,N'*-diisobutylacetamides **1-3** (1 eq, 3 mmol) and methyl iodide (1.87 mL, 10 eq, 30 mmol) was left at room temperature for 2 d. The reaction mixture was concentrated under reduced pressure to give ammonium iodide **29-31** in quantitative yields.

Dipropylmethyl-2-(*N,N'*-diisobutyl)acetamidoammonium iodide 29

^1H NMR (500 MHz, CDCl_3): δ 0.87 (6 H, d, $J = 7$ Hz, $2 \times \text{Me}_A\text{Me}_B\text{CH}$), 0.94-1.03 (12 H, m, $2 \times \text{Me}_A\text{Me}_B\text{CH}$, $2 \times \text{CH}_3\text{CH}_2$), 1.70-1.85 (4 H, m, $2 \times \text{CH}_2\text{CH}_2\text{N}$), 1.91-2.02 (2 H, m, $2 \times \text{CHMe}_2$), 3.17 (2 H, d, $J = 8$ Hz, $\text{NCH}_2\text{CHMe}_2$), 3.35 (2 H, d, $J = 8$ Hz, $\text{NCH}_2\text{CHMe}_2$), 3.50 (3 H, s, NCH_3), 3.59 (2 H, dt, $J = 12.5$ Hz, $J = 6$ Hz, $\text{CH}_2\text{CH}_2\text{N}$), 3.89 (2 H, dt, $J = 12$ Hz, $J = 6$ Hz, $\text{CH}_2\text{CH}_2\text{N}$), 4.65 (2 H, s, CH_2CO).

^{13}C NMR (150 MHz, CDCl_3): δ 10.5 (2 C), 16.4 (2 C), 19.8 (2 C), 20.0 (2 C), 26.2, 27.6, 50.7, 53.0, 54.7, 59.0, 64.6 (2 C), 163.3.

MALDI-TOF: m/z 412.49 (M), 285.37 (M-I).

Calcd. for $\text{C}_{17}\text{H}_{37}\text{IN}_2\text{O}$: C, 49.51; H, 9.04; N, 6.79%; Found C, 49.68; H, 9.18; N, 6.88%.

Dihexylmethyl-2-(*N,N'*-diisobutyl)acetamidoammonium iodide 30

^1H NMR (500 MHz, CDCl_3): δ 0.82-0.90 (12 H, m, $2 \times \text{Me}_A\text{Me}_B\text{CH}$, $2 \times \text{CH}_3\text{CH}_2$), 1.01 (6 H, d, $J = 7$ Hz, $2 \times \text{Me}_A\text{Me}_B\text{CH}$), 1.24-1.40 (12 H, m, $2 \times \text{CH}_3(\text{CH}_2)_3$), 1.62-1.75 (4 H, m, $2 \times \text{CH}_2\text{CH}_2\text{N}$), 1.93-2.03 (2 H, m, $2 \times \text{CHMe}_2$), 3.18 (2 H, d, $J = 7$ Hz,

NCH_2CHMe_2), 3.37 (2 H, d, $J = 7.5$ Hz, NCH_2CHMe_2), 3.48 (3 H, s, NCH_3), 3.57 (2 H, dt, $J = 12.5$ Hz, $J = 5.5$ Hz, CH_2CH_2N), 3.94 (2 H, dt, $J = 12$ Hz, $J = 6$ Hz, CH_2CH_2N), 4.69 (2 H, s, CH_2CO).

^{13}C NMR (125 MHz, $CDCl_3$): δ 13.8 (2 C), 19.9 (2 C), 20.1 (2 C), 22.3 (2 C), 22.7 (2 C), 25.8 (2 C), 26.3, 27.6, 31.1 (2 C), 50.8, 53.1, 54.7, 59.2, 63.2 (2 C), 163.4.

MALDI-TOF - m/z 369.39 (M-I).

Calcd. for $C_{23}H_{49}IN_2O$; C, 55.63; H, 9.95; N, 5.64%; Found C, 55.89; H, 9.71; N, 5.63%.

Dioctylmethyl-2-(*N,N'*-diisobutyl)acetamidoammonium iodide 31

1H NMR (500 MHz, $CDCl_3$): δ 0.83-0.90 (12 H, m, $2 \times Me_A Me_B CH$, $2 \times CH_3CH_2$), 1.00 (6 H, d, $J = 7$ Hz, $2 \times Me_A Me_B CH$), 1.18-1.39 (20 H, m, $2 \times CH_3(CH_2)_5$), 1.61-1.74 (4 H, m, $2 \times CH_2CH_2N$), 1.93-2.03 (2 H, m, $2 \times CHMe_2$), 3.18 (2 H, d, $J = 8$ Hz, NCH_2CHMe_2), 3.37 (2 H, d, $J = 7.5$ Hz, NCH_2CHMe_2), 3.47 (3 H, s, NCH_3), 3.57 (2 H, dt, $J = 12.5$ Hz, $J = 5.5$ Hz, CH_2CH_2N), 3.93 (2 H, dt, $J = 12$ Hz, $J = 6$ Hz, CH_2CH_2N), 4.69 (2 H, s, CH_2CO).

^{13}C NMR (150 MHz, $CDCl_3$): δ 13.9, 19.8, 20.0, 22.4 (2 C), 22.7 (2 C), 26.1 (2 C), 26.2, 27.6, 28.9 (4 C), 28.9 (3 C), 31.5 (2 C), 50.7, 53.0, 54.7, 59.2, 63.0 (2 C), 163.4.

MALDI-TOF - m/z 425.45 (M-I).

Calcd. for $C_{27}H_{57}IN_2O$; C, 58.68; H, 10.4; N, 5.07%; Found C, 58.6; H, 10.27; N, 4.9%.

Dipropylmethyl-2-(*N,N'*-diisobutyl)acetamidoammonium nitrate 32

Silver nitrate (510 mg, 1 eq, 3 mmol) was added to a stirred solution of dipropylmethyl-2-(*N,N'*-diisobutyl)acetamido ammonium iodide **29** (1.24 g, 1 eq, 3 mmol) in acetonitrile (mL) and the mixture was stirred for 30 min at room temperature. The

precipitated silver iodide was filtered off and the filtrate was concentrated to give dipropylmethyl-2-(*N,N'*-diisobutyl)acetamido ammonium nitrate **32** (1.02 g, 98%).

Ruthenium feed solutions

Ruthenium nitrosyl nitrate solutions were prepared by dissolving appropriate amount of ruthenium nitrosyl nitrate in nitric acid. For solvent extraction studies concentration of Ru was 200 mg/L for all experiments except for selectivity test. For selectivity studies concentration of all metal ions was 100 mg/L. The concentration of nitric acid used for the extraction studies was varied between 0.1 M and 2.0 M. For sorption studies by impregnated resin, Ru concentration range was 50 to 1800 mg/L. Quantitative determination of ruthenium was carried out using ICP-AES (Inductively coupled plasma atomic emission spectrophotometry). Quantification limit was 1 mg/L and detection limit for ruthenium was 0.1 mg/L. Error in ruthenium analysis was within $\pm 5.0\%$.

Solvent extraction studies

For determination of distribution ratio (D_{Ru}), organic phase was equilibrated with equal volume of aqueous phase containing Ru for 30 min in a glass vial. All the extraction experiments were carried out in a thermostated water bath maintained at temperature 25 ± 1 °C. After phase separation by centrifugation, the organic and the aqueous phases were separated and the aqueous phase was analyzed for ruthenium by ICP-AES after suitable dilutions. The concentration of ruthenium in the organic phase was calculated by mass balance. The distribution ratio D_{Ru} was determined as the ratio of metal concentration in organic phase to that in aqueous phase at equilibrium.

Method of impregnation of extractant **29** on XAD-4 resin

Four different methods are commonly used for impregnation of an extractant on the solid polymeric supports *viz* the dry method, wet method, dynamic column method and modifier addition method [182, 201-204]. The impregnation of Amberlite XAD-4 with extractant **29** was achieved using wet method that included several steps. To remove the various organic and inorganic impurities present in the Amberlite XAD-4 resin, it was soaked in methanol for 6 h, filtered, washed with deionized water and left for dryness overnight. Finally, the resin beads were dried under vacuum at 20 mm Hg for 8 h. For impregnation, dry Amberlite XAD-4 resin was immersed into a saturated solution of the required amount of extractant **29** in methanol and stirred slowly at room temperature for 4 h. SIR beads were then separated by filtration using a sintered glass funnel, washed with 30% methanol-deionized water and air dry overnight followed by drying under vacuum at 20 mm Hg for 8 h. The ratio of resin to extractant (w/w) was varied from 1:0.5 to 1:3 to find the maximum loading of extractant on resin. The pictures of Amberlite XAD-4 resin before and after maximum impregnation are shown in Figure 5.17.

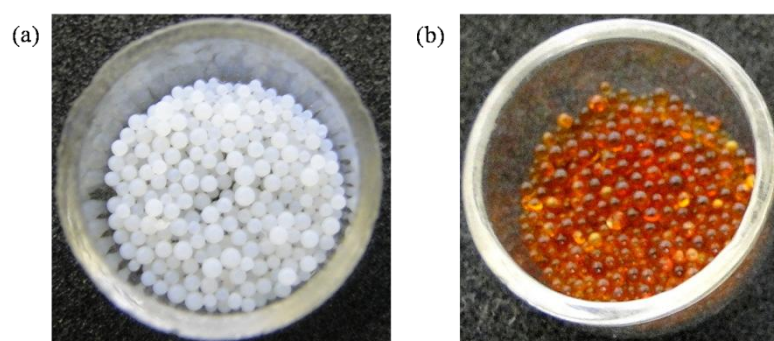


Fig. 5.17 Amberlite XAD-4 resin beads; (a) before and (b) after impregnation.

Analytical methods used for characterization of impregnated resin

Impregnated resin was characterized using IR (Shimadzu instrument using ATR diamond probe) and Scanning Electron Microscopy (SEM) (Philips XL 30 ESEM at

room temperature). The thermogravimetric analysis (TGA) was carried out using STAR[®] System METTLER TOLEDO instrument. A few milligram of the sample was taken in the alumina sample holder and the thermogravimetric curves were recorded from 25 °C to 550 °C at a heating rate of 5 °C min⁻¹ under dynamic condition in N₂ atmospheres (50 mL min⁻¹). The % loading of extractant on the resin was determined from the thermogravimetric data.

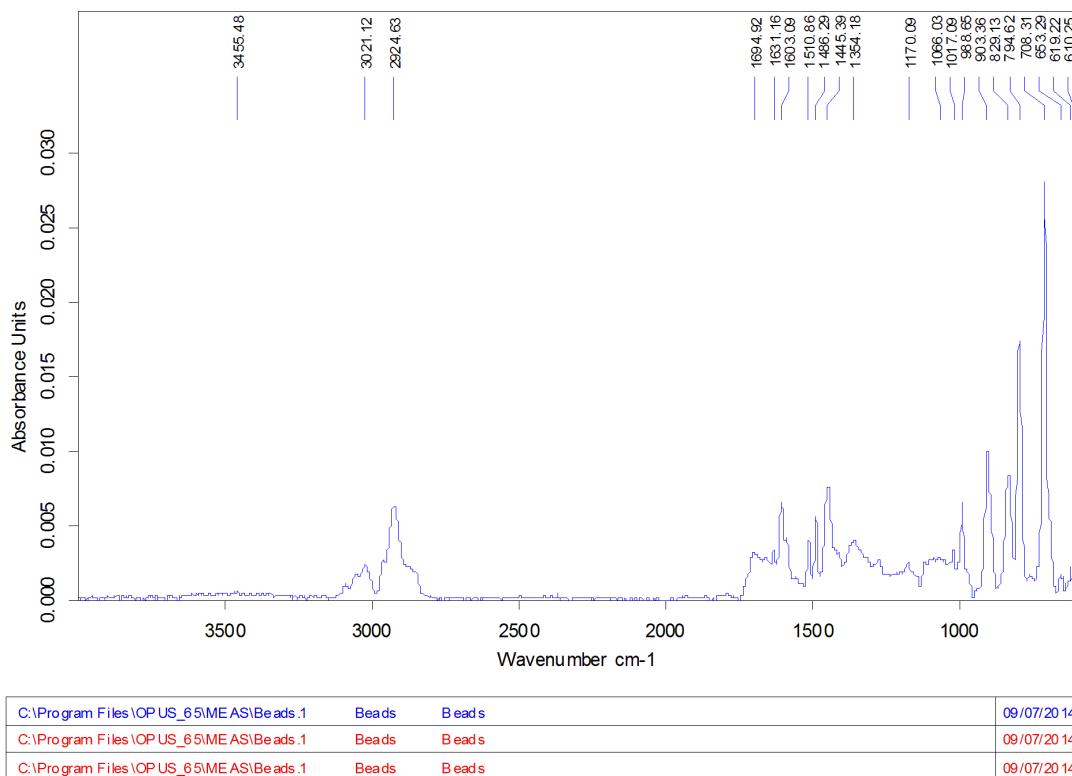
Sorption studies

For sorption studies, 50 mg of impregnated resin and 1 mL solution of different concentrations of Ru in HNO₃ were poured into different vials. The vials were placed in a constant water bath shaker at 25 °C. The steady state was attained within 1 h of contact time. Therefore, the contact time was kept 1.5 h for all the experiments. The mixture was then filtered and the concentrations of metal ion in aqueous phase, before and after equilibration were measured using ICP-AES. The concentration of ruthenium in solvent impregnated XAD resin was calculated by mass balance. The distribution coefficient (K_d , mL.g⁻¹) and equilibrium sorption capacity (Q_e , mg/g) were calculated from the Equations 5.9 and 5.10, respectively.

$$K_d = \frac{C_0 - C_e}{C_e} \left(\frac{V}{M} \right) \text{ (mL.g}^{-1}\text{)} \quad (5.9)$$

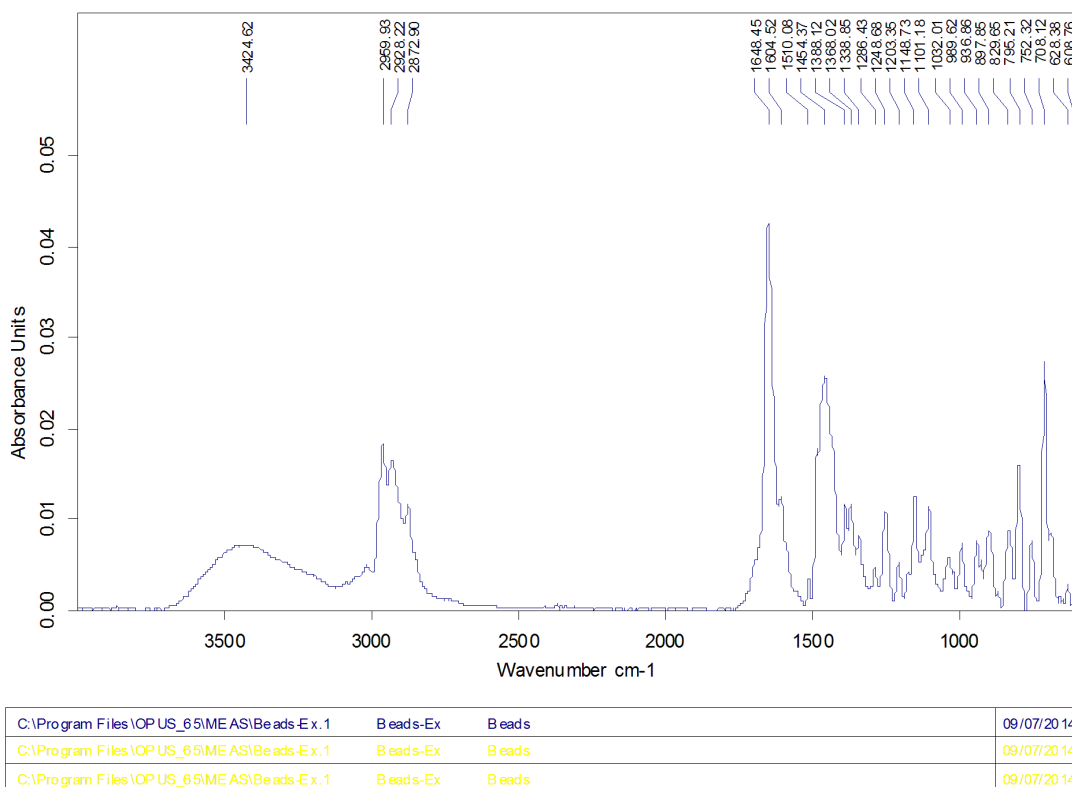
$$Q_e = (C_0 - C_e) \left(\frac{V}{M} \right) \text{ (mg.g}^{-1}\text{)} \quad (5.10)$$

Where C_0 is the initial Ru concentration in aqueous phase before contact, C_e is the final metal concentration after contact, V the volume of aqueous phase and M is the mass of the impregnated resin used.



Page 1/1

Fig. 5.18 IR spectrum of XAD-4 resin before impregnation of extractant.



Page 1/1

Fig. 5.19. IR spectrum of XAD-4 resin after impregnation of extractant.

References

1. IAEA Nuclear technology Review, IAEA, Vienne, Austria, 2009.
2. H. J. Arnikaar, *Essentials of Nuclear Chemistry*, Wiley Eastern Limited, New Delhi, 2nd edn., 1988.
3. S. S. Bajaj and A. R. Gore, *Nucl. Eng. Des.*, 2006, **236**, 701.
4. B. A. Semenov and N. Oi, Nuclear Fuel Cycles- Adjusting to new realities, IAEA Bulletin, Vienna, Austria, 1993.
5. Classification of Radioactive Waste, IAEA Safety Standards No GSG-1, IAEA, Vienna, Austria, 2009.
6. C. McCombie, *Phys. Today*, 1997, **50**, 56.
7. J.V. Holder, *Radiochim. Acta*, 1978, **25**, 171.
8. Actinide and Fission Product Partitioning and Transmutation—Status and Assessment report, OECD/NEA, Paris, 1999.
9. J. Magill, V. Berthou, D. Haas, J. Galy, R. Schenkel, H.-W. Wiese, G. Heusener, J. Tommasi and G. Youinou, *Nuclear Energy*, 2003, **42**, 263.
10. W. Schulz, J. D. Navratil and A. E. Talbot, *Science and technology of tributyl phosphate*, CRC Press, Florida, 1984.
11. L. Maya, *J. Inorg. Nucl. Chem.*, 1981, **43**, 385.
12. B. J. Mincher, G. Modolo and S. P. Mezyk, *Solvent Extr. Ion Exch.*, 2009, **27**, 1.
13. Potential Benefits and Impacts of Advanced Nuclear Fuel Cycles with Actinide Partitioning and Transmutation, in *Nuclear Science*, OECD/NEA, Paris, 2011.
14. J. N. Mathur, M. S. Murali and K. L. Nash, *Solvent Extr. Ion Exch.*, 2001, **19**, 357.

15. Mobile Fission and Activation Products in Nuclear Waste Disposal, in *Nuclear Science*, ISBN 978-92-64-99072-2, OECD/NEA, 6310, La Baule, France, 2007.
16. W. W. Schulz and L. A. Bray, *Sep. Sci. Technol.*, 1987, **22**, 191.
17. P. Swain, M. Chellanadar, S. Kannan, N. K. Pandey, S. Rajagopalachari, K. M. Uthandi and N. Rajamani, *Prog. Nucl. Energy*, 2014, **75**, 198.
18. B. Remenec, *Czech. J. Phys.*, 2006, **56**, D645.
19. X. Liu, J. Liang and J. Xu, *Solvent Extr. Ion Exch.*, 2004, **22**, 163.
20. J. N. Mathur, M. S. Murli, P. R. Natarajan, L. P. Badheka, A. Banerji, A. Ramanujam, P. S. Dhami, V. Gopalakrishnan, R. K. Dhumwad and M. K. Rao, *Waste Manage.*, 1993, **13**, 317.
21. S. Tachimori and H. Nakamura, *J. Nucl. Sci. Technol.*, 1982, **19**, 326.
22. E. Dziwinski and J. Szymanowski, *Solvent Extr. Ion Exch.*, 1998, **16**, 1515.
23. Y. J. Zhu, J. Chen and R. Z. Jiao, *Solv. Extr. Ion Exch.*, 1996, **14**, 61.
24. V. K. Manchanda and P. N. Pathak, *Sep. Purif. Technol.*, 2004, **35**, 85.
25. S. J. Ansari, P. Pathak, P. K. Mohapatra and V. K. Manchanda, *Chem. Rev.*, 2012, **112**, 1751.
26. Y. Sasaki, Y. Sugo, S. Suzuki and S. Tachimori, *Solv. Extr. Ion. Exch.*, 2001, **19**, 91.
27. H. H. Dam, D. N. Reinhoudt and W. Verboom, *Chem. Soc. Rev.*, 2007, **36**, 367.
28. P. Nekovář and D. Schrötterová, *Solvent Extr. Ion Exch.*, 1999, **17**, 163.
29. M. Johansson, J. Alstad, J. P. Omtvedt and G. Skarnemark, *Radiochim. Acta*, 2001, **89**, 619.
30. T. A. Todd, T. A. Batcheller, J. D. Law and R. S. Herbst, Cesium and Strontium Separation Technologies Literature Review, Idaho National Engineering and

- Environmental Laboratory Idaho Falls, INEEL/EXT-04-01895, U.S. Department of Energy, Idaho 83415, 2004.
31. M. J. Hudson, L. M. Harwood, D. M. Laventine and F. W. Lewis, *Inorg. Chem.*, 2013, **52**, 3414.
32. J. Rydberg, M. Cox, C. Musikas and G. R. Choppin, *Solvent Extraction Principles and Practice Revised and Expanded*, Marcel Dekker, USA, 2nd edn., 2004.
33. H. J. Fendler, *J. Membr. Sci.*, 1987, **30**, 323.
34. M. Ghaedi, B. Karami, Sh. Ehsani, F. Marahel and M. Soylak, *J. Hazard. Mater.*, 2009, **172**, 802.
35. R. Takayama, K. Ooe, W. Yahagi, H. Fujisawa, Y. Komori, H. Kikunaga, T. Yoshimura, N. Takahashi, K. Takahisa, H. Haba, Y. Kudou, Y. Ezaki, A. Toyoshima, M. Asai, Y. Nagame, T. Saito, T. Mitsugashira and A. Shinohara, *Proc. Radiochim. Acta*, 2011, **1**, 157.
36. P. K. Parhi, K.H. Park, H. I. Kim and J. T. Park, *Hydrometallurgy*, 2011, **105**, 195.
37. M. R. Antonio, D. R. McAlisterb and E. P. Horwitz, *Dalton Trans.*, 2015, **44**, 515.
38. S. Kannan, M. A. Moody, C. L. Barnes and P. B. Duval, *Inorg. Chem.*, 2008, **47**, 4691.
39. S. Sriram, R. Veeraraghavan and V. K. Manchanda, *Radiochim. Acta*, 1999, **84**, 153.
40. R.G. Pearson, *J. Am. Chem. Soc.*, 1963, **85**, 3533.
41. M. Benedict, T. H. Pigford and H. W. Levi, *Nuclear Chemical Engineering*, McGraw Hill Book Company, US, 2nd edn., 1981, pp.165.

42. M. Benedict, T. H. Pigford and H. W. Levi, *Nuclear Chemical Engineering*, McGraw Hill Book Company, US, 2nd edn., 1981, pp.172.
43. F. Poineau, J. D. Mazaubrun, D. Ford, J. Fortner, J. Kropf, G. W. C. Silva, N. Smith, K. Long, G. Jarvinen and K. Czerwinski, *Radiochim. Acta*, 2008, **96**, 527.
44. R. Shanker and K. S. Venkateswarlu, *Sep. Sci.*, 1976, **11**, 591.
45. W. C. Eckelman, *J. Am. Coll. Cardiol. Img.*, 2009, **2**, 364.
46. J. Vučina and D. Lukić, *Phys. Chem. Technol.*, 2002, **2**, 235.
47. A. Linz, *Ind. Eng. Chem.*, 1955, **47**, 1492.
48. J. Marchese, F. Valenzuela, C. Basualto and A. Acosta, *Hydrometallurgy*, 2004, **72**, 309.
49. J. Y. Lee, J. R. Kumar, H. S. Jeon and J. S. Kim, *Chem. Eng.*, 2010, **54**, 27.
50. L. E. Noronha, G. S. Kamble, S. S. Kolekar and M. A. Anuse, *Int. J. Chem. Sci. Tech.*, 2013, **3**, 15.
51. J. R. Kumar, J. S. Kim, J. Y. Lee and H. S. Yoon, *J. Radioanal. Nucl. Chem.*, 2010, **285**, 301.
52. N. I. Gerhardt, A. A. Palant, V. A. Petrova and R. K. Tagirov, *Hydrometallurgy*, 2001, **60**, 1.
53. R. R. Rao and S. M. Khopkar, *Analyst*, 1983, **108**, 346.
54. V. R. Bhandiwad, R. Swarup and S. K. Patil, *J. Radioanal. Nucl. Chem.*, 1979, **52**, 5.
55. M. Ghadiri, S. N. Ashrafizadeh and M. Taghizadeh, *Hydrometallurgy*, 2014, **144–145**, 151.
56. E. A. Mezhev, V. V. Druzhenkov and A. N. Sirotinin, *Radiochemistry*, 2002, **44**, 146.

57. D. Desideri, L. Feduzi, M. A. Meli and C. Roselli, *Microchem. J.*, 2011, **97**, 264.
58. H. Ramebäck, Y. Albinsson, M. Skålberg, U. B. Eklund, L. Kjellberg and L. Werme, *J. Nucl. Mater.* 2000, **277**, 208.
59. A. Senol, *Sep. Purif. Technol.*, 2014, **131**, 35.
60. Y. Xu, S. Y. Kim, T. Ito, H. Tokuda, K. Hitomi and K. Ishii, *J. Chromatogr. A*, 2013, **1312**, 37.
61. P. Nekovář and D. Schrötterová, *Chem. Eng. J.*, 2000, **79**, 229.
62. T. Coşar and R. Ziyadanoğullari, *Turk. J. Chem.*, 1998, **22**, 379.
63. E. Goralska, M. T. Coll, A. Fortuny, C. S. Kedari, and A. M. Sastre, *Solvent Extr. Ion Exch.*, 2007, **25**, 65.
64. M. C. Ali, T. Kawasaki, M. Nogami, M. Saeki, Y. Sasaki and Y. Ikeda, *Prog. Nucl. Energy*, 2011, **53**, 1005.
65. M. C. Ali, T. Suzuki, Y. Tachibana, Y. Sasaki and Y. Ikeda, *Sep. Purif. Technol.*, 2012, **92**, 77.
66. Y. Sasaki, M. Ozawa, T. Kimura and K. Ohashi, *Solvent Extr. Ion Exch.*, 2009, **27**, 378.
67. E. P. Horwitz, A. C. Muscatello, D. G. Kalina and L. Kaplan, *Sep. Sci. Technol.* 1981, **16**, 417.
68. E. P. Horwitz, K. A. Martin, H. Diamond and L. Kaplan, *Solvent Extr. Ion Exch.*, 1986, **4**, 449.
69. V. Kumar, J. N. Sharma, P. V. Achuthan and R. C. Hubli, *RSC Adv.*, 2014, **4**, 805.
70. M. Cindrić, Z. Veksli and B. Kamenara, *Croat. Chem. Acta*, 2009, **82**, 345.
71. M. T. Pope and A. Miiller, *Angew. Chem. Inr. Ed. Engl.*, 1991, **30**, 34.

72. E. Kapetanakis, A. M. Douvas, D. Velessiotis, E. Makarona, P. Argitis, N. Glezos and P. Normand, *Org. Electron.*, 2009, **10**, 711.
73. D. E. Katsoulis, *Chem. Rev.*, 1998, **98**, 359.
74. E. Kapetanakis, A. M. Douvas, D. Velessiotis, E. Makarona, P. Argitis, N. Glezos and P. Normand, *Adv. Mater.*, 2008, **20**, 4568.
75. (a) E. Coronado, C. Gimenezsaiz and C. Gomezgarcia, *Coordination Chem. Rev.*, 2005, **249**, 1776; (b) M. T. Pope, Springer-Verlag, Berlin, Germany, 1983; (b) A. Müller, *Nature*, 1991, **352**, 115; (c) A. Müller, M. T. Pope, F. Peters and D. Gatteschi, *Chem. Rev.*, 1998, **98**, 239; (d) C. L. Hill, *Chem. Rev.*, 1998, **98**, 1; (e) D. L. Long, E. Burkholder and L. Cronin, *Chem. Soc. Rev.*, 2007, **36**, 105; (f) G. J. T. Cooper and L. Cronin, *J. Am. Chem. Soc.*, 2009, **131**, 8368.
76. V. Shivaiah, *Inorg. Chem. Commun.*, 2006, **9**, 1191.
77. M. X. Li, H. L. Chen, J. P. Geng, X. He, M. Shao, S. R. Zhu and Z. X. Wang, *Cryst. Eng. Commun.*, 2011, **13**, 1687.
78. Y. Shi, W. Yang, G. Xue, H. Hu and J. Wang, *J. Mol. Struct.*, 2006, **784**, 244.
79. B. Modec, J. V. Brenčič and J. Zubieta, *Inorg. Chem. Commun.*, 2003, **6**, 506.
80. S. L. Linguito, X. Zhang, M. Padmanabhan, A. V. Biradar, T. Xu, T. J. Emge, T. Asefaab and J. Li, *New J. Chem.*, 2013, **37**, 2894.
81. S. Zhou, B. Liu, Y. G. Chen, X. M. Li and D. X. Wang, *RSC Adv.*, 2013, **3**, 24910.
82. H. Y. Zang, K. Tan, W. Guan, S. L. Li, G. S. Yang, K. Z. Shao and L. K. Yana, *Cryst. Eng. Commun.*, 2010, **12**, 3684.

83. B. K. Koo and U. Lee, *Inorg. Chimica. Acta.*, 2006, **359**, 2067.
84. A. S. Kertes, in *Solvent extraction chemistry of metals*, ed. H. A. C. McKey, T. V. Healy, I. L. Jetkins and A. Naylor, MacMillan, London, 1965, pp. 377.
85. A. Keshav, K. L. Wasewar, S. Chand and H. Uslu, *Fluid Phase Equilib.*, 2009, **275**, 21.
86. M. A. Olazabal, M. M. Orive, L. A. Fernández and J. M. Madariaga, *Solvent Extr. Ion Exch.*, 1992, **10**, 623.
87. D. Banerjea, *Inorganic Chemistry: A Modern Treatise*, Asian Books Pvt. Ltd., New Delhi, 2012.
88. R. Xi, B. Wang, K. Isobe, T. Nishioka, K. Toriumi and Y. Ozawa, *Inorg. Chem.*, 1994, **33**, 833.
89. (a) A. F. Masters, S. F. Ghellu, R. T. Brownlee, M. J. O'Connor and A. G. Wedd, *Inorg. Chem.*, 1980, **19**, 3866; (b) M. T. Pope, *Inorg. Chem.*, 1991, **30**, 181; (c) M. L. Niven, J. J. Cruywagen and J. B. B. Heyns, *J. Chem. Soc., Dalton Trans.*, 1991, 2007; (d) D. Hagrman, C. Zubieta, D. J. Rose, J. Zubieta and R. C. Haushalter, *Angew. Chem., Int. Ed.*, 1997, **36**, 873; (e) J. O. Xu, R. Z. Wang, G. Y. Yang, Y. H. Xing, D. M. Li, W. M. Bu, L. Ye, Y. G. Fan, G. D. Yang, Y. Xing, Y. H. Lim and H. Q. Jia, *Chem. Commun.*, 1999, 983.
90. D. Xiao, Y. Hou, E. Wang, S. Wang, Y. Li, L. Xu and C. Hu, *Inorg. Chim. Acta*, 2004, **357**, 2525.
91. The structure of **3** was confirmed by single-crystal X-ray data. CCDC 1401083 contains the supplementary crystallographic data for this paper. These data can be obtained free of charge from The Cambridge Crystallographic Data Centre via www.ccdc.cam.ac.uk/data_request/cif.

92. The structure of 4 was confirmed by single-crystal X-ray data. CCDC 1401084 contains the supplementary crystallographic data for this paper. These data can be obtained free of charge from The Cambridge Crystallographic Data Centre via www.ccdc.cam.ac.uk/data_request/cif.
93. R. C. Clark and J. S. Reid, *Acta Cryst.*, 1995, **A51**, 887.
94. G. M. Sheldrick, *Acta Cryst.*, 2008, **A64**, 112.
95. O. V. Dolomanov, L. J. Bourhis, R. J. Gildea, J. A. K. Howard and H. Puschmann, *J. Appl. Cryst.*, 2009, **42**, 339.
96. E. R. Irish and W. H. Reas, *The PUREX process-a solvent extraction reprocessing method for irradiated uranium*, General Electric, Washington, 1996.
97. A. Wright and P. Paviet-Hartman, *Sep. Sci. Technol.*, 2010, **45**, 1753.
98. B. J. Mincher, G. Modolo and S. P. Mezyk, *Solvent Extr. Ion Exch.*, 2009, **27**, 331.
99. B. J. Mincher, G. Elias, L. R. Martin and S. P. Mezyk, *J. Radioanal. Nucl. Chem.*, 2009, **282**, 645.
100. W. Davis Jr., In *Radiolytic behavior*, ed. W. Schulz, J. D. Navratil and A. E. Talbot, CRC Press, Florida, 1984, pp. 221.
101. S. C. Tripathi, A. Ramanujam, K. K. Gupta and P. Bindu, *Sep. Sci. Technol.*, 2001, **36**, 2863.
102. J. N. Sharma, R. Ruhela, K. K. Singh, M. Kumar, C. Janardhanan, P. V. Achutan, S. Manohar, P. K. Wattal and A. K. Suri, *Radiochim. Acta*, 2010, **98**, 485.
103. Z. Nowak, *Nukleonika*, 1977, **22**, 155.

104. D. Lasage, H. Virelizier, C. K. Jankowski and J. C. Tabet, *Spectroscopy*, 1997, **13**, 275.
105. C. Lamouroux, H. Virelizier, C. Moilin and C. K. Jankowski, *J. Chromatogr.* 2001, **917**, 261.
106. D. Lasage, H. Virelizier, C. K. Jankowski and J. C. Tabet, *Eur. J. Mass. Spectrom.*, 1998, **4**, 47.
107. C. Ginisty and B. Guillame, *Sep. Sci. Technol.*, 1990, **25**, 1941.
108. H. He, M. Lin, Y. Muroya, H. Kudo and Y. Katsumura, *Phys. Chem. Chem. Phys.*, 2004, **6**, 1264.
109. B. J. Mincher, S. P. Mezyk and L. R. Martin, *J. Phys. Chem.*, 2008, **112**, 6275.
110. A. Tahraoui and J. H. Morris, *Sep. Sci. Technol.*, 1995, **30**, 2603.
111. Z. Nowak, M. Nowak and A. Seydel, *Radioanal. Lett.*, 1979, **38**, 343.
112. T. Tsujino and T. J. Ishihara, *Nucl. Sci. and Technol.*, 1966, **3**, 320.
113. Y. Kawaguchim, K. Morimoto, T. Kitao, K. Ohyama and E. Omori, *Atom. Ener. Soc. Jpn.*, 2009, **8**, 221.
114. S. C. Tripathi, P. Bindu and A. Ramanujam, *Sep. Sci. Technol.*, 2001, **36**, 1463.
115. S. C. Tripathi, S. Sumathi and A. Ramanujam, *Sep. Sci. Technol.*, 1999, **34**, 2887.
116. R. W. Wilkinson and T. F. Williams, *J. Chem. Soc.*, 1961, 4098.
117. J. Kuruc, V. E. Zubarev, L. T. Bugaenko and F. Macášek, *J. Radioanal. Nucl. Chem. Lett.*, 1988, **127**, 37.
118. L. Melander and W. H. Saunders Jr., *Reaction Rates of Isotopic Molecules*, John Wiley and Sons, New York, 1980.
119. R. P. Bell, *The tunnel effect in chemistry*, Chapman and Hall, London, 1980.
120. T. Gillbro and A. Lund, *Chem. Phy. Lett.*, 1974, **27**, 300.

121. G. T. Miwa, J. S. Walsh, G. L. Kedderis and P. F. Hollenberg, *J. Biol. Chem.* 1983, **258**, 14445.
122. F. H. Westheimer, *Chem. Rev.*, 1961, **61**, 265.
123. W. A. Van Hook, *Nukleonika*, 2011, **56**, 217.
124. C. J. Collins and N. S. Bowman, *Isotope effects in chemical reactions*, Van Nostrand Rheinhold, New York, 1970.
125. J. Bigeleisen and M. Wolfsberg, *Adv. Chem. Phys.*, 1958, **1**, 15.
126. A. Kohen and H. H. Limbach (eds), *Isotope effects in chemistry and biology*, Taylor and Francis, Boca Raton. 2006
127. M. Wolfsberg, W. A. Van Hook, P. Paneth and L. P. N. Rebelo, *Isotope effects in the chemical, geological, and bio sciences*, Springer, Dordrecht, 2010.
128. G. Jancso, in *Isotope effects*, ed. A. Vertes, S. Nagy and Z. Klencsar, Handbook of isotope chemistry, Kluwer Academic Pub, Dordrecht, 2003, 4, pp. 85.
129. C. Hennig, R. B. Oswald and S. J. Schmatz, *Phys. Chem. A*, 2006, **110**, 3071.
130. M. Tashiro, H. Tsuzuki, S. Mataka and T. J. Yonemitsu, *Label Compd. Radiopharm.*, 1991, **29**, 691.
131. B. J. Mincher and R. D. Curry, *Appl. Radiat. Isot.*, 2000, **52**, 189.
132. J. W. T. Spinks and R. J. Woods, *An introduction to radiation chemistry*, 3rd edn. Wiley, New York, 1990.
133. D. R. Peterman, B. J. Mincher, C. L. Riddle and R. D. Tillotson, Summary report on gamma radiolysis of TBP/*n*-dodecane in the presence of nitric acid using the hydrolysis/ radiolysis test loop, INL/EXT-10-19866, Aug. 2010.
134. K. A. Venkatasan, B. Robertselvan, M. P. Antony, T. G. Srinivasan and P. R. Vasudeva Rao, *Solvent Extr. Ion Exch.*, 2006, **24**, 747.

135. L. B. Kumbahre, D. R. Prabhu, G.R. Mahajan, S. Sriram, V. K. Manchanda, and L. P. Badheka, *Nucl. Tech.*, 2002, **139**, 253.
136. S. A. Ansari, P. N. Pathak, V. K. Manchanda, M. Hussain, A. K. Prasad and V. S. Parmar, *Solvent Extr. Ion Exch.*, 2005, **23**, 463.
137. G. Modolo, H. Asp, C. Schreinemachers and H. Vijgen, *Solvent Extr. Ion Exch.*, 2007, **25**, 703.
138. S. Manohar, J. N. Sharma, B. V. Shah and P. K. Wattal, *Nucl. Sci. Eng.*, 2007, **156**, 96.
139. Z. X. Zhu, Y. Sasaki, H. Suzuki, S. Suzuki and T. Kimura, *Analytica Chimica Acta*, 2004, **527**, 163.
140. H. Suzuki, Y. Sasaki, Y. Sugo, A. Apichaibuol and T. Kimura, *Radiochim. Acta*, 2004, **92**, 463.
141. V. Kumar, A. Kumar, S. Mondal, J. N. Sharma, R. C. Hubli, P. K. Wattal and A. K. Suri, *Sep. Purif. Tech.*, 2012, **98**, 118.
142. J. Ravi, A. S. Suneesh, T. Prathibha, K. A. Venkatesan, M. P. Antony, T. G. Srinivasan and P. R. Vasudeva Rao, *Solvent Extr. Ion Exch.*, 2011, **29**, 86.
143. G. R. Mahajan, D. R. Prabhu, V. K. Manchanda and L. P. Badheka, *Waste Manage.*, 1998, **18**, 125.
144. Y. Sasaki, Y. Kitatsuji, Y. Sugo, Y. Tsubata, T. Kimura and Y. Morita, *Solvent Extr. Res. Dev.*, 2012, **19**, 51.
145. M. Iqbal, J. Huskens, W. Verboom, M. Sypula and G. Modolo, *Supramol. Chem.*, 2010, **22**, 827.
146. L. Wu, Y. Fang, Y. Jia, Y. Yang, J. Liao, N. Liu, X. Yang, W. Feng, J. Ming and L. Yuan, *Dalton Trans.*, 2014, **43**, 3835.
147. P. K. Mohapatra, A. Sengupta, M. Iqbal, J. Huskens, S. V. Godbole and W. Verboom, *Dalton Trans.*, 2013, **42**, 8558.

148. D. Jańczewski, D. N. Reinhoudt, W. Verboom, C. Hill, C. Allignol and M. T. Duchesne, *New J. Chem.*, 2008, **32**, 490.
149. M. T. Murillo, A. G. Espartero, J. Sánchez-Quesada, J. de Mendoza and P. Prados, *Solv. Extr. Ion Exch.* 2009, **27**, 107.
150. L. Boyadzhiev and Z. Lazarova, in *Membrane Separations Technology: Principles and Applications*, ed. R. D. Noble and S.A. Stern, Elsevier Science B. V., 1995, pp.283.
151. P. K. Mohapatra and V. K. Manchanda, *Indian J. Chem.*, 2003, **42A**, 2925.
152. D. L. Hofman, W. M. Craig, E. M. Buchalter, R. S. Birkill, and J. J. Smit; Supported liquid membrane technology applied to the recovery of useful isotopes from reactor pool water. I. Chem. E. Symposium Series No. 103, Extraction '87, EFCE Publication Series No. 347, pp. 180 – 182.
153. W. C. Babcock, R. W. Baker, E. D. Lachapelle and K. L. Smith, *J. Membr. Sci.*, 1980, **7**, 89.
154. A. M. Sastre, A. Kumar, J. P. Shukla and R. K. Singh, *Sep. Purif. Methods*, 1998, **27**, 213.
155. S. Panja, R. Ruhela, S. K. Misra, J. N. Sharma, S. C. Tripathi and A. Dakshinamoorthy, *J. Membr. Sci.*, 2008, **325**, 158.
156. S. A. Ansari, P. K. Mohapatra, D. R. Prabhu and V. K. Manchanda, *J. Membr. Sci.*, 2006, **282**, 133.
157. S. A. Ansari, P. K. Mohapatra, D. R. Prabhu and V. K. Manchanda, *J. Membr. Sci.*, 2007, **298**, 169.
158. S. Sriram, P. K. Mohapatra, A. K. Pandey, V. K. Manchanda and L. P. Badheka, *J. Membr. Sci.*, 2000, **177**, 163.
159. P. K. Mohapatra, D. S. Lakshmi, D. Mohan and V. K. Manchanda, *J. Membr. Sci.*, 2004, **232**, 133.

160. A. Bhattacharyya, P. K. Mohapatra, A. Roy, T. Gadly, S. K. Ghosh and V. K. Manchanda, *Hydrometallurgy*, 2009, **99**, 18.
161. J. N. Sharma, R. Ruhela, K. N. Harindaran, S. L. Mishra, S. K. Tangri and A. K. Suri, *J. Radioanal. Nucl. Chem.*, 2008, **278**, 173.
162. R. Ruhela, S. Panja, J. N. Sharma, B. S. Tomar, S. C. Tripathi, R. C. Hubli and A. K. Suri, *J. Hazard. Mater.*, 2012, **229–230**, 66.
163. S. Panja, R. Ruhela, S. C. Tripathi, A. K. Singh, P. M. Gandhi and R. C. Hubli, *J. Membr. Sci.*, 2014, **449**, 67.
164. A. J. B. Kemperman, D. Bargeman, T. V. D. Boomgaard and H. Strathmann, *Sep. Sci. Technol.*, 1996, **31**, 2733.
165. P. K. Mohapatra, Ph. D. Thesis, University of Bombay, 1993.
166. R. M. Izzat, D. K. Roper, R. L. Bruening and J. D. Lamb, *J. Membr. Sci.*, 1989, **45**, 73.
167. A. D. Becke, *Phys. Rev. A*, 1988, **38**, 3098.
168. J. P. Perdew, *Phys. Rev. B: Condens. Matter*, 1986, **33**, 8822.
169. TURBOMOLE is program package developed by the Quantum Chemistry Group at the University of Karlsruhe, Germany, 1988.
170. R. Ahlrichs, M. Bär, M. Häser, H. Horn and C. Kölmel, *Chem. Phys. Lett.*, 1989, **162**, 165.
171. A. Tokarev, A. Grandjean, Y. Guari, J. Larionova, R. Pflieger and C. Guérin, *J. Nucl. Mater.*, 2010, **400**, 25.
172. J. M. Fletcher, I. L. Jenkins, F. M. Lever, F. S. Martin, A. R. Powell and R. Todd, *J. Inorg. Nucl. Chem.*, 1955, **1**, 378.
173. F. Mousset, F. Bedioui and C. Eysseric, *Electrochem. Commun.*, 2004, **6**, 351.
174. K. Singh, N. L. Sonar, T. P. Valsala, Y. Kulkarni, T. Vincent and A. Kumar, *Desalin. Water Treat.*, 2014, **52**, 514.

175. M. Blicharska, B. Bartoś, S. Krajewski and A. Bilewicz, *J. Radioanal. Nucl. Chem.*, 2013, **298**, 1713.
176. N. A. Barbosa, L. A. R. da Rosa, A. Facure and D. Braz, *Radiat. Phys. Chem.*, 2014, **95**, 224.
177. S. J. Kokate and S. R. Kuchekar, *J. Saudi Chem. Soc.*, 2010, **14**, 41.
178. B. Rezaei and M. Keyvanfard, *J. Hazard. Mater.*, 2008, **151**, 456.
179. H. Wei, X. Yan, X. Li, S. He and C. Sun, *J. Hazard. Mater.*, 2013, **244–245**, 478.
180. S. Muhammad, P. R. Shukla, M. O. Tade and S. Wang, *J. Hazard. Mater.*, 2012, **215–216**, 183.
181. R. Navarro, I. Saucedo, A. Núñez, M. Ávila and E. Guibal, *React. Funct. Polym.*, 2008, **68**, 557.
182. B. Saha, R. J. Gill, D. G. Bailey, N. Kabay and M. Arda, *React. Funct. Polym.*, 2004, **60**, 223.
183. K. Raj, K. K. Prasad and N. K. Bansal, *Nucl. Eng. Des.*, 2006, **236**, 914.
184. M. Karve and R. V. Rajgor, *Desalination*, 2008, **232**, 191.
185. A. Warshawsky, *Talanta*, 1974, **21**, 644.
186. R. Huang, B. Yang, Q. Liu and Y. Liu, *J. Appl. Polym. Sci.*, 2014, **131**, 39903.
187. M. L. Delacour, E. Gailliez, M. Bacquet and M. Morcellet, *J. Appl. Polym. Sci.*, 1999, **73**, 899.
188. G. A. Meligi, *Polym.-Plast. Technol. Eng.*, 2008, **47**, 106.
189. G. Absalan and M. A. Mehrdardi, *Sep. Purif. Technol.*, 2003, **33**, 95.
190. S. D. Çekiç, H. Filik and R. Apak, *Anal. Chim. Acta*, 2004, **505**, 15.
191. A. W. Trochimczuk, N. Kabay, M. Arda and M. Streat, *React. Funct. Polym.*, 2004, **59**, 1.
192. E. A. El-Sofany, *J. Hazard. Mater.*, 2008, **153**, 948.

193. T. Saitoh, F. Nakane and M. Hiraide, *React. Funct. Polym.*, 2007, **67**, 247.
194. E. Hallaba and R. A. I. Azzam, *Z. Anorg. Allg. Chem.*, 1962, **314**, 53.
195. W. J. Maeck, G. L. Booman, M. E. Kussy and J. E. Rein, *Anal. Chem.*, 1961, **33**, 1775.
196. M. M. Fieberg and R. I. Edwards, US patent 4,105,442, 1978.
197. S. Panigrahi, T. Dash, K. C. Nathsarma and K. Sarangi, *Sep. Sci. Technol.*, 2014, **49**, 545.
198. S. Kedari, M. T. Coll, A. Fortuny, E. Goralska and A. M. Sastre, *Sep. Sci. Technol.*, 2005, **40**, 1927.
199. J. N. Sharma, A. Kumar, V. Kumar, S. Pahan, C. Janardanan, V. Tessi and P. K. Wattal, *Sep. Purif. Technol.*, 2014, **135**, 176.
200. A. O. Dada, A. P. Olalekan, A. M. Olatunya and O. DADA, *IOSR J. Appl. Chem.*, 2012, **3**, 38.
201. R. S. Juang, *Proc. Natl. Sci. Counc. ROC (A)*, 1999, **23**, 353.
202. M. Rovira, L. Hurtado, J. L. Cortina, J. Arnaldos and A. M. Sastre, *React. Funct. Polym.*, 1998, **38**, 279.
203. D. Muraviev, L. Ghantous and M. Valiente, *React. Funct. Polym.*, 1998, **38**, 259.
204. R. N. Mendoza, I. S. Medina, A. Vera and M. A. Rodriguez, *Solvent Extr. Ion Exch.*, 2000, **18**, 319.